THE JOURNAL
OF
CHEMICAL PHYSICS

VOLUME 19, NUMBER 9 SEPTEMBER, 1951

Diffusion through an Interface

E. J. SCOTT
Department of Mathematics

AND

L. H. TUNG AND H. G. DRICKAMER
Department of Chemistry,
University of Illinois, Urbana, Illinois

(Received June 1, 1951)

The diffusion equation has been solved for the case of two cells of finite length with an interface between the cells. The effect of an interfacial resistance to mass transfer has been considered. It is shown that the situation where there is equilibrium (no resistance) at the interface is a special case of our solution. Several important cases are considered numerically.

MOST practical mass transfer operations involve the transport of molecules between phases (liquid-solid, liquid-liquid, or liquid-gas). Usually the fluids are in convective flow, and the following assumptions are made.

(1) A laminar film exists at the boundary of each liquid phase. In this laminar film the transport is entirely the result of molecular diffusion. This transport in this film is slow compared with turbulent transport in the main body. (2) The two phases are at equilibrium at the interface, and therefore the interface offers no resistance to mass transfer.

The first assumption rests on fairly sound grounds, but the second assumption has been made purely for convenience. In this paper it is proposed to treat two-phase diffusion with resistance in the interface, to demonstrate that the case of no resistance (equilibrium) at the interface arises as a special case of the general treatment, and to show the effect of various interfacial resistances on the characteristics of the mass transfer.

Consider a cell as shown below at $t=0$.

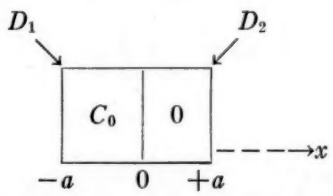

The differential equation for transport in the region $-a$ to 0 is

$$C_t(x, t)=D_1C_{xx}(x, t) \tag{1}$$

and in the region 0 to a

$$C_t(x, t)=D_2C_{xx}(x, t). \tag{2}$$

The following boundary conditions obtain:

the initial condition—

$$C(x, 0)=C_0, \qquad -a<x<0, \tag{3}$$

$$C(x, 0)=0, \qquad 0<x<a; \tag{4}$$

no diffusion is taking place across the boundary at the ends of the cell—

$$C_x(-a, t)=0, \tag{5}$$

$$C_x(a, t)=0; \tag{6}$$

continuity at the interface—

$$-D_1C_x(0_-, t)=-D_2C_x(0_+, t)=\mathbf{J}[C(0_-, t), C(0_+, t)]. \tag{7}$$

The flux at the interface is assumed to be of the following form:

$$\mathbf{J}[C(0_-, t)C(0_+, t)]=\alpha[C(0_-, t)-mC(0_+, t)]$$

m is the distribution coefficient of the diffusion substance in the two phases, namely when equilibrium is established $C_-=mC_+$. Hence Eq. (7) may be rewritten

as

$$-D_1C_x(0_-, t)=-D_2C_x(0_+, t)$$
$$=\alpha[C(0_-, t)-mC(0_+, t)]. \quad (8)$$

α is the transfer coefficient at the interface. Thus, in the case of no resistance at the interface, α will approach infinity; and since equilibrium is maintained at the interface, $C(0_-, t)=mC(0_+, t)$. Equation (8) then reduces to

$$-D_1C_x(0_-, t)=-D_2C_x(0_+, t). \quad (9)$$

We shall make use of the laplace transform method to solve our differential equations. Letting $L\{C(x, t)\}=c(x, p)$, the problem in the transform of $C(x, t)$ is then

$$pc(x, p)-C_0=D_1c_{xx}(x, p) \quad (-a<x<0), \quad (10)$$

$$pc(x, p)=D_2c_{xx}(x, p) \quad (0<x<a), \quad (11)$$

$$c_x(-a, p)=0, \quad c_x(a, p)=0, \quad (12)$$

$$-D_1c_x(0_-, p)=-D_2c_x(0_+, p)$$
$$=\alpha[c(0_-, p)-mc(0_+, p)]. \quad (13)$$

The solutions of (10) and (11) are

$$c(x, p)=A_1\cosh(x+a)\left(\frac{p}{D_1}\right)^{\frac{1}{2}}+\frac{C_0}{p} \quad (-a<x<0), \quad (14)$$

$$c(x, p)=A_2\cosh(x-a)\left(\frac{p}{D_2}\right)^{\frac{1}{2}} \quad (0<x<a). \quad (15)$$

Differentiating (14) and (15) and making use of the first two terms of (13), we have

$$D_1A_1\left(\frac{p}{D_1}\right)^{\frac{1}{2}}\left[\sinh a\left(\frac{p}{D_1}\right)^{\frac{1}{2}}\right]$$
$$=-D_2A_2\left(\frac{p}{D_2}\right)^{\frac{1}{2}}\left[\sinh a\left(\frac{p}{D_2}\right)^{\frac{1}{2}}\right],$$

from which

$$A_1=-A_2\left(\frac{D_2}{D_1}\right)^{\frac{1}{2}}\frac{\sinh a\left(\frac{p}{D_2}\right)^{\frac{1}{2}}}{\sinh a\left(\frac{p}{D_1}\right)^{\frac{1}{2}}}. \quad (16)$$

From (13) we also have

$$-D_2c_x(0_+, p)=\alpha[c(0_-, p)-mc(0_+, p)].$$

Therefore,

$$D_2A_2\left(\frac{p}{D_2}\right)^{\frac{1}{2}}\left[\sinh a\left(\frac{p}{D_2}\right)^{\frac{1}{2}}\right]$$
$$=\alpha\left\{A_1\left[\cosh a\left(\frac{p}{D_1}\right)^{\frac{1}{2}}\right]+\frac{C_0}{p}-mA_2\left[\cosh a\left(\frac{p}{D_2}\right)^{\frac{1}{2}}\right]\right\}.$$

Substituting the value of A_1 in (16) into the preceding expression and solving for A_2, we obtain

$$A_2=\frac{\alpha C_0(D_1)^{\frac{1}{2}}\sinh a\left(\frac{p}{D_1}\right)^{\frac{1}{2}}}{p\left\{\alpha m(D_1)^{\frac{1}{2}}\left[\cosh a\left(\frac{p}{D_2}\right)^{\frac{1}{2}}\right]\left[\sinh a\left(\frac{p}{D_1}\right)^{\frac{1}{2}}\right]+\alpha(D_2)^{\frac{1}{2}}\left[\sinh a\left(\frac{p}{D_2}\right)^{\frac{1}{2}}\right]\left[\cosh a\left(\frac{p}{D_1}\right)^{\frac{1}{2}}\right]\right.}$$
$$\left.+(pD_1D_2)^{\frac{1}{2}}\left[\sinh a\left(\frac{p}{D_2}\right)^{\frac{1}{2}}\right]\left[\sinh a\left(\frac{p}{D_1}\right)^{\frac{1}{2}}\right]\right\}. \quad (17)$$

Using this value of A_2, we get from (16)

$$A_1=\frac{-\alpha C_0\sinh a\left(\frac{p}{D_2}\right)^{\frac{1}{2}}}{p\left\{\alpha m(D_1)^{\frac{1}{2}}\left[\cosh a\left(\frac{p}{D_2}\right)^{\frac{1}{2}}\right]\left[\sinh a\left(\frac{p}{D_1}\right)^{\frac{1}{2}}\right]+\alpha(D_2)^{\frac{1}{2}}\left[\sinh a\left(\frac{p}{D_2}\right)^{\frac{1}{2}}\right]\right.}$$
$$\left.+(pD_1D_2)^{\frac{1}{2}}\left[\sinh a\left(\frac{p}{D_2}\right)^{\frac{1}{2}}\right]\left[\sinh a\left(\frac{p}{D_1}\right)^{\frac{1}{2}}\right]\right\}. \quad (18)$$

Let us make the substitutions

$$k=\left(\frac{D_1}{D_2}\right)^{\frac{1}{2}}, \quad \mu=\left(\frac{p}{D_1}\right)^{\frac{1}{2}}, \quad \lambda=\left(\frac{p}{D_2}\right)^{\frac{1}{2}}=k\mu. \quad (19)$$

Then, making use of (17) and substituting in (15) yields for the interval $0<x<a$ the expression

$$c(x,p)=\frac{\alpha kC_0(\sinh\mu a)[\cosh k\mu(x-a)]}{p[k\mu(D_1D_2)^{\frac{1}{2}}(\sinh k\mu a)(\sinh\mu a)+\alpha km(\cosh k\mu a)(\sinh\mu a)+\alpha(\cosh\mu a)(\sinh k\mu a)]}.$$

This function is a single-valued function of μ with simple poles at $p=0$ and $p=-D_1\eta n^2$, where $\pm\eta_n$, $n=1, 2, 3, \cdots$ are the roots (all real and simple) of

$$k(D_1D_2)^{\frac{1}{2}}\eta(\sin k\eta a)(\sin\eta a)-\alpha km(\cos k\eta a)(\sin\eta a)-\alpha(\cos\eta a)(\sin k\eta a)=0. \tag{20}$$

The residue of $c(x, p)e^{pt}$ at $p=0$ is

$$C_0/(m+1).$$

The residue at $p=-D_1\eta_n^2$ is

$$\frac{k\alpha C_0(\sinh(-i\eta_n a)(\cosh ik\eta_n(x-a))\exp(-D_1\eta_n^2t)}{p(d/dp)[k(D_1D_2)^{\frac{1}{2}}\mu(\sinh k\mu a)(\sinh\mu a)+k\alpha m(\cosh k\mu a)(\sinh\mu a)+\alpha(\cosh\mu a)(\sinh k\mu a)]_{p=-D_1\eta_n^2}}$$

$$=\frac{-2\alpha kC_0(\sin\eta_n a)(\cos k\eta_n(x-a))\exp(-D_1\eta_n^2t)}{\eta_n[\alpha a(k^2m+1)(\sin\eta_n a)(\sin k\eta_n a)-\alpha ak(m+1)(\cos\eta_n a)(\cos k\eta_n a)}.$$

$$+k(D_1D_2)^{\frac{1}{2}}\{(\sin ka\eta_n)(\sin a\eta_n)+\eta_n a(k(\sin\eta_n a)(\cos ka\eta_n)+(\sin k\eta_n a)(\cos\eta_n a))\}]$$

Therefore, by the inversion theorem we have for the interval $0<x<a$

$$C(x,t)=[C_0/(m+1)]$$

$$-\sum_{n=1}^{\infty}\frac{2\alpha kC_0(\sin\eta_n a)(\cos k\eta_n(x-a))\exp(-D_1\eta_n^2t)}{\eta_n[\alpha a(k^2m+1)(\sin\eta_n a)(\sin k\eta_n a)-\alpha ak(m+1)(\cos\eta_n a)(\cos k\eta_n a)}. \tag{21}$$

$$+k(D_1D_2)^{\frac{1}{2}}\{(\sin ka\eta_n)(\sin a\eta_n)+\eta_n a(k(\sin\eta_n a)(\cos ka\eta_n)+(\sin k\eta_n a)(\cos\eta_n a))\}]$$

Making use of (19) and substituting A_1 into (14), we get for the interval $-a<x<0$

$$c(x,p)=\frac{C_0}{p}-\frac{\alpha C_0(\sinh k\mu a)(\cosh\mu(x+a))}{pk[\mu(D_1D_2)^{\frac{1}{2}}(\sinh k\mu a)(\sinh\mu a)+k\alpha m(\cosh k\mu a)(\sinh\mu a)+\alpha(\cosh\mu a)(\sinh k\mu a)]}.$$

The inverse of the first term on the right is C_0 and the poles of the second term on the right are identical with the case when $0<x<a$. Evaluating the residues at these poles and applying the inversion theorem, we obtain for the interval $-a<x<0$

$$(Cx,t)=[C_0m/(m+1)]$$

$$+\sum_{n=1}^{\infty}\frac{2\alpha C_0(\sin\eta_n ka)(\cos\eta_n(x+a))\exp(-D_1\eta_n^2t)}{\eta_n[\alpha a(k^2m+1)(\sin\eta_n a)(\sin k\eta_n a)-\alpha ak(m+1)(\cos\eta_n a)(\cos k\eta_n a)}. \tag{22}$$

$$+k(D_1D_2)^{\frac{1}{2}}\{(\sin ka\eta_n)(\sin a\eta_n)+\eta_n a(k(\sin\eta_n a)(\cos ka\eta_n)+(\sin k\eta_n a)(\cos\eta_n a))\}]$$

In the case of no resistance (equilibrium) $\alpha\to\infty$, and we see that the solutions (20) and (21) reduce to

$$C(x,t)=\frac{C_0m}{(m+1)}-\sum_{n=1}^{\infty}\frac{2kC_0(\sin\eta_n a)(\cos k\eta_n(x-a))\exp(-D_1\eta_n^2t)}{\eta_n[a(k^2m+1)(\sin\eta_n a)(\sin k\eta_n a)-ak(m+1)(\cos\eta_n a)(\cos k\eta_n a)]} \quad (0<x<a), \tag{23}$$

$$C(x,t)=\frac{C_0m}{(m+1)}+\sum_{n=1}^{\infty}\frac{2C_0(\sin\eta_n ka)(\cos\eta_n(x+a))\exp(-D_1\eta_n^2t)}{\eta_n[a(k^2m+1)(\sin\eta_n a)(\sin k\eta_n a)-ak(m+1)(\cos\eta_n a)(\cos k\eta_n a)]} \quad (-a<x<0). \tag{24}$$

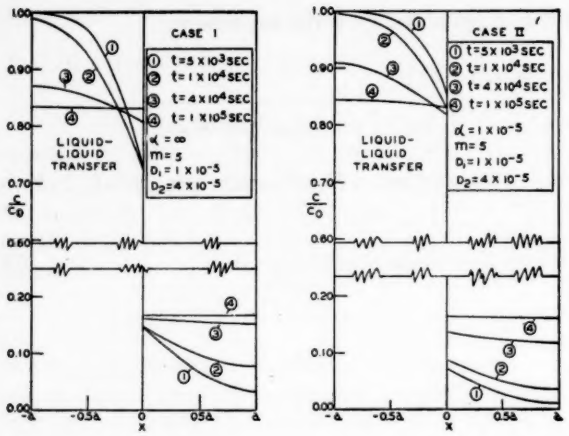

FIG. 1. Concentration profile as a function of time. Case I. Equilibrium at the interface. Case II. Interfacial resistance is of the same order as diffusional resistance.

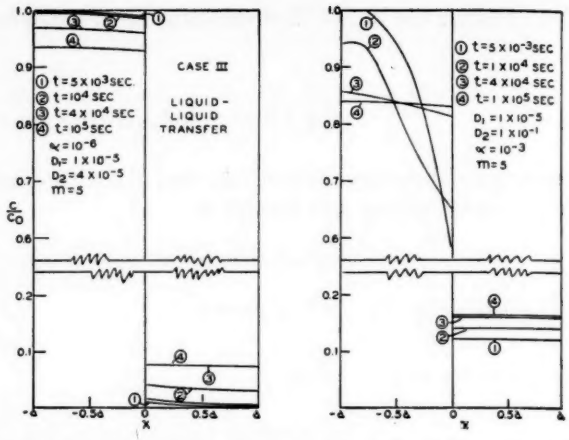

FIG. 2. Concentration profiles as a function of time. Case III. Interfacial resistance is large compared with diffusional resistance. Case IV. Gas-liquid transfer. Interfacial resistance of same order as diffusional resistance.

Equation (20) becomes

$$km\cos k\eta a\sin\eta a+\cos\eta a\sin k\eta a=0, \qquad (25)$$

whose roots are all real and simple.

Four cases have been considered numerically.

Case I	Case II
$D_1=1\times10^{-5}$ cm²/sec	$D_1=1\times10^{-5}$ cm²/sec
$D_2=4\times10^{-5}$ cm²/sec	$D_2=4\times10^{-5}$ cm²/sec
$m=5$	$m=5$
$a=1$ cm	$a=1$ cm
$\alpha=\infty$	$\alpha=1\times10^{-5}$ cm/sec
Case III	**Case IV**
$D_1=1\times10^{-5}$ cm²/sec	$D_1=1\times10^{-5}$ cm²/sec
$D_2=4\times10^{-5}$ cm²/sec	$D_2=1\times10^{-1}$ cm²/sec
$m=5$	$m=5$
$a=1$ cm	$a=1$ cm
$\alpha=1\times10^{-6}$ cm/sec	$\alpha=10^{-3}$ cm/sec

Cases I to III correspond to liquid-liquid transfer, Case IV to liquid-vapor transfer. In Case I there is no resistance (equilibrium) at the interface. In Case II the interfacial resistance is the same order as the resistance in the liquids, in Case III the interfacial resistance is higher by a factor of ten then the liquid resistance. The results are shown in Figs. 1 and 2. For the case of equilibrium the concentration ratio at the interface remains constant and equal to m. In the other cases it varies markedly. The concentration profile at various points in the cell as a function of time is widely different for the various cases.

This solution provides a means of establishing α and of characterizing the situation at the interface from experimental data. If the diffusion coefficients in the two phases are known, and the concentration at any point in the cell can be measured as a function of time with the two phases in contact, α can be calculated. It is hoped to obtain a generalized means of predicting α as a function of the molecular properties.

NOMENCLATURE

A_1, A_2 = constants of integration.
a = half-length of the diffusion cell.
C = concentration.
C_0 = initial concentration at left half of the diffusion cell in Medium 1.
D_1 = diffusion coefficient of the diffusing material in Medium 1.
D_2 = diffusion coefficient of the diffusing material in Medium 2.
J = mass flux at the interface.
$k=(D_1/D_2)^{\frac{1}{2}}$.
m = the distribution coefficient of the diffusing component between the phases at equilibrium.
p = transformation variable.
t = time.
x = distance coordinate.
α = transfer coefficient at the interface.
$\eta=i\mu$.
$\mu=(p/D_1)^{\frac{1}{2}}$.

Studies on the Photovoltaic Effect. II*

IRVIN LEVIN† AND CHARLES E. WHITE
Department of Chemistry, University of Maryland, College Park, Maryland
(Received April 30, 1951)

Benzaldehyde dissolved in alcohol in concentrations less than 0.1 *M* yields a positive photopotential and in greater concentrations the photopotential is negative. The production of the negative photopotential is attributed to the presence of peroxybenzoic acid. In general, oxygen in the peroxide linkage seems to cause negative photopotentials and oxygen in a carbonyl group yields positive photopotentials. Strong inorganic oxidizing agents produce negative photopotentials. Inorganic reducing agents and salts which are not oxidizing agents yield little or no photopotentials. A polar solvent is necessary for the production of a photopotential. A photopotential-spectrum curve which in general follows the light absorption curve is derived for anthraquinone. High photopotentials can be obtained at wavelengths where light absorption is low if a high intensity light source is used.

INTRODUCTION

IN a previous paper,[1] a method of measuring the photopotentials produced by certain organic substances in solution was described. This method utilizes a platinum point as the irradiated electrode and a sheet of platinum foil as the dark electrode, and both electrodes are immersed in the solution. The photopotential is measured by a vacuum-tube electrometer which prevents any polarizing current from going through the photovoltaic cell.

The primary purpose of the present work is to find what types of structures are responsible for the production of the photopotential.

A. Anomaly of Benzaldehyde

Experimental

The anomalous photovoltaic behavior of benzaldehyde in producing a stable negative photopotential has been noted.[1] This negative photopotential was the first to be obtained from all the organic compounds studied. The result of changing the mole-fraction of the ethyl alcohol and benzaldehyde on the photopotential is summarized in Curve *A* of Fig. 1. Curves *B* and *C* of Fig. 1 indicate the usual photovoltaic behavior of organic substances in solution at a given wavelength of light. In all of the experiments reported in this paper the light used was from a high pressure mercury vapor lamp. The chief wavelength emitted by this lamp is at 3660A and all of the emission is over 3000A. Benzaldehyde was found to yield a positive photopotential of 450 galvanometer units when dissolved in absolute ethyl alcohol at a concentration of 0.1 molar. A series of alcoholic solutions were tested through a wide range of concentrations. It was found that the so-called "pure" benzaldehyde yielded a negative photopotential of approximately −400 galvanometer units which decreased in a positive direction on dilution, resulting in the curve *A* of Fig. 1.

In order to find the source of the negative photopotential the following experiments were performed. Several distillations of a sample of benzaldehyde opened to the air did not affect the negative photopotential. Addition of benzoic acid, benzoin, and benzil had no effect in altering the negative photopotential of benzaldehyde. Also, at intermediate mole-fraction concentrations of benzaldehyde in ethyl alcohol, a transient photoinductive effect was present. The transient effect consisted of the galvanometer indicating a positive range of values during the first moments of irradiation and then assuming a negative value.

A stock sample of benzaldehyde in a sealed cell gradually decreased its negative photopotential from approximately −400 to −14 units in four days, and afterwards very slowly decreased asymptotically towards zero in ten months.

DISCUSSION

The experiments described above indicate that the negative photopotential was due to an intermediate product in the oxidation of benzaldehyde. Gatterman

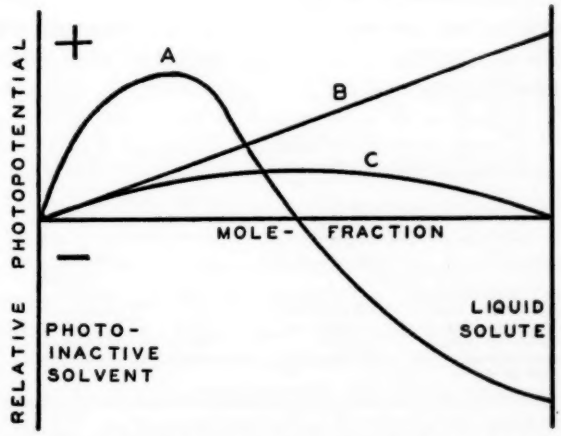

FIG. 1. Effect of mole-fraction on a photoactive liquid in solution.

* This work was sponsored by the ONR under Contract N8onr-76500.
† Present address: Department of Biophysical Instrumentation, Army Medical Center, Washington 12, D. C.
[1] I. Levin and C. E. White, J. Chem. Phys. **18**, 417 (1950).

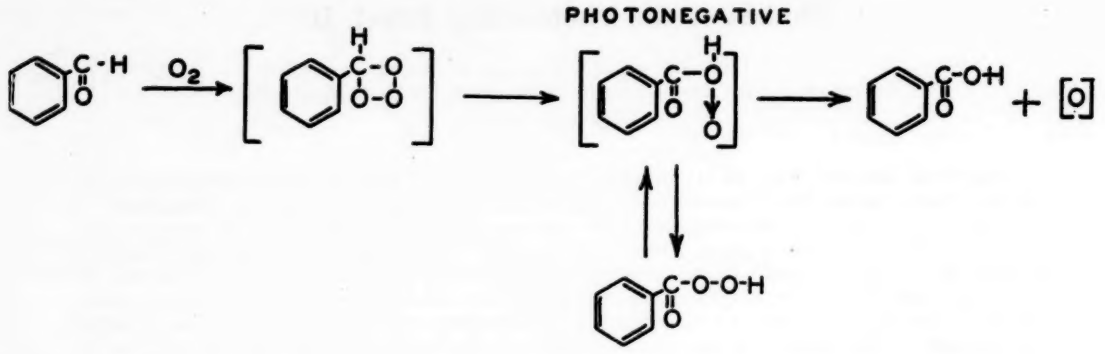

and Wieland[2] propose the following mechanism for the oxidation of benzaldehyde: The nacent oxygen atom may be claimed by another benzaldehyde molecule to form benzoic acid. If it is assumed that the peroxybenzoic acid is responsible for the negative photopotential, all of the above results can be readily explained. Peroxybenzoic acid is continually formed from benzaldehyde in the presence of oxygen; therefore the negative photopotential can always be observed in the presence of air. In the absence of oxygen, the peroxybenzoic acid gradually becomes converted to benzoic acid and the negative photopotential disappears. The transient photoinductive effect noted above was probably due to a competitive action between the photopositive benzaldehyde molecule and the photonegative peroxybenzoic acid.

Cinnamaldehyde behaved similarly to benzaldehyde but to a lesser degree. It appears that the aldehydes which can form peroxides with molecular oxygen behave like benzaldehyde and present a curve of type *A*, while those aldehydes which do not form peroxides, produce a positive photopotential.

The results here indicate that an oxygen atom in a peroxide linkage yields a negative photopotential, while an oxygen atom in carbonyl linkage produces a positive photopotential. The peroxide is apparently electron-saturated and can probably act as an electron source by freeing photoelectrons. The carbonyl oxygen, however, may probably behave as an electron sink which is capable of attracting electrons to it when photoactivated.

TABLE I.

Solvent	Iodine	Solute Bromine	Chlorine
Water	photoinactive	−4.7	photonegative tendency
Ethyl alcohol (95%)	−13	−8.0	reactive
Ethyl alcohol (abs.)	photoinactive	−11	reactive
Chloroform (dry)	46	3.6	photoinactive
Chloroform (wet)	58	250	photoinactive
Carbon tetrachloride (wet or dry)	photoinactive	photoinactive	photoinactive

[2] Gatterman and Wieland, *Laboratory Methods of Organic Chemistry* (Macmillan Company, New York, 1932), p. 203.

B. The Behavior of Inorganic Compounds

Experimental

The theory that the peroxide group was responsible for the production of the negative potential in the oxidized benzaldehyde led to the testing of inorganic compounds such as hydrogen peroxide and various oxidizing and reducing agents. The source of light used in these experiments was a high pressure mercury vapor lamp described above. The temperature was that of the room, approximately 25°C.

The Halogens. Practically all previous photochemical studies on chlorine, bromine and iodine in solution have been made in water. For example,[3] chlorine in water, on strong illumination with the proper wavelengths of light, produces hydrochloric acid and gaseous oxygen;

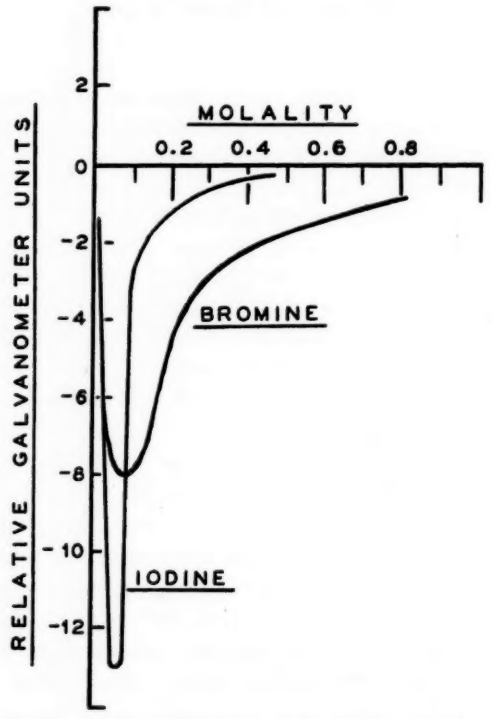

FIG. 2. Photovoltaic behavior of bromine and iodine in ethyl alcohol.

[3] J. W. Mellor, *A Comprehensive Treatise on Inorganic and Theoretical Chemistry*, Vol. II, (London, 1922).

weak irradiation may produce chloric acid. In the present work, water, ethyl alcohol, chloroform, and carbon tetrachloride were used as the solvents for the three halogens except in cases where a chemical reaction occurred immediately on mixing.

Chlorine in water. Chlorine water was prepared by bubbling chlorine gas from a manganese dioxide-hydrochloric acid generator into distilled water until saturation seemed apparent. The gas was passed through a potassium permanganate solution to remove hydrochloric acid which might come over from the reaction vessel. Approximately 0.5 gram of chlorine dissolves in 100 grams of water at room temperature.[4] The saturated solution was not allowed to stand but was placed in the photovoltaic cell immediately for study. The results are shown in Table I.

Bromine in water. A saturated solution of bromine in distilled water was prepared at 25°C. This solution yielded a small photonegative effect of −4.7 galvanometer units as shown in Table I. A curve of the photopotentials of bromine at varying concentrations in water was derived and is shown in Fig. 2.

Iodine in water. Solid resublimed iodine in excess was shaken in distilled water for 24 hours. The result was a light brown solution which did not produce a photopotential. Approximately 0.09 gram of iodine per 100 ml of water is the reported concentration.[3,4]

Chlorine in ethyl alcohol. Chlorine in ethyl alcohol was not studied because of the immediate chemical reactivity between these two substances.

Bromine in ethyl alcohol. When the concentration of bromine is high in ethyl alcohol, a chemical reaction takes place readily. With low concentrations, immediate reactivity will not occur if the solution is kept at room temperature. Fig. 2 indicates the results obtained with bromine in absolute ethyl alcohol and in 95 percent ethyl alcohol.

Iodine in ethyl alcohol. Solutions of iodine in absolute and 95 percent ethyl alcohols were studied and the results are shown in Fig. 2. The importance of the minima of bromine and iodine will be discussed below.

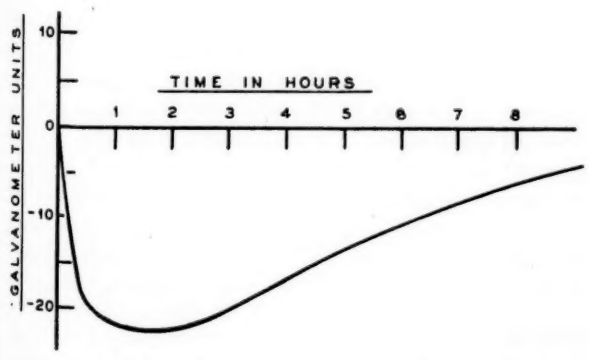

FIG. 3. Variation of photopotential of hydrogen peroxide with time.

[4] Estimated from Lange's *Handbook of Chemistry*, sixth edition (Sandusky, Ohio, 1946).

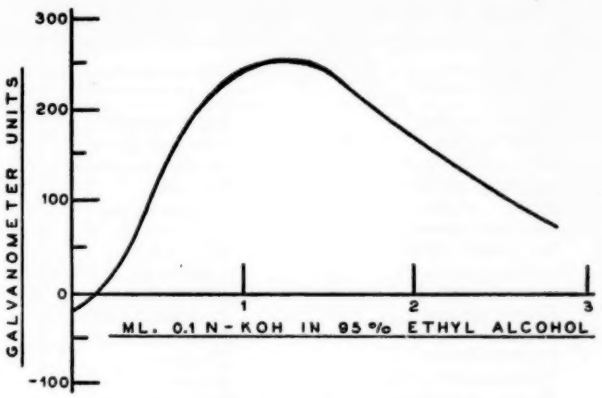

FIG. 4. Photovoltaic behavior of potassium dichromate with potassium hydroxide.

Chlorine in chloroform. This solution was found to be photo-inactive as indicated in Table I.

Bromine in chloroform. This halogen gave interesting results. With commercial chloroform taken from a stock bottle, a positive photopotential of 250 galvanometer units was obtained. Drying the chloroform over calcium chloride and distilling it gave 3.6 galvanometer units as shown in Table I.

Iodine in chloroform. This element yielded a positive photopotential of 58 galvanometer units in wet chloroform and 46 units in dry chloroform as shown in Table I.

The results of the three halogens in carbon tetrachloride are shown in Table I.

Oxidizing agents. Oxidizing agents in general showed photonegative properties. These include potassium permanganate, hydrogen peroxide, potassium peroxysulfate, potassium dichromate, ammonium dichromate, and the halogens in ethyl alcohol as described above. Potassium permanganate yielded a negative photopotential of −9.4 units at a concentration of 0.2 gram in 100 ml of water; more concentrated or more dilute solutions yielded lower photopotentials.

Hydrogen peroxide yielded a negative photopotential whose magnitude varied with time as shown in Fig. 3. This substance illustrates the use of the photovoltaic effect in studying certain reaction mechanisms. 30 percent cp hydrogen peroxide solution from the stock container gave −8 units. 20 percent hydrogen peroxide produced −1 galvanometer unit; this reading gradually increased for about one hour to −20 units and then slowly, in a few hours, decreased towards zero.

The dichromates and chromates showed peculiar properties when dissolved in 95 percent ethyl alcohol. Potassium and ammonium dichromates freshly dissolved in 95 percent ethyl alcohol yielded negative photopotentials but the addition of a small amount of alkali, which converted these compounds to chromates, produced a positive photopotential. This is shown in Fig. 4. This photonegative behavior of the chromate is probably an important factor in the photo-oxidation by chromates of alcohols, gelatine, glue, albumin, gum

TABLE II. Behavior of benzoin in various solvents.

Solvents producing a photopotential	Solvents producing no photopotential
Methyl alcohol	Lauryl alcohol
Ethyl alcohol	Ethylene glycol
n-Propyl alcohol	Diethylene glycol
Isopropyl alcohol	Glycerine
n-Butyl alcohol	Cyclohexane
sec-Butyl alcohol	Cyclohexene
tert-Butyl alcohol	Paraldehyde
Isobutyl alcohol	Carbon tetrachloride
n-Amyl alcohol	Ethyl ether
Benzyl alcohol	Petroleum ether
Acetone	Phenyl ether
Cyclohexanone	Dioxane
Glacial acetic acid	Anisole
Acetic anhydride	Benzene
Chloroform	Toluene
Acetonitrile	Ethyl benzene
Benzonitrile	Xylene (comm'l)
Aniline	Carbon disulfide
Pyridine	Nitrobenzene
Ethyl bromide	
Bromobenzene	
Ethyl acetate	
Ethyl benzoate	

arabic, dextrin, sugars, glycerine, casein, paper, and other organic compounds.

Potassium peroxysulfate freshly saturated in water was photoinactive, but when saturated in 95 percent ethyl alcohol yielded −15 units.

Reducing agents. Very few inorganic reducing compounds produced photopotentials with the light used in these experiments. Sodium nitrite and potassium nitrite yielded small positive photopotentials. The value found for equimolar water solutions was 10 galvanometer units for sodium nitrite and 30 for potassium nitrite. In 95 percent ethyl alcohol both readings were increased by about 25 units.

Salts. Salts other than oxidizing or reducing agents in either alcohol or water solutions proved to be inactive under the conditions of these experiments.

Discussion

As indicated in Fig. 2, iodine shows a sharp photopotential maximum at a concentration of 0.025 molar, while bromine has a broader characteristic and yields a smaller maximum at 0.05 molarity. This may be explained from the fact that iodine has its outer electrons in a freer state and absorbs more light energy than bromine in the same concentration.

The production of a negative photopotential by inorganic oxidizing agents, such as potassium permanganate and potassium dichromate, may indicate that the oxygen atoms coordinate to the metal serve as an electron-source and produce a negative photopotential similar to the oxygen-to-oxygen coordination in peroxides. Lone-pair electrons would be excited in either case. Conversely, covalent oxygen atoms, as in the carbonyl group, may probably tend to act as electron-sinks to yield a positive photopotential.

The behavior of hydrogen peroxide shown in Fig. 3 may be accounted for by postulating a mechanism similar to that given above for benzaldehyde. This phenomenon with hydrogen peroxide may be described as follows: It is probable that the coordinate form is the one which produces the negative photopotential. This is substantiated by the fact that an induction period takes place before the maximum photopotential is reached as indicated in Fig. 3.

C. The Effect of Solvent on the Photopotential

Experimental

A photoactive substance must be in a suitable solvent medium in order to display its photovoltaic properties. The effect of the solvent was studied with benzoin as a photopositive compound at a concentration of either 0.06 molar or saturation, and with iodine as the photonegative compound at an optimum concentration of 0.025 molar. The glass-covered high pressure mercury vapor lamp which emits wavelengths not shorter than 3000A was used as a source of excitation. Table II summarizes the work with benzoin, while Table III shows the results with iodine.

Discussion

From the results tabulated in Tables II and III, the dielectric constant and the density of the solvent appears to have little direct effect on the production of the photopotential. Properties of the solvents, which apparently determine whether a photopotential will be produced are the resistivity of the solvent, and the ability of the solvent to associate with the solute. It appears that the solvent should be polar to allow association with the solute.

The relation of the resistivity of the solvent to the production of a photopotential is illustrated in Table II. Benzoin produced a photopotential when used with the solvents in the first column of Table II. All of the solvents in this column have electrical resistivities ranging from 10^7 to 10^{10} ohms per cc.[5] The compounds listed in the second column have resistivities from 10^8 to 10^{17} ohms per cc and failed to give a photopotential with benzoin. It is obvious that the solvents in which photopotentials were produced not only have a lower re-

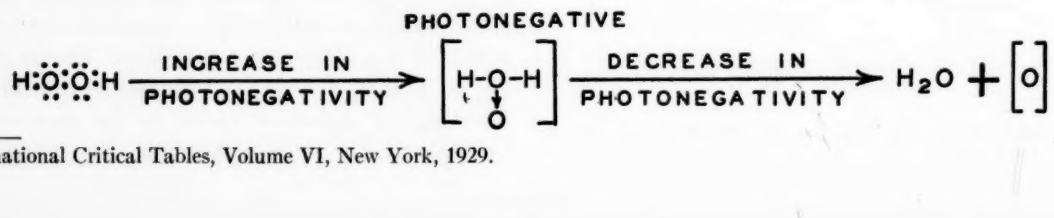

[5] International Critical Tables, Volume VI, New York, 1929.

sistivity but also are types which are capable of association with benzoin. Exceptions to the concepts of association between solute and solvent and resistivity of solvent for the production of the photopotential are the polyhydroxy compounds, the glycols, glycerine, and paraldehyde in the second column of Table II. A greater number of hydroxyl groups on a ring may probably cause a solute to become photoinactive; examples are hydroquinone and pyrogallol. There may be a greater tendency for the polyhydroxy molecules to associate with themselves instead of with another kind, and the production of a photopotential may thus be prevented. The increase in the size of the alcohol molecule, from methyl to lauryl alcohol, that caused a lowering in the photopotential was probably due to the decrease in the tendency of association with benzoin and the mono-hydroxy alcohol. With iodine, as shown in Table III, it was found that certain solvents such as the lower alcohols produce negative photopotentials, whereas other solvents, such as acetone and chloroform produce positive photopotentials. Still other solvents such as benzene, carbon tetrachloride and dioxane produced no photoactivity, probably because of their

TABLE III. Behavior of iodine in various solvents.

Solvent	Photopotential with I_2 as solute
Methyl alcohol	−4.4
Acetone	2.0
Ethyl ether	photoinactive
Pyridene	photoinactive
Nitrobenzene	−2.0
Benzene	photoinactive
Dioxane	photoinactive
Glacial acetic acid	photoinactive
Chloroform (dry)	46
Chloroform (wet)	58
Ethyl alcohol (95 percent)	13
Ethyl alcohol (absolute)	photoinactive
Carbon tetrachloride (wet or dry)	photoinactive

being highly resistive. The concept of association between solute and solvent being necessary to produce a photopotential with a low resistive solvent seems to apply generally here too. The photopotentials with iodine in the various solvents of Table III are much smaller than with benzoin.

The three curves of Fig. 1 were partly discussed in Section A above. Curve *A* of Fig. 1 was attributed to the presence of a photonegative impurity in a photopositive substance. Curve *B* is probably the normal behavior of a photopositive compound with variations in concentration. The converse of these curves might also result with photoactive solutes of opposite polarities. Curve *C* of Fig. 1 is a peculiar type which may be due to a light absorption effect with concentration changes or the formation of a photoactive complex between solute and solvent.

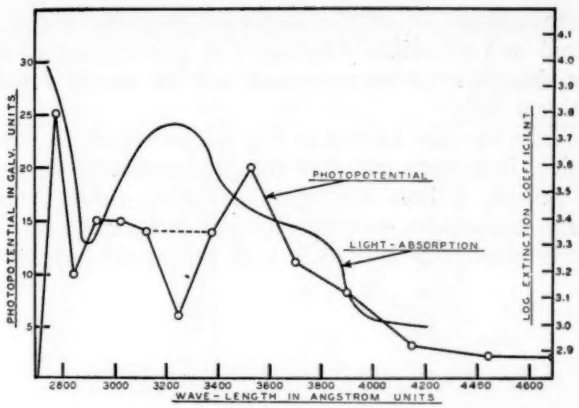

FIG. 5. Comparison of light absorption and photopotential for anthraquinone—0.0024 molar in absolute ethyl alcohol.

D. The Effect of Light Absorption on the Photopotential

In light absorption, certain groups of the molecule produce peculiar shapes in the light absorption curve. Analogous effects may probably occur when a curve is derived of photopotential *vs* wavelength. An attempt was therefore made to derive the photopotential wavelength characteristic of compounds which absorb light in the ultraviolet region. Organic compounds which absorb visible light are generally more complex in structure than those which absorb in the ultraviolet region. Therefore, simpler compounds such an anthraquinone, benzaldehyde, benzil, benzoin, and benzophenone which produce a photopotential and absorb in the range from 2200A to 4000A were chosen for study. A medium-sized quartz Hilger-Cornu spectrograph was set up in conjunction with an iron-tungsten arc, for the production of a fairly continuous range of wavelengths of ultraviolet light. An attempt was made to place the probe point at positions of high intensity throughout the spectrum. The erratic results indicated that this objective was not always achieved. The best correlation of photopotential with light absorption was obtained using anthraquinone as is shown in Fig. 5. A point-to-point curve was drawn for the photopotentials since the light source was not continuous and not of uniform intensity. The light absorption curve was obtained from the literature.[6]

It is believed that the low readings obtained at the portion of the curve, indicated by the dotted line, were the result of the low intensity of the arc. All of the compounds used gave low results in this range and intensity measurements of the spectrum showed many low points in this area. The greater intensity of the arc at 3500A and longer than at 2800A should be taken into account in comparing photopotentials at these points. Experiments conducted by Mr. Wiebush in this laboratory with mercury vapor lamps at 2537A and 3660A, with equal intensities, indicate that the photopotential of

[6] L. Marchlewski and A. Moroz, Bull. soc. chim. France **35**, 474 (1924).

anthraquinone at 2537A should be about 40 as compared to 1 at 3660A. This result is quite in line with the absorption of the compound and the energy of the incident light.

While the data plotted in Fig. 5 is admittedly qualitative, it is apparent that the photopotential curve, in general, follows the light absorption curve. This curve and others derived with the compounds listed above show that relatively high photopotentials can be obtained at points of low absorption if light of sufficiently high intensity is used. It is also evident from the curves that even though the arc gave very intense lines above 3800A, and the compounds were still absorbing in that range, only very low photopotentials were produced. For example, with approximately equal intensities and equal absorption, benzil gave a photopotential of 160 units at 3700A and only 50 units at 3900A.

THE JOURNAL OF CHEMICAL PHYSICS VOLUME 19, NUMBER 9 SEPTEMBER, 1951

Force Constants and Calculated Thermodynamic Properties for SiF_4

FRED L. VOELZ, ARNOLD G. MEISTER, AND FORREST F. CLEVELAND
Spectroscopy Laboratory, Department of Physics, Illinois Institute of Technology, Chicago, Illinois
(Received June 1, 1951)

Using observed fundamental frequencies and the Wilson *FG* matrix method, sets of force constants for SiF_4 have been determined using the most general second degree potential energy function. While no unique set of force constants can be given, limits are set for the force constants. Also the calculations indicate that if the Si—F bond interaction constant is ignored, too high a value for the Si—F bond stretching force constant results. Finally, the heat content, free energy, entropy, and heat capacity for the ideal gaseous state at 1 atmos pressure were calculated for 11 temperatures ranging from 100–1000°K, using a rigid rotator, harmonic oscillator approximation.

RECENTLY Jones, Kirby-Smith, Woltz, and Nielsen[1] reinvestigated the Raman and infrared spectra of SiF_4 and obtained very accurate values for the fundamental frequencies. Since they did not calculate force constants for this molecule and because no modified valence force treatment could be found in the literature, the present investigation was carried out. Also, no previous calculation of thermodynamic functions could be located so these were calculated because of the better values of the fundamental frequencies which are now available.

FORCE CONSTANTS

Force constants were determined previously by several investigators[2–4] using central force and valence force potential energy functions. However, in no case

TABLE I. Force constants of the SiF_4 molecule (millidynes/A).

f_{dd}/f_d	Set	f_d	f_{dd}	$f_{d\alpha}-f_{d\alpha'}$	$f_\alpha-f_{\alpha\alpha}$	$f_\alpha-f_{\alpha\alpha'}$	f_α	$f_{\alpha\alpha}$	$f_{\alpha\alpha'}$
0.00	*A*	7.1628	0	2.6407	1.2902	2.3124	—	—	—
	B	7.1628	0	0.61906	0.37025	0.47250	0.47250	0.10225	0
0.05	*A*	6.2285	0.31143	2.5649	1.4669	2.6658	—	—	—
	B	6.2285	0.31143	0.12901	0.35798	0.44801	0.44801	0.09003	0
0.10	*A*	5.5098	0.55098	2.3901	1.5499	2.8317	—	—	—
	B	5.5098	0.55098	−0.13330	0.40154	0.53512	0.53512	0.13358	0
0.15	*A*	4.9398	0.74097	2.1895	1.5874	2.9068	—	—	—
	B	4.9398	0.74097	−0.27870	0.35012	0.43228	0.43228	0.08216	0
0.20	*A*	4.4768	0.89536	1.9842	1.5987	2.9294	—	—	—
	B	4.4768	0.89536	−0.35424	0.53452	0.80110	0.80110	0.26658	0
0.25	*A*	4.0930	1.0232	1.7790	1.5918	2.9147	—	—	—
	B	4.0930	1.0232	−0.38200	0.60794	0.94792	0.94792	0.33998	0
0.50	*A*	2.8651	1.4326	0.67798	1.3686	2.4692	—	—	—
	B	2.8651	1.4326	−0.026035	1.0482	1.8285	1.8285	0.7833	0

[1] Jones, Kirby-Smith, Woltz, and Nielsen, J. Chem. Phys. **19**, 242 (1951).
[2] A. Eucken and A. Bertram, Z. physik. Chem. **B31**, 361 (1936).
[3] R. Ananthakrishnan, Proc. Indian Acad. Sci. **5A**, 447 (1937).
[4] G. Herzberg, *Infrared and Raman Spectra* (D. Van Nostrand Company, Inc., New York, 1945), pp. 167, 182.

TABLE II. Fundamental frequencies of the SiF_4 molecule.

Designation	Wave number (cm^{-1})	Degeneracy
ν_1	800*	1
ν_2	268*	2
ν_3	1031	3
ν_4	391	3

* Liquid.

was the most general second-degree potential energy function used, as in the present investigation. Unfortunately, it is not possible to give values for all the force constants since only four fundamental frequencies are available for determining the seven force constants required for the potential energy function.

The force constants used were the following: f_d = Si−F bond stretching; f_{dd} = interaction between two Si−F bonds; f_α = F−Si−F angle bending; $f_{\alpha\alpha}$ = interaction between two F−Si−F angles having a side in common; $f_{\alpha\alpha'}$ = interaction between two F−Si−F angles having no sides in common; $f_{d\alpha}$ = interaction between Si−F bond and F−Si−F angle having the SiF bond as one side; and $f_{d\alpha'}$ = interaction between Si−F bond and F−Si−F angle not having this bond as a side.

In order to calculate more than four force constants f_{dd} was assumed to be a reasonable fraction (0 to 0.50) of f_d. The force constants so determined are given in Table I and were obtained using the Wilson *FG* matrix method.[5] Tetrahedral angles were assumed and the following constants were used:

for the reciprocals of the masses of the atoms

$$\mu_{Si}=2.1464\times10^{22}\ g^{-1};$$
$$\mu_F=3.1699\times10^{22}\ g^{-1};$$

and for the equilibrium bond distance[6–8]

$$Si-F=1.54A.$$

All the sets of force constants given in Table I will reproduce the fundamental frequencies to the nearest cm^{-1}.

One notices from Table I that the value of f_d depends considerably on the value of f_{dd} used so that when this constant is arbitrarily made zero, too high a value for f_d results. Also two sets of constants (*A* and *B*) are given for $f_{d\alpha}-f_{d\alpha'}$, $f_\alpha-f_{\alpha\alpha}$, and $f_\alpha-f_{\alpha\alpha'}$ since a quadratic equation is obtained in solving for these constants. One sees that the *A* sets have much larger bending constants than the *B* sets and for this reason it appears that the *B* sets should be preferred. If one assumes $f_{\alpha\alpha'}=0$, since $f_{\alpha\alpha'}$ should be smaller than $f_{\alpha\alpha}$, then it is possible to give values for f_α and $f_{\alpha\alpha}$ as has been done in Table I. It is not possible to separate $f_{d\alpha}$ and $f_{d\alpha'}$ in a similar manner since $f_{d\alpha'}$ should be larger than $f_{\alpha\alpha'}$.

It seems difficult to choose the best set of force constants from Table I, but it is possible to set limits for some of the force constants. Since the set with $f_{dd}/f_d=0.25$ gives a large value for f_{dd}, it seems that all sets having f_{dd}/f_d ratios lower than this should be used in setting the limits. So from Table I one has the following results: $f_d=7.1628-4.4768$; $f_{dd}=0-0.89536$; $f_{d\alpha}-f_{d\alpha'}=0.61906-(-0.35424)$; $f_\alpha-f_{\alpha\alpha}=0.37025-0.53452$; and $f_\alpha-f_{\alpha\alpha'}=0.47250-0.80110$ millidyne/A.

It will be noted that the force constants have been given to 5 significant figures which is greater than the number occurring in the frequencies used to determine the force constants. This greater number of significant figures was retained to insure that all the sets of force constants would reproduce the fundamental frequencies to the nearest cm^{-1}; the force constants cannot be considered as being reliable to five significant figures.

TABLE III. Heat content, free energy, entropy, and heat capacity of SiF_4 for the ideal gaseous state at 1 atmos pressure (cal $mole^{-1}$ deg^{-1}).

T(°K)	$(H^0-H_0^0)/T$	$-(F^0-H_0^0)/T$	S^0	C_p^0
100	8.40	44.83	53.23	9.94
200	10.38	51.24	61.62	14.50
298.16	12.27	55.50	67.77	17.56
300	12.31	55.82	68.13	17.61
400	13.92	59.59	73.51	19.84
500	15.28	62.84	78.12	21.40
600	16.39	65.73	82.12	22.47
700	17.32	68.33	85.64	23.22
800	18.09	70.71	88.80	23.75
900	18.74	72.86	91.61	24.14
1000	19.30	74.87	94.17	24.44

THERMODYNAMIC PROPERTIES

The heat content, free energy, entropy, and heat capacity of SiF_4 were calculated for temperatures from 100° to 1000°K to a rigid rotator, harmonic oscillator approximation. The calculated values are for the ideal gaseous state at 1 atmos pressure. Using a Si−F bond distance of 1.54A and tetrahedral angles, one finds for the moments of inertia $I_{xx}=I_{yy}=I_{zz}=147$awu.A^2. Birge's 1941 values[9] of the physical constants and a symmetry number of 12 were used throughout the calculations. The values of the fundamental frequencies and their degeneracies are given in Table II while the calculated thermodynamic properties are given in Table III. Since two of the four values for the fundamental frequencies are for the liquid state, the values of the thermodynamic properties in Table III may be slightly larger than those for the ideal gaseous state.

[5] E. B. Wilson, Jr., J. Chem. Phys. **7**, 1047 (1939); **9**, 76 (1941).
[6] L. O. Brockway and F. T. Wall, J. Am. Chem. Soc. **56**, 2373 (1934).
[7] L. Pauling and L. O. Brockway, J. Am. Chem. Soc. **57**, 2684 (1935).
[8] H. Braune and P. Pinnow, Z. physik. Chem. **B35**, 239 (1937).
[9] R. T. Birge, Revs. Modern Phys. **13**, 233 (1941).

The Asymmetric Rotor. IX. The Heavy Water Bands at 2787 cm^{-1} and 5373 cm^{-1}*

K. KEITH INNES AND PAUL C. CROSS
Department of Chemistry and Chemical Engineering, University of Washington, Seattle, Washington

AND

PAUL A. GIGUÈRE†
California Institute of Technology, Pasadena, California

(Received April 30, 1951)

The combination band (110) of the two stretching fundamentals of D_2O is reported and analyzed to yield $\nu_0=5373.2$ cm^{-1} and the excited state moments of inertia 1.910, 3.931, and 5.929×10^{-40} g cm^2. The same method of analysis applied to the unsymmetrical fundamental band (100) envelope gives $\nu_0=2787.5$ cm^{-1} and the excited state moments 1.881, 3.876, and 5.843×10^{-40} g cm^2.

INTRODUCTION

A SUMMARY of the work to date on the analysis of vibration and rotation spectra of heavy water vapor is presented in Table I.

Fuson, Randall, and Dennison[1] obtained an expression for the effective reciprocal moments of inertia of heavy water as functions of the vibrational quantum numbers by computing the isotope effect on the constants in the analogous expression for water. Using the inertial constants for the ground state as given by this expression and applying a crude classical correction for centrifugal distortion they obtained calculated "key" energies as an aid to the building of an "experimental" term scheme from the pure rotation spectrum. The difference between the calculated and constructed term values are given in the column $W-W_k$ of their Table IV. They did not, apparently, investigate the possibility of minimizing these differences with the objective of obtaining "best values" of the inertial constants. For instance, an inspection of these differences for the low τ-levels indicates that they could be consistently reduced by an increase of 0.01 cm^{-1} in the inertial constant C. In fact, such an increase was found necessary by King[2] in his band envelope analysis of the bending fundamental by punched-card machine methods.

DN[3] obtained two infrared active fundamentals at high resolution and analyzed both by deducing the excited state term values in the manner of Fuson, Randall, and Dennison, apparently using the experimental term values for the ground state given in reference 1. They then chose effective moments which best represented their excited state term schemes at low J values, remarking that the moments given by King yielded a poorer fit for the (001) band.

This paper presents the results of the first analysis of a combination band of heavy water as well as an investigation of the data for the unsymmetrical stretching fundamental[3] by the band envelope method.[4]

EXPERIMENTAL

Frequencies of the absorption peaks observed in the region 5250 to 5490 cm^{-1} are recorded in Table II.

TABLE I. Vibration-rotation parameters of heavy water.

Analysis data	a a	b c	b c	d d	d d	e d	e e
$(n_3n_1n_2)$	(000)	(000)	(001)	(001)	(100)	(100)	(110)
ν_0 obs			1179	1178.3	2787.2	2787.5	5373.2
ν_0 calc			1178.8	1178.8	2787.6	2787.6	5372.8
A_{obs}	15.38	15.38	16.50	16.60	14.88	14.88	14.65
B_{obs}	7.25	7.25	7.33	7.35	7.24	7.22	7.12
C_{obs}	4.83	4.84	4.79	4.84	4.84	4.79	4.72
A_{calc}	15.385	15.385	16.50	16.50	14.88	14.88	14.59
B_{calc}	7.255	7.255	7.33	7.33	7.21	7.21	7.12
C_{calc}	4.830	4.830	4.77	4.77	4.77	4.77	4.71
Δ_{obs}	0.115	0.105	0.329	0.288	0.035	0.086	0.088
Δ_{calc}	0.105	0.105	0.329	0.329	0.088	0.088	0.088

[a] See reference 1.
[b] See reference 2.
[c] E. F. Barker and W. W. Sleator, J. Chem. Phys. **3**, 660 (1935).
[d] See reference 3.
[e] This work.

* The work herein reported was supported in part by the ONR under Contract N8onr 52010.
† Now at the Department of Chemistry, Laval University, Quebec, Canada.
[1] Fuson, Randall, and Dennison, Phys. Rev. **56**, 982 (1939).
[2] G. W. King, J. Chem. Phys. **15**, 85 (1947).
[3] F. P. Dickey and H. H. Nielsen, Phys. Rev. **73**, 1164 (1948). Hereafter referred to as DN.
[4] Allen, Cross, and Wilson, J. Chem. Phys. **18**, 691 (1950).

The heavy water used was 99.5 percent pure; the absorption cell was one meter long and the pressure, about 200 mm. The spectrum was studied with an automatic recording vacuum spectrometer[5] using the first order of an échelette grating with 7500 lines to the inch. Overlapping orders were eliminated successfully by means of a special plastic filter[6] kindly supplied by the Polaroid Corporation. The photosensitive element was a lead sulfide cell operating at room temperature. The resolution was of the order of 2 cm^{-1} with a slit width of 0.05 cm corresponding to 0.9 cm^{-1} in the region covered. Calibration for wavelength was based on the infrared lines of argon. Scanning was done at the rate of 15A per minute.

The present band coincides almost exactly with the fairly intense $\nu_2+\nu_3$ band of ordinary water, which may explain why it has not been reported before. For the same reason it was important to avoid all absorption due to atmospheric moisture.

ANALYSIS

Absorption in the region 5250 to 5500 cm^{-1} was evidently due to an A-type band which was accordingly given the combination assignment (110). The band center calculable from potential constants[7] for the molecule was 5372.8 cm^{-1}.

The Fuson, Randall, and Dennison expression yielded a first approximation to the moments of the upper state as listed in the last column of Table I. Using these, the observed ground state constants of King and published tables,[8] the energies of permitted transitions were calculated. The trial spectrum was completed with the calculation of relative line intensities.[9] To be consistent with the analysis of King, a centrifugal distortion correction was not employed.

Preparation of a table of derivatives of upper state energies with respect to the inertial constants facilitated adjustment of the computed spectrum to a best fit of the data. That best fit is presented under the data in Fig. 1 in which all transitions (about 150) arising from levels up through $J=12$ and having intensity greater than 0.5 (on an arbitrary scale) are included. The excited state constants giving rise to that spectrum are also listed in the last column of Table I.

King assumed that rigid rotor energies could be used

TABLE II. Observed absorption peaks of the combination band $\nu_1+\nu_3$ of heavy water (ν_{vac}, cm^{-1}).*

5253.6	5374.9
5259.4	5376.1
5261.1	5380.2
5263.1	5383.1
5265.1	5385.2
5271.2	5389.7
5274.0	5393.5
5276.6	5396.2
5278.0	5398.8
5280.2	5403.9
5282.7	5406.3
5284.7	5407.9
5288.7	5411.0
5290.9	5413.3
5294.3	5415.3
5296.9	5416.8
5299.3	5422.6
5301.3	5426.6
5303.5	5430.9
5305.9	5433.5
5309.3	5437.2
5313.9	5438.0
5317.2	5440.9
5319.2	5444.2
5321.7	5445.6
5327.2	5449.0
5328.4	5453.2
5332.4	5456.2
5333.8	5458.8
5338.0	5460.2
5339.6	5461.9
5344.4	5466.8
5346.2	5468.5
5348.9	5471.9
5351.4	5474.3
5354.5	5477.7
5357.5	5480.5
5361.0	5481.9
5363.7	5485.8
5365.9	5487.3
5369.7	5491.8
5371.3	5495.5

* Computed results are not included here. Positions and intensities of rotational transitions may be calculated by using the constants of the last column of Table I with tables in references 8 and 9.

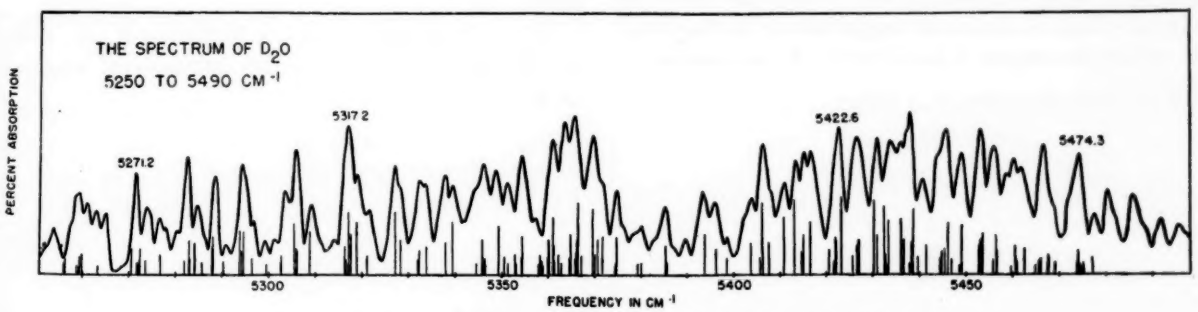

FIG. 1. Calculated and observed combination band $\nu_1+\nu_3$ at 5373.2 cm^{-1}.

[5] Badger, Zumwalt, and Giguère, Rev. Sci. Instr. **19**, 861 (1948).
[6] Blout, Amon, Shepherd, Thomas, West, and Land, J. Opt. Soc. Am. **36**, 460 (1946).
[7] B. T. Darling and D. M. Dennison, Phys. Rev. **57**, 128 (1940).
[8] King, Hainer, and Cross, J. Chem. Phys. **11**, 27 (1943).
[9] Cross, Hainer, and King, J. Chem. Phys. **12**, 210 (1944).

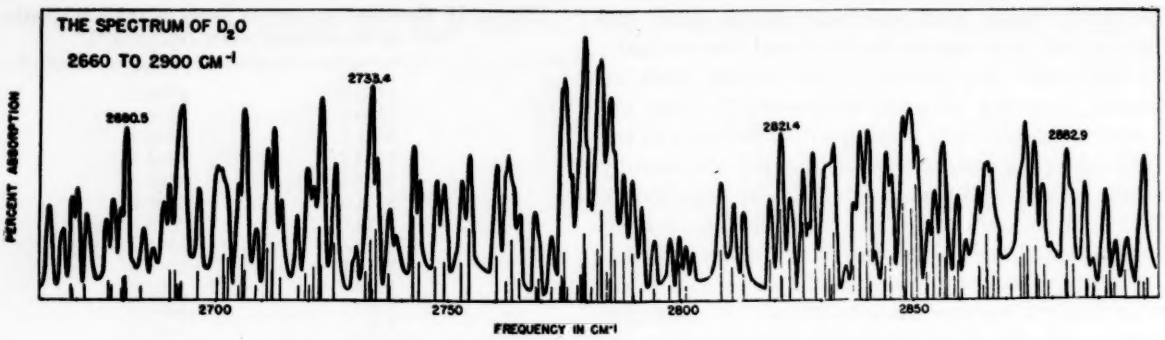

FIG. 2. Calculated and observed perpendicular stretching fundamental at 2787.5 cm^{-1}. (Experimental curve according to Dickey and Nielsen (see reference 3)).

in such analyses without serious error because important lines arise from levels of low τ-value for which distortion is small and, in any case, discrepancies tend to cancel in the term differences.

The effect on *this* spectrum of the classical centrifugal correction of Cross[10] was observed by correcting each energy level of both states and recalculating the spectrum. Only one-fourth of the lines were shifted by as much as one-fifth of a wave number and only a fourth of those by more than two-fifths of a wave number. It should be pointed out that King analyzed a parallel-type band for which allowed transitions are between levels of more widely separated τ-values than for the band considered above. This circumstance will decrease the effect of canceling of the corrections which, themselves, amount to as much as eight wave numbers for some levels important in the spectrum.

The puzzling lack of agreement of the two methods used for the analysis of the 1179 cm^{-1} band led to a preliminary survey of the data given by DN. Energies for ground and excited states were calculated using, in turn, constants given by DN and King. Resulting transitions were compared with experimental positions of the lines as identified by DN. Though the analysis was not pursued it appeared that the constants given by King led to a better fit of the data and that, especially for $J=4$, 5, 6, a number of peaks had been associated with the wrong transitions in the later analysis.[3] This conclusion is supported by the fact that one would not expect $I_C(=h/8\pi^2cC)$ to be smaller for the excited than for the ground state. Indeed, one may observe that for all water bands analyzed the reverse is the case.[7] The magnitude of the disagreement of calculated and observed Δ's also seems unreasonably large. This shows up in the discrepancies between observed and predicted values of the inertial constants.

For these reasons it was thought worthwhile to reinvestigate the DN data for ν_3, extending the analysis, as for the (110) band, through $J=12$ for all lines of appreciable intensity. The fit illustrated in Fig. 2 was obtained with the constants listed in column seven of Table I. Note that the constants employed for this best fit preserve agreement between the calculated and observed values of Δ.

The assignment of transitions to observed peaks by DN checked well with ours within 60 cm^{-1} of either side of the band center. However, for transitions involving $J=5$ or greater, the agreement is sometimes poor. For example, the transition $5_{-3}-6_{-4}$ contributed to a peak at 2710.9 in our analysis but was assigned to 2705.9 cm^{-1} by DN.

The band envelope method depends only on the adjustment of seven parameters: the band center and the three inertial constants of each of the two states. Difficulties of building term schemes from such spectra are illustrated in the two figures from which it is seen that, in general, each peak is an envelope of several lines.

The authors are grateful to Professor R. M. Badger for the use of his spectrograph and general laboratory facilities.

[10] P. C. Cross, Phys. Rev. 47, 7 (1935).

Microwave Spectroscopic Investigation of the Kinetics of the Heterogeneous Ammonia-Deuterium Exchange*

J. WEBER† AND KEITH J. LAIDLER
U. S. Naval Ordnance Laboratory, Silver Spring, Maryland
and
Departments of Physics and Chemistry, The Catholic University of America, Washington, D. C.
(Received April 2, 1951)

A method is described for analyzing a mixture of gases using microwave spectroscopy. Relatively simple microwave measurements are employed on single resolved collision broadened spectral lines. For binary mixtures, only the peak absorption coefficients need to be measured if the microwave collision diameters are known. Mixtures of isotopically substituted molecules can also be analyzed because the microwave absorption lines of the isotopic species are easily resolved.

The technique is applied to determining the mole fraction of NH_3 in mixtures of deuterated ammonias, and to a study of the kinetics of the NH_3-D_2 isotopic exchange reaction on a singly promoted iron catalyst. It is found that rates of desorption of molecules from surfaces are markedly increased on adsorption of other molecules, a fact that can be explained only in terms of strong interactions between adsorbed molecules. The rate of the exchange reaction is proportional to the square root of the deuterium pressure. With increasing ammonia pressure the rate passes through a maximum, showing that the mechanism involves reaction between adsorbed ammonia and adsorbed deuterium atoms. The activation energy diminishes significantly with increasing ammonia pressure, providing additional evidence for the existence of strong interactions between adsorbed molecules.

INTRODUCTION

THE theory of the collision broadening of spectral lines provides a means of determining the number of molecules of an absorbing substance in a mixture of gases. Spectral lines in both the optical and microwave regions have an observable breadth which is due to "natural" breadth, the Doppler effect, broadening by collisions with other gas molecules, and broadening by collisions with the walls of the vessel. In the microwave region, at pressures above forty microns, gas-collision broadening accounts for at least ninety-nine percent of the line breadth, and under these conditions the absorption coefficient for a collision-broadened spectral line has been shown[1] to be given by

$$\alpha=\frac{8\pi^2\nu^2N_{jk}|\mu_{jk}|^2}{3ckT}\times\left[\frac{\Delta\nu}{(\Delta\nu)^2+(\nu_0-\nu)^2}+\frac{\Delta\nu}{(\Delta\nu)^2+(\nu_0+\nu)^2}\right]. \quad (1)$$

Here ν is the frequency, N_{jk} the number of molecules per unit volume in the state characterized by the quantum numbers j and k, μ_{jk} is the matrix element corresponding to the dipole moment, c is the velocity of light, T is the absolute temperature, k is Boltzmann's constant, ν_0 is the frequency of maximum absorption, and $\Delta\nu$ is the half-width of the spectral line at half-intensity.

The area underneath the spectral line is, for a mixture of gases, given by

$$\text{Area}=\int_0^\infty \alpha d\nu=[8\pi^3\nu^2|\mu_{jk}|^2/3ckT](N_{jk}). \quad (2)$$

This area is therefore a measure of N_{jk}. Expressions (1) and (2) also hold for the pure gas. It follows that the ratio of areas for the pure absorbing gas and the mixture enables the mole fraction of the absorbing gas in the mixture to be determined. Equivalent to measuring the area is simultaneous measurement of the peak absorption, line breadth, and pressure. Other simplifications are possible if one has a binary mixture, and these are discussed in subsequent sections.

In the present work the method has been applied to a study of the kinetics of the heterogeneous exchange reaction between ammonia and deuterium, the technique being used to determine the amount of NH_3 in a mixture of NH_3, NH_2D, NHD_2, and ND_3. The microwave method is particularly valuable for the analysis of mixtures of isotopically substituted molecules, the absorption frequencies of the isotopic species having a substantial separation. We have found the technique to be a very powerful one for kinetic studies, to which it has apparently not previously been applied.

Theory of the Microwave Method for Analysis of Binary Mixtures

If α_0 is the maximum value of absorption coefficient, Eq. (1) gives

$$\alpha_0=8\pi^2\nu_0^2N_{jk}|\mu_{jk}|^2/3ckT\Delta\nu. \quad (3)$$

Since N_{jk} is proportional to $\alpha_0\Delta\nu$, it follows that if α_0 and $\Delta\nu$ are measured, together with the pressures, the mole fraction of the absorber gas is determined uniquely. This method was not the one used, however, since line breadths cannot easily be measured with an accuracy greater than several percent. The method actually em-

* Abstracted from a dissertation submitted by J. Weber in partial fulfillment of the requirements for the Degree of Doctor of Philosophy in Physics at the Catholic University of America.

† Present address: Department of Electrical Engineering, University of Maryland, College Park, Maryland.

[1] J. H. Van Vleck and V. Weisskopf, Revs. Modern Phys. **17**, 227 (1945).

ployed depends upon the fact that the line breadth is proportional to the molecular collision frequency, which can be calculated if the molecular collision diameters are known.

For such a mixture of an absorbing and a nonabsorbing gas, it follows from Eq. (3) that

$$N_1/N_0=\alpha_1(\Delta\nu)_1/\alpha_0(\Delta\nu)_0. \quad (4)$$

Here N_1 is the number of absorbing molecules per unit volume of the mixture, α_1 is the peak absorption coefficient of the mixture, and $(\Delta\nu)_1$ is the line breadth for the mixture; N_0, α_0, and $(\Delta\nu)_0$ are the corresponding quantities for the pure gas. The line breadths $(\Delta\nu)_1$ and $(\Delta\nu)_0$ are proportional to the molecular collision frequencies. For a mixture of any two gases, denoted by subscripts i and j, the collision frequency f_{ij} for a collision of the ith species with the jth species is given[2] by

$$f_{ij}=[(8RT/\pi M_i)(1+M_i/M_j)]^{\frac{1}{2}}N_jS_{ij}, \quad (5)$$

where S_{ij} is the collision cross section for species i with species j, M_i and M_j are the molecular weights, R is the gas constant, and N_j is the number of molecules of type j per unit volume. A similar expression holds for f_{ii}, i.e., for collisions of species i with other molecules of its own kind, in which case $i=j$.

For a mixture the collision frequency for the ith species is given by

$$f=f_{ii}+f_{ij}. \quad (6)$$

Equations (4), (5), and (6) give rise to

$$\frac{N_1}{N_1+N_2}=\frac{(\alpha_1S_{12}/\alpha_0S_{11})(1+M_1/M_2)^{\frac{1}{2}}}{\sqrt{2}(1-\alpha_1/\alpha_0)+(\alpha_1S_{12}/\alpha_0S_{11})(1+M_1/M_2)^{\frac{1}{2}}}. \quad (7)$$

The procedure is then to measure α_0 initially for the pure absorbing gas and S_{12}/S_{11} for a mixture of the absorbing gas and the other gas. It is then necessary only to measure α_1 subsequently in order to obtain the mole fraction $N_1/(N_1+N_2)$ of the absorbing gas in any mixture of the two gases.

In the above it is assumed that the work is being done in the medium pressure region where the peak absorption coefficient of the pure absorbing gas is independent of the pressure, and the Van Vleck-Weisskopf formula applies; this was always so in the work to be described. Otherwise, the variation of peak absorption coefficient with pressure would have to be taken into account.

The method of determining the ratio S_{12}/S_{11} of collision cross sections is as follows. Equations (5) and (6) give rise to

$$\frac{S_{12}}{S_{11}}=\frac{(\Delta\nu)_1P_0}{(\Delta\nu)_0P_1}\left(1-\frac{\alpha_1}{\alpha_0}\right)\times\left(\frac{2M_2}{M_1+M_2}\right)^{\frac{1}{2}}\left(1-\frac{\alpha_1(\Delta\nu)_1P_0}{\alpha_0(\Delta\nu)_0P_1}\right)^{-1}, \quad (8)$$

where P_0 is the partial pressure of the pure absorbing gas and P_1 is the total pressure. S_{12}/S_{11} and the composition of the gas can therefore be determined by measuring α_1 and $(\Delta\nu)_1$ for the mixture, and then α_0 and $(\Delta\nu)_0$ for the pure gas. This was done for a number of mixtures of the ammonias taken from the reaction vessel at the ends of runs, the hydrogen being first removed by separation in a cold trap. Similar measurements were then made on pure NH_3, and the results enabled actual cross sections as well as ratios to be obtained.

In this work the microwave method was used to determine the mole fraction of NH_3 in a mixture of deuterated ammonias. The assumption is made that the collision diameters of all of the deuterated ammonias are sufficiently alike that the mixture can be treated as a mixture of only two gases, the absorbing gas (NH_3) and the nonabsorbing gas (NH_2D, NHD_2, and ND_3). This introduces only a negligible error, since the kinetic data apply to initial rates, under which circumstances the NH_2D predominates.

Surface Exchange Reaction between Ammonia and Deuterium

Bimolecular surface reactions may proceed by either of two main types of mechanism. In the first, which corresponds to the formulations of Langmuir[3] and Hinshelwood,[4] both molecules must be adsorbed side by side in order for reaction to occur; in the second, proposed by Rideal,[5] reaction takes place between an absorbed molecule and a molecule in the gas phase. It appears that the majority of reactions occur by Langmuir-Hinshelwood mechanisms,[6] and indeed there appears to be no unequivocal evidence for a Rideal mechanism in any single case. For a time it appeared likely that the para-ortho hydrogen conversions were of this nature,[7] but recent work by Rideal and Trapnell[8] has thrown considerable doubt upon this, and has suggested that the original mechanism of Bonhoeffer,

[2] J. H. Kennard, *Kinetic Theory of Gases* (McGraw-Hill Book Company, Inc., New York, 1938), p. 112; see also B. Bleaney and R. P. Penrose, Proc. Phys. Soc. (London) **60**, 540 (1948).

[3] I. Langmuir, Trans. Faraday Soc. **17**, 621 (1921).

[4] C. N. Hinshelwood, *Kinetics of Chemical Change* (Oxford University Press, New York, 1926), p. 145; *ibid.* (1940), p. 187.

[5] E. K. Rideal, Proc. Cambridge Phil. Soc. **35**, 130 (1939); Chemistry and Industry **62**, 335 (1943).

[6] K. J. Laidler, *Chemical Kinetics* (McGraw-Hill Book Company, Inc., New York, 1950), Chapter 6.

[7] D. D. Eley and E. K. Rideal, Proc. Roy. Soc. (London) **A178**, 429 (1941); D. D. Eley, Trans. Faraday Soc. **44**, 216 (1948).

[8] E. K. Rideal and B. M. W. Trapnell, Faraday Soc. Discussions **8**, 114 (1950).

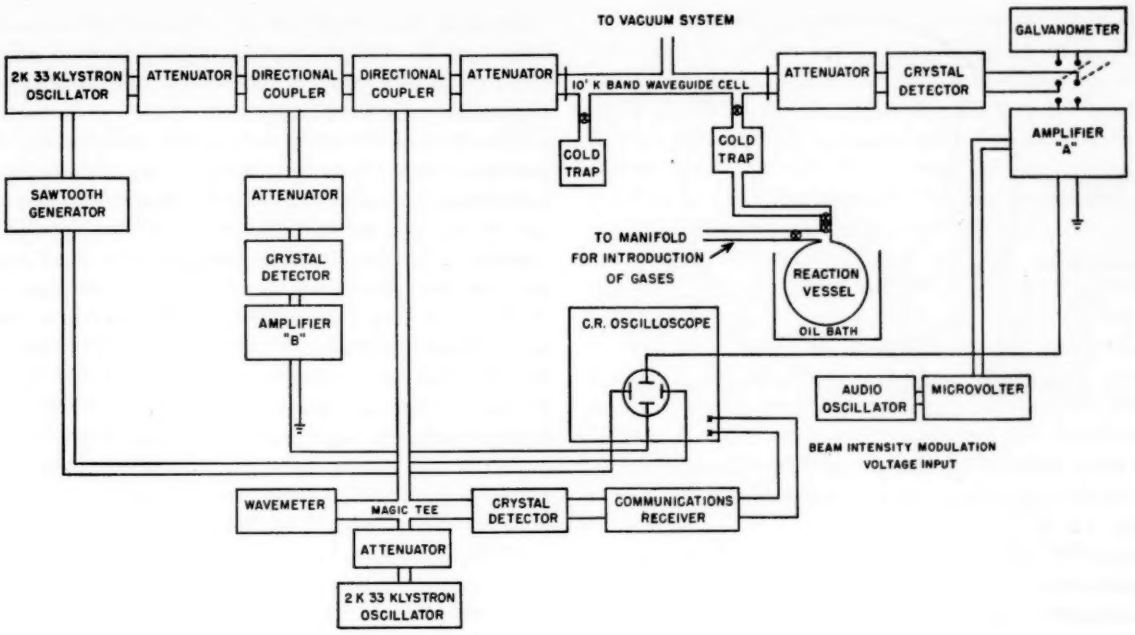

FIG. 1. Block diagram of apparatus.

Farkas, and Rummel[9] is probably correct. The hydrogenation of ethylene is believed by some[10] to occur by interaction between adsorbed ethylene and gaseous hydrogen, but the kinetics seem to be more satisfactorily explained in terms of the assumption that reaction occurs between ethylene and hydrogen molecules both of which are adsorbed.[11]

One other reaction which, it has been suggested,[12] may occur by a Rideal mechanism is the exchange reaction between ammonia and deuterium. The kinetics of this reaction were first studied by A. Farkas[13] on a pure iron surface, and was found to be of zero order with respect to ammonia and of the one-half order with respect to deuterium. These facts can be explained[14] on the basis of a Langmuir-Hinshelwood mechanism if the deuterium is weakly adsorbed atomically, the rate then being proportional to $p_{D_2}{}^{\frac{1}{2}}p_{NH_3}/(1+ap_{NH_3})^2$, where a is a constant at a given temperature. The rate is seen to pass through a maximum as the ammonia pressure is increased, owing to the displacement of deuterium by ammonia, and Farkas' zero-order behavior can be explained on the assumption that his ammonia pressures were in the region of the maximum. A Rideal mechanism will also account for Farkas' results, if it be assumed that the ammonia is adsorbed strongly but that the reaction is between gaseous NH_3 and adsorbed deuterium; the treatment[14] of this case has shown that the rate is proportional to $p_{D_2}{}^{\frac{1}{2}}p_{NH_3}/(1+ap_{NH_3})$. In this case, there is no falling off of the rate at high ammonia pressures.

It is evident that the above mechanisms can be distinguished on the basis of whether, at high pressures of ammonia, the rate diminishes, since such behavior cannot be accounted for on the basis of the Rideal type of mechanism. The main object of the present work was to investigate this point; and very careful rate measurements have been made over a range of deuterium and ammonia pressures, using a singly-promoted iron catalyst.

EXPERIMENTAL

Microwave Technique

All measurements were made on the 3–3 inversion line of ammonia, at 23,870 megacycles. The apparatus employed, a block diagram for which is shown in Fig. 1, is similar to that used by Good;[15] and only its special features will be described. The large variation of klystron power output over its mode would cause the spectral line to be displayed on a curved base, with consequent error in half-width determinations. In order to present the absorption line on a horizontal base, some of the power was taken out before the absorption cell, and its rectified envelope subtracted from the cell output by the amplifier-oscilloscope arrangement shown in the figure. It is essential that amplifiers A and B have identical frequency and phase characteristics, and that the crystal detectors and crystal mounts are of the

[9] Bonhoeffer, Farkas, and Rummel, Z. physik. Chem. **B21**, 225 (1933); A. Farkas, Trans. Faraday Soc. **35**, 943 (1939).
[10] G. Twigg, Faraday Soc. Discussions **8**, 152 (1950).
[11] K. J. Laidler, Faraday Soc. Discussions **8**, 47, 90 (1950).
[12] D. D. Eley, in *Advances in Catalysis* (Academic Press, New York, 1948), p. 157; Quart. Revs. **3**, 209 (1949).
[13] A. Farkas, Trans. Faraday Soc. **32**, 416 (1936); see also H. S. Taylor and J. C. Jungers, J. Am. Chem. Soc. **57**, 660 (1935).
[14] K. J. Laidler, Am. Chem. Soc. Symposium on "Anomalies in Chemical Kinetics," Minneapolis, June, 1950, to be published in J. Phys. Colloid Chem. (1951).
[15] W. E. Good, Phys. Rev. **69**, 639 (1946); **70**, 213 (1946).

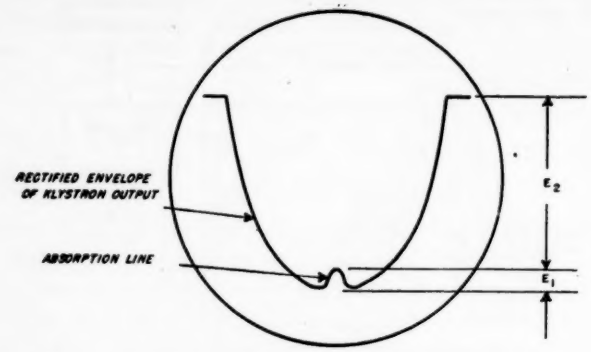

FIG. 2. Oscilloscope display of absorption line, without subtracted signal.

same kind and are carefully matched. The absorption lines are shown, without and with the subtracted signal, in Figs. 2 and 3.

Frequency markers were placed on the oscilloscope by combining the outputs of the swept klystron and a fixed frequency klystron in a crystal mixer. The mixer output was amplified by a communications receiver, tuned to half the frequency of the desired marker separation, the receiver output being used for intensity-modulation of the oscilloscope trace. Whenever the frequency of the swept klystron differs from that of the fixed klystron by the frequency to which the communications receiver is tuned, the crystal mixer output is amplified and intensity-modulates the trace. This occurs twice each sweep cycle (swept oscillator above and then below the frequency of the fixed oscillator), and the markers therefore have a frequency spacing twice that to which the receiver is tuned.

The variation of klystron power over its mode brings about some distortion even when the spectral line is viewed on a horizontal base, but the distortion over the half-width portion is negligible.

For the determination of collision cross sections the absorption coefficients were measured using the oscilloscope. The oscilloscope display is shown diagrammatically in Fig. 2. The absorption coefficient was measured by determining the ratio of the height of the absorption line, displayed on a horizontal base, to the height of the swept klystron signal-rectified envelope (channel B off), using a 2000-cycle calibrated signal on the oscilloscope for comparison.

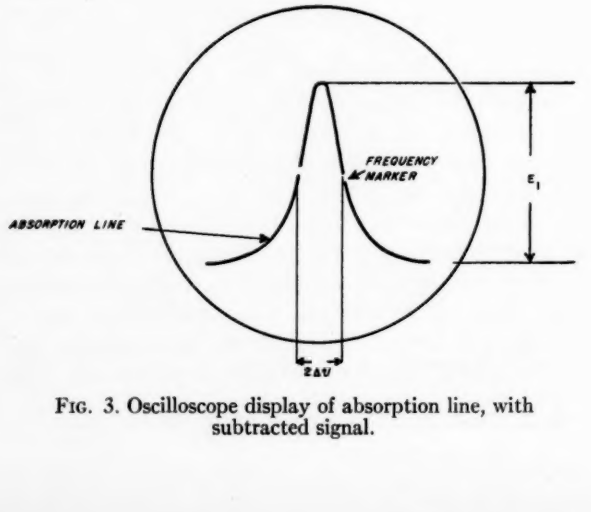

FIG. 3. Oscilloscope display of absorption line, with subtracted signal.

The crystal detector was a Sylvania 1N26, determined to be a 2.2-power device by measurements with a calibrated attenuator. A correction to the line width has to be applied for distortion of the spectral line because of the fact that the crystal obeys the 2.2-power law, and for broadening due to collisions with the walls. A kinetic theory calculation showed that in a K-band wave guide at 40μ pressure, collisions with the walls broaden the ammonia line by somewhat less than one percent. The contribution to the line width due to Doppler effect is negligible because the Doppler broadening is an independent effect and combines quadratically with the collision broadening.[17]

With these corrections Eq. (8) gives $S_{12}/S_{11}=0.90 \pm 0.02$. From the line-width data for pure NH_3, the value of the collision cross section for the 3–3 line in pure NH_3 was found to be 604×10^{-16} cm^2, and for an NH_3 deuterated ammonia mixture the value is 544×10^{-16} cm^2, the probable errors being 1.5 percent. In making the calculations the weighted mean value of 18.5 was employed for the molecular weight of the deuterated ammonias. The value obtained for the cross section of NH_3 in pure NH_3 agrees within experimental error with the most recent value, 598×10^{-16} cm^2, obtained by Howard and Smith.[18]

For reasons given in the sections on results and discussion it was found to be necessary to make the gas analyses in the wave guide at a higher pressure than was used for determining the cross sections, 1 to 2 mm being used. At such pressures the 3–3 line was too broad for convenient display on the oscilloscope, and an alternative method, a modification of that used by Bleaney and Penrose,[19] was employed. The wave guide was pumped down to 10^{-4} mm, at which pressure the 3–3 line is barely visible even with high amplification; and the klystron was tuned very slightly to one side of it, to avoid residual errors. The klystron sweep was then turned off, the crystal output switched over to a galvanometer, and the reading taken. The gas sample was admitted, and from the galvanometer readings before and after admission of gas the absorption coefficient was calculated. The cell was then pumped out rapidly, cold traps being used for additional pumping speed, and the galvanometer read again. This procedure reduced errors due to changes in klystron power during the introduction of the gas.

The use of the wave guide for work at higher pressures has the advantage over the resonant cavity of Bleaney and Penrose[19] that slight changes in oscillator frequency have almost no effect on the measured ab-

[17] The authors are indebted to Dr. K. F. Herzfeld for a discussion of this point.

[18] R. H. Howard and W. V. Smith, Phys. Rev. **89**, 128 (1950).

[19] B. Bleaney and R. P. Penrose, Proc. Roy. Soc. (London) **A189**, 358 (1947).

sorption coefficients. For weak absorption coefficients a resonant cavity may be more suitable than a wave guide, but will be less accurate unless frequency drifts are made very small. It is essential that the klystron power output be constant during the measurements. This was achieved using a very well-regulated klystron beam voltage supply, battery supply for focus, repeller, and filament voltages, and a "well-trained" klystron. An electronically regulated 110-volt supply, in addition to the regulated beam supply, was found to be desirable. Voltage regulators which employ saturable reactors are not suitable because the distortion of the line voltage introduces harmonics into the regulated supply for which its circuits were not designed. Care was taken to avoid corona discharge around high voltage points in the klystron supply.

Using this high pressure technique, absorption coefficients were found to be reproducible to 0.1 percent under good conditions. This is more than an order of magnitude better than any previously reported. The uncertainty in the ratio of cross sections is about 1.5 percent, but this introduces an error of only 0.5 percent at mole fractions near 0.5, and less elsewhere.

One matter that had to be considered in connection with this method of carrying out gas analysis was the possibility of the deuterated ammonias reacting together on the walls of the wave guide. Direct tests showed this effect to be unimportant. The procedure was to analyze mixtures of the ammonias by the method described, to add a known proportion of NH_3 and to analyze again by the microwave method. The results agreed with the calculated values to within 0.3 percent, showing that the equilibria had not shifted to an appreciable extent.

Kinetic Procedure

The ammonia-deuterium exchange reaction was studied on a singly-promoted iron catalyst (No. 631) kindly supplied to us by Dr. P. H. Emmett. This was reduced at 400°C in an atmosphere of dry hydrogen, and when not in use was maintained throughout the entire period of the investigations in contact with dry hydrogen at 110°C or more. Extreme care was taken to avoid admitting air to the catalyst, and it was found at the end of the investigations that the early runs were reproducible within the experimental error. The deuterium used was supplied by the Stuart Oxygen Company and was 99.5 percent pure; it was dried by passing through a trap cooled with liquid nitrogen. The ammonia was dried by bubbling through liquid ammonia in a trap cooled by acetone and dry ice.

The reaction vessel was a two-liter Pyrex flask which was maintained at a temperature accurate to 0.3°C in a thermostatically controlled oil bath. Before each run the vessel was pumped down to 5×10^{-4} mm, and the catalyst "washed" twice with ammonia at 25-cm pressure. As a result of this washing, the necessity for which will be explained later, the runs all started with an adsorbed layer of ammonia on the catalyst (or of species produced from ammonia, e.g., NH_2, H, NH, N). To carry out a run deuterium was introduced at the desired pressure; the reaction was started by heating a cold trap containing ammonia until the pressure reached the desired value and then closing off the trap and the reaction vessel. The amount of ammonia present after various intervals of time was determined using the microwave technique. Small samples were removed from the reaction vessel by trapping them between two stopcocks, and the wave guide was first washed with several such samples, for reasons to be explained. The sample to be analyzed was then introduced into the liquid nitrogen trap, the hydrogen pumped off, and the mixture of ammonias was introduced at a pressure of 1 to 2 mm into the wave guide and analyzed.

RESULTS AND DISCUSSION

Adsorption and Desorption Effects

It was originally planned to study the exchange reaction by following the disappearance of NH_3 using the low pressure technique with the oscilloscope, similar to that described for the determination of collision cross sections. Under these conditions, at 40μ pressure, the extent of adsorption on the wave guide was found to be such that there was more gas on the surface than in the gas phase. This alone does not affect the analyses, which give the mole fraction of NH_3 and therefore do not depend on the total amount of gaseous ammonia, but for practical reasons (to accelerate the pumping-out of the guide after each determination) it was considered desirable to reduce the amount of adsorption as much as possible. This was done by coating the surface with a thin layer of Glyptal which was then baked; the average coating thickness was found to be 0.0003 in. In this way the adsorption was very much reduced without appreciably affecting the electrical losses.

The procedure originally planned was to pump the wave guide down to less than 10^{-4} mm, after which the gas sample would be admitted and the microwave analysis carried out. It was expected that under these conditions there would be no error due to desorption of ammonias from the walls of the wave guide, since it had been shown directly, both by observation of the increase of pressure and of the pressure broadening of the 3–3 line, that after pumping to 10^{-4}-mm pressure, the rate of desorption is very low; it corresponded to a pressure rise of less than 5μ per minute, which would not be sufficient to affect the analysis of the sample subsequently introduced. However, the procedure was found to be unsatisfactory, since the rate of desorption was found to be very greatly increased on admission of the sample to the wave guide. Consequently, the results of the analysis of the sample were found to be very seriously affected by the last sample that had been in the wave guide. No reasonable amount of preliminary pumping was found to be sufficient to avoid this difficulty.

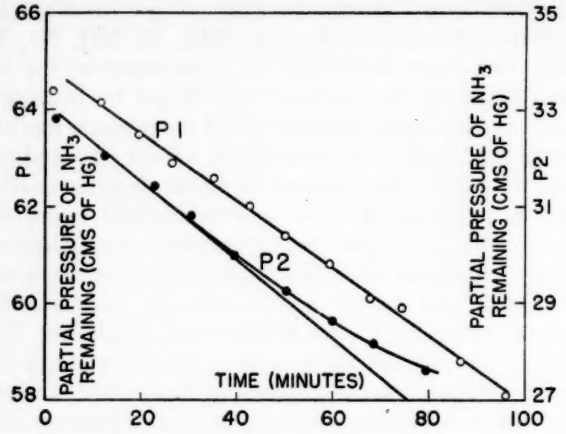

FIG. 4. Pressure-time curves for initial NH_3 pressures in the regions of 33 cm and 64 cm. $T=122.3°C$.

These results were evidently due to the fact that the rate of desorption of a substance may be very markedly increased by increase of gas pressure, i.e., by adsorption of additional molecules.‡ Some measurements of rates of desorption from the wave guide were made; but these are only of a semiquantitative nature, since some of the rates were too rapid for accurate determination. It was found that at a pressure of 10^{-4} mm, the rate of desorption of NH_3 corresponded to an initial pressure rise of about 5μ per minute. On introducing a mixture of deuterated ammonias at a pressure of 0.4 mm, the rate of desorption of ammonia was found to be increased by a factor of at least 100; the time required to make the measurements limits the accuracy, and it is possible that the increase in desorption rate is very much greater than this.

Some similar measurements were also made on the activated iron catalyst, at 122°C. In this case a mixture of the deuterated ammonias at high pressure was originally present, and the vessel was rapidly pumped down to less than one micron, and closed off from the pumps. The total rate of desorption of the ammonias was found to be approximately 5×10^{-9} mole sec^{-1}. NH_3 was then added to the reaction system and samples taken and analyzed at various times; the rate of desorption of deuterated ammonia could then be determined. At an NH_3 pressure of 20 cm the rate of desorption was found to be about 1.4×10^{-6} mole sec^{-1}, the increase being by a factor of about 300; in the two-liter vessel ammonia corresponding to a pressure of 1 cm is, in fact, desorbed in less than 10 minutes.

It was observed also that admission of ammonia to the reaction vessel, at 20 cm of pressure, increased the desorption rate of deuterium from the catalyst surface by at least an order of magnitude.

These results on rates of desorption are of some theoretical interest from the standpoint of interaction forces existing on surfaces. The simplest explanation of the results, and the one we assumed earlier,[20] is that an adsorbed molecule is put into a state of higher potential energy when other molecules are adsorbed close to it, owing to repulsive interactions between the molecules, and that it is therefore desorbed more rapidly. An alternative explanation, suggested to us by Dr. P. H. Emmett after the publication of our preliminary note, is that two molecules adsorbed side by side may change places. It may be supposed that the molecules that are not desorbed when the system is pumped down are adsorbed on particularly active sites. These molecules cannot easily pass to less active sites (since there will be an increase of free energy); but after adsorption of a second molecule on a neighboring and less active site, an exchange of molecules may occur, the first molecule passing to the less active site from which it can be more readily desorbed. It is not possible to distinguish experimentally between these two possibilities, since both give rise to the same behavior. However, we consider

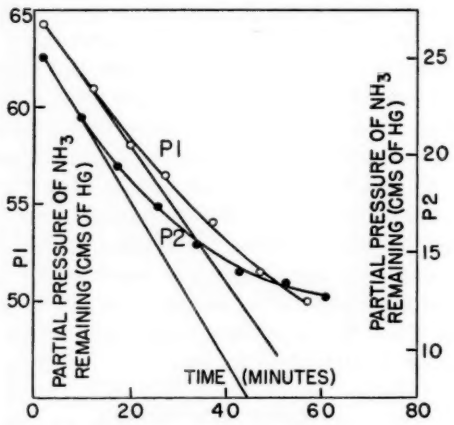

FIG. 6. Pressure-time curves for initial NH_3 pressures in the regions of 25 cm and 64 cm. $T=163.8°C$.

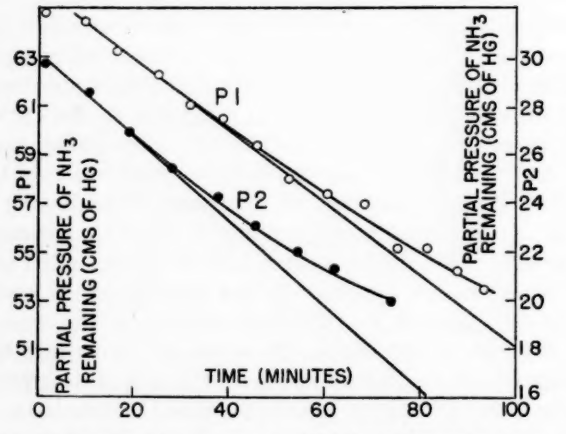

FIG. 5. Pressure-time curves for initial NH_3 pressures in the regions of 30 cm and 65 cm. $T=141.5°C$.

‡ Since publishing a preliminary report on this result (reference 20), we have been informed by Dr. P. H. Emmett of somewhat similar results obtained by him and J. T. Kummer, using carbon monoxide in normal and isotopic forms. Some similar results of Farkas and Farkas are considered later.

[20] J. Weber and K. J. Laidler, J. Chem. Phys. 18, 1418 (1950).

on theoretical grounds that the second explanation is unlikely on the wave guide at room temperatures, since such exchange reactions may be expected to occur only with difficulty. We have, in fact, made some rough calculations of the amount of bond stretching that would be required for two adsorbed NH_3 molecules to pass one another. Making the most favorable assumptions, we find that such a process would involve at least a doubling of the length of the bond connecting the ammonia to the surface. This would involve practically complete dissociation of both molecules, and would only occur slowly at the temperature of the experiments.§

In any case, we can refer to the desorption phenomenon observed as due to "interaction" between neighboring molecules. Previous evidence for surface interactions, being mostly based on heat of adsorption measurements,[21] has always been capable of alternative explanation in terms of the variability of the surface sites. The present results are not inconsistent with the idea of active centers, but require for their explanation the concept of interaction between adsorbed molecules.

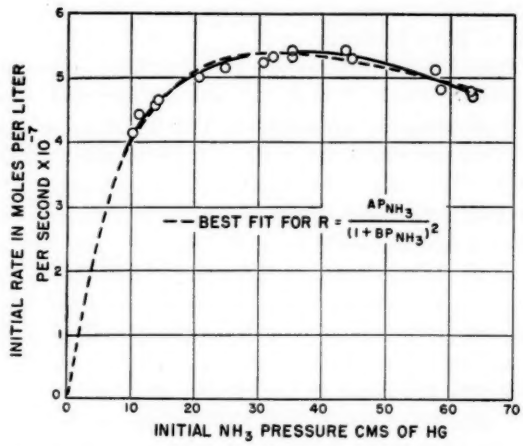

FIG. 7. Rate *vs* initial ammonia pressure at $T=122.3°C$, initial deuterium pressure = 8.2 cm.

The Ammonia-Deuterium Exchange Reaction

Owing to the rapid desorption from the wave guide on introducing samples of deuterated ammonias, it was found that the low pressure analytical procedure was unsatisfactory, the results being profoundly influenced by the gas that had previously been in the wave guide. For this reason the higher pressure procedure, using the galvanometer and "washing" the surface before making the determinations, was used; this was found to be completely satisfactory.

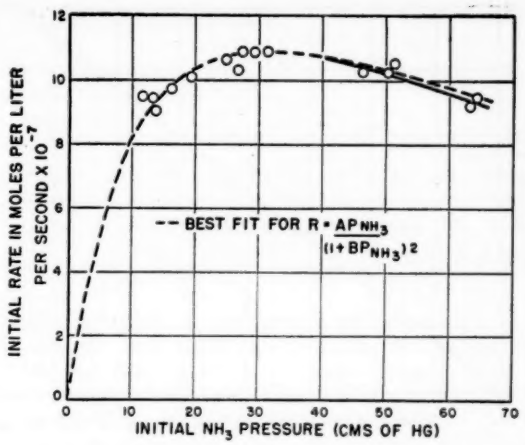

FIG. 8. Rate *vs* initial ammonia pressure at $T=141.5°C$; same initial deuterium concentration as for Fig. 7.

In each kinetic run the partial pressure of ammonia was determined at various times, and the initial rates were obtained graphically by drawing initial tangents. Typical pressure-time curves are shown in Figs. 4, 5, and 6. The curves are initially nearly linear at high ammonia or deuterium pressures, but have marked curvature at lower pressures. The pressure-time laws are complex, but fortunately it is not necessary to have them in explicit form for the present investigations. There is generally an induction period, and this is longer the greater the deuterium pressure. This is attributed to the slowness with which deuterium and ammonia adjust themselves on a surface already covered to a certain degree with strongly held species (NH_2,

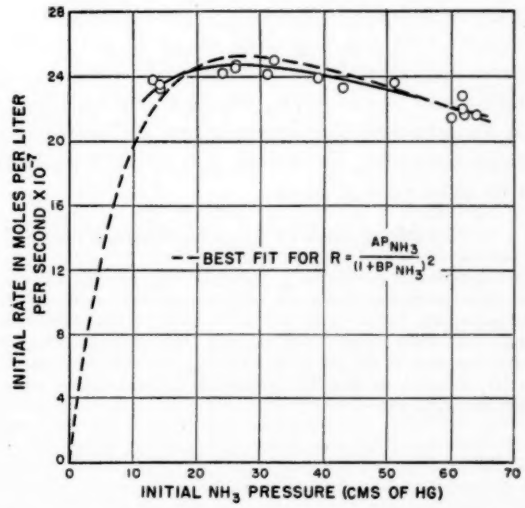

FIG. 9. Rate *vs* initial ammonia pressure at $T=163.8°C$; same initial deuterium concentration as for Fig. 7.

§ Somewhat similar results to ours have been observed by A. Farkas and L. Farkas, Trans. Faraday Soc. **31**, 821 (1935), with H_2 and D_2 on a quartz surface at 720°C. In this system there is undoubtedly rapid atomic exchange, $H_2+D_2 \rightleftharpoons 2HD$, and Emmett's explanation may well apply. In the case involving the wave guide the atomic exchange processes are, as mentioned earlier, slower than the effects observed, and simple repulsive interactions appear to offer the only interpretation. Atomic exchange processes of the type $NH_3+ND_3 \rightleftharpoons NH_2D+NHD_2$ may, however, be important on the catalyst; but atomic exchange cannot have any bearing on the influence of ammonia on the desorption rate of deuterium.

[21] Especially J. K. Roberts' work; see A. R. Miller, *The Adsorption of Gases on Solids* (Cambridge University Press, London, 1949).

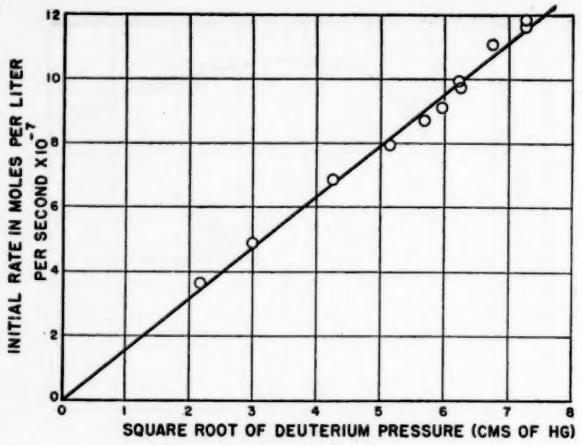

FIG. 10. Rate *vs* square root of deuterium pressure at 122.3°C; initial ammonia pressure is 18.4 cm.

NH, N, and H) arising from the preliminary washing with ammonia.

The investigation was particularly concerned with establishing the relationship between rate and initial ammonia pressure. The data for the three temperatures 122.3°C, 141.5°C, and 163.8°C are shown in Figs. 7, 8, and 9. All of these runs correspond to the same initial deuterium concentration (8.2 cm at 122.3°C). Figure 10 shows the variation of initial rate with the square root of the initial deuterium pressure, at a constant initial ammonia pressure of 18.4 cm. Practical considerations limit the investigations to the temperature range used; over 165°C the rates are too rapid to observe accurately, while at lower temperatures the effects due to the gas adsorbed in the previous run were found to be very important

The results obtained are consistent with those of Farkas,[13] but the more accurate technique has revealed that the rate does pass through a significant maximum with increasing ammonia pressure. The present results also show that the rate is proportional to $p_{D_2}^{\frac{1}{2}}$ over the range investigated, i.e., up to 50 cm deuterium pressure.‖

The fact that the rate falls off at higher ammonia pressures indicates that a Langmuir-Hinshelwood type of mechanism is occurring, reaction taking place between an adsorbed deuterium atom and an adsorbed ammonia molecule. The kinetic law for this mechanism is, in its most general form,

$$v=kp_{NH_3}p_{D_2}^{\frac{1}{2}}/(1+ap_{NH_3}+bp_{D_2}^{\frac{1}{2}})^2, \qquad (9)$$

‖ In a preliminary note in J. Chem. Phys. **19**, 381 (1951), we stated that deviations from the square root law occurred at the higher pressures. Later work, however, showed that this was not the case. The error arose from the fact that at higher deuterium pressures the rate of diffusion of NH_3 into the reaction vessel was markedly reduced, so that the ammonia concentrations were not as great as supposed.

TABLE I. Activation energies.

Pressure (cm)	Activation energy (kcal per mole)
12	13.8
25	12.8
40	12.3
60	12.3

where k, a, and b are constants. The fact that the rate is proportional to $p_{D_2}^{\frac{1}{2}}$ indicates that the term $bp_{D_2}^{\frac{1}{2}}$ may be neglected in the denominator; the law obeyed is thus

$$v=kp_{NH_3}p_{D_2}^{\frac{1}{2}}/(1+ap_{NH_3})^2. \qquad (10)$$

It may be seen in Figs. 7–9 that the data are very well fitted by a curve following this equation. It is to be emphasized that the falling off of the rate at high ammonia pressures is not due to an irreversible poisoning of the catalyst, since the early runs could be reproduced within the experimental error at the end of the series of investigations.

Activation energies at various ammonia pressures¶ are given in Table I; they are seen to diminish significantly with increasing pressure. The simple treatments, neglecting interaction forces and assuming a smooth surface, all predict an increase of activation energy with increasing pressure,[11] whether the mechanism be a Langmuir-Hinshelwood or a Rideal one. The assumption of a variable surface cannot reverse this conclusion, since at lower pressures the reaction proceeds on the more active centers, with low activation energy. The results actually obtained appear to be only explicable on the basis of the assumption of interaction forces, and therefore provide additional evidence that these are important. As a result of these forces between adsorbed molecules an increase of pressure puts the system into a state of higher potential energy, so that less energy is required to reach the activated state.

ACKNOWLEDGMENT

Grateful acknowledgment is made to the staff of the U. S. Naval Ordnance Laboratory, in particular Mr. L. R. Alldredge, for their cooperation in allowing this investigation to be carried out at the Laboratory, and for providing all the necessary equipment. Thanks are also due to Professor K. F. Herzfeld for valuable suggestions and advice, and to Dr. P. H. Emmett for supplying the catalyst and for valuable comments.

¶ The activation energies were, in fact, calculated at constant concentration and not pressure; the pressures quoted in the table are approximate.

THE JOURNAL OF CHEMICAL PHYSICS VOLUME 19, NUMBER 9 SEPTEMBER, 1951

Nucleation in Very Rapid Vapor Expansions

ARTHUR KANTROWITZ
Cornell University, College of Engineering, Ithaca, New York
(Received May 14, 1951)

In the Volmer theory, sub-critical droplets (embryos), with vapor pressure greater than their surroundings, nevertheless, grow statistically, because they exist in sufficiently greater numbers than neighboring larger droplets. Thus the formation of nuclei against the thermodynamic barrier presupposes the presence of very large numbers of embryos of all sizes.

An approximate lower bound for the time (nucleation time) required for the formation of this system of embryos can be calculated readily by (1) neglecting the thermodynamic barrier which impedes their formation; (2) assuming that when droplets contain a certain supercritical number, Γ, of molecules they grow very rapidly because their vapor pressure is considerably lower than their surroundings; (3) assuming that the formation of the embryo system begins when the vapor first becomes saturated. The equation for the rate of formation of embryos then reduces to the heat conduction equation yielding a simple solution. The lower bound sought is found to be inversely proportional to the fourth power of the degree of supercooling. Comparison with the experiments of Wegener and Smelt indicates that in some nozzle expansions the occurrence of nucleation is determined by this process.

On this theory the thermal accommodation coefficient which determines the heat transfer and especially the accommodation coefficient for growth, which determines the probability of a molecule sticking to the surface, play a much more prominent role than they do in the Volmer steady-state theory. Comparison with experimental time lags for the condensation of H_2O in air at -30 to -60°C gives the order of magnitude of the accommodation coefficient for growth as 5×10^{-4}.

INTRODUCTION

WHEN a gas is expanded adiabatically its vapor pressure generally falls faster than its pressure. Shortly after the saturation point is passed condensation begins on any foreign condensation nuclei which may be present. However, foreign nuclei are not usually present in sufficient numbers to seriously affect rapid expansion processes (for example, in nozzles or in closed chambers from which foreign nuclei have been removed) and, therefore, in those processes appreciable condensation does not occur until the gas spontaneously generates nuclei.

The spontaneous generation of nuclei has been treated by Volmer and others and the theory has been brought to its present state by Becker and Doering.[1] It has been demonstrated by Volmer and Flood[2] that this theory accounts quantitatively for the degree of supersaturation actually observed in the Wilson closed chamber expansion of various gases. Condensation in nozzles has been detected by the pressure and density increases, which it produces. It has been shown by Oswatitsch[3] that the occurrence of condensation in certain steam nozzle flows can also be accounted for by the Becker-Doering ($B-D$) treatment. Recent experiments by Wegener and Smelt[4] have shown however that the degree of (water vapor) supersaturation which is reached in the expansion of moist air in small nozzles is much greater than that predicted from the $B-D$ theory. It was found furthermore that the supersaturation increases rapidly with the time rate of expansion.

The time required for the growth of droplets of appreciable size from nuclei has been calculated by Oswatitsch. Since this time may be comparable with the other times involved in the problem, the droplet growth time will play a role in rapid expansions. However (from the $B-D$ theory) the rate of nucleation varies extremely rapidly with the degree of supersaturation. Thus it would be expected that in a situation where the supersaturation is increasing rapidly with the time the formation and growth of new nuclei will condense more vapor than the continued growth of old nuclei.*

In the early stages of condensation the highly variable nucleation rate will therefore dominate the process and, after condensation has reduced the supersaturation to a point where nucleation disappears, the droplet growth process will govern the return to equilibrium. Therefore, the initial appearance of condensation is determined by nucleation and the dependence of the degree of supersaturation on the rate of expansion in the experiments of Wegener and Smelt[4] indicates that the nucleation process requires an appreciable time.

The purposes of this paper are to estimate this nucleation time lag, to find its dependence on supersaturation, and to compare these results with the experiments of Wegener and Smelt.

Sometime after the original presentation of this work,[5] earlier treatments of the nucleation time lag

[1] R. Becker and W. Doering, Ann. Physik (5) **24**, 719 (1935).
[2] M. Volmer and H. Flood, Z. physik. Chem. (A) **170**, 273 (1934)
[3] K. Oswatitsch, Z. ang. Math. und Mech. (ZAMM) **22** Heft **1**, (1942).
[4] P. Wegener and R. Smelt, Naval Ordnance Laboratory Memorandum 10772, 15 February, 1950.

* A rough calculation based on the $B-D$ theory and the approximation that the radii of supercritical drops grow linearly with the time will illustrate this point. Consider an expansion in which the supersaturation increases linearly with the time. Then it can be shown that the droplet size which contributes the largest total surface area at a time t_2 seconds after saturation passed through its critical size at a time t_1 where

$$\Delta\phi(t_1)/kT > t_1/(t_2-t_1),$$

$\Delta\phi(t_1)$ is the free energy required to produce a critical droplet at time t_1. The $>$ sign appears in consequence of the fact the critical radius has been neglected in comparison with the droplet radius at time t_2. In view of the fact that for most cases $\Delta\phi/kT \gg 1$ this indicates that recently formed droplets contribute most of the surface area available for condensation in the early stages of the process while the supersaturation is increasing.

[5] A. Kantrowitz, "Nucleation in very rapid vapor expansions,"

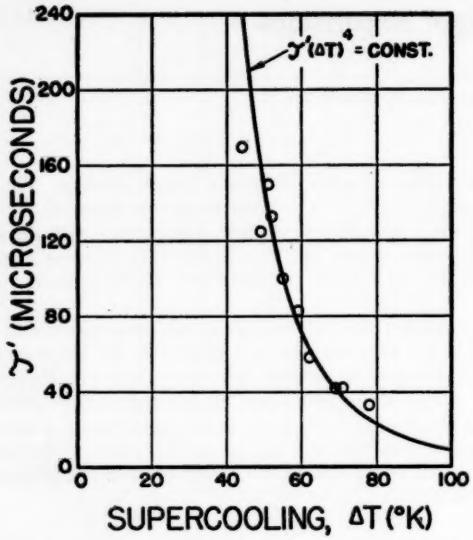

FIG. 1. The transit time from saturation to condensation *versus* the final degree of supercooling. The experimental points were obtained by Wegener and Smelt (reference 4) and the solid line has the theoretical form with the constant chosen for best fit.

problem with special reference to cavitation by Zeldovitch[6] and to crystallization by Turnbull[7] were called to the author's attention by Dr. Turnbull. In treating the problem of droplet formation in gases it will be more convenient to start from the general equations given by Frenkel than to adapt either of the above treatments. Also since the original presentation of this work, Probstein[8] extended it by including the effect of the thermodynamic barrier which is neglected in this treatment. He was able to confirm our assumption that the nucleation time lag is not greatly affected by the thermodynamic barrier (see below).

THEORY OF THE NUCLEATION PROCESS

Volmer[9] has demonstrated that the steady-state rate of formation of nuclei is given by

$$I=Ce^{-\Delta\Phi/kT}, \tag{1}$$

where I is the number of nuclei formed per second per cc, $\Delta\Phi$ is the (Gibbs) free energy excess of a droplet of critical size, k is Boltzmann's constant, T is absolute temperature, and C is a large number (of the order of magnitude of the number of molecular collisions per second in the cc of gas) which does not vary greatly with the degree of supersaturation.

In the steady-state theory the nucleation rate is dominated by the highly variable exponential factor. For typical examples it is only necessary to know the value of C to a factor of 10^3 to calculate the critical degree of supersaturation to within 10 percent or 15 percent. However, the kinetic factors which control the factor C also determine the time required for the appearance of a system of embryos and it now becomes important to evaluate these kinetic factors more accurately.

If now we restrict ourselves to very rapid expansions the chief impediment to nucleation will be the time required to grow the required system of embryos. Thus for a time we must expect nucleation rates far below the result of the steady-state theory. During this period we will neglect the thermodynamic barrier and concentrate our attention on the "diffusion" process by which the system of embryos is formed.

We shall start by following the formalism of Frenkel[10] and will depart from his treatment first taking into account kinetic factors which were neglected in previous treatments. Later we shall arrive at a time dependent differential equation (Eq. (9)) for the growth of the system of embryos formally identical with his result but with a different value of the diffusivity. We shall then neglect the term representing the thermodynamic barrier to obtain a simple solution applicable to very rapid expansions.

Let us assume that there exists a density, f_g, of embryos containing g molecules and that their total surface area is $S_g f_g$. Let β be the number of molecules of the vapor impinging each second on unit area and assume that a fraction A_G (the "accommodation coefficient for growth") sticks to the surface. Assume also that α_g molecules evaporate each second from unit surface area of embryos containing g molecules. Then the net number of embryos growing from $g-1$ to g molecules per second (per unit volume) is

$$I_g=f_{g-1}S_{g-1}\beta_1 A_G-f_g S_g\alpha_g. \tag{2}$$

If L is the latent heat of evaporation per molecule then the f_g embryos must dissipate an amount of heat $I_g L$ per unit time. If the embryos are at an average temperature θ_g degrees above their surroundings and they are bombarded by β_1 vapor molecules with a thermal accommodation coefficient A_1 and β_2 noncondensable molecules with a thermal accommodation coefficient A_2, then heat balance requires

$$I_g L=f_g S_g\theta_g(\beta_1 C'v_1 A_1+\beta_2 C'v_2 A_2), \tag{3}$$

where $C'v_1$ and $C'v_2$ are the augmented† heat capacities of the gases.

We shall calculate an average evaporation rate $\alpha_g(\theta_g)$ by assuming that all the embryos are heated an equal amount θ_g above their surroundings. From the Clausius-Capeyron equation (and assuming the vapor

presented at the Sixth meeting of the Fluid Dynamics Division, American Physical Society, Urbana, Illinois, May 13, 1950.

[6] J. B. Zeldovitch, Acta Physicochim. U.R.S.S. **XVIII**, No. 1, 1 (1943).

[7] D. Turnbull, Metals Tech. (June, 1948).

[8] R. F. Probstein, "Time lag in the self-nucleation of a supersaturated vapor," Princeton Univ. Aero. Engrs. Lab. Report No. 168, November 27, 1950.

[9] M. Volmer, *Kinetik der Phasenbildung* (Verlag Steinkopff, Dresden und Leipzig, 1949).

[10] J. Frenkel, *Kinetic Theory of Liquids* (Oxford University Press, London, 1946), Chapter 7.

† These are the normal heat capacities plus $R/2$ and are used in this case since we are dealing with samples "found" crossing a surface rather than molecules of average energy.

a perfect gas) we readily find (for small θ_g),

$$\alpha_g(\theta_g)=\alpha_g[1+(L/RT^2-1/2T)\theta_g], \quad (4)$$

where α_g is the evaporation rate at the temperature of the surroundings.

We are now in a position to rewrite Eq. (2) making allowance for the heating of the embryos by condensation (replacing α_g by $\alpha_g(\theta_g)$). Eliminating θ_g and $\alpha_g(\theta_g)$ by Eqs. (3) and (4) we get

$$I_g\left(1+\alpha_g\frac{\nu}{\beta_{th}}\right)=f_{g-1}S_{g-1}\beta_1A_g-f_gS_g\alpha_g, \quad (5)$$

where we have used the abbreviations $\nu\equiv L^2/RT^2-L/2T$, and $\beta_{th}\equiv\beta_1C'v_1A_1+\beta_2C'v_2A_2$.

We will only consider embryos for which $g\gg1$ so that $S_g\approx S_{g-1}$. We can generalize Frenkel's thermodynamic relation (Eq. (21b), p. 393) between the evaporation and condensation rates to give

$$\alpha_g=\beta_1A_G\exp(1/kT\partial\Delta\Phi\partial g).$$

Where $\partial\Delta\Phi/\partial g$ is the rate of change of thermodynamic potential with the droplet size. Following Frenkel's passage from differences to differentials Eq. (5) becomes

$$I_g=-D(\partial f_g/\partial g)-(D/kT)f_g(\partial\Delta\Phi/\partial g), \quad (6)$$

where the "diffusivity"

$$D\equiv\frac{\beta_1A_GS_g}{1+\alpha_g\nu/\beta_{th}}. \quad (7)$$

Now if we consider cases where f_g is not steady in time we readily get (Frenkel Eq. (22b), p. 394)

$$\partial f_g/\partial t=I_g-I_{g+1}. \quad (8)$$

Passing to differentials and substituting Eq. (6), (8) becomes

$$\frac{\partial f}{\partial t}=\frac{\partial}{\partial g}\left(D\frac{\partial f}{\partial g}\right)+\frac{1}{kT}\frac{\partial}{\partial g}\left(Df\frac{\partial\Delta\Phi}{\partial g}\right). \quad (9)$$

We shall now neglect the thermodynamic barrier term, the last term in Eq. (9), to obtain a simple solution which will be valid for the interval during which the nucleation rate is small compared to the steady-state result. Furthermore, we shall suppress the dependence of the diffusivity on the embryo size and adopt an average D. Then Eq. (9) becomes

$$\partial f/\partial t=D(\partial^2f/\partial g^2), \quad (10)$$

the standard diffusion equation.

The order of magnitude of the time (nucleation time) required for an appreciable nucleation rate to occur in a supersaturated gas can be found by solving Eq. (10) subject to the following boundary conditions: (a) That no embryos exist, $f_g=0$, for $t=0$. (b) That after embryos have grown to contain Γ molecules, they grow so rapidly that $f_\Gamma=0$ for all t. To obtain the order of magnitude of the nucleation time it will be sufficient to estimate $\Gamma=2g^*$. (c) That $f_{g=0}$ is some constant f_0. This means that we assume the existence of a constant number of vapor molecules and that we are using Eq. (10) down to very small values of g.

The solution of Eq. (10) with these boundary conditions can be found in standard references (see Carslaw, *Heat Conduction in Solids*, p. 67). The nucleation rate is (using Eq. (6) without the last term):

$$I_\Gamma=-D\left(\frac{\partial f}{\partial g}\right)_{g=\Gamma}=\frac{Df_0}{\Gamma}+\frac{2Df_0}{\Gamma}\sum_{n=1}^{\infty}(-1)^n\exp\left(-\frac{n^2\pi^2}{\Gamma^2}Dt\right). \quad (11)$$

Using the Poisson summation formula the series in Eq. (11) can be put into a form which converges much more rapidly for small t. We get

$$I_\Gamma=2f_0(D/\pi t)^{\frac{1}{2}}\sum_{n=1}^{\infty}\exp[-\Gamma^2/4Dt(2n-1)^2]. \quad (12)$$

For small t we need retain only the first term and finally

$$I_\Gamma=2f_0(D/\pi t)^{\frac{1}{2}}\exp(-\Gamma^2/4Dt). \quad (13)$$

To obtain large rates of nucleation we must have t of the order of magnitude of τ where $\tau\equiv\Gamma^2/4D=g^{*2}/D$.

The effect of our neglect of the thermodynamic barrier can be readily found by comparing the nucleation rate as calculated from Eq. (13) with the values obtained by Probstein (reference 8). It is found for example that the time required, for a typical case,‡ before the nucleation rate reaches $\frac{1}{10}$ of Probstein's final value, is about 50 percent greater, using Probstein's calculations, than from Eq. (13). We shall therefore use the results of Eq. (13) in our further considerations rather than the slowly converging (for small t) series given by Probstein. (Note the application of the Poisson summation transformation to his series leads to difficult integrations.)

These boundary conditions under which we solved Eq. (10) correspond to a sudden supersaturation from an unsaturated condition. However, in an experimental situation the supersaturation will increase with time until appreciable condensation occurs. To take this into account we should use a value of Γ which decreases with time. However, if we use a value of Γ obtained from the value of g^* appropriate to the conditions at which appreciable nucleation finally occurs, then we cannot make a large error since f_Γ will be very small if not zero during the period before appreciable nucleation begins. It can be shown that the error made in this way is small as long as t is small compared to τ which is the interesting period for this analysis.

APPLICATION TO THE EXPERIMENTS OF WEGENER AND SMELT

In view of the fact that we do not know even the order of magnitude of the accommodation coefficients

‡ The case calculated was for the condensation of nitrogen with $g^*=15$. For the purposes of this calculation his estimated $\Gamma/g^*=4/3$ and his values of D and the other constants for nitrogen were employed.

(especially A_G) which enter into the average diffusivity D we cannot calculate meaningful values of τ directly. However, it will be possible to calculate the variation of $\tau=g^{*2}/D$ with the degree of supersaturation since we can assume that the relatively small changes in temperature and pressure involved will not affect the values of the accommodation coefficients. From the definition of the diffusivity D (Eq. (7)) it can be seen that only the value of the typical surface area S_g of the droplets which is to be used in computing the average diffusivity will change rapidly with the degree of supersaturation. This typical surface area will vary with the surface area of the critical droplets and thus with $(g^*)^{2/3}$. Hence D will be proportional to $(g^*)^{2/3}$ and τ will be proportional to $(g^*)^{4/3}$. Using the Clausius-Capeyron equation and assuming the vapor a perfect gas, the Gibbs relation between the critical droplet radius and the degree of supersaturation ΔT can be written approximately.§

$$r^*=\frac{2\sigma M}{dRT(L/RT^2)\Delta T}, \tag{14}$$

where σ is the surface tension, d is the liquid density, M is the molecular weight, ΔT is the temperature at which the gas would be saturated at the local vapor pressure minus the local gas temperature.

Since r^* is proportional to $(g^*)^{1/3}$, $(g^*)^{4/3}$ is proportional to $(\Delta T)^4$ from Eq. (14). Thus we should expect τ and the nucleation time to vary inversely as the fourth power of the degree of supersaturation.

This expectation can be compared with the experimental results of Wegener and Smelt.[4] These investigators expanded room temperature air with a humidity of 70 percent to 76 percent through a small nozzle (2.5×2.5 cm cross section). They detected condensation of the water vapor by the resultant condensation shock which was observed with a shadowgraph. The nozzle was constructed so that the rate of temperature drop could be varied by varying the divergence of the nozzle walls.

It was found that the attainable degree of supersaturation increased as the rate of temperature drop was increased. They computed the "transit" time (which we shall denote by τ'), i.e., the time required for a particle to travel from the saturation point to the condensation shock and their results are presented as circles‖ on Fig. 1.

On the basis of our argument in the introduction we must expect that these delays in the appearance of condensation are not due to droplet growth times but are proportional to our nucleation time, i.e., these times should be proportional to τ. Thus we should expect that the transit time would vary inversely with the fourth power of the final degree of supersaturation. The curve $\tau'=\text{const}(\Delta T)^{-4}$ is also reproduced on Fig. 1, the constant having been determined as 936 sec $(°K)^4$ by averaging the experimental values of $\tau'(\Delta T)^4$. It is seen that the agreement between the experimental and theoretical variations of transit time with supersaturation is better than could have been anticipated.

It can also be shown from the definition of the diffusivity that τ should be inversely proportional to the humidity (for humidity small enough so that β_{th} is not appreciably dependent on the heat transferred to H_2O vapor). This is also in apparent agreement with the experimental results although insufficient information was provided to make a quantitative comparison possible.

ACCOMMODATION COEFFICIENTS

If we accept this explanation of the nucleation time lag we can utilize the data of Wegener and Smelt to obtain order of magnitude information about the accommodation coefficients. In view of the fact that the $B-D$ theory predicts very large values of the nucleation rate for the degree of supersaturation which exists in these experiments, τ must be considerably larger than τ'. We shall assume $\tau=10\tau'$ which means that the nucleation rate is e^{-10} times the steady-state value. Then

$$\tau(\Delta T)^4=10\tau'(\Delta T)^4=9360 \text{ sec } (°K)^4$$

and

$$\tau=g^{*2}/D=9360/(\Delta T)^4.$$

Employing the definition of D (Eq. (7)) and inserting $\alpha g=\beta_1 A_G$, i.e., the value appropriate to the critical droplet size we can obtain a relation between the accommodation coefficients. Inserting values appropriate to the experimental conditions we get,

$$A_G=\frac{1}{1900-(640/3.5A_1+140A_2)}. \tag{15}$$

(The stream temperature at the condensation shock ranged from $-30°$ to $-60°$C.)

Clearly if the thermal accommodation coefficients for H_2O and air (A_1 and A_2) are of the same order of magnitude only A_2 will be important. Also unless $A_2\lesssim 0.01$ it will not affect A_G which will be 5×10^{-4}.

This very small indicated value of A_G is not in disagreement with other qualitative information on the condensation of water vapor at low temperatures. For example, it has frequently been found difficult to condense water vapor on very cold surfaces. Since there can be little doubt that the gas is very cold in these cases a low value of A_G is indicated here also.

ACKNOWLEDGMENTS

This work was partially supported by Sverdrup and Parcel, Inc. operating under contract with the U. S. Air Force. The author is very grateful to Mr. S. C. Lin who suggested the transformation of Eq. (11) by the Poisson summation formula and who carried out numerous other calculations in connection with this work.

§ The Clausius-Capeyron differential equation has been used as a finite difference equation over the range ΔT in deriving Eq. (14).

‖ One apparently spurious point has been recomputed from their data.

Double Refraction of Flow: Numerical Evaluation of Extinction Angle and Birefringence as a Function of Velocity Gradient

HAROLD A. SCHERAGA,
Department of Chemistry, Cornell University, Ithaca, New York

JOHN T. EDSALL,
University Laboratory of Physical Chemistry, Related to Medicine and Public Health, Harvard University, Boston, Massachusetts

AND

J. ORTEN GADD, JR.,
Computation Laboratory, Harvard University, Cambridge, Massachusetts

(Received May 21, 1951)

The method of double refraction of flow in systems containing large asymmetrical molecules gives experimental data which, when interpreted in light of the theory of Peterlin and Stuart, enable one to calculate molecular lengths; information about the polydispersity of the system and about the optical properties of the solute particles may also be obtained from such data. Heretofore, this theory had been developed so that the data could be interpreted only under the limiting condition of low velocity gradient where the degree of orientation of the solute particles is very small. With the aid of the Mark I computer of the Harvard Computation Laboratory, the necessary equations have been solved to provide numerical values over a much wider range of velocity gradients, greatly increasing the usefulness of flow birefringence measurements for the study of macromolecular systems.

INTRODUCTION

OPTICAL measurements of the double refraction produced when a solution of large asymmetrical molecules is subject to a shearing force can be used to determine the dimensions of the dissolved molecules.[1–4] The method has already been extensively applied,[5–10] but many of the data obtained or obtainable could not heretofore be interpreted because the theory had been developed to give numerical values only under certain limiting conditions. The present work was undertaken in order to extend the applicability of the theory to a much wider range of experimental conditions, thus greatly increasing the usefulness of flow birefringence measurements as a tool in the determination of particle sizes and the characterization of polydisperse systems of macromolecules.

EXPERIMENTAL OBSERVATION

Double refraction is produced, in a liquid containing large asymmetrical molecules or colloidal particles, when a velocity gradient is set up in the liquid. This is most readily achieved by forcing the liquid through a capillary tube, or by subjecting it to shear between two concentric cylinders, one of which rotates while the other is held fixed. The latter procedure is best for quantitative measurements, and was employed in 1870 by J. Clerk Maxwell, who was apparently the first to describe the phenomenon, using Canada balsam as the liquid for study. This is also the method which has been adopted in most studies on double refraction of flow.[1–16]

In the concentric-cylinder-type of system, the liquid is placed in the annular space between the cylinders, the suspended particles assuming random orientation

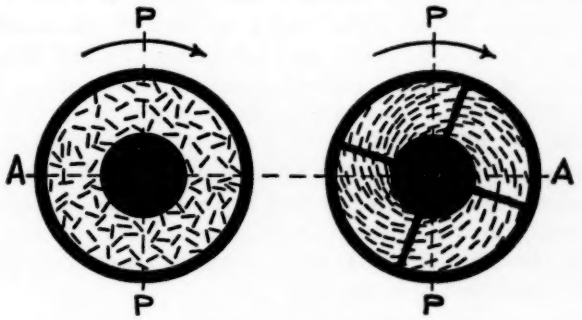

FIG. 1(a). Particles, each schematically represented by a line indicating its optic axis, at rest.

FIG. 1(b). Orientation caused by motion of external cylinder.

FIG. 1. Orientation of particles in a doubly refractive fluid placed between concentric cylinders (reference 12).

[1] J. T. Edsall, Advances in Colloid Sci. **1**, 269 (1942).
[2] E. J. Cohn and J. T. Edsall, *Proteins, Amino Acids, and Peptides* (Reinhold Publishing Corporation, New York, 1943), p. 506.
[3] A. Peterlin and H. A. Stuart, Hand. u. Jahrb. d. chem. Physik, Bd. 8, Abt. IB (1943).
[4] O. Snellman and Y. Bjornstahl, Kolloid-Beihefte **52**, 403 (1941).
[5] R. Signer and H. Gross, Z. physik. Chem. (A)**165**, 161 (1933).
[6] J. W. Mehl, Cold Spring Harbor Symposia Quant. Biol. **6**, 218 (1938).
[7] M. A. Lauffer and W. M. Stanley, J. Biol. Chem. **123**, 507 (1938).
[8] J. F. Foster and J. T. Edsall, J. Am. Chem. Soc. **67**, 617 (1945).
[9] Edsall, Foster, and Scheinberg, J. Am. Chem. Soc. **69**, 273 (1947).
[10] J. T. Edsall and J. F. Foster, J. Am. Chem. Soc. **70**, 1860 (1948).
[11] Edsall, Gordon, Mehl, Scheinberg, and Mann, Rev. Sci. Instr. **15**, 243 (1944).
[12] A. L. von Muralt and J. T. Edsall, J. Biol. Chem. **89**, 315, 351 (1930).
[13] J. T. Edsall and J. W. Mehl, J. Biol. Chem. **133**, 409 (1940).
[14] C. Sadron, J. phys. et radium (7) **7**, 263 (1936).
[15] A. J. de Rosset, J. Chem. Phys. **9**, 766 (1941).
[16] Lawrence, Needham, and Shen, J. Gen. Physiol. **27**, 201 (1944).

when both cylinders are at rest as shown in Fig. 1(a). When one of the cylinders (e.g., the outer one) is set in motion, laminar flow is produced in the liquid, and a velocity gradient is set up across the gap.[17] The resulting shearing forces produce an orientation of the suspended particles, which are here assumed to be rigid ellipsoids of revolution.[18] This orientation is represented schematically in Fig. 1(b). If the cylinders are mounted between crossed Nicol prisms, where AA and PP represent the planes of transmission of the analyzing and polarizing Nicol, respectively, then the field appears dark when the cylinders are at rest (Fig. 1(a)) and, when one cylinder is rotating, becomes light in all regions except for a dark cross (Fig. 1(b)).

To characterize the observed phenomena, two quantities must be measured: (1) the extinction angle, χ, the smaller of the two angles between this "cross of isocline" and the planes of transmission of the Nicols (this is also the angle between the optic axis in the flowing liquid and the direction of the stream lines); (2) the magnitude of the double refraction, Δn,—i.e., the difference in refractive index between light transmitted with its electric vector parallel, and light with its electric vector perpendicular, to the optic axis. The problem is to measure χ and Δn as a function of velocity gradient and relate them to the dimensions of the suspended particles.

Empirically, it is found, for solutions containing a single type of large molecule, that χ approaches 45° as the velocity gradient, G, approaches zero, and approaches 0° asymptotically as G increases to very large values, provided the flow is laminar. Δn is zero when $G=0$, is a linear function of G at low G values, and gradually approaches a constant limiting saturation value at very high values of G. Very elongated particles, like those of myosin (the structural protein of muscle), or tobacco mosaic virus, which are several thousand angstrom units in length, give low values of χ and high values of Δn even at low velocity gradients ($G=10$ to 300 sec^{-1} in water which has a viscosity of 0.01 poise at 20°). Molecules, like human serum albumin and gamma-globulin, near 200A in length, require much higher velocity gradients and solvent media of high viscosity as well to attain a significant degree of orientation ($G=1000$ to 10,000 sec^{-1}, or more; viscosity 50 to 100 times that of water).[8–10]

THEORY

Colloidal particles or large asymmetrical molecules in the flowing solution are subject to shearing forces due to the velocity gradient, G, which tends to orient their major axes.[19] In addition to the hydrodynamic forces, the particles are subject to rotary brownian movement which causes a random fluctuation of the orientation. The brownian movement is characterized by a rotary diffusion constant, Θ. The relation of χ and Δn to the molecular dimensions has been developed chiefly by Boeder,[20] Peterlin and Stuart,[3,21,22] and Snellman and Bjornstahl.[4] This is expressed as a function of the parameter α (or σ in the notation of Peterlin and Stuart) which is equal to G/Θ. If Θ is known, the length of the semimajor axis, a, of the molecule can be evaluated.[1–4,23,24] The crux of the problem, therefore, is the determination of Θ from the experimental measurements of χ and G.

The double refraction, Δn, is the product of an optical factor which is evaluated independently[22] and an orientation factor f. Like the extinction angle χ, f is a function of α and p.

We shall further define[25] the quantity R,

$$R=(p^2-1)/(p^2+1), \quad \text{where} \quad p=a/b. \tag{1}$$

R is thus equal to unity for an infinitely thin rod ($a/b=\infty$), to zero for a sphere ($a/b=1$), and to -1 for a flat disk without thickness ($a/b=0$).

Peterlin and Stuart obtained expressions for χ and f in terms of slowly converging infinite series in α and p. At very low values of α (<1.5), corresponding to χ-values between 45° and 38°, these series converge sufficiently rapidly to enable one to evaluate the rotary diffusion constant from a simple limiting equation. However, the errors in the experimental data are generally greatest at low gradients; that is, at low values of α. The data are more accurate at somewhat higher gradients, but it has not been possible hitherto to evaluate from theory the numerical relation between χ and α under these conditions. Moreover, it is very important experimentally to determine whether a given solution under study contains only one or more than one constituent capable of orientation by the velocity gradients employed. The only way to be sure of this is

[17] Above a critical speed of rotation the flow becomes turbulent (see reference 1), but we are here concerned only with conditions in which the flow is laminar.

[18] The assumption that the suspended particles are rigid ellipsoids of revolution is considered a moderately good approximation to the shape of a protein molecule, but is not applicable to flexible chain molecules such as many synthetic polymers.

[19] G. B. Jeffery, Proc. Roy. Soc. (London), **A102**, 161 (1922–23).

[20] P. Boeder, Z. Physik **75**, 258 (1932).

[21] A. Peterlin, Z. Physik **111**, 232 (1938).

[22] A. Peterlin and H. A. Stuart, Z. Physik **112**, 1, 129 (1939).

[23] F. Perrin, J. phys. et radium (7)**5**, 497 (1934).

[24] For example, for prolate ellipsoids ($a>b$), rotary brownian movement of the a-axis about the b-axis is characterized (reference 23) by the rotary diffusion constant Θ_b and a relaxation time τ_a, where

$$\frac{\Theta_b}{\Theta_0}=\frac{\tau_0}{\tau_a}=\frac{3q^2(2-q^2)(1-q^2)^{-\frac{1}{2}}\ln\{[1+(1-q^2)^{\frac{1}{2}}]/q\}-3q^2}{2(1-q^4)},$$

where $q=1/p=b/a$, and the zero subscript refers to quantities for a sphere of the same volume. If $a>5b$, the following approximation is valid within 1 percent:

$$\Theta_b=1/2\tau_a=(3kT/16\pi\eta a^3)(2\ln 2p-1),$$

where η is the viscosity of the solvent.

It is thus easily seen that Θ_b is not a very sensitive function of the axial ratio, p, as compared with the length of the semimajor axis, a. Therefore, p can be determined with sufficient accuracy for present purposes from viscosity measurements, and may be taken as a known quantity. A determination of Θ_b from flow birefringence data thus gives the molecular length, $2a$.

[25] This quantity is denoted as b by Peterlin and Stuart.

to make measurements over a wide range of velocity gradients and compare the measured χ-values with values calculated from the appropriate theoretical curve.[26] However, since only a small portion of the theoretical curve is given by the limiting formulas of Peterlin and Stuart, this method of analysis could not be satisfactorily carried out. A semi-empirical method has been tried,[9] but it was considered essential to have the complete theoretical curves using a rigid ellipsoid of revolution as a molecular model.[18] If these were available it would be possible not only to infer whether only a single type of elongated molecule is present, but also, if several such components are present, to draw some important inferences concerning their relative sizes and concentrations in the solution. An observed χ-value, in such a multicomponent system, is a function of all the values of both χ and f that would be found for each of the components, if it were present in the solution alone, at the same velocity gradient. The ability to analyze such complex systems would greatly increase the range and power of the method of double refraction of flow.

We shall, therefore, present the Peterlin and Stuart theory,[3,21,22] wherein we have evaluated the quantities required to obtain χ and f values over a wide range of α values by the use of the Mark I computer of the Harvard Computation Laboratory.

If rigid ellipsoidal particles are suspended in a continuous medium under conditions of laminar flow, the state of the system may be characterized by a distribution function, F, which depends on α and R and is given by the differential equation [3,4]

$$\partial F/\partial t=\Theta\Delta F-\mathrm{div}(F\omega), \tag{2}$$

where Δ is the laplacian operator and ω is the angular velocity of the particle, being a function of G and R. This equation shows the analogy between the rotational problem and the similarly expressed problem of translational diffusion embodied in Fick's laws. In the steady state $\partial F/\partial t=0$. The substitution of Jeffery's expressions[19] for ω and performance of the indicated vector operations leads to the following equation:

$$\Delta F/\alpha=\tfrac{1}{2}(1+R\cos 2\varphi)(\partial F/\partial\varphi)$$
$$+\tfrac{1}{2}R\sin\theta\cos\theta\sin 2\varphi(\partial F/\partial\theta)-\tfrac{3}{2}R\sin^2\theta\sin 2\varphi(F). \tag{3}$$

The meaning of θ and φ may be understood by reference to Fig. 2, which is a section of the gap between the concentric cylinders, the inner one rotating. X is the direction of the stream lines at 0; Z is the direction of the velocity gradient between the concentric cylinders; Y is parallel to the cylinder axis and is normal to the streaming plane; x, y, z are the directions of the principal axes of the index of refraction ellipsoid of the birefringent system, and χ is the angle between the z and X axes, x and z being coplanar with X and Z. An *individual* particle at 0 has its major axis in the ξ-direction where ξ, η, ζ is a set of axes fixed in the particle. θ is the angle between Y and ξ, while φ is the angle between the YZ and $Y\xi$ planes. This is the usual notation of spherical coordinates with volume element $d\Omega=\sin\theta d\theta d\varphi$.

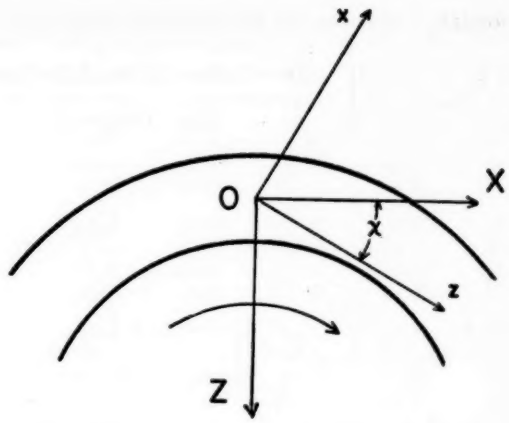

FIG. 2. Coordinate system in Couette cylinder apparatus. X, Y, Z axes are fixed in the fluid and x, y, z axes are the principal axes of the index of refraction ellipsoid in the birefringent system (reference 22).

As will be shown later, the determination of χ and f involves the evaluation of certain mean values. The distribution function, F, is required for this purpose and is evaluated as follows. (See Peterlin,[21] and Peterlin and Stuart.[3,22])

Express F as a power series in R:

$$F=\sum_{j=0}^{\infty}R^jF_j. \tag{4}$$

Each F_j then satisfies an inhomogeneous equation of the type

$$(1/\alpha)\Delta F_j-\tfrac{1}{2}\partial F_j/\partial\varphi=\tfrac{1}{2}[\cos 2\varphi(\partial F_{j-1}/\partial\varphi)$$
$$+\sin\theta\cos\theta\sin 2\varphi(\partial F_{j-1}/\partial\theta)-3\sin^2\theta\sin 2\varphi\cdot F_{j-1}]. \tag{5}$$

F_j may be expressed in terms of series of spherical harmonics as

$$F_j=\tfrac{1}{2}\sum_{n=0}^{\infty}a_{n0,\,j}P_{2n}$$
$$+\sum_{n=1}^{\infty}\sum_{m=1}^{n}(a_{nm,\,j}\cos 2m\varphi+b_{nm,\,j}\sin 2m\varphi)P^{2m}{}_{2n}, \tag{6}$$

where P_{2n} is a Legendre polynomial of the first kind and

$$P^{2m}{}_{2n}=\sin^{2m}\theta\cdot d^{2m}P_{2n}/(d\cos\theta)^{2m}.$$

Since F_j is a function of α and is independent of R, the $a_{nm,\,j}$ and $b_{nm,\,j}$ coefficients will also have this dependency.

Substituting Eq. (6) in Eq. (5) and making use of the orthogonality and recurrence relations for these

[26] The problem of calculations based on double refraction of flow measurements in polydisperse systems will be considered in a later paper.

polynomials,[27] one obtains the following recurrence formulas for $a_{nm,j}$ and $b_{nm,j}$:

$$\frac{n(2n+1)}{\alpha}a_{n0,j}=-\frac{1}{4}\left[-\frac{(2n-3)(2n-2)(2n-1)2n(2n+1)}{(4n-3)(4n-1)}b_{n-1,1;j-1}+\frac{3(2n-1)2n(2n+1)(2n+2)}{(4n-1)(4n+3)}b_{n,1;j-1}\right.$$
$$\left.+\frac{2n(2n+1)(2n+2)(2n+3)(2n+4)}{(4n+3)(4n+5)}b_{n+1,1;j-1}\right], \quad (7)$$

$$b_{n0,j}=0 \quad (8)$$

$$\frac{2n(2n+1)}{\alpha}a_{nm,j}+mb_{nm,j}=-\frac{1}{4}\left[\frac{2n+1}{(4n-3)(4n-1)}b_{n-1,m-1;j-1}-\frac{3}{(4n-1)(4n+3)}b_{n,m-1;j-1}\right.$$
$$-\frac{2n}{(4n+3)(4n+5)}b_{n+1,m-1;j-1}-\frac{(2n-2m-3)(2n-2m-2)(2n-2m-1)(2n-2m)(2n+1)}{(4n-3)(4n-1)}b_{n-1,m+1;j-1}$$
$$+\frac{3(2n-2m-1)(2n-2m)(2n+2m+1)(2n+2m+2)}{(4n-1)(4n+3)}b_{n,m+1;j-1}$$
$$\left.+\frac{2n(2n+2m+1)(2n+2m+2)(2n+2m+3)(2n+2m+4)}{(4n+3)(4n+5)}b_{n+1,m+1;j-1}\right] \quad (m\neq 0), \quad (9)$$

$$-ma_{nm,j}+\frac{2n(2n+1)}{\alpha}b_{nm,j}=-\frac{1}{4}\left[\frac{2n+1}{(4n-3)(4n-1)}a_{n-1,m-1;j-1}-\frac{3}{(4n-1)(4n+3)}a_{n,m-1;j-1}\right.$$
$$-\frac{2n}{(4n+3)(4n+5)}a_{n+1,m-1;j-1}-\frac{(2n-2m-3)(2n-2m-2)(2n-2m-1)(2n-2m)(2n+1)}{(4n-3)(4n-1)}a_{n-1,m+1;j-1}$$
$$+\frac{3(2n-2m-1)(2n-2m)(2n+2m+1)(2n+2m+2)}{(4n-1)(4n+3)}a_{n,m+1;j-1}$$
$$\left.+\frac{2n(2n+2m+1)(2n+2m+2)(2n+2m+3)(2n+2m+4)}{(4n+3)(4n+5)}a_{n+1,m+1;j-1}\right] \quad (m\neq 0). \quad (10)$$

Normalization, i.e., $\int F d\Omega=1$, gives $a_{00,0}=1/2\pi$ and all other $a_{00,j}=0$. The complete distribution function is given by Eq. (4) after the F_j's are thus evaluated.

The evaluation of the coefficients $a_{nm,j}$ and $b_{nm,j}$ as solutions of the simultaneous Eqs. (7)–(10) is a formidable task and would have been hopeless without the aid of the Mark I computer. It should be pointed out that not all the coefficients are required for the double refraction of flow problem, but, as has been shown by Peterlin and Stuart, only the $a_{11,j}$ and $b_{11,j}$ terms. However, many other terms are required in order to evaluate these particular ones. The task is somewhat eased by the vanishing of many of these terms for certain values of the indices.[28]

Making use of the distribution function, F, of the particles it is possible to calculate the effect of the interaction of this oriented system with a beam of polarized light, i.e., the double refraction. Results of such a computation are

$$\tan 2\chi=\frac{\overline{2\cos(\xi X)\cos(\xi Z)}}{\overline{\cos^2(\xi X)-\cos^2(\xi Z)}} \quad (11)$$

[27] E. Jahnke and F. Emde, *Tables of Functions* (Dover Publications, New York, 1945), p. 107.

[28] The mathematical details for the formulation of the problem for the Mark I computer and several general relations between the $a_{11,j}$ and $b_{11,j}$ coefficients are described more fully in the Annals of the Harvard Computation Laboratory. This report also contains more extended versions of Tables I and II. Several generalizations which hold for the relations between the terms in Eqs. (5) to (10), inclusive, were found to be of major importance in the computation problem. They are listed here for the convenience of other investigators:

1. All terms with negative indexes are zero.
2. $a_{nm,0}=0$, and $a_{00,j}=0$, except $a_{00,0}=1/2\pi$.
3. $b_{nm,0}=b_{n0,j}=b_{0m,j}=0$.
4. If m is even and j is odd, $a_{nm,j}=0$, and $b_{nm,j}=0$.
5. If m is odd and j is even, $a_{nm,j}=0$, and $b_{nm,j}=0$.
6. If $n>j$, or if $m>j$, $a_{nm,j}=0$, and $b_{nm,j}=0$.
7. In this problem, terms where $m>n$ need not be computed as they do not affect the values of $a_{11,j}$ or $b_{11,j}$.

TABLE I. Extinction angle, χ, as function of α for various axial ratios, p.[a]

α \ p	1.00	2.00	3.00	4.00	5.00	7.00	10.00	16.00	25.00	50.00	∞
0.00	45.00	45.00	45.00	45.00	45.00	45.00	45.00	45.00	45.00	45.00	45.00
0.25	43.81	43.81	43.81	43.81	43.81	43.81	43.81	43.81	43.81	43.81	43.81
0.50	42.62	42.62	42.62	42.62	42.62	42.62	42.62	42.62	42.62	42.62	42.62
0.75	41.44	41.44	41.44	41.44	41.45	41.45	41.45	41.45	41.45	41.45	41.45
1.00	40.27	40.28	40.29	40.29	40.29	40.30	40.30	40.30	40.30	40.30	40.30
1.25	39.12	39.14	39.15	39.16	39.16	39.17	39.17	39.17	39.17	39.17	39.17
1.50	37.98	38.02	38.04	38.05	38.06	38.07	38.07	38.07	38.07	38.07	38.08
1.75	36.87	36.92	36.96	36.98	36.99	37.00	37.01	37.01	37.01	37.01	37.01
2.00	35.78	35.86	35.91	35.94	35.96	35.97	35.98	35.98	35.99	35.99	35.99
2.25	34.72	34.82	34.90	34.94	34.96	34.98	34.99	35.00	35.00	35.00	35.00
2.50	33.69	33.82	33.93	33.98	34.01	34.03	34.04	34.05	34.05	34.06	34.06
3.00	31.72	31.93	32.09	32.17	32.21	32.25	32.27	32.28	32.29	32.29	32.29
3.50	29.87	30.18	30.41	30.52	30.58	30.63	30.66	30.68	30.69	30.69	30.69
4.00	28.16	28.56	28.87	29.02	29.09	29.17	29.21	29.23	29.24	29.25	29.25
4.50	26.57	27.08	27.47	27.66	27.75	27.85	27.89	27.93	27.94	27.95	27.95
5.00	25.10	25.73	26.20	26.42	26.54	26.65	26.71	26.75	26.77	26.77	26.78
6.00	22.50	23.35	23.98	24.29	24.45	24.60	24.68	24.73	24.75	24.76	24.76
7.00	20.30	21.35	22.13	22.51	22.71	22.90	23.00	23.06	23.09	23.10	23.11
8.00	18.43	19.65	20.57	21.02	21.26	21.48	21.60	21.68	21.70	21.72	21.73
9.00	16.84	18.20	19.25	19.75	20.02	20.27	20.41	20.50	20.53	20.55	20.55
10.00	15.48	16.95	18.09	18.66	18.96	19.24	19.39	19.49	19.53	19.54	19.55
12.50	12.82	14.45	15.80	16.48	16.84	17.18	17.37	17.49	17.54	17.56	17.56
15.00	10.90	12.60	14.07	14.84	15.25	15.64	15.86	16.00	16.05	16.08	16.09
17.50	9.46	11.16	12.72	13.55	14.00	14.44	14.68	14.84	14.89	14.92	14.93
20.00	8.35	10.02	11.62	12.51	13.00	13.47	13.74	13.90	13.97	14.00	14.01
22.50	7.46	9.08	10.71	11.64	12.16	12.67	12.97	13.14	13.21	13.24	13.26
25.00	6.75	8.30	9.95	10.91	11.46	12.00	12.31	12.50	12.58	12.62	12.63
30.00	5.66	7.08	8.71	9.72	10.32	10.91	11.26	11.48	11.57	11.61	11.62
35.00	4.86	6.17	7.76	8.80	9.43	10.07	10.45	10.69	10.78	10.83	10.85
40.00	4.27	5.46	7.00	8.04	8.70	9.38	9.79	10.06	10.16	10.21	10.23
45.00	3.80	4.90	6.37	7.41	8.08	8.79	9.23	9.51	9.62	9.68	9.69
50.00	3.42	4.43	5.84	6.87	7.54	8.28	8.74	9.03	9.15	9.22	9.23
60.00	2.86	3.73	5.00	5.99	6.66	7.41	7.89	8.20	8.33	8.40	8.42
80.00	2.14	2.82	3.88	4.75	5.36	6.08	6.55	6.86	6.98	7.05	7.08
100.00	1.72	2.27	3.15	3.90	4.45	5.09	5.52	5.80	5.92	5.98	6.00
200.00	0.86	1.14	1.62	2.04	2.35	2.74	2.99	3.16	3.23	3.27	3.28

[a] Values of χ for α-values above 60 are of uncertain validity. See appendix.

and

$$\Delta n=(2\pi c/n)(g_1-g_2)\{[\overline{\cos^2(\xi Z)}-\overline{\cos^2(\xi X)}]^2+[\overline{4\cos(\xi Z)\cos(\xi X)}]^2\}^{\frac{1}{2}}$$

$$=(2\pi c/n)(g_1-g_2)f(\alpha, p), \tag{12}$$

where c is the concentration of the particles expressed as volume fraction, n is the index of refraction of the isotropic solution at rest, and (g_1-g_2) is an optical factor depending on the axial ratio and indices of refraction of the particle.[22] Since $\cos(\xi X)=\sin\theta\sin\varphi$, and $\cos(\xi Z)=\sin\theta\cos\varphi$, it follows that

$$2\cos(\xi X)\cos(\xi Z)=\tfrac{1}{3}\sin 2\varphi\cdot P^2_2$$

and

$$\cos^2(\xi Z)-\cos^2(\xi X)=\tfrac{1}{3}\cos 2\varphi\cdot P^2_2. \tag{13}$$

The mean values of these functions are evaluated by multiplying by F and integrating, giving

$$-\tan 2\chi=\sum_{j=1}^{\infty} R^{j-1}b_{11,j}/\sum_{j=1}^{\infty} R^{j-1}a_{11,j}, \tag{14}$$

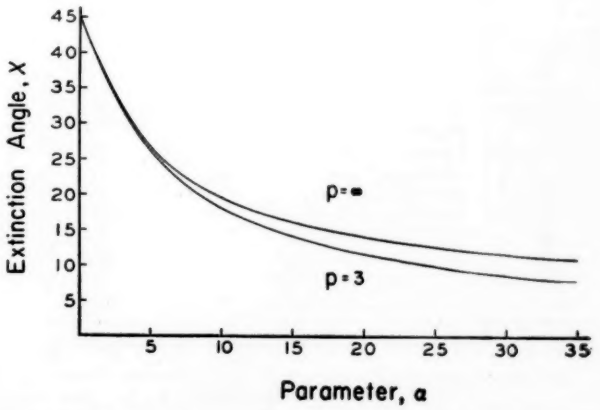

FIG. 3. Extinction angle, χ, *vs* parameter α together with its dependence on axial ratio, p.

TABLE II. Orientation factor, f, as function of α for various axial ratios, p.[a]

α \ p	1.00	2.00	3.00	4.00	5.00	7.00	10.00	16.00	25.00	50.00	∞
0.00	0.00000	0.0000	0.0000	0.0000	0.0000	0.0000	0.0000	0.0000	0.0000	0.0000	0.0000
0.25	0.00000	0.0100	0.0133	0.0147	0.0154	0.0160	0.0163	0.0165	0.0166	0.0166	0.0167
0.50	0.00000	0.0199	0.0266	0.0293	0.0307	0.0319	0.0325	0.0329	0.0331	0.0332	0.0332
0.75	0.00000	0.0298	0.0397	0.0437	0.0458	0.0476	0.0486	0.0492	0.0494	0.0495	0.0496
1.00	0.00000	0.0394	0.0525	0.0579	0.0606	0.0630	0.0643	0.0651	0.0654	0.0656	0.0656
1.25	0.00000	0.0489	0.0651	0.0718	0.0751	0.0781	0.0797	0.0807	0.0811	0.0813	0.0813
1.50	0.00000	0.0581	0.0774	0.0853	0.0892	0.0927	0.0947	0.0958	0.0963	0.0965	0.0966
1.75	0.00000	0.0671	0.0893	0.0984	0.1029	0.1069	0.1092	0.1105	0.1110	0.1113	0.1114
2.00	0.00000	0.0757	0.1007	0.1110	0.1161	0.1206	0.1231	0.1246	0.1252	0.1255	0.1256
2.25	0.00000	0.0840	0.1118	0.1231	0.1287	0.1338	0.1366	0.1382	0.1388	0.1392	0.1393
2.50	0.00000	0.0920	0.1223	0.1348	0.1409	0.1464	0.1494	0.1512	0.1519	0.1523	0.1524
3.00	0.00000	0.1069	0.1421	0.1565	0.1636	0.1700	0.1735	0.1756	0.1764	0.1768	0.1769
3.50	0.00000	0.1204	0.1601	0.1762	0.1842	0.1914	0.1954	0.1977	0.1986	0.1991	0.1992
4.00	0.00000	0.1326	0.1763	0.1941	0.2029	0.2108	0.2152	0.2177	0.2187	0.2192	0.2194
4.50	0.00000	0.1436	0.1909	0.2103	0.2198	0.2284	0.2331	0.2359	0.2370	0.2376	0.2377
5.00	0.00000	0.1534	0.2041	0.2249	0.2351	0.2444	0.2494	0.2524	0.2536	0.2542	0.2544
6.00	0.00000	0.1700	0.2268	0.2502	0.2617	0.2721	0.2778	0.2812	0.2825	0.2832	0.2834
7.00	0.00000	0.1835	0.2456	0.2712	0.2839	0.2954	0.3017	0.3054	0.3069	0.3076	0.3079
8.00	0.00000	0.1945	0.2613	0.2891	0.3028	0.3153	0.3222	0.3262	0.3278	0.3286	0.3289
9.00	0.00000	0.2035	0.2746	0.3044	0.3191	0.3326	0.3399	0.3443	0.3460	0.3469	0.3472
10.00	0.00000	0.2111	0.2860	0.3176	0.3334	0.3477	0.3556	0.3603	0.3621	0.3630	0.3633
12.50	0.00000	0.2253	0.3086	0.3444	0.3624	0.3788	0.3879	0.3933	0.3953	0.3964	0.3968
15.00	0.00000	0.2351	0.3254	0.3649	0.3848	0.4032	0.4133	0.4193	0.4216	0.4228	0.4232
17.50	0.00000	0.2421	0.3383	0.3810	0.4028	0.4229	0.4340	0.4406	0.4431	0.4444	0.4449
20.00	0.00000	0.2473	0.3485	0.3942	0.4177	0.4393	0.4513	0.4585	0.4612	0.4626	0.4631
22.50	0.00000	0.2513	0.3568	0.4052	0.4302	0.4533	0.4661	0.4737	0.4766	0.4782	0.4787
25.00	0.00000	0.2544	0.3637	0.4147	0.4412	0.4659	0.4796	0.4878	0.4910	0.4926	0.4932
30.00	0.00000	0.2589	0.3744	0.4299	0.4592	0.4867	0.5020	0.5113	0.5148	0.5166	0.5173
35.00	0.00000	0.2619	0.3823	0.4418	0.4736	0.5037	0.5206	0.5308	0.5347	0.5367	0.5374
40.00	0.00000	0.2640	0.3883	0.4513	0.4854	0.5181	0.5366	0.5478	0.5521	0.5543	0.5551
45.00	0.00000	0.2656	0.3930	0.4589	0.4952	0.5304	0.5505	0.5626	0.5673	0.5698	0.5706
50.00	0.00000	0.2667	0.3967	0.4653	0.5037	0.5413	0.5630	0.5763	0.5814	0.5841	0.5850
60.00	0.00000	0.2683	0.4021	0.4750	0.5169	0.5590	0.5838	0.5991	0.6051	0.6083	0.6094
80.00	0.00000	0.2699	0.4082	0.4868	0.5338	0.5826	0.6125	0.6314	0.6389	0.6429	0.6442
100.00	0.00000	0.2707	0.4114	0.4933	0.5434	0.5966	0.6298	0.6511	0.6596	0.6642	0.6657
200.00	0.00000	0.2718	0.4161	0.5034	0.5588	0.6199	0.6592	0.6850	0.6954	0.7010	0.7029

[a] Values of f for α-values above 60 are of uncertain validity. See appendix.

and

$$f(\alpha, R)=\frac{16\pi R}{5}[(\sum_{j=1}^{\infty} R^{j-1}a_{11,j})^2+(\sum_{j=1}^{\infty} R^{j-1}b_{11,j})^2]^{\frac{1}{2}}. \quad (15)$$

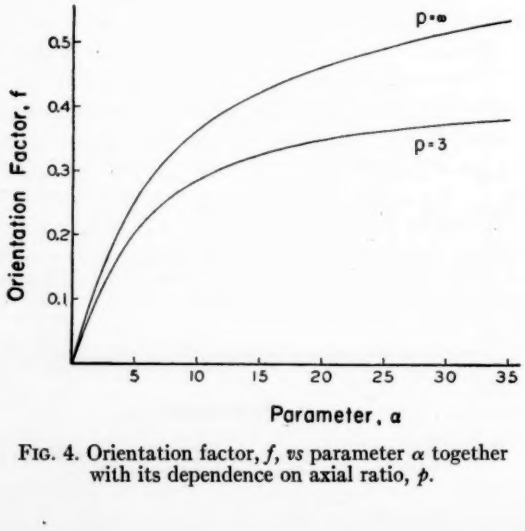

FIG. 4. Orientation factor, f, *vs* parameter α together with its dependence on axial ratio, p.

Heretofore, these equations have been useful for valid computation only in the following limiting forms which hold for $\alpha<1.5$,

$$\chi=\frac{\pi}{4}-\frac{\alpha}{12}\left[1-\frac{\alpha^2}{108}\left(1+\frac{24R^2}{35}\right)+\cdots\right], \quad (16)$$

$$f(\alpha, R)=\frac{\alpha R}{15}\left[1-\frac{\alpha^2}{72}\left(1+\frac{6R^2}{35}\right)+\cdots\right]. \quad (17)$$

By machine computation of the $a_{11,j}$ and $b_{11,j}$ terms, the sums which appear in Eqs. (14) and (15) have been evaluated for values of α up to $\alpha=200$. At these high α-values χ has fallen practically to zero from the initial value of 45° at $\alpha=0$. However, f is still significantly far from its saturation value f_∞, which it would have at $\alpha=\infty$. The convergence of these series is much more dependent upon the rate of decrease of the values of the $a_{11,j}$ and $b_{11,j}$ terms, as j increases, than upon the decreasing values of R^{j-1}, especially since R approaches

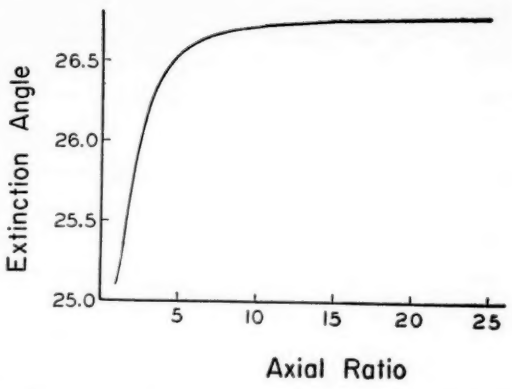

FIG. 5. Dependence of extinction angle on axial ratio for $\alpha=5$.

unity very rapidly as p increases.[28] A short discussion of the behavior of the coefficients is given in the Appendix. These series were evaluated for various values of the axial ratio, p, and the data are summarized in Tables I and II. The greater dependence on p at low p values is immediately apparent and is, of course, a consequence of the rapidity with which R approaches unity as p increases. χ and f become insensitive to p at about $p=16$, where they differ by very little from their values for the case $p=\infty$. By far the greatest dependence on p occurs below $p=10$. These results are illustrated graphically in Figs. 3–6.

The values in Tables I and II are given for prolate ellipsoids ($p>1$). However, the curves for an oblate ellipsoid of axial ratio $1/p$ are identical with those of a prolate ellipsoid of axial ratio p. This ratio enters into Eqs. (14) and (15) only through the function R. From Eq. (1) it is clear that when p changes to $1/p$, R changes sign: $R(p)=-R(1/p)$. However, in the summations $\sum R^{j-1}a_{11,j}$ and $\sum R^{j-1}b_{11,j}$, only the a and b coefficients for which j is odd have values different from zero. Hence, only even powers of R enter into the summations, from which it follows that $\chi(\alpha, p)=\chi(\alpha, 1/p)$, and $f(\alpha, p)=-f(\alpha, 1/p)$.[29] These relations were clearly recognized by Peterlin and Stuart[22] (see their figures for χ and f as functions of α), but not explicitly stated by them. From Eq. (14),[30]

$$\lim_{R\to 0}\tan 2\chi=\frac{-b_{11,1}}{a_{11,1}}\frac{6}{\alpha}=-\frac{6}{\alpha}. \tag{18}$$

The equation $\lim_{\alpha\to 0}\tan 2\chi=6/\alpha$, which had already been derived by Boeder[20] for the case of thin rods ($R=1$), becomes identical with Eq. (16) as α approaches zero.

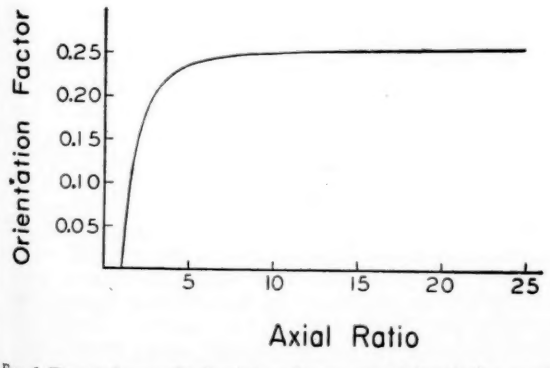

FIG. 6. Dependence of orientation factor on axial ratio for $\alpha=5$.

[29] The change of sign in the equation for f, when p changes to $1/p$, is due to the factor R before the parentheses in Eq. (15).

TABLE III. Values of $-\Sigma a_{11,j}$ as function of j for various values of α.

j \ α	25	40	60	100	200
1	0.037622	0.038913	0.039395	0.039646	0.039753
3	0.045133	0.048785	0.050268	0.051071	0.051419
5	0.046291	0.052465	0.055325	0.056967	0.057700
7	0.045537	0.053452	0.057790	0.060498	0.061765
9	0.044715	0.053261	0.058821	0.062630	0.064509
11	0.044315	0.052705	0.059032	0.063820	0.066313
13	0.044244	0.052205	0.058871	0.064424	0.067487
15	0.044290	0.051896	0.058608	0.064699	0.068260
17	0.044338	0.051754	0.058368	0.064802	0.068783
19	0.044361	0.051713	0.058191	0.064821	0.069127
21	0.044367	0.051715	0.058079	0.064804	0.069338
23	0.044366	0.051729	0.058013	0.064771	0.069460

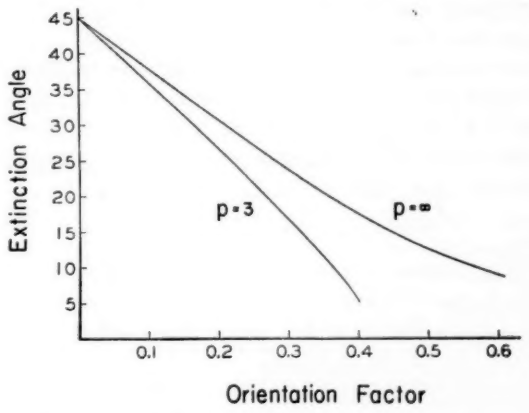

FIG. 7. Extinction angle *vs* orientation factor together with its dependence on axial ratio.

TABLE IV. Values of $\Sigma b_{11,j}$ as function of j for various values of α.

j \ α	25	40	60	100	200
1	0.009029	0.005837	0.003939	0.002379	0.001193
3	0.015774	0.010806	0.007460	0.004560	0.002298
5	0.019813	0.014767	0.010583	0.006605	0.003359
7	0.021399	0.017518	0.013207	0.008500	0.004385
9	0.021545	0.019029	0.015137	0.010092	0.005295
11	0.021256	0.019628	0.016389	0.011325	0.006051
13	0.020927	0.019723	0.017107	0.012225	0.006651
15	0.020828	0.019616	0.017461	0.012848	0.007110
17	0.020818	0.019482	0.017597	0.013258	0.007451
19	0.020833	0.019383	0.017620	0.013519	0.007699
21	0.020844	0.019328	0.017595	0.013677	0.007874
23	0.020849	0.019303	0.017563	0.013768	0.007997

[30] $a_{11,1}=-\frac{1}{8\pi}\frac{1}{1+36/\alpha^2}$, and $b_{11,1}=\frac{3}{4\pi\alpha}\frac{1}{1+36/\alpha^2}$.

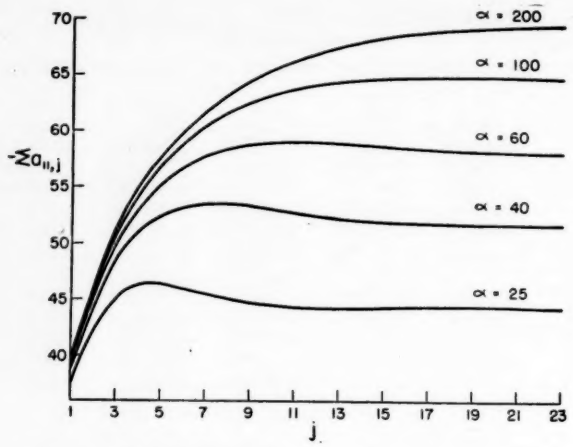

FIG. 8. $-\Sigma a_{11,j}$ as function of j for various values of α.

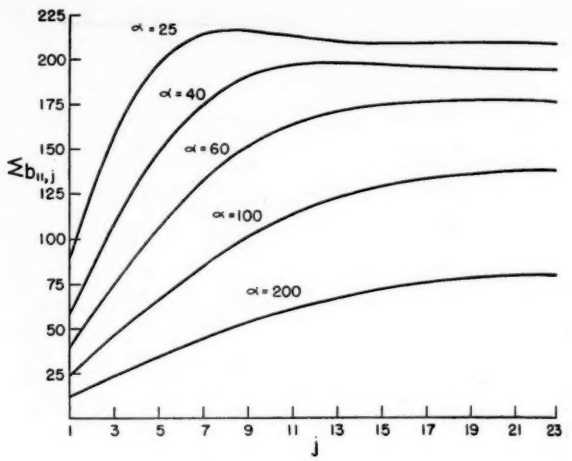

FIG. 9. $\Sigma b_{11,j}$ as function of j for various values of α.

Thus in all cases, when α approaches zero and the degree of orientation becomes very small, f approaches zero, and $\tan 2\chi = 6/\alpha$. This holds for all p values, and, in the limiting case where p approaches 1—that is, the ellipsoid approaches a sphere—these relations hold also for all values of α.

If experimental values of χ *vs* Δn are plotted, the data may be fitted by a theoretical curve of χ *vs* kf, where k is an adjustable constant used to fit the data to the curve. When determined, it gives the optical factor $(g_1 - g_2)$, since

$$k = 2\pi c(g_1 - g_2)/n. \tag{19}$$

If this procedure is adopted, it is unnecessary to extrapolate to low α-values where the experimental errors are large.[9,10] The nature of the χ *vs* f curve and its dependence on p is shown in Fig. 7.

Some question may arise as to the validity of the Peterlin and Stuart solution, especially since the viscosity problem, treated by Peterlin with the same distribution function, is at variance with the results of Simha,[31,32] whose treatment is considered to be the valid one.[33] The Simha treatment of viscosity is also identical with that of Kuhn and Kuhn[34] for low gradient. However, the disagreement in the viscosity theories does not arise from the use of an incorrect distribution function,[35] but rather from Peterlin's omission of certain terms in the hydrodynamic equations, which were taken into account by Simha. Thus, the inadequacy of the viscosity theory in no way affects the valid use of this distribution function for the treatment of double refraction of flow.

If the omitted terms were taken into account, Peterlin's viscosity treatment would presumably be valid. During the course of the computation in connection with the present problem numerous other coefficients besides the $a_{11,j}$ and $b_{11,j}$ terms were evaluated. The availability of these additional terms may be of use for a viscosity theory formulated on a similar basis.

APPENDIX. BEHAVIOR OF $a_{11,j}$ AND $b_{11,j}$ TERMS[28]

To be sure that the limiting values of the slowly converging series were obtained, it is necessary to know the magnitude of the uncomputed terms. Although no accurate estimate of the size of the remainder terms could be made, some idea of the rate of convergence of these series at high α values may be obtained from the data of Tables III and IV, where the values of the $-\Sigma a_{11,j}$ and $\Sigma b_{11,j}$ series are given for several values of α. These data are also plotted in Figs. 8 and 9. It will be noted that the b terms converge much more slowly than do the a terms. It will also be noted that the series for $\alpha = 200$ and $\alpha = 100$ clearly have not converged. For infinite p and large α the proportional error in χ is approximately equal to the proportional error in the series of $b_{11,j}$ terms, while the proportional error in f is approximately equal to that in the series of $a_{11,j}$ terms.

It is felt that, for $\alpha \leqq 60$, the error that has been committed is well under 1 percent, but that, for $\alpha = 80$, 100, or 200, the results listed in Tables I and II are significantly in error for all but the very small values of p. These "bad" results have been included in the tables in the hope that they may shed some light on the question of convergence. If they had been included in Fig. 7, for the case $p = \infty$, they would lie significantly lower than the curve shown, so that the extrapolated value of f at $\chi = 0$ would be about 0.75 instead of the value 1 as it should be and as, in fact, it appears to be when the values at $\alpha = 80$, 100, and 200 are omitted.

It is believed that no error has been made at any stage of the computation except in the truncation of the series of $a_{11,j}$ and $b_{11,j}$ terms. Thus, it is felt that the results contained in Tables I and II are entirely accurate within the number of figures reported when either α or p is very small, and are probably accurate to well within 1 percent in all cases except when $\alpha = 80$, 100, or 200.

[31] R. Simha, J. Phys. Chem. **44**, 25 (1940).
[32] F. Eirich, Repts. Prog. Phys. **7**, 329 (1940).
[33] Personal communications with Onsager, Peterlin, and Simha.
[34] W. Kuhn and H. Kuhn, Helv. Chim. Acta **28**, 97 (1945). See especially Eqs. (73) and (74). The recent important paper of J. G. Kirkwood and P. L. Auer, J. Chem. Physics **19**, 281 (1951), should also be consulted in this connection.
[35] This distribution function appears to be correct although its convergence has not been established. An indication of the possibility of the convergence was obtained during the computation procedure.

Studies on Tellurium-Selenium Alloys*

E. GRISON†
Laboratory for Insulation Research, Massachusetts Institute of Technology, Cambridge, Massachusetts
(Received April 30, 1951)

Tellurium and metallic (hexagonal) selenium were shown to give solid solution in any concentration. The variation of the cell dimensions with composition departs only slightly from linearity: c shows a certain tendency to contraction (this corresponds to a smaller valency angle in the chains of atoms than is required by a linear variation): a varies much less (2 percent between Se and Te) and in a manner which depends upon the preparation of the alloy (as already observed for pure selenium by H. Krebs).

The presence of sharp $(hk \cdot l)$ lines with $l \neq 0$ in all the alloys suggests that these must be composed not of homogeneous chains (i.e., Se chains, Te chains packed together), but of composite chains, in which the homogeneous sequences must be fairly short.

I. INTRODUCTION

VON HIPPEL[1] has pointed out that in the sequence of elements in the VI_b group in the periodic table, S, Se, Te, Po, the physical properties gradually change from those of an insulator (sulfur) to those of a metal (polonium). In a parallel manner, the intermolecular binding goes from the simple van der Waals to the metallic bond: thus in polonium each atom is surrounded by six equidistant neighbors, whereas in sulfur each atom has two nearest neighbors, covalently bound, and four next neighbors. The intermediate elements, the semiconductors Se and Te, are isomorphous and their atomic arrangement is shown in Fig. 1.

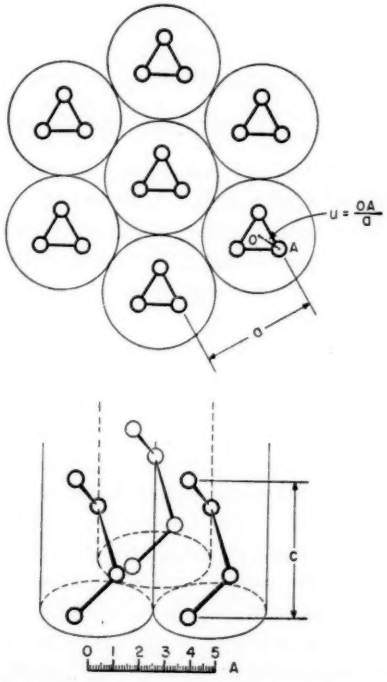

FIG. 1. Structure of metallic selenium and tellurium.

It consists of infinite chains of atoms spiraling around the c axis, the bonding between neighboring atoms in the same chain being covalent. Between atoms belonging to neighboring chains, the bonding seems to be intermediate between the metallic bond (as found in polonium) and the van der Waals contact (as found in sulfur).

Solid solutions of Se and Te form a continuous link in the transition from insulators to metals, and we may expect that a better knowledge of the properties of these solutions will be of interest for the understanding of the properties of this class of semiconductors.

The existence of these solutions for every concentration has been hitherto questioned. There exists conflicting evidence,[2] but the discovery of natural crystals isomorphous with tellurium and selenium and containing 30 percent Se and 70 percent Te,[3] and the solidification curve of Se-Te mixtures as given by Pellini[4] (Fig. 2) are very strong indications in favor of the miscibility of these elements in all proportions. It must be realized that these solid solutions are of a special kind which cannot be compared to the familiar types of solid solutions where an atom in a metal, or an ion or a

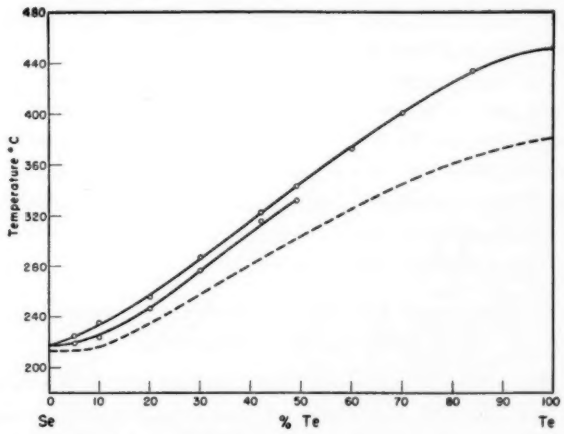

FIG. 2. Liquidus-solidus curves of Te-Se alloys.

* Sponsored by the ONR, the Army Signal Corps, and the Air Force under ONR Contract N5ori-07801. A more detailed description of this work, with tables, under the same title, is given in Technical Report XXXVIII, ONR Contract N5ori-07801, Lab. Ins. Res., M.I.T., March, 1951.

† Present address, Laboratoire Central des Services Chimiques de l'État, Paris.

[1] A. von Hippel, J. Chem. Phys. **16**, 372 (1948).

[2] Gmelins Handbuch der anorganischen Chemie, 8th edition (1940), system number 11, p. 361.

[3] E. S. Dana and H. L. Wells, Am. J. Sci. [3] **40**, 78 (1890).

[4] G. Pellini and G. Vio, Gazz. chim. ital. **36**, Pt. 2, 469 (1906).

molecule in an ionic or molecular lattice is replaced by an atom, ion, or molecule of the solute. Since Se and Te are infinite chain polymers, these alloys must be either a mixture of these polymers, or a copolymer, involving a covalent bond Te-Se.

II. PREPARATION OF Te-Se Alloys

Mixtures of tellurium‡ and selenium,‡ in proportions varying from 10 to 90 percent by steps of 10 percent were enclosed in vacuum-sealed Pyrex tubes.

A first set of samples was heated in sequence in an oven at 500°C for 3 hours. From time to time the tubes were shaken thoroughly in order to insure good homogeneity. A second set was heated as a group at the same temperature for 24 hours. At the end of this time the tubes were quenched as rapidly as possible.

The alloys, after cooling or quenching and subsequent grinding, give an x-ray powder pattern consisting of broad and blurred lines. To increase the degree of order in their structure, annealing was required.

The most favorable conditions for this annealing treatment have been determined empirically. If the temperature rises above a certain value (indicated in Fig. 2 by the dotted line), sintering takes place, and monocrystalline grains grow very rapidly. It is therefore necessary to keep the samples below this temperature. Although varying the annealing time has not been systematically studied, it was found that longer annealing times are required for alloys which are richer in Se. A pure tellurium powder after annealing for only 2 hours will give sharp x-ray lines up to high diffraction angles; on the other hand, Krebs[5] has shown that annealing times up to 3 weeks were necessary in the case of pure selenium to achieve a much inferior result. In practice, we have limited ourselves to annealing times ranging from 3 hours (for 90 percent Te) to 2 days (for 10 percent Te).

Grinding of the specimen causes a broadening of the lines. This has been checked on alloys which were annealed and then ground again.

The temperature at which the alloy has been prepared has no effect on the final pattern. For instance, the 66 percent Te alloy was heated in a vacuum-sealed Vycor tube in one case for 3 hours at 1000°C, in another case 24 hours at 800°C and in a third, 67 hours at 390°C. No systematic change in the unit-cell dimensions or in the x-ray pattern could be detected.

III. VARIATION OF THE UNIT-CELL DIMENSIONS WITH CONCENTRATION

The x-ray powder patterns confirm the indications of the thermal analysis: tellurium and selenium are miscible in all proportions and these solutions form a continuous transition from one element to the other. We may therefore expect to find a continuous variation of the unit cell dimensions, a and c.

A. Method of Measurement

The x-ray patterns have been recorded with the Philips camera of diameter 114.6 mm, using CuKα radiation. The photographic film is mounted in this camera according to the Straumanis method in order to eliminate the error due to the shrinkage of the film. However, as the alloys give only broad lines in the region of "back-reflection," we were not able to take full advantage of this technique and therefore had to assume a constant value for the effective camera circumference, based on an average of values obtained in previous determinations.

In order to eliminate, as far as possible, systematic errors induced by eccentric mounting of the sample, absorption, etc., we chose the method of Cohen[6] as modified by Heavens and Cheesman.[7] The least squares treatment was applied to observational equations (one for each x-ray line) put into the following form for hexagonal symmetry:

$$As^2+Cl^2+Df(\theta)=\sin^2\theta_{\text{obs}},$$

where l is the l index of the $(hk\cdot l)$ reflection observed at a glancing angle θ_{obs}; s^2 is equal to h^2+hk+k^2; A, C, and D are the unknowns; A and C are functions of the unit cell dimensions a and c, $A=\lambda^2/3a^2$, $C=\lambda^2/4c^2$ (λ, wavelength of the X radiation); D is an unknown numerical constant; and $Df(\theta)$ is the systematic error which affects $\sin^2\theta$. The function $f(\theta)$ is

$$f(\theta)=(\sin^2 2\theta)(1/\theta+1/\sin\theta).$$

This function, determined empirically by Nelson and Riley[8] and justified theoretically by Taylor and Sinclair,[9] gives the best correction of the systematic errors. The average value of D from 19 x-ray patterns of the annealed alloys has been found to be 3.7×10^{-4}. For this value of D, and for the maximum value 3.0 of $f(\theta)$ reached when $\theta=35°$, the systematic error in $\sin^2\theta$ is 11×10^{-4}, whereas the accidental error to be expected from the measurement of the angle θ in reading the position of the lines on the film does not exceed 4×10^{-4} for $\sin^2\theta$, in the neighborhood of $\theta=35°$, where most of the observed lines are situated.

The root-mean-square of the residuals of the observational equations stays around a value $\Delta\sin^2\theta=2.3\times10^{-4}$.

The uncertainties in the unknowns A, C, and D may be computed from the residuals. The uncertainty ΔD of D appears to range from 0.4 to 1.0×10^{-4}, a significant fraction of the value of D itself. From the uncertainties in A and C, the uncertainties in a and c

‡ High Purity Grade, American Smelting and Refining Company, New York.

[5] H. Krebs, Z. Physik **126**, 769 (1949).

[6] M. U. Cohen, Rev. Sci. Instr. **6**, 68 (1935).

[7] O. S. Heavens and G. H. Cheesman, Acta Cryst. **3**, 197 (1950).

[8] J. B. Nelson and D. P. Riley, Proc. Phys. Soc. (London) **57**, 160 (1945).

[9] A. Taylor and H. Sinclair, Proc. Phys. Soc. (London) **57**, 126 (1945).

can be computed. These are found to range from 0.001 to 0.004A. But the systematic error $Df(\theta)$ being important and its correction being subject to a fairly large uncertainty, as shown above, it seems reasonable to set the upper limit of error in a and c at 0.004 and 0.008A, respectively (the errors in A and C being the same, the error in c will be double that in a, as is easily seen from the formulas relating a and A, c, and C).

B. Results of the Measurements

The measurements of the unit-cell dimensions a and c for alloys of various concentrations are shown in Figs. 3 and 4. It will be noted that: (1) it is possible in the case of annealed alloys (open circles in the figures) to draw a continuous curve for the variation of c which fits closest to the experimental values within the limits of error discussed above. This curve falls below the straight line joining the extreme values for Te and Se. (2) It is impossible to draw a corresponding curve for the a axis, even in the case of the annealed alloys. The values obtained for a lie, on the average, above the straight line which joins the two extremes, and below the dashed curve. This curve represents the theoretical variation of a, which should result when c varies according to the experimental curve given above, and when Vegard's law§ is obeyed. (3) In the case of the quenched alloys, the excessive scattering of the experimental points makes it impossible to drawn any consistent curve for the variation of a or c. Nevertheless one can observe that the values of c are systematically larger than for the same alloy after annealing.

These results may be compared with the observation of Krebs[5] that the length of the c axis of pure selenium varies very little with different thermal treatments, whereas the a axis shows a much wider variation. It is apparently the same for the tellurium-selenium alloys: the variation of c is regular, while the variation of a exhibits irregularities.

IV. INTERPRETATION OF THE EXPERIMENTAL RESULTS. STRUCTURE OF THE ALLOYS Te-Se

We have seen that the isomorphous structures of Te, Se, and their alloys, consist of infinite chains of atoms bound to their two nearest neighbors by covalent bonds, the axis of these chains being parallel with the c axis.

The structure of these alloys can be described in terms of two alternate hypotheses: (1) homogeneous chains consisting of one kind of atom only. The alloy would then be a true solid solution of selenium chains and tellurium chains adjacent to each other. (2) Compound chains containing covalent bonds Te-Se. In this case, the alloy would be a true copolymer and the question arises as to what the average length of the homogeneous chain sections would be.

Let us first consider hypothesis (1).

§ The volume of the unit cell varies linearly with the concentration.

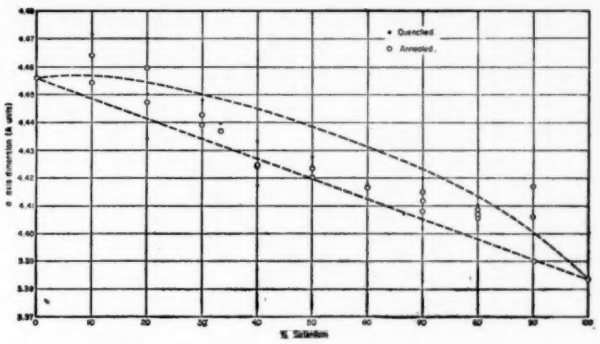

FIG. 3. Variation of the a axis dimension with concentration.

In the x-ray pattern of annealed alloys all the lines up to $\theta=50°$ are equally sharp, which indicates that the lattice is ordered in all three dimensions. This would not exclude random displacements of the atoms from an average position, as is the case in the solid solution of two metals of different atomic radii.

The c dimensions of Te and Se differ by 20 percent; therefore, if chains of Te and Se were placed, undistored and in random fashion, next to one another (Fig. 5), this random packing of homogeneous chains could not give an x-ray pattern with $(hk\cdot l)$ lines in which $l\neq 0$. The $(00\cdot l)$ lines would be "one-dimensional lines" arising from the incoherent superposition of the intensities scattered by the single chains. This is obviously not what we observe.

We may now imagine that neighboring chains of tellurium and selenium might be distorted by this

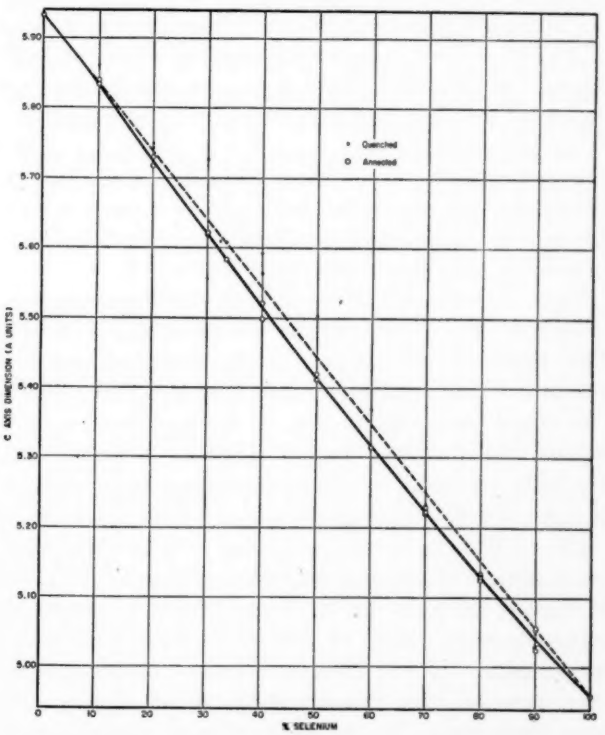

FIG. 4. Variation of the c axis dimension with concentration.

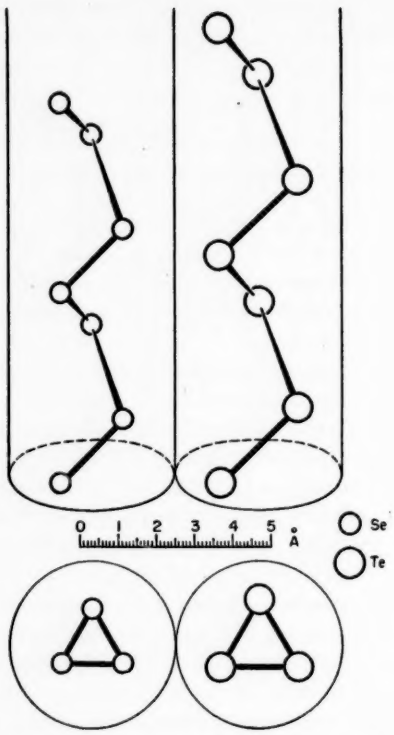

FIG. 5. One chain of tellurium and one of selenium.

proximity in such a way that the tellurium chain would contract and the selenium chain expand to the same c value. A simple computation shows that, in the case of an equimolecular alloy having a value of $c=(C_{Te}+C_{Se})/2$, the contraction of the valency angle of tellurium would be from 102° to 98°, and the expansion of that of selenium from 105° to 113°. The diameter of such distorted chains (a-axis dimension) would be 4.65 and 4.28A for Te and Se, respectively. If we imagine each chain enclosed in a cylinder of diameter a (see Fig. 1), we would then have a packing of cylinders with diameters differing by 9 percent but having the same period along the c axis. Such a structure would give sharp lines, as was observed.

Such deformations of the valency angle as were considered for the 50–50 mixture are physically possible. The difference in diameter of the cylinders remains within the limits tolerated by solid solutions of metals. For alloys very rich in one of the constituents, the required distortions would, however, become appreciably greater: a solution containing a small amount of tellurium would require a contraction of the valency angle to 91°, and one containing a correspondingly small amount of selenium would have to stretch to 124°. Moreover, these distortions would be due to the interaction between chains of two kinds, and if the local concentration of one element happens to be greater than average, thus concentrating chains of only one type, these would tend to return to their normal shape. Hence one should observe fluctuations in the value of c giving rise to a broadening of the $(hk\cdot l)$ lines, and this broadening should be enhanced by the annealing process. The opposite is observed: annealing reduces the fluctuations of c. In terms of the distortion hypothesis this could be explained only by the unreasonable assumption that annealing leads to tension instead of releasing it.

Thus the more reasonable hypothesis seems to be that the alloy is a copolymer. If, in this case, the homogeneous sequences along the chains are long, we are led to the same structure and the same objections as above. Such long periods would result if the average length of the selenium chains, estimated by Krebs and Morsch[10] to be 100 atoms in the molten state, would remain intact in the solid solution.

We, therefore, limit ourselves to the case where homogeneous sequences are short, so that in neighboring chains the atoms remain close to an "average" position, without any deformation of the chain. For instance, in the equimolecular alloy, where the value of c differs by 10 percent from that of each constituent, homogeneous sequences of more than 4 or 5 atoms could not exist without the definition of "average" position losing its physical meaning (Fig. 6).

The x-ray pattern will then show sharp lines. The diameters of the cylinders would differ by less than 2 percent, and the c periods would adjust themselves automatically.

On quenching, the cylinders would pack closely in good order, as their diameters are almost the same, but the helixes might not have exactly the same pitch. This would explain why the x-ray pattern would then show sharp $(hk\cdot 0)$ lines, and increased broadening of $(hk\cdot l)$ lines for increasing l values. The annealing proc-

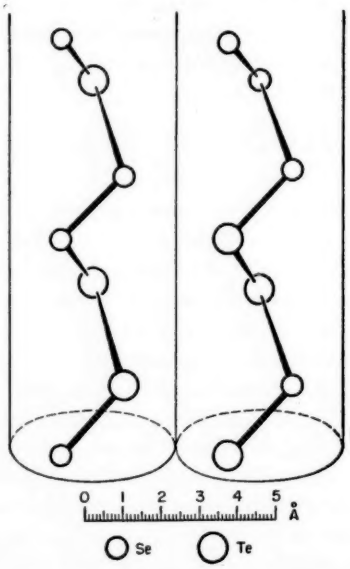

FIG. 6. Alloys Se-Te: compound chains with random sequence (composition *ca* 50 percent).

[10] H. Krebs and W. Morsch, Z. anorg. u. allgem. Chem. **263**, 305 (1950).

ess would relieve the tensions between chains by aligning their atoms closer to the "average" positions.

This second hypothesis seems the more likely because it does not require any extensive deformation of the chains. In addition, the existence of a Te-Se covalent bond appears very probable. We know that the selenium chains may break and recombine, even at room temperature, in the process of crystallization of amorphous selenium, or in the transition from the β-modification to metallic selenium. It is therefore likely that in the liquid state these chains could break and recombine with tellurium chains, especially as a Se-Te bond will be slightly more stable (the difference in electronegativity between these elements is 0.3). The reaction would occur with reasonable speed as soon as the selenium chains have enough mobility. This would explain why the alloys formed at low and high temperatures show no detectable difference.

The results observed for the variation of a and c with concentration can be interpreted in terms of structure as follows: the c dimension depends only upon the valency angle α and the covalent bond length d:

$$c=d\left(3\left[4\sin^2\frac{\alpha}{2}-1\right]\right)^{\frac{1}{2}}.$$

The (apparent) variation of d with concentration must obviously be linear as we cannot assume any change of the bond length Se-Se or Te-Te in the alloy, and as the bond length Se-Te, if present, will be equal to the mean value of the bond lengths Se-Se and Te-Te.

Therefore, assuming a linear variation of d, one can compute the variation of α with concentration. The dashed curve in Fig. 7 gives the variation of α assuming that c varies linearly, while the full curve is computed assuming that c varies according to the curve of Fig. 3. This shows that the chains have a tendency to contract

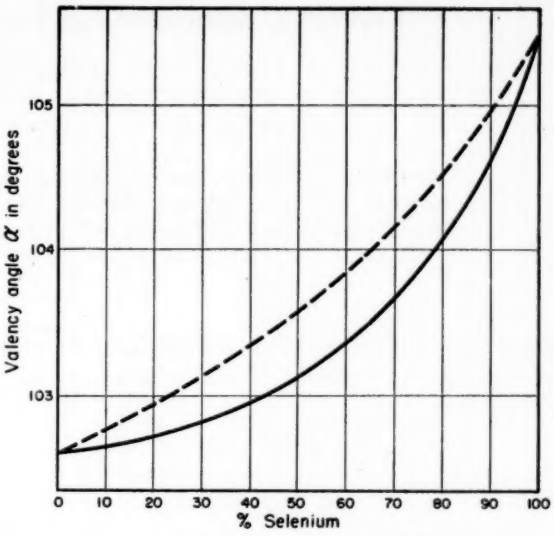

FIG. 7. Variation of apparent valency angle *vs* concentration.

to less than the length required by a linear law. Thus, in quenched alloys the chains are stretched, and the effect of annealing is to allow them to contract.

The systematic discrepancy from Vegard's law shown by Fig. 4, together with the tendency of the alloy to have a higher density, corresponds to a shortening of the van der Waals distance between chains; this shortening is very slight, being smaller than 0.01A.

ACKNOWLEDGMENT

The author wishes to express his thanks to Professor A. R. von Hippel for his continued interest and constant support throughout this work, to Professor B. E. Warren for several very helpful discussions, and to J. Kalnajs for his most competent help and advice in many experimental problems.

Contact Distances of Ion Pairs in the Isomeric Dichloroethanes

KURT H. STERN, FRANK HEALEY, JR.,* AND ARTHUR E. MARTELL
Department of Chemistry, Clark University, Worcester, Massachusetts
(Received May 7, 1951)

The effective dielectric constant of ethylene chloride is calculated from known dissociation constants of various ion pairs in ethylene and ethylidene chloride according to the method of Denison and Ramsey. The average value of the effective dielectric constant is used for the calculation of contact distances of various ion pairs in ethylene chloride. The variation of contact distance with size and structure of the ions is discussed.

THE Bjerrum[1] relationship for the thermodynamic dissociation constant of a uni-univalent electrolyte has the form:

$$K^{-1}=4\pi N/1000(\epsilon^2/DkT)^3Q(b)$$

$$Q(b)=\int_z^b e^y y^{-4}dy$$

$$b=\epsilon^2/(aDkT),$$

where K is the dissociation constant, D is the macroscopic dielectric constant of the medium, a is the contact distance (distance between centers of charge) of the two oppositely charged ions, and $y=\epsilon^2/(rDkT)$. The other symbols have their usual meaning. Bjerrum assumed the ions to be rigid spheres in a medium of uniform dielectric constant. On the basis of these assumptions deviations would be expected for systems which differ from this model.

The isomeric dichloroethanes offer an example of the way in which two apparently similar solvents may behave differently with respect to the dissociation of electrolytes. The molecules of ethylidene chloride are known to exist in only one form. On the other hand, Mizushima *et al.*[2] have recently estimated the ratio of ethylene chloride molecules in the gauche form (having an angle of 60° between the C−Cl bonds when the molecule is viewed in the direction of the C−C bond) to those in the *trans*-form to be 1.3:1 at 25°C in the liquid solvent. It is to be expected that the more polar (gauche) isomer is present in larger proportion about an ion than in the body of the solution. These isomeric solvents, therefore, afford a convenient comparison of two media which differ from the Bjerrum model in that one is much less uniform than the other with respect to the dielectric.

In a recent communication Denison and Ramsey[3] used the dissociation constants of ion pairs in ethylene and in ethylidene chlorides in the light of the ion-association theory of Bjerrum[1] and Fuoss and Kraus[4] to calculate an "effective" dielectric constant for ethylene chloride which differed appreciably from the ordinary, or "macroscopic", dielectric constant. Although these isomeric solvents have nearly the same bulk dielectric constants, and even though Walden's rule holds almost exactly for a number of salts in these solvents,[5]† the dissociation constants of ion pairs calculated by the method of Fuoss and Kraus[6] are much greater in ethylene chloride than in ethylidene chloride. Thus dissociation constants have been reported by Denison and Ramsey to be from seven- to tenfold greater in ethylene chloride than in ethylidene chloride. Also, similar data reported more recently by two of us[5] for other salts indicated dissociation constants in most cases to be about five times greater in ethylene than ethylidene chloride, except for tetraethylammonium nitrate which gave a ratio of ten to one. It was first pointed out by Ramsey and Colichman[7] that the usual interpretation of the differences of ionic association constants in terms of differences in a values did not seem to apply here on the basis of differences in dipole moments and polarizabilities of the two solvents. Later, from the known existence of two isomers of ethylene chloride, Denison and Ramsey[2] were led to the conclusion that the gauche molecules (of ethylene chloride) were attracted preferentially by ions in this solvent. This enhancement of the relative population of the gauche form of ethylene chloride in the vicinity of an ion over the average population in the pure solvent, would make the effective dielectric constant in ethylene chloride greater than the macroscopic dielectric constant of this solvent. Thus the measured K value would be greater than that calculated by the Bjerrum equation. Also of interest in this connection is the suggestion by Healey and Martell[5] that the differences in behavior of these two solvents might be due, at least in part, to (1) the greater polarizability of ethylene chloride and (2) the partial fixation of ethylene chloride

* Present address: Department of Chemistry, Lehigh University, Bethlehem, Pennsylvania.

[1] N. Bjerrum, Kgl. Danske Videnskab, Mat.-fys. Medd. **7** No. 9 (1926).

[2] Mizushima, Morino, Watanabe, Simanouti, and Yamaguchi, J. Chem. Phys. **17**, 591 (1949).

[3] J. T. Denison and J. B. Ramsey, J. Chem. Phys. **18**, 770 (1950).

[4] R. M. Fuoss and C. A. Kraus, J. Am. Chem. Soc. **55**, 1019 (1933).

[5] F. H. Healey and A. E. Martell, paper to be presented, Division of Physical and Inorganic Chemistry, General Meeting of the American Chemical Society, Chicago, Illinois, September, 1950. (Also see F. H. Healey and A. E. Martell, J. Am. Chem. Soc. **73**, 3296 (1951).)

† Adherence to Walden's rule indicates that the ionic radii are nearly the same in these solvents.

[6] R. M. Fuoss and C. A. Kraus, J. Am. Chem. Soc. **55**, 476 (1933). R. M. Fuoss, *ibid.*, **57**, 488 (1935).

[7] J. B. Ramsey and E. L. Colichman, J. Am. Chem. Soc. **69**, 3041 (1947).

dipoles in the vicinity of an ion. The latter suggestion involves an increase of the gauche forms of ethylene chloride when ions are present, whereas Denison and Ramsey suggest a redistribution of the forms already present. Thus it has been recognized for some time by those working in this field, that it is necessary to look further than merely to the dielectric constant of a solvent in estimating or predicting its ionizing power, and that constitutive factors, such as dipole moment, polarizability and steric effects play an important part.

In view of these findings and implications, it was considered of interest to use our data along the lines suggested by Denison and Ramsey. In Table I are listed the calculated contact distances of ion pairs (distances of closest approach) of various salts in ethylidene chloride. These were calculated from the dissociation constants previously reported using the treatment of Bjerrum[3] and of Fuoss and Kraus.[4] It was possible to make a comparison with ethylene chloride in six cases. Dissociation constants in ethylene chloride of tetraethyl-, tetrapropyl-, tetrabutyl- and tetraamylammonium picrates and of tetraethylammonium nitrate have been given by Tucker and Kraus[8] while that of octadecyltrimethylammonium picrate was recently reported by Pickering and Kraus.[9] No data on ethylene chloride are available for the remaining salts listed.

TABLE I. Determination of *D*-effective of ethylene chloride.

Salt	Contact distance a in ethylidene chloride	D-effective of ethylene chloride
$(Et)_4NPi$	4.37	11.6
$(Pr)_4NPi$	4.44	12.0
$(Bu)_4NPi$	4.51	11.7
$(Am)_4NPi$	4.57	11.8
Octadecyl $(Me)_3NPi$	3.74	11.5
Octadecyl $(Bu)_3NPi$	4.60	
$(Et)_4NCNS$	3.87	
$(Et)_4NClO_4$	4.05	
$(Et)_4NNO_3$	3.70	12.0
		Av. = 11.8

Using the approach of Denison and Ramsey, we assume the "a" value of any salt in ethylene chloride to be the same as that found for the salt in ethylidene chloride, by use of the Bjerrum equation in which the macroscopic dielectric constant of ethylidene chloride is used. With this "a" value and the dissociation constant obtained for the salt in ethylene chloride, the effective dielectric constant of ethylene chloride is calculated by a series of approximations. This is listed in the third column of Table I. The average value of 11.8 is almost identical to that calculated by Denison and Ramsey (11.9), and the individual values agree with those calculated by Denison and Ramsey within the limit of reliability of the equations. The variation of the logarithm of the dissociation constant in ethylidene chloride with "a" is summarized in Fig. 1. The shape of the curve is about what one would expect from the equations employed in calculating "a." The fact that the points lie close to the curve is not a test of either the theory or the data, but rather a reflection of the self-consistency of the calculations.

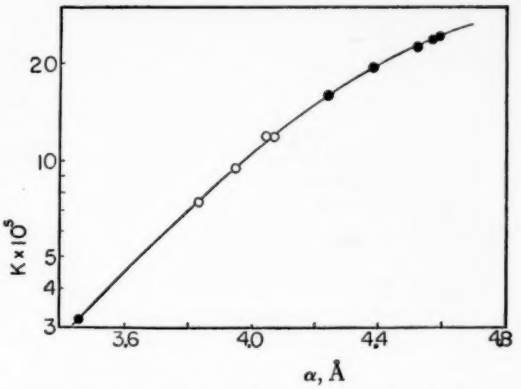

FIG. 1. Variation of dissociation constants of ion pairs with contact distance in ethylidene chloride.

The average value of the effective dielectric constant of ethylene chloride, so obtained, was then used to calculate new "a" values for a large number of salts in this solvent by use of the dissociation constants of these salts reported by Kraus and co-workers.[6,7] The results of these calculations, summarized in Table II, provide ionic contact distances for a number of salts in ethylene chloride for which data are not yet available in ethylidene chloride. The values thus obtained show some interesting relationships. The contact distances of the picrates in ethylene and ethylidene chlorides, and of the nitrates in ethylene chloride increase in the same

TABLE II. Contact distances in ethylene and in ethylidene chlorides.

	Picrates in ethylidene chloride		Picrates in ethylene chloride[a]		Nitrates in ethylene chloride		Picrate-nitrate
Cation	a, A	Δa	a, A	Δa	a, A	Δa	Δa, A
$(Me)_4N^+$			3.46				
				0.79			
$(Et)_4N^+$	4.37		4.25		3.84		0.41
		0.07		0.13		0.11	
$(Pr)_4N^+$	4.44		4.38		3.95		0.43
		0.07		0.14		0.10	
$(Bu)_4N^+$	4.51		4.52		4.05		0.47
		0.06		0.06		0.05	
$(Am)_4N^+$	4.57		4.58		4.10		0.48
				0.07		0.02	
$(IAm)_4N^+$			4.59		4.07		0.52

[8] L. M. Tucker and C. A. Kraus, J. Am. Chem. Soc. **69**, 454 (1947).

[9] H. L. Pickering and C. A. Kraus, J. Am. Chem. Soc. **71**, 3288 (1949).

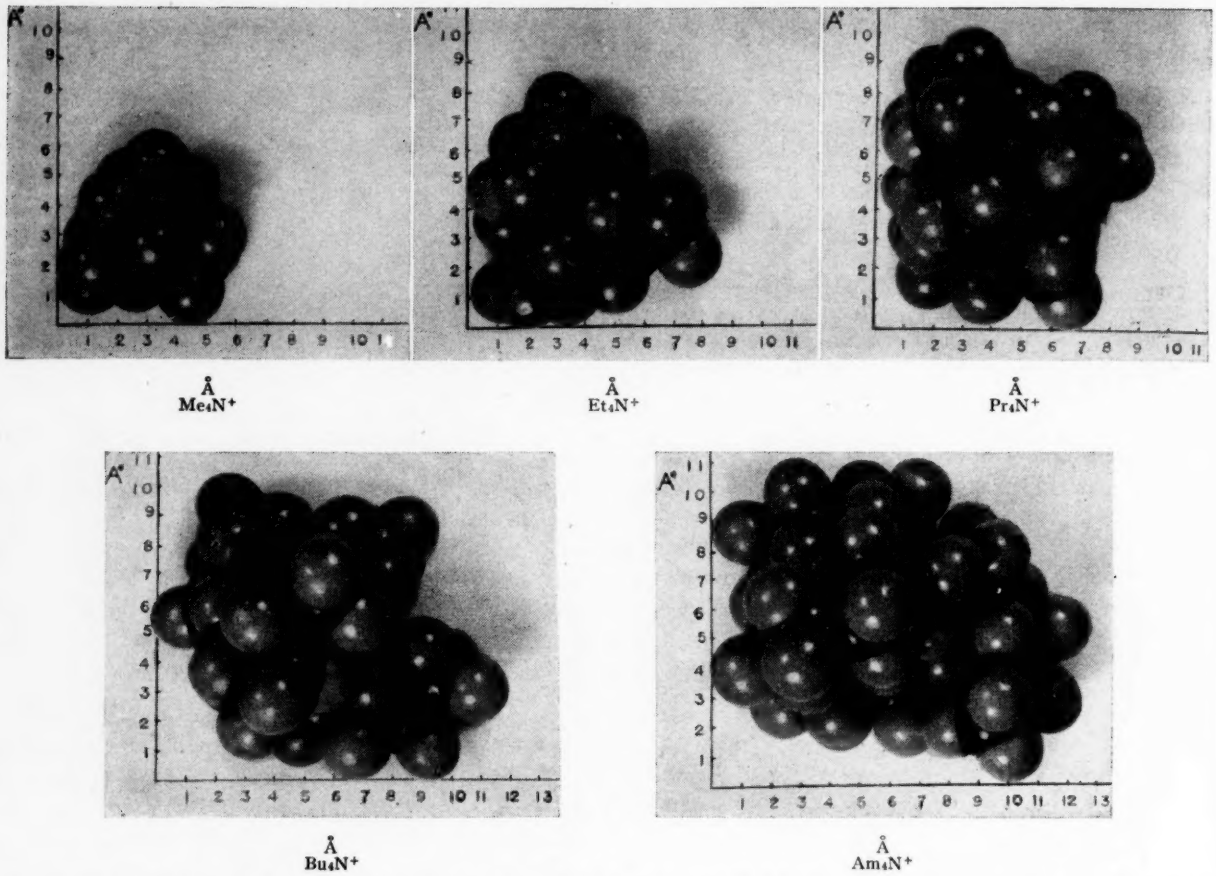

FIG. 2. Models of tetraalkylammonium ions. The carbon chains have been coiled back on each other so as to give the smallest possible ion but so as to retain an approximately spherical shape.

manner with increase in length of the alkyl chain. This increase in contact distance (indicated by Δa-values in Table II) is greatest from methyl to ethyl, and drops off rapidly as the length of the chain increases. It is not readily obvious why the Δa values decrease as rapidly as observed, although a marked effect would be expected. An examination of molecular models of the quaternary ammonium ions indicates, however, that assuming the ions to be relatively spherical, a somewhat different behavior would be observed. In Fig. 2 are illustrated Fischer-Hirschfelder models of symmetrical quaternary ammonium ions with alkyl groups containing one to five carbon atoms. Examination of these models indicates a radius of $\sim$3A for the tetramethylammonium ion, and an increase of about 0.5A for the ethyl, propyl, and butyl derivatives, with smaller increases for higher homologs. If, on the other hand, models are set up with the carbon chains swept back as much as possible from one side of the ion, so as to allow a closer approach of the positive nitrogen to some negative ion, it is found that beyond a slight increase from methyl to ethyl there is no significant difference in these homologous series in the shortest distance between the nitrogen atom and a negative ion. It is seen from the Δa values given in Table II that, in terms of these structural considerations, the alkyl groups exist principally in the "swept-back" form thereby permitting the distance of closest approach of the negative ion to the positive nitrogen atom to be substantially the same in all the tetraalkylammonium salts from ethyl to amyl.

Also of interest are the differences in the contact distances of the quaternary ammonium picrates and nitrates given in Table II. It is seen that there is a significant increase in "a" as the size of the quaternary ammonium ion increases. Assuming as a first approximation that the size of the nitrate ion does not change,‡ it is apparent that the size of the picrate ion increases with a corresponding increase in the size of the positive ion. Since this effect can take place for the ion pairs only, it is probably due to decreased interaction (i.e., less flattening) of the picrate ion with increase in size of the positive ion.

The contact distances in Table I for the tetraalkylammonium picrates are in general agreement with the theoretical predictions of Bjerrum[3] and of Fuoss and Kraus.[4] As the size of the symmetrical cations increases, the distance between the centers of charge in an ion-

‡ The nitrate ion is very much smaller and, hence, less deformable then the picrate ion.

pair would also increase. If Coulomb's law is obeyed, the result will be a decrease in the binding energy between the ions in an ion-pair and a consequent increase in the dissociation constant. Octadecyltributylammonium picrate has the highest "*a*" value of all salts measured, as would be expected. Note, however, that it is only slightly more than that of tetraamylammonium picrate. On the other hand, it is interesting to note that octadecyltrimethylammonium picrate has the lowest "a" value of any *picrate*. Apparently the distance of closest approach of the picrate anion to the charge within the cation is the smallest for this cation, and considerably less than for the tetraethylammonium ion. In this connection it is interesting to note that Kraus[4] found the dissociation constant of methyltributylammonium picrate to be less than that of tetraethylammonium picrate. This may also be possibly interpreted as being due to the approach of the picrate ion to the positive nitrogen at the methyl position. The structure visualized for these three ion pairs is indicated schematically by Fig. 3. The experimental data seem to indicate definite orientation effects in the formation of these ion pairs.

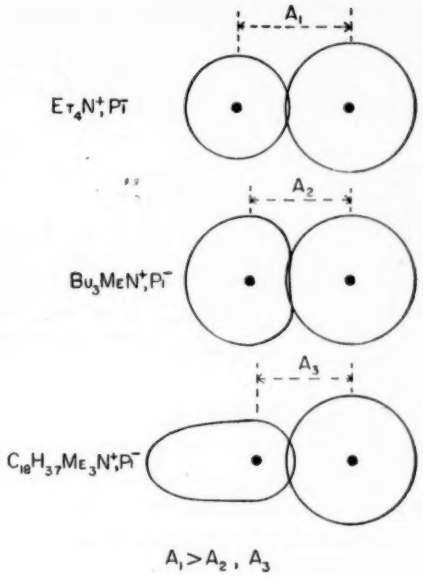

FIG. 3. Schematic comparison of contact distances of selected ion pairs in ethylidene chloride.

ACKNOWLEDGMENT

The authors are greatly indebted to Professor J. B. Ramsey for valuable suggestions and criticism.

THE JOURNAL OF CHEMICAL PHYSICS VOLUME 19, NUMBER 9 SEPTEMBER, 1951

The Analysis of the Infrared Spectrum of Chlorine Monofluoride*

ALVIN H. NIELSEN AND ERNEST A. JONES†
K-25 Laboratories, Carbide and Carbon Chemicals Division, Union Carbide and Carbon Corporation, Oak Ridge, Tennessee, and The University of Tennessee, Knoxville, Tennessee

(Received May 5, 1951)

The vibration-rotation fine-structure of the fundamental and first overtone of ClF has been resolved with grating spectrometers utilizing an 1800 lines-per-inch and a 3600 lines-per-inch grating. An analysis of the observed bands is given and the ω_e and $x_e\omega_e$ for $Cl^{35}F^{19}$ and $Cl^{37}F^{19}$ were found to be 786.34 cm^{-1}, 6.23 cm^{-1}, and 778.82 cm^{-1}, and 6.11 cm^{-1}, respectively.

INTRODUCTION

THE electronic band spectrum of chlorine monofluoride was observed in 1942 by Wahrhaftig[1] who analyzed the spectrum and calculated the vibrational and rotational constants. In 1947, Schmitz and Schumacher[2] reported additional electronic band spectra investigations of ClF in which they also give a set of vibrational constants. The vibrational constants obtained in these two investigations are not in agreement with each other. In 1949, the infrared prism spectrum was observed by Parkinson, Jones, and Nielsen[3] who reported the fundamental and first overtone. Because it was not then possible to resolve these bands into rotational lines, no analysis could be made, and the band centers obtained were not sufficiently accurate to be anything but in general agreement with both sets of electronic data. Recently, Gilbert, Roberts, and Griswold[4] observed the pure rotation spectrum in the microwave region. These authors give an exceedingly accurate set of rotational constants for both $Cl^{35}F^{19}$ and $Cl^{37}F^{19}$.

In an attempt to distinguish between the two differing sets of vibrational constants, an experiment was performed to resolve the fundamental and first overtone

* This document is based on work performed for the AEC by Carbide and Carbon Chemicals Division, UCC, at Oak Ridge, Tennessee. This problem was part of a paper presented at the Symposium on Molecular Spectra at the Ohio State University, Columbus, Ohio, June, 1950.

† Now in the Department of Physics, Vanderbilt University, Nashville, Tennessee.

[1] A. L. Wahrhaftig, J. Chem. Phys. **10**, 248 (1942).

[2] H. Schmitz and H. J. Schumacher, Z. Naturforsch. **2A**, 359 (1947).

[3] Parkinson, Jones, and Nielsen, Phys. Rev. **76**, 199 (1949).

[4] Gilbert, Roberts, and Griswold, Phys. Rev. **76**, 1723 (1949).

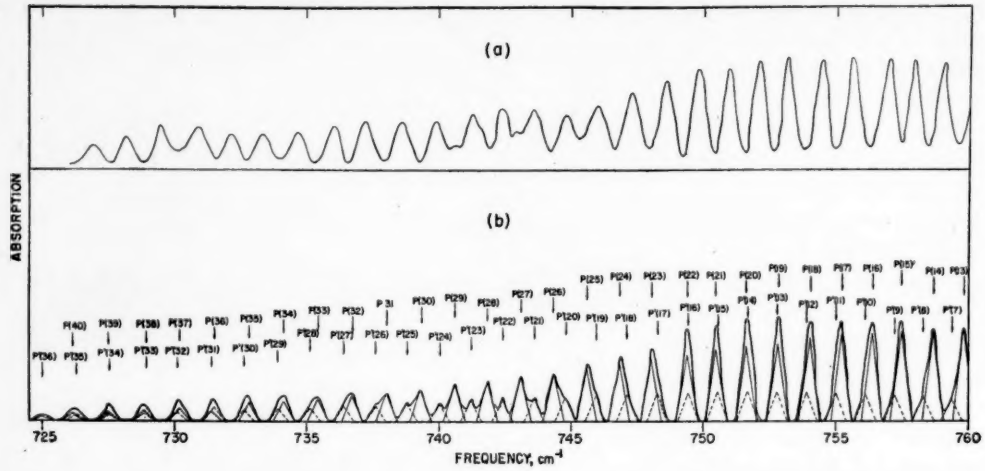

FIG. 1(a). Observed spectrum of the fundamental of ClF, 725 cm^{-1}–760 cm^{-1}. (b). Theoretical spectra of $Cl^{35}F^{19}$ (solid triangles) and $Cl^{37}F^{19}$ (dotted triangles) and the resultant curve.

bands into rotational structure. This paper gives the results of the observations made and an analysis of the data obtained.

EXPERIMENTAL DETAILS

The chlorine monofluoride used in this experiment was prepared in this laboratory by Mr. A. V. Faloon and Mr. W. B. Kenna. To observe the fundamental vibration of this molecule, the gas was contained at a pressure of 10–15 cm of mercury in a 10-cm fluorothene absorption cell[5] closed with rocksalt windows. For the overtone, the same cell was filled to atmospheric pressure.

Measurements on the fundamental were made on an automatically-recording prism-grating spectrometer[6] utilizing an 1800 lines-per-inch replica grating and a Golay detection system feeding its signal to a Leeds and Northrup Type-G Speedomax recorder. The effective slit width throughout was about 0.4 cm^{-1}.

Measurements on the overtone were carried out at the Ohio State University, utilizing the vacuum spectrograph described by Bell, Noble, and Nielsen.[7] A 3600 lines-per-inch replica grating was used, and again the effective slit width was about 0.4 cm^{-1}. Use of a vacuum spectrograph was necessary because the overtone lies in the midst of the intense 6.26μ atmospheric water band and it was otherwise impossible to resolve the closely spaced ClF lines from the background interference.

EXPERIMENTAL RESULTS

That the fundamental and first overtone were quite well resolved may be seen in Figs. 1(a), 2(a), 3(a), and 4(a) where the curves shown have been replotted from the actual records to a more convenient scale.‡ The thermal agitation noise which usually rides on the records has been eliminated in the redrawing. The lines are fairly

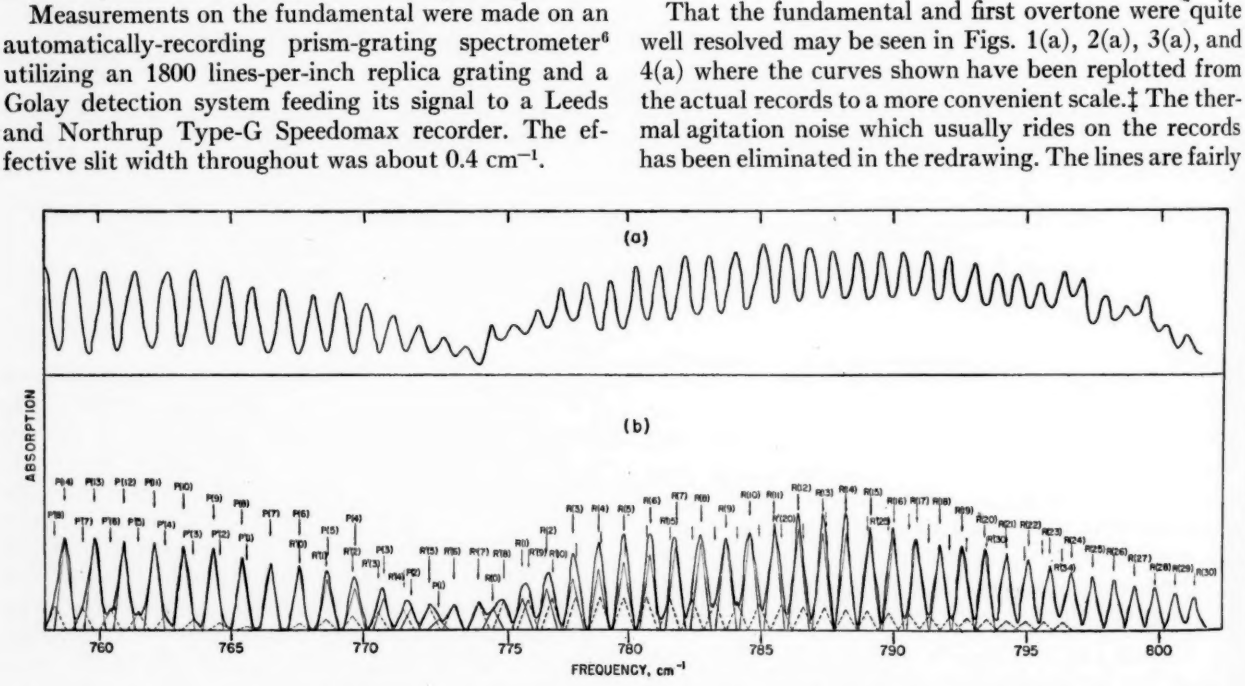

FIG. 2(a). Observed spectrum of the fundamental of ClF, 760 cm^{-1}–800 cm^{-1}. (b). Theoretical spectra of $Cl^{35}F^{19}$ (solid triangles) and $Cl^{37}F^{19}$ (dotted triangles) and the resultant curve.

[5] J. S. Kirby-Smith and E. A. Jones, J. Opt. Soc. Am. **39**, 780 (1949).
[6] A. H. Nielsen, J. Tenn. Acad. Sci. XXII, No. 4, 241 (1947).
[7] Bell, Noble, and Nielsen, Rev. Sci. Instr. **18**, 48 (1947).
‡ Because of the unwieldy length of the records, both fundamental and overtone are shown in two halves, with the split coming approximately at the half-way mark in cm^{-1}.

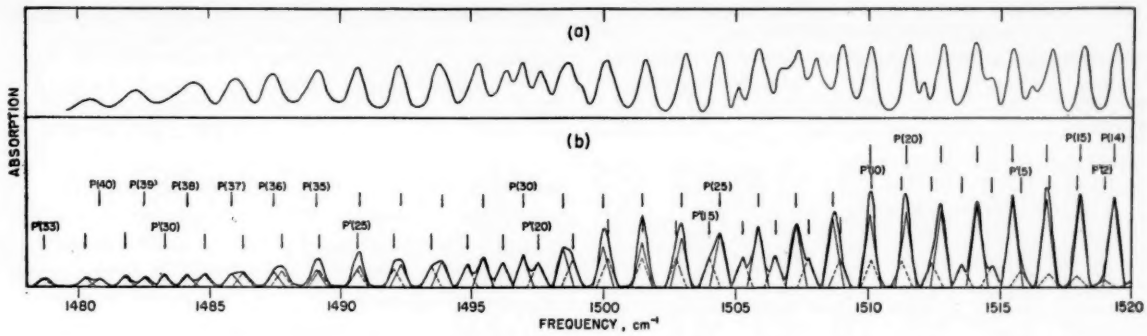

FIG. 3. (a) Observed spectrum of first overtone of ClF, 1480 cm^{-1}–1520 cm^{-1}. (b) Theoretical spectra of $Cl^{35}F^{19}$ (solid triangles) and $Cl^{37}F^{19}$ (dotted triangles) and the resultant curve.

evenly spaced at about 1 cm^{-1} or less, throughout. Diatomic molecules, not possessing angular momentum about the internuclear axis, have no Q branches and there is, thus, a gap at the band center of width about $4B$, which serves to identify the band center. No such gap exists in the fundamental and first overtone of ClF. This fact makes the choice of the band center very difficult. Inasmuch as Cl^{37} is one-third as abundant as Cl^{35}, the $Cl^{37}F^{19}$ lines will be fairly intense throughout. It therefore seems quite reasonable from the amount of the isotope shift that a $Cl^{37}F^{19}R'$§ line should fall just at the $Cl^{35}F^{19}$ band center. The observed rotation lines in general are composites of the two isotopic species and are, therefore, somewhat displaced to higher or lower frequencies depending upon the phase effect of the $Cl^{37}F^{19}$ lines. The only real evidence of the lines getting out of step in the fundamental may be seen between $P(24)$ and $P(40)$ of $Cl^{35}F^{19}$ in Fig. 1(a) where several P' lines are actually resolved. The confusion resulting from overlap is, perhaps, better seen in the overtone in Figs. 3(a) and 4(a). It is also clear from Figs. 3 and 4 that the convergence is fairly large as only a few lines are resolved in the R branch. As no repeatable resolution is apparent beyond about 1550 cm^{-1}, the experimental curve is not reproduced beyond this frequency.

Attempts to assign proper J-values to the fundamental lines in Figs. 1(a) and 2(a) simply from a study of the spectral record were not successful as they led to values of B_e and α_e which were in poor agreement with the microwave values. J-values were consequently assigned in both the fundamental and overtone by a method discussed in the next section. Column 2 in Tables I–IV inclusive gives a list of the observed frequencies in cm^{-1} for both bands corrected to vacuum. The accuracy of measurement of these lines in the fundamental is about ± 0.10 cm^{-1} and in the overtone about ± 0.25 cm^{-1}.

DISCUSSION OF THE ANALYSIS

A study of the record in Figs. 1(a) and 2(a) indicates that the most likely location of the band center of $Cl^{35}F^{19}$ is between 772.0 cm^{-1} and 775.0 cm^{-1}. This is in agreement with predictions from electronic band spectra as the band center from Schmitz and Schumacher's work is 772.4 cm^{-1} and from Wahrhaftig's data it is 773.4 cm^{-1}. If either of these positions is chosen as the band center, the lines observed at 772.4 cm^{-1} and 773.4 cm^{-1} would of necessity be R' lines. If now the lines were numbered $R(0)$, $R(1)$, etc., and $P(1)$, $P(2)$, etc., outwardly from either of these positions, the results were inconsistent with the microwave data.

As this approach to the analysis did not prove satisfactory, a method utilizing the microwave data was attempted. Of the two previous choices for the band center the one by Wahrhaftig was estimated to be the most likely from a study of Fig. 2(a). The rotation lines

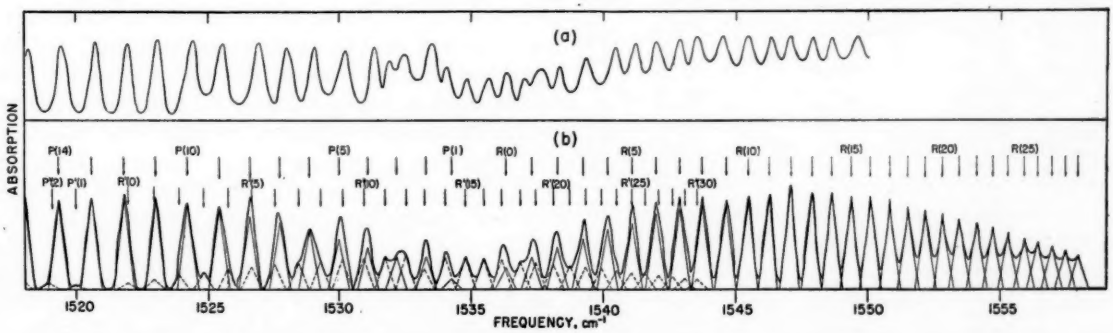

FIG. 4. (a) Observed spectrum of first overtone of ClF, 1520 cm^{-1}–1550 cm^{-1}. (b) Theoretical spectra of $Cl^{35}F^{19}$ (solid triangles) and $Cl^{37}F^{19}$ (dotted triangles) and the resultant curve.

§ The prime on P and R will be used to denote lines of $Cl^{37}F^{19}$.

TABLE I. Table of observed and calculated frequencies in the fundamental of $Cl^{35}F^{19}$.

Identification	Obs. freq. cm^{-1}	Calc. freq. cm^{-1}	Δ cm^{-1}	Identification	Obs. freq. cm^{-1}	Calc. freq. cm^{-1}	Δ cm^{-1}
$R(0)$							
$R(1)$	776.03[a]	775.90	+0.13	$P(1)$	772.54[a]	772.84	−0.30
$R(2)$	776.99	776.90	+0.09	$P(2)$	771.61[a]	771.80	−0.29
$R(3)$	777.94	777.90	+0.04	$P(3)$	770.67	770.76	−0.09
$R(4)$	778.86	778.88	−0.02	$P(4)$	769.66	769.70	−0.04
$R(5)$	779.83	779.86	−0.03	$P(5)$	768.64	768.64	0.00
$R(6)$	780.75	780.83	−0.08	$P(6)$	767.59	767.57	+0.02
$R(7)$	781.72	781.79	−0.07	$P(7)$	766.49	766.49	0.00
$R(8)$	782.63[a]	782.74	−0.11	$P(8)$	765.32	765.40	−0.08
$R(9)$	783.65	783.68	−0.03	$P(9)$	764.32	764.30	+0.02
$R(10)$	784.66	784.61	+0.05	$P(10)$	763.18	763.19	−0.01
$R(11)$	785.55	785.53	+0.02	$P(11)$	762.13	762.08	+0.05
$R(12)$	786.42	786.45	−0.03	$P(12)$	760.92	760.95	−0.03
$R(13)$	787.29	787.36	−0.07	$P(13)$	759.78	759.82	−0.04
$R(14)$	788.21	788.26	−0.05	$P(14)$	758.60	758.68	−0.08
$R(15)$	789.10	789.14	−0.04	$P(15)$	757.46	757.53	−0.07
$R(16)$	789.91	790.02	−0.11	$P(16)$	756.65	756.37	+0.28
$R(17)$	790.82	790.90	−0.08	$P(17)$	755.15	755.20	−0.05
$R(18)$	791.64	791.76	−0.12	$P(18)$	754.00	754.02	−0.02
$R(19)$	792.61	792.58	+0.03	$P(19)$	752.83	752.83	0.00
$R(20)$	793.45	793.43	+0.02	$P(20)$	751.67	751.67	0.00
$R(21)$	794.22	794.26	−0.04	$P(21)$	750.51	750.47	+0.04
$R(22)$	795.09	795.08	+0.01	$P(22)$	749.32	749.26	+0.06
$R(23)$	795.97	795.89	+0.08	$P(23)$	748.13	748.05	+0.08
$R(24)$	796.64	796.70	−0.06	$P(24)$	746.84	746.83	+0.01
$R(25)$	797.56	797.49	+0.07	$P(25)$	745.57	745.59	−0.02
$R(26)$	798.31	798.28	+0.03	$P(26)$	744.36	744.35	+0.01
$R(27)$	799.02	799.06	−0.04	$P(27)$	743.15	743.11	+0.04
$R(28)$	799.81	799.82	−0.01	$P(28)$	741.95[a]	741.85	+0.10
$R(29)$	800.58	800.58	0.00	$P(29)$	740.83[a]	740.59	+0.24
				$P(30)$	739.43[a]	739.31	+0.12
				$P(31)$	738.09	738.03	+0.06
				$P(32)$	736.74	736.75	−0.01
				$P(33)$	735.46	735.45	+0.01
				$P(34)$	734.18	734.14	+0.04
				$P(35)$	732.92	732.83	+0.09
				$P(36)$	731.56	731.51	+0.05
				$P(37)$	730.44[b]	730.18	+0.26
				$P(38)$	729.00[b]	728.85	+0.15
				$P(39)$	727.72[b]	727.50	+0.22
				$P(40)$	726.41[b]	726.15	+0.27

[a] The lines are displaced or unobserved because of overlapping.
[b] The lines are weak and badly overlapped.

TABLE II.[a] Table of observed and calculated frequencies in the fundamental band of $Cl^{37}F^{19}$.

	R branch				*P* branch		
Identification	Obs. freq. cm^{-1}	Calc. freq. cm^{-1}	Δ cm^{-1}	Identification	Obs. freq. cm^{-1}	Calc. freq. cm^{-1}	Δ cm^{-1}
$R'(0)$	767.59[a]	767.60	−0.01				
$R'(1)$	768.64[a]	768.59	+0.05	$P'(1)$	[b]	765.59	
$R'(2)$	769.66[a]	769.58	+0.08	$P'(2)$	[b]	764.57	
$R'(3)$	770.67[a]	770.55	+0.12	$P'(3)$	[b]	763.55	
$R'(4)$	771.61[a]	771.52	+0.09	$P'(4)$	[b]	762.51	
$R'(5)$	772.54[a]	772.47	+0.07	$P'(5)$	[b]	761.47	
$R'(6)$	773.40	773.42	−0.02	$P'(6)$	[b]	760.42	
$R'(7)$	774.34	774.36	−0.02	$P'(7)$	[b]	759.36	
$R'(8)$	775.21	775.29	−0.08	$P'(8)$	[b]	758.29	
$R'(9)$	776.03[a]	776.21	−0.18	$P'(9)$	[b]	757.21	
$R'(10)$	776.99[a]	777.13	−0.14	$P'(10)$	[b]	756.12	
$R'(11)$	777.94[a]	778.03	−0.09	$P'(11)$	755.15[a]	755.02	+0.13
$R'(12)$	778.86[a]	778.93	−0.07	$P'(12)$	754.00[a]	753.92	+0.08
$R'(13)$	779.83[a]	779.82	+0.01	$P'(13)$	752.83[a]	752.81	+0.02
$R'(14)$	780.75[a]	780.70	+0.05	$P'(14)$	751.67[a]	751.68	−0.01
$R'(15)$	781.72[a]	781.57	+0.15	$P'(15)$	750.51[a]	750.55	−0.04
$R'(16)$	782.63[a]	782.43	+0.20	$P'(16)$	749.32[a]	749.42	−0.10
$R'(17)$	[b]	783.28		$P'(17)$	748.13[a]	748.27	−0.14
$R'(18)$	[b]	784.12		$P'(18)$	[b]	747.11	
$R'(19)$	[b]	784.93		$P'(19)$	[b]	745.95	
$R'(20)$	[b]	785.76		$P'(20)$	[b]	744.81	
$R'(21)$	[b]	786.57		$P'(21)$	[b]	743.62	
$R'(22)$	787.29[a]	787.37	−0.08	$P'(22)$	742.45	742.44	+0.01
$R'(23)$	788.21[a]	788.17	+0.04	$P'(23)$	741.15	741.24	−0.09
$R'(24)$	789.10[a]	788.95	+0.15	$P'(24)$	740.12	740.04	+0.08
$R'(25)$	789.91[a]	789.73	+0.18	$P'(25)$	[b]	738.83	
$R'(26)$	[b]	790.50		$P'(26)$	[b]	737.61	
$R'(27)$	[b]	791.26		$P'(27)$	[b]	736.38	
$R'(28)$	[b]	792.00		$P'(28)$	[b]	735.15	
$R'(29)$	[b]	792.76		$P'(29)$	[b]	733.90	
$R'(30)$	[b]	793.48		$P'(30)$	[b]	732.65	
$R'(31)$	[b]	794.20		$P'(31)$	731.56[a]	731.39	+0.17
$R'(32)$	[b]	794.91		$P'(32)$	730.44[a]	730.13	+0.31
$R'(33)$	[b]	795.61		$P'(33)$	729.00[a]	728.85	+0.15
$R'(34)$	[b]	796.31		$P'(34)$	727.72[a]	727.57	+0.15
				$P'(35)$	726.41[a]	726.28	+0.13

[a] Where the $Cl^{37}F^{19}$ overlap is very close the nearest observed line is listed in Table II.
[b] Lines thus marked were unobserved because of overlap.

may then be calculated from the relations given in (1).

$$\left.\begin{matrix} R(J-1) \\ P(J) \end{matrix}\right\} = 773.40 \pm (B'+B'')J + (B'-B'')J^2 \mp 4D_eJ^3 \quad (1)$$

where $J=1, 2, 3, \cdots$, etc., and B' and B'' are the rotational constants in the upper and lower vibrational states respectively. These were computed from the microwave values of B_e and α_e. D_e is the centrifugal stretching constant.

The band center for $Cl^{37}F^{19}$ may be computed with good accuracy from the relation $\nu' = (\mu/\mu')^{\frac{1}{2}}\nu$, where μ and μ' are the reduced masses for the two isotopic species. This may be seen by writing the band centers in terms of ω_e and $x_e\omega_e$, taking into account the reduced mass dependence as shown in Eqs. (2).

$$\begin{aligned} \nu(Cl^{35}F^{19}) &= \omega_e - 2x_e\omega_e \\ \nu'(Cl^{37}F^{19}) &= (\mu/\mu')^{\frac{1}{2}}\omega_e - 2(\mu/\mu')x_e\omega_e. \end{aligned} \quad (2)$$

For $Cl^{35}F^{19}$ and $Cl^{37}F^{19}$ the quantities $(\mu/\mu')=0.981$ and $(\mu/\mu')^{\frac{1}{2}}=0.990$. It may, therefore, be seen that $x_e\omega_e$ and $x_e\omega_e'$ differ by less than 2 percent. Thus, whether Schmitz and Schumacher's value of $x_e\omega_e=4.0$ cm^{-1} or Wahrhaftig's value of 9.9 cm^{-1} is used, the error incurred in computing ν' cannot be greater than 0.4

TABLE III. Table of observed and calculated frequencies in the first overtone of $Cl^{35}F^{19}$.

	R branch				*P* branch		
Identification	Obs. freq. cm^{-1}	Calc. freq. cm^{-1}	Δ cm^{-1}	Identification	Obs. freq. cm^{-1}	Calc. freq. cm^{-1}	Δ cm^{-1}
$R(0)$	1536.26	1536.31	−0.05				
$R(1)$	[a]	1537.31		$P(1)$	[a]	1534.27	
$R(2)$	1538.26	1538.28	−0.02	$P(2)$	1533.48	1533.23	+0.25
$R(3)$	1539.27	1539.24	+0.03	$P(3)$	[a]	1532.16	
$R(4)$	1540.39	1540.18	+0.21	$P(4)$	1531.27	1531.08	+0.19
$R(5)$	1541.16	1541.11	+0.05	$P(5)$	1530.15	1529.98	+0.17
$R(6)$	1541.90	1542.01	−0.11	$P(6)$	1529.00	1528.87	+0.13
$R(7)$	1542.73	1542.90	−0.17	$P(7)$	1527.91	1527.73	+0.18
$R(8)$	1543.43	1543.76	−0.33	$P(8)$	1526.89	1526.58	+0.29
$R(9)$	1544.43	1544.63	−0.20	$P(9)$	1525.49	1525.41	+0.08
$R(10)$	1545.38	1545.47	−0.09	$P(10)$	1524.41	1524.23	+0.18
$R(11)$	1546.21	1546.28	−0.07	$P(11)$	1523.04	1523.02	+0.02
$R(12)$	1546.92	1547.09	−0.17	$P(12)$	1521.90	1521.80	+0.10
$R(13)$	1547.79	1547.87	−0.08	$P(13)$	1520.66	1520.57	+0.09
$R(14)$	1548.46	1548.64	−0.18	$P(14)$	1519.39	1519.31	+0.08
$R(15)$	1549.50	1549.39	+0.11	$P(15)$	1518.10	1518.04	+0.06
				$P(16)$	1516.90	1516.75	+0.15
				$P(17)$	1515.44	1515.44	0.00
				$P(18)$	1514.03	1514.12	−0.09
				$P(19)$	1512.77	1512.77	0.00
				$P(20)$	1511.55	1511.44	+0.10
				$P(21)$	1510.10	1510.07	+0.03
				$P(22)$	1509.05	1508.68	+0.37
				$P(23)$	1507.26	1507.27	−0.01
				$P(24)$	1505.90	1505.85	+0.05
				$P(25)$	1504.35	1504.41	−0.06
				$P(26)$	1503.11	1502.95	+0.16
				$P(27)$	1501.59	1501.47	+0.12
				$P(28)$	1500.07	1499.99	+0.08
				$P(29)$	1498.63	1498.49	+0.14
				$P(30)$	1496.90	1496.95	−0.05
				$P(31)$	1495.23	1495.41	−0.18
				$P(32)$	1493.74	1493.85	−0.11
				$P(33)$	1492.20	1492.28	−0.08
				$P(34)$	1490.64	1490.68	−0.04
				$P(35)$	1489.10	1489.07	+0.03
				$P(36)$	1487.27	1487.44	−0.17
				$P(37)$	1485.86	1485.81	+0.05
				$P(38)$	1484.32	1484.14	+0.18
				$P(39)$	1482.10	1482.47	−0.37
				$P(40)$	1480.49	1480.78	−0.29

[a] Lines marked with an a are masked by or shifted by $Cl^{37}F^{19}$ lines.

TABLE IV. Table of observed and calculated frequencies in the first overtone of $Cl^{37}F^{19}$.

Identification	Obs. freq. cm^{-1}	Calc. freq. cm^{-1}	Δ cm^{-1}	Identification	Obs. freq. cm^{-1}	Calc. freq. cm^{-1}	Δ cm^{-1}
$R'(0)$	[a]	1521.97					
$R'(1)$	[a]	1522.95		$P'(1)$	[a]	1519.97	
$R'(2)$	[a]	1523.90		$P'(2)$	[a]	1518.95	
$R'(3)$	[a]	1524.84		$P'(3)$	[a]	1517.90	
$R'(4)$	[a]	1525.76		$P'(4)$	1516.90	1516.84	+0.06
$R'(5)$	[a]	1526.67		$P'(5)$	1516.12	1515.76	+0.36
$R'(6)$	[a]	1527.55		$P'(6)$	1514.64	1514.67	−0.03
$R'(7)$	[a]	1528.42		$P'(7)$	[a]	1513.55	
$R'(8)$	[a]	1529.28		$P'(8)$	1512.09	1512.42	−0.33
$R'(9)$	[a]	1530.11		$P'(9)$	[a]	1511.28	
$R'(10)$	[a]	1530.93		$P'(10)$	[a]	1510.11	
$R'(11)$	1531.76	1531.73	+0.03	$P'(11)$	[a]	1508.93	
$R'(12)$	1532.39	1532.52	−0.13	$P'(12)$	1508.09	1507.73	+0.36
$R'(13)$	1533.05	1533.29	−0.24	$P'(13)$	1506.71	1506.50	+0.21
$R'(14)$	1533.91	1534.04	−0.13	$P'(14)$	1505.12	1505.27	−0.15
$R'(15)$	1534.72	1534.77	−0.05	$P'(15)$	[a]	1504.02	
$R'(16)$	1535.43	1535.48	−0.05	$P'(16)$	[a]	1502.75	
$R'(17)$	1536.26	1536.18	+0.08	$P'(17)$	[a]	1501.46	
$R'(18)$	1536.96	1536.86	+0.10	$P'(18)$	[a]	1500.16	
$R'(19)$	1537.62	1537.49	+0.13	$P'(19)$	1499.19	1498.84	+0.35
$R'(20)$	1538.26	1538.14	+0.12	$P'(20)$	1497.61	1497.53	+0.08
$R'(21)$	1538.89	1538.75	+0.14	$P'(21)$	1496.35	1496.18	+0.17
$R'(22)$	1539.27	1539.36	−0.09	$P'(22)$	[a]	1494.81	
$R'(23)$	1539.65	1539.95	−0.30	$P'(23)$	1493.74	1493.42	+0.32
$R'(24)$	1540.39	1540.51	−0.12	$P'(24)$	[a]	1492.03	
$R'(25)$	1541.16	1541.07	+0.09	$P'(25)$	[a]	1490.61	
$R'(26)$	1541.69	1541.60	+0.09	$P'(26)$	[a]	1489.17	
$R'(27)$	1542.11	1542.11	0.00	$P'(27)$	[a]	1487.72	
$R'(28)$	1542.73	1542.61	+0.12	$P'(28)$	[a]	1486.26	
$R'(29)$	1543.32	1543.09	+0.23	$P'(29)$	[a]	1484.77	
$R'(30)$	1543.43	1543.55	−0.12	$P'(30)$	[a]	1483.27	

[a] Lines are masked by $Cl^{35}F^{19}$, and are unobserved except in their effect on the $Cl^{35}F^{19}$ lines.

cm^{-1}. The rotation lines of $Cl^{37}F^{19}$ may now be calculated from (1) by substituting the computed band center 766.13 cm^{-1} and appropriate B-values. The intensities of the absorption lines of both isotopic species were calculated taking account of the relative abundances of Cl^{35} and Cl^{37}. Theoretical spectra for both species for the fundamental were plotted with intensities as ordinates and frequencies as abscissas as shown in Figs. 1(b) and 2(b). Each line is represented as a triangle with the altitude proportional to the intensity and the base equal to twice the effective slit width. The heavy solid line in Figs. 1(b) and 2(b) is the resultant spectrum when the ordinates are added. Over a lightbox the actual record, Figs. 1(a) and 2(a), and the theoretical spectrum, Figs. 1(b) and 2(b), were compared until the line-positions and line-intensities in the two curves were in virtually complete agreement. Such agreement was achieved when a correction of +0.48 cm^{-1} was made to the assumed band center 773.40 cm^{-1} making the value 773.88 cm^{-1}. Columns 3 and 7 in Tables I and II give the frequencies of the lines calculated from this band center and appropriate B-values for both isotopic molecules. The identification of the lines is given in columns 1 and 5. Discrepancies between observed and calculated frequencies are given in columns 4 and 8. Comparison of the observed and calculated line-positions, together with a study of Figs. 1 and 2, shows the agreement achieved is to about ±0.1 cm^{-1}, which is within the experimental error. With the $R(J)$ and $P(J)$ values given in Tables I and II the relation $\frac{1}{2}[R(J-1)+P(J)]$ plotted *versus* J^2 give excellent straight lines and band centers of 773.88 cm^{-1} and 766.61 cm^{-1} for $Cl^{35}F^{19}$ and $Cl^{37}F^{19}$, respectively. These band centers with the values of $(\mu/\mu')^{\frac{1}{2}}$ and (μ/μ') when substituted into Eqs. (2) give ω_e, ω_e', $x_e\omega_e$, and $x_e\omega_e'$ as 786.34 cm^{-1}, 778.82 cm^{-1}, 6.23 cm^{-1} and 6.11 cm^{-1}, respectively. Table V lists the molecular constants of ClF obtained by the various investigators up to the present. It will be noted that the microwave B and α are somewhat smaller than those given by Wahrhaftig, and the ω_e and $x_e\omega_e$ herein determined, lie between the previous values of Wahrhaftig and Schmitz and Schumacher.

TABLE V. Table of molecular constants for ClF.

Molecular constant[a]	Wahrhaftig[1]	Schmitz and Schumacher[3]	Nielsen and Jones	Gilbert, Roberts and Griswold[4]
B_e	0.518 ±0.001 cm^{-1}			0.516508$_8$ cm^{-1}
B_e'				0.506685$_7$ cm^{-1}
α_e	0.006 ±0.002 cm^{-1}			0.00435879 cm^{-1}
α_e'				0.00433514 cm^{-1}
D_e				8.773 ×10^{-7} cm^{-1}
D_e'				8.440 ×10^{-7} cm^{-1}
ω_e	793.2 cm^{-1}	780.4 cm^{-1}	786.34 cm^{-1}	
$x_e\omega_e$	9.9 cm^{-1}	4.0 cm^{-1}	6.23 cm^{-1}	
ω_e'	785.6 cm^{-1} (calc.)		778.82 cm^{-1}	
$x_e\omega_e'$	9.7 cm^{-1} (calc.)		6.11 cm^{-1}	

[a] The primes indicate values for $Cl^{37}F^{19}$.

As a check on these vibrational constants they and the microwave values of B and α were used to predict the rotation-line positions for the first overtone of $Cl^{35}F^{19}$ and $Cl^{37}F^{19}$. These predicted lines plotted as triangles with the altitude proportional to the intensity and the base twice the effective slit width may be seen in Figs. 3(b) and 4(b). The heavy line is drawn to give the resulting theoretical curve. Just above, in Figs. 3(a) and 4(a), is shown, plotted to the same scale, the $v=2\leftarrow v=0$ transition as observed. Because of the overlap of lines in the spectrum the accuracy of the measured lines is probably between ±0.20 cm^{-1} and ±0.30 cm^{-1}, and it may be seen that most of the discrepancies are smaller than that, but a few are worse. Because it was possible to predict these lines with such good accuracy, it is believed that the values of ω_e and $x_e\omega_e$ for both isotopic species are quite well determined. Tables III and IV list the line assignments, observed frequencies and calculated frequencies, as well as the discrepancies, for both isotopic species.

The authors wish to thank Dr. E. E. Bell of the Department of Physics and Astronomy at the Ohio State University for arranging a recording schedule on their vacuum spectrograph and assistance in obtaining records. Thanks are due Messrs. A. V. Faloon and W. B. Kenna for careful sample preparation. A Frederick Gardner Cottrell Grant-in-Aid from the Research Corporation to one of us (A. H. Nielsen) made possible the completion of the University of Tennessee grating spectrograph on which these measurements were made.

The Oscillator Strength of H_2^+, $1s\sigma-2p\sigma$

DAVID R. BATES
University College, London, England
(Received March 21, 1951)

The $1s\sigma-2p\sigma$ transition of H_2^+ is investigated using exact two center wave functions and using approximate wave functions based on a linear combination of atomic orbitals (with both the dipole length and the dipole velocity formulas). It is found that at the equilibrium internuclear distance, 2.00 a_0, the true oscillator strength of the transition is 0.319; with the dipole length formula, the LCAO approximation yields a value some 1.4 times greater, and with the dipole velocity formula it yields a value some 0.54 times smaller. Results are given for internuclear distances between 0 and 9 a_0.

MANY calculations on molecular oscillator strengths have been performed since the publication of the first[1] of Mulliken's series of papers on the subject. In general, rather crude wave functions such as are provided by a linear combinations of atomic orbitals (LCAO) have to be employed. It is clearly important to accumulate as much evidence as possible on the accuracy that is achieved; and it is desirable to investigate whether the formula based on the dipole velocity has any advantage over the usual one based on the dipole length. In connection with another problem, tables of exact wave functions for the hydrogen molecular ion have recently been prepared by the writer in collaboration with Professor H. S. W. Massey, Mr. A. L. Stewart, and Mrs. K. Ledsham.[2] The opportunity was taken of carrying out a precise computation of the oscillator strength of the transition H_2^+, $1s\sigma-2p\sigma$, and of comparing the results with those obtained from approximate wave functions. Apart from the interest attached to this comparison, detailed information on the transition is required in several astrophysical applications.

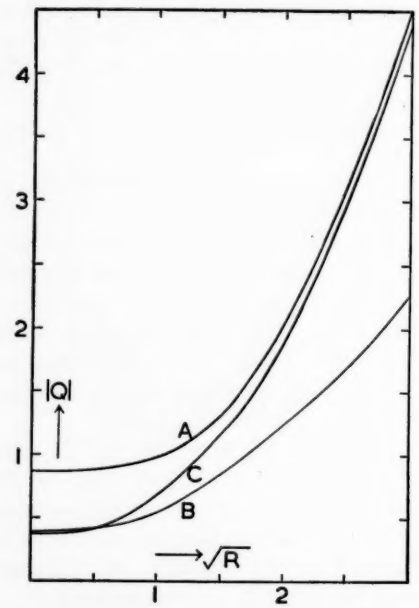

FIG. 1. Curves of $|Q|$ *versus* $R^{\frac{1}{2}}$ (both in atomic units). Curve A is LCAO dipole length (formula (5)), B is LCAO dipole velocity (formula (8)), and C is the two center wave function result (formulas (10) and (11)).

The oscillator strength f can be expressed as

$$f=(8\pi^2m/3h)\nu G|Q|^2 \tag{1}$$

with

$$|Q|=\left|\int_\tau \chi_i(\mathbf{r})\mathbf{r}\chi_j^*(\mathbf{r})d\tau\right| \tag{2a}$$

or with

$$|Q|=(h/4\pi^2m\nu)\left|\int_\tau \chi_i(\mathbf{r})\nabla\chi_j^*(\mathbf{r})d\tau\right|$$

$$=(h/4\pi^2m\nu)\left|\int_\tau \chi_j^*(\mathbf{r})\nabla\chi_i(\mathbf{r})d\tau\right|, \tag{2b}$$

where m is the electronic mass, h is Planck's constant, ν is the frequency of the radiation, G is the orbital degeneracy factor, $\mathbf{r}$ is the position vector, and $\chi_i(\mathbf{r})$ and $\chi_j(\mathbf{r})$ are the wave functions of the states involved.[1] Chandrasekhar[3] has pointed out that although the dipole length formula (2a) and the dipole velocity formula (2b) are identical when exact wave functions are employed they are not necessarily of equal merit in other circumstances.

Denoting the distances of the electron from the two nuclei by r_A and r_B, and the internuclear distance by R, we have that the LCAO approximations to $\chi_{1s\sigma}(\mathbf{r})$ and $\chi_{2p\sigma}(\mathbf{r})$ are

$$\{e^{-r_A}+e^{-r_B}\}/\{2\pi(1+S)\}^{\frac{1}{2}} \tag{3}$$

and

$$\{e^{-r_A}-e^{-r_B}\}/\{2\pi(1-S)\}^{\frac{1}{2}}, \tag{4}$$

respectively, S being the function

$$e^{-R}(1+R+\tfrac{1}{3}R^2).$$

On substituting in Eq. (2a), Mulliken[4] finds

$$|Q| \text{ (LCAO dipole length)}=R/2(1-S^2)^{\frac{1}{2}}. \tag{5}$$

[1] R. S. Mulliken, J. Chem. Phys. **7**, 14 (1939).
[2] Bates, Ledsham, Massey, and Stewart, (to be published). I wish to thank my colleagues for allowing me to use the results of this paper prior to their publication.
[3] S. Chandrasekhar, Astrophys. J. **102**, 223 (1945), see also H. Shull, Astrophys. J. **112**, 352 (1950).
[4] R. S. Mulliken, J. Chem. Phys. **7**, 20 (1939).

Both $|Q|$ and R are here in the appropriate atomic units (a_0, the radius of the first Bohr orbit).

Using instead Eq. (2b), and writing the energy $h\nu$ as E Rydbergs, we obtain

$$|Q|\,(\text{LCAO dipole velocity})$$

$$= \left| \int_\tau (e^{-r_1}+e^{-r_2}) \times \left(\frac{e^{-r_1}}{r_1}\mathbf{r}_1 - \frac{e^{-r_2}}{r_2}\mathbf{r}_2 \right) d\tau \right| \Big/ \pi E(1-S^2)^{\frac{1}{2}} \quad (6)$$

$$= \left| \int_\tau e^{-(r_1+r_2)} \left(\frac{1}{r_1}\mathbf{r}_1 - \frac{1}{r_2}\mathbf{r}_2 \right) d\tau \right| \Big/ \pi E(1-S^2)^{\frac{1}{2}} \quad (7)$$

$$= 2R(1+R)e^{-R}/3E(1-S^2)^{\frac{1}{2}}. \quad (8)$$

In carrying out the computations it was judged best to use the true value of E rather than the value associated with the LCAO approximation.

The exact two centers wave functions available are in elliptical coordinates,

$$\lambda = (r_A + r_B)/R, \quad \mu = (r_A - r_B)/R. \quad (9)$$

With these, the two alternative formulas are equivalent, but it is easier to compute (2a) which becomes simply

$$|Q| = \tfrac{1}{8}\pi R^4 \left| \int_{-1}^{+1} \int_1^\infty \chi_{1s\sigma}(\lambda,\mu)\chi_{2p\sigma}(\lambda,\mu) \times \{\lambda\mu(\lambda^2-\mu^2)\} d\lambda d\mu \right|. \quad (10)$$

The variables are separable, but the integration has to be carried out by numerical methods.* It can be seen from (2b) that we have also

$$|Q| = \frac{\pi R^2}{E} \left| \int_{-1}^{+1} \int_1^\infty \chi_{1s\sigma}(\lambda,\mu) \times \left[\left\{ \frac{\partial \chi_{2p\sigma}(\lambda,\mu)}{\partial \lambda} \right\} \mu(\lambda^2-1) + \left\{ \frac{\partial \chi_{2p\sigma}(\lambda,\mu)}{\partial \mu} \right\} \lambda(1-\mu^2) \right] d\lambda d\mu. \quad (11)$$

A limited use was made of this as a check on the work.

The results are displayed in Fig. 1 which gives the values of $|Q|$ obtained by the three methods as a function of the square-root of the internuclear distance. It will be noted that at the equilibrium $R(2.00a_0)$, the true $|Q|$ lies almost midway between $|Q|$ (LCAO dipole length) and $|Q|$ (LCAO dipole velocity); the former being a factor of 1.2 high and the latter a factor of 0.73 low.† With formula (2a) the LCAO approximation gives rise to serious error at small R (as would be expected), but as R increases it improves, at first quite rapidly and then extremely slowly. In contrast with formula (2b), it gives remarkable precision at small R (perhaps due in some measure to chance), and as R increases it becomes steadily less satisfactory—indeed, it underestimates $|Q|$ by a factor of 2 when the internuclear distance is infinite. This last discrepancy might appear surprising, since at very large R the LCAO wave functions can usually be regarded as accurate. However, the reason for it can readily be understood. Thus on referring to Eqs. (6) and (7) it can be seen that all contributions to the transition integral cancel except that arising from the overlap between the atomic orbital based on one nucleus and the derivative of the atomic orbital based on the other nucleus; and this overlap is unlikely to be properly represented when R is great. Obviously, gross cancellation must always occur if the

TABLE I. Data on the $1s\sigma - 2p\sigma$ transition of H_2^+.

Internuclear distance R (atomic units)	Photon energy E (Rydbergs)	Oscillator strength f
0.0	3.000	0.139
0.2	2.852	0.150
0.4	2.580	0.175
0.6	2.294	0.207
0.8	2.023	0.240
1.0	1.774	0.269
1.2	1.547	0.292
1.4	1.344	0.309
1.6	1.165	0.317
1.8	1.007	0.321
2.0	0.8702	0.319
2.2	0.7516	0.315
2.4	0.6493	0.310
2.6	0.5610	0.304
2.8	0.4848	0.297
3.0	0.4189	0.289
3.2	0.3620	0.281
3.4	0.3128	0.271
3.6	0.2702	0.261
3.8	0.2332	0.250
4.0	0.2011	0.238
4.2	0.1732	0.226
4.4	0.1491	0.213
4.6	0.1281	0.201
4.8	0.1100	0.188
5.0	0.0942_6	0.175
5.5	0.0637_1	0.144
6.0	0.0426_5	0.116
6.5	0.0283_1	0.090_9
7.0	0.0186_4	0.069_8
7.5	0.0122_1	0.052_8
8.0	0.0079_3	0.039_2
8.5	0.0051_3	0.028_8
9.0	0.0033_0	0.020_9

* My gratitude is due to the departmental computer, Mrs. K. Ledsham, for her able assistance in this computation.

† The corresponding factors for the oscillator strengths are, of course, 1.4 and 0.54, respectively.

product $|Q|E$ is small and if the wave functions of the states concerned do not lie mainly in different regions of space. In cases in which this effect does not arise the dipole velocity formula would seem useful, and probably the best procedure in practice is to evaluate both it and the dipole length formula. Inspection of the form of the transition integrals should, of course, always be carried out to see if there is any feature which would make either formula unreliable. If there is none, it is perhaps most judicious to adopt the mean of the two sets of results.

The oscillator strengths at various internuclear distances were obtained by inserting in Eq. (1) (with G put equal to unity) the data on $|Q|$ and E derived from the two center calculations. The results are presented in Table I. With a view to certain astrophysical applications, an unusually wide R range is covered. The accumulation of errors in the lengthy computational work involved may have introduced slight inaccuracies in the f values. These may conceivably be as much as 3 percent; but it is thought probable that they are actually considerably less.

THE JOURNAL OF CHEMICAL PHYSICS VOLUME 19, NUMBER 9 SEPTEMBER, 1951

The Outer Electron Configuration in Metallic Copper

A. I. SNOW
Institute for the Study of Metals, University of Chicago, Chicago, Illinois
(Received May 10, 1951)

The effect on the atomic scattering factor of metallic copper of the $3d^{7.75}\,4s^1\,4p^{2.25}$ outer electron configuration, demanded by the Pauling valence of 5.50, is computed. Approximately a 6 percent lowering in intensity of the (111) reflection when compared with the atomic scattering factor computed on the basis of a Hartree-Fock calculation for the $3d^{10}\,4s^1$ configuration is predicted if the Pauling model is the correct one. Differences for other reflections are also computed. Available intensity data for metallic copper are discussed in the light of these results.

INTRODUCTION

IN connection with the theory of the metallic state it would be of interest to have at hand definite experimental evidence concerning the electronic configuration of the elements. A specific example is metallic copper whose outer electronic configuration on the Mott[1] picture is $3d^{10}\,4s^1$ as contrasted with the configuration $3d^{7.75}\,4s^1\,4p^{2.25}$ demanded by the Pauling[2] valence of 5.50. The difference between these two configurations seems great enough to be susceptible to experimental check and x-ray diffraction suggests itself as one possible method. Ageev and Ageeva[3] have attempted to obtain the electron density distribution by means of a fourier series based on x-ray diffraction data but their methods of handling the series are open to serious question.[4] Since the outer electronic configuration will affect the intensities of only a very few low order reflections it should be possible, if x-ray diffraction methods can be used at all, to obtain some idea of the electronic configuration by examination of these reflections alone without the use of a fourier series with all of its attendant difficulties.

I shall first calculate the decrease in atomic scattering factor (hereafter designated as ASF) of a (111) reflection due to the removal of 2.25 electrons from the $3d^{10}$ group. The removal of these electrons will cause a change in screening for the remaining 7.75 electrons which will increase their scattering power and which will be calculated. I shall then discuss the effect of a nonspherically symmetrical electron distribution. Finally, a comparison will be made of the results obtained with available experimental data.

CONTRIBUTION OF 3d ELECTRONS TO ASF

Viervoll and Ögrim[5] list data for the contribution of a $3d$ electron to the ASF. Their table is based on a Hartree[6] self-consistent field radial distribution function computed without taking exchange effects into account. I shall discuss the effect of neglect of exchange later. From Viervoll and Ögrim's data the contribution of a $3d$ electron to the copper ASF for a (111) reflection is 0.570. Removal of 2.25 $3d$ electrons therefore causes a decrease in ASF of 1.283.

If the ASF of an electron in a group is plotted against $[\sin\theta/(Z-S)\lambda]$ where Z is the atomic number of the atom concerned and S is a screening parameter, then by a proper choice of S it is possible to make the ASF curves for the same group in different atoms superimpose.[7] The S value for the $3d^{10}$ group in copper is 23.0[5] whereas the S value for the same group in rubidium is

[1] N. F. Mott and H. Jones, *The Theory of the Properties of Metals and Alloys* (Clarendon Press, London, 1936).
[2] L. Pauling, Proc. Roy. Soc. (London) **A196**, 355 (1948).
[3] N. V. Ageev and D. L. Ageeva, Izvest. Akad. Nauk. SSSR Otdel Khim Nauk, 273 (1948).
[4] A. I. Snow, Acta Cryst. (to be published).
[5] H. Viervoll and O. Ögrim, Acta Cryst. **2**, 277 (1949).
[6] D. R. Hartree, Proc. Roy. Soc. (London) **A141**, 282 (1933).
[7] R. W. James and G. W. Brindley, Phil. Mag. **12**, 81 (1931).

TABLE I. Difference in contribution to ASF between $3d^{10}$ and $3d^{7.75}$ electrons in copper.

Reflection indices (1)	Contribution of one electron in a $3d^{10}$ configuration to ASF[5] (2)	Contribution of 2.25 electrons in a $3d^{10}$ configuration to ASF (3)	Contribution of one electron in a $3d^{7.75}$ configuration to ASF (4)	Difference between contribution of one electron in a $3d^{10}$ and a $3d^{7.75}$ configuration to ASF (5)	Difference between contribution of 7.75 electrons in a $3d^{10}$ and $3d^{7.75}$ configuration to ASF (6)	Total change in ASF of a $3d$ group due to removal of 2.25 electrons (7)
(111)	0.570	1.283	0.648	0.078	0.605	−0.678
(200)	0.488	1.098	0.582	0.094	0.729	−0.369
(220)	0.289	0.650	0.384	0.095	0.737	0.087
(311)	0.216	0.486	0.296	0.080	0.620	0.134

27.0[5]. Assuming linearity between these values when plotted against atomic number we see that a change of +1 in nuclear charge leads to a change of 0.5 in screening parameter S. Assuming the same change of 0.5 for the removal of one $3d$ electron and using a plot of the $3d$ contribution to ASF *versus* $[\sin\theta/(Z-S)\lambda]$ we find that the contribution per electron of the remaining 7.75 electrons is increased from 0.570 to 0.648 so that the contribution of the remaining 7.75 electrons to ASF is increased by 0.605 over what they would contribute as part of a $3d^{10}$ group. This change of 0.5 per electron for S is probably too high since the $4s$ and $4p$ electron distribution will overlap with the $3d^{7.75}$ distribution somewhat and so will tend to screen the $3d^{7.75}$ group at least slightly. Since the value 0.605 is probably too high we are on the safe side in our calculation.

The difference in ASF for a (111) reflection between a $3d^{10}$ configuration and a $3d^{7.75}$ configuration is therefore (1.283−0.605) or 0.678. Differences for the first few reflections calculated in the manner described are listed in column seven of Table I.

The difference in ASF for a copper (111) reflection between the use of a radial distribution function based on a self-consistent field calculation with consideration of exchange and Viervoll and Ögrim's data, based on a calculation with neglect of exchange, is 0.07 per $3d$ electron. This value is fairly independent of angle decreasing only to 0.06 for a (311) reflection. If the exchange contribution to the remaining 7.75 electrons after removal of the 2.25 $4p$ electrons, is about the same as that corresponding to the value when they are present as part of a $3d^{10}$ group, then the absolute value of the difference in ASF in column seven of Table I will be approximately 0.16 too low so that again we would be on the safe side in neglect of this effect.

CONTRIBUTION OF 4s AND 4p ELECTRONS TO ASF

To evaluate the contribution of the $4s\ 4p^{2.25}$ electrons to the scattering I shall use James and Brindley's[7] calculations for the ASF of Rb+. The effective nuclear charge $(Z-S)$ for the $4s$ and $4p$ electrons of Rb+ should be in the range 5–7 and that for $4s$ and $4p$ electrons for copper in the range 1.1 to 2.5. Using the Rb+ data as a basis and taking the ratio of $(Z-S)$ values of Rb+ to copper to be 2.0 we find on correction for change in effective nuclear charge that the total contribution of the $4s^1\ 4p^{2.25}$ electrons to the scattering, on this basis, is −0.278. Even though exchange effects would tend to increase this value somewhat it is doubtful that these effects would make the contributions of these electrons to the scattering become greatly positive, where we may define "greatly positive" as a total contribution greater than 0.15. We also have some protection in having used the most unfavorable and unlikely ratio of $(Z-S)$ values. Any larger ratio should have the ultimate effect of lowering the extent of contribution of these electrons to the ASF. We shall, therefore, fairly safely, ignore the contributions of the $4s^1\ 4p^{2.25}$ electrons to the ASF.

The extent to which electrons are moved into a covalent bond from an originally spherically symmetrical distribution is a point on which there is still some disagreement. On examination of the electron density distributions, obtained by x-ray methods in various organic compounds Cochran[8] concludes that, "The electron density in a covalent bond is very little more than is obtained by placing two 'non-interacting' atoms one bond length apart." Brill[9] and Franklin[10] conclude that there is a relatively large concentration of electrons at the centers of covalent bonds (in diamond and graphite, respectively). If Cochran's conclusions can be extrapolated to copper we already have obtained an estimate of the effect of the $3d^{7.75}\ 4s^1\ 4p^{2.25}$ configuration on the scattering. It is of interest, however, to make an estimate of the effect of directional bonding on the scattering. We start with the general expression,

$$\Delta F=\int\int\int \rho[\exp 2\pi i(hx+ky+lz)]d\tau,$$

where ΔF is the contribution to the structure factor of the electrons in a bond above the number present due to overlap of spherical atoms; ρ is the increase in electron density due to this effect, h, k, l are Miller indices; x, y, z are fractions of the lattice constant a; and the integration is to be taken over a region containing these extra electrons in the bond. For purposes of calculation we will assume that ρ is constant and that the extra

[8] W. Cochran, Acta Cryst. **4**, 81 (1951).
[9] R. Brill, Acta Cryst. **3**, 333 (1950).
[10] R. E. Franklin, Nature (London) **165**, 71 (1950).

TABLE II.[a] Comparison of calculated and observed ASF copper.

Reflection indices (1)	f (based on Hartree-Fock treatment-$3d^{10}$ configuration) (2)	f observed (Zn radiation) (3)	Δf (Zn radiation) (4)	Deviation from dispersion correction ($\Delta f+3.9$) (5)	f observed (Cu radiation) (6)	Δf (Cu radiation) (7)	Deviation from dispersion ($\Delta f+3.0$) (8)
(111)	21.9	18.3	−3.6	+0.3	18.9	−3.0	0.0
(200)	20.6	15.6	−5.0	−1.1	17.2	−3.4	−0.4
(220)	16.6	12.6	−4.0	−0.1	13.5	−3.1	−0.1
(311)	14.6	10.6	−4.0	−0.1	11.5	−3.1	−0.1
(331)	11.3	7.55	−3.8	+0.1	8.4	−2.9	+0.1
(420)	11.0	7.15	−3.8	+0.1	8.0	−3.0	0.0

[a] With the exception of columns 5 and 8 this table appears in *The Optical Principles of the Diffraction of X-Rays* by R. W. James, (G. Bell and Sons, London, 1948), p. 186.

electrons are in a rectangular box of square cross section with the unique axis directed toward nearest neighbors (i.e., along a cube face diagonal). Using these ideas one obtains the following equation for the measured contribution Δf_{111} of the extra electrons to the (111) ASF.

$$\Delta f_{111}=\frac{(3.6)^3(8)(12)\rho \sin 2\pi z_0}{4(2\pi)^2\sqrt{2}} \times[x_0 \sin 2\pi\sqrt{2}y_0-y_0 \sin 2\pi\sqrt{2}x_0]$$

where x_0, y_0, and z_0 are each half of one of the dimensions of the box and y_0 is equal to z_0. For the (200) reflection we obtain

$$\Delta f_{200}=\frac{(3.6)^3 8z_0}{4}\left[\frac{8x_0 \sin 4\pi y_0}{4\pi}-\frac{16 \sin 2\pi\sqrt{2}x_0 \sin 2\pi\sqrt{2}y_0}{8\pi^2}\right].$$

If $x_0=y_0=z_0$ then Δf_{111} is identically zero. For a volume where $2x_0=\sqrt{2}a/8$ and $2y_0=2z_0=\sqrt{2}a/16$ the total contribution to (111) is 0.01ρ. If we assume this volume and that ρ is equal to one electron per cubic angstrom, then this corresponds to moving a total of approximately 0.4 electron from each atom into the covalent bonds. For the volume chosen, the length of box in the face diagonal direction is equal to $\frac{1}{4}$ of the interatomic distance which seems to be a very safe maximum for this direction. For any volume chosen where the length of a side is less than or equal to $\sqrt{2}a/8$ the effect of the contribution to the (111) reflection is negligibly small.

The contribution to the (200) reflection ASF is always negative and is equal to -0.15ρ for the box of volume $\sqrt{2}/8\times\sqrt{2}/16\times\sqrt{2}a^3/16$. For a box of volume $[\sqrt{2}a/16]^3$ it is -0.54ρ. If ρ is equal to 1 the former volume corresponds to a shift of 3.17 electrons from each atom into covalent bonds and the latter volume to a shift of 1.09 electrons from each atom. If, as seems reasonable, the volume in which the extra electrons would appear is smaller than that chosen, then the contribution to the (200) reflection will be less than that calculated here. An electron density of one seems to be a maximal value because it is larger than that obtained by Ageev and Ageeva for the total electron density of copper in the bond and their calculations were carried out in such a manner that one would expect them to obtain too great an electron density in the bond (see reference 4).

We see, therefore, that a difference of −0.65 seems a fair estimate for the difference in ASF caused by a change from $3d^{10}\,4s^1$ to the $3d^{7.75}\,4s^1\,4p^{2.25}$ configuration for the (111) reflection. This is, of course, not a certain value but, as noted, we have been rather careful, in doubtful cases, to take values which seemed to be on the safe side. For the (200) reflection the number of extra electrons moved into the bond and the volume in which they are contained causes a great effect and this number is uncertain. A fair minimum value seems to be −0.36.

COMPARISON WITH AVAILABLE DATA

Brindley and Spiers[11] have obtained the atomic scattering factors listed in column six of Table II using copper radiation and Rusterholz obtained the data in column three with zinc radiation. Ageev and Ageeva[3] have independently obtained intensity data for copper with copper radiation and their data agree extremely well with that of Brindley and Spiers, after scaling by making the intensity of one reflection agree with that obtained by Brindley and Spiers. Unfortunately, since the radiations used are close to the absorption edge of copper a large dispersion effect is present. This dispersion correction is independent of angle since it depends only on the k electrons. To evaluate the dispersion correction we subtract the measured ASF from the ASF computed from a Hartree-Fock self-consistent field radial distribution function and in the standard fashion assume that the differences for the higher order reflections are due to dispersion. If we take 3.0 for dispersion correction for Cu radiation and 3.9 for the dispersion correction for Zn radiation and subtract these values from those in columns six and four, respectively, we obtain the effect of other influences than dispersion on the ASF.

The data in columns five and eight of Table II show two points of consistency: (1) The difference between the calculated ASF and the experimental ASF for the (111) reflection is essentially equal to the dispersion correction, and (2) the large negative deviation for the (200) reflection. In connection with the first point it should be pointed out that conceivable experimental

[11] G. W. Brindley, Phil. Mag. **21**, 778 (1936).

errors such as those due to extinction are negative in sign, are directly proportional to the intensity of a reflection, and therefore should affect the (111) reflection the most since it is the most intense. It is difficult to conceive of reasonable errors in the reverse direction. If the data for the (111) reflection is seriously accepted it would, of course, support the $3d^{10}\ 4s^1$ configuration since the observed ASF is equal to the calculated ASF for that configuration. The marked negative deviation for the (200) reflection is puzzling. As shown, a movement of a large number of electrons into the bond on the Pauling model will account for this deviation but the largeness of the number of electrons needed to be moved into the bond makes this possibility seem unlikely. This deviation may have something to do with systematic errors in measuring intensities since the data of Brindley[11] for aluminum where any directional bonding would have no effect on the intensities show that the (200) reflection here is also weaker than it should be when corrected for dispersion.

CONCLUSIONS

Calculation has shown that a measurable difference in atomic scattering factor is predicted for the outer electron configuration $3d^{7.75}\ 4s^1\ 4p^{2.25}$ in copper as compared with the other postulated configuration $3d^{10}\ 4s^1$. This difference amounts to 3 percent in the ASF of a (111) reflection which corresponds to a 6 percent difference in intensity. For a (200) reflection the difference is at least 3.7 percent in intensity and for other reflections it is much smaller. Comparison with available data has shown that the observed value of ASF for a (111) reflection is equal to that calculated on the basis of a $3d^{10}\ 4s^1$ configuration (after correction for dispersion). Comparison of data for the (200) reflection showed an anomalous difference between observed and calculated values which may be due to experimental uncertainties. Therefore, the available data, while suggestive, are probably not reliable enough from which to draw any final conclusions about the outer electron configuration in metallic copper.

A word might be said in conclusion about the measurement of ASF for the low order reflections. To be certain of the difference of 6 percent calculated for the (111) reflection an experimental accuracy of about 2 percent would be necessary, which should be obtainable with careful technique. The best data would be that for which the dispersion effect is quite small, such as that obtained with tungsten K radiation. This leads to problems in intensity measurements since a Geiger counter will be inefficient at this wavelength. The use of scintillation counter techniques with a heavily absorbing phosphor suggest themselves. What can most easily be done is to check the copper radiation data in order to resolve the (200) ASF anomaly. It seems, therefore, at the edge of possibility that an accurate determination of the outer electron configuration in copper should be possible in the near future.

I would like to thank Drs. R. S. Mulliken and T. H. Walnut for helpful discussions.

Thermal Analysis of the System $PbBr_2$–PbO

L. M. KNOWLES
Ethyl Corporation Research Laboratories, Detroit, Michigan
(Received June 19, 1951)

A thermal analysis of the system $PbBr_2$–PbO proved the existence of four compounds intermediate between $PbBr_2$ and PbO, namely $PbBr_2 \cdot PbO$, $PbBr_2 \cdot 2PbO$, $PbBr_2 \cdot 3PbO$, and $PbBr_2 \cdot 7PbO$. The compound $PbBr_2 \cdot PbO$ was unstable above 497°C whereas the others were stable at their melting points. Pure $PbBr_2 \cdot PbO \cdot H_2O$ (or Pb(OH)Br) was prepared and was found to decompose into $PbBr_2 \cdot PbO$ at temperatures above 150°C. This work offers an explanation for the discrepancies among data reported in the literature for the melting point of lead bromide.

THE present paper reports a determination, by thermal analysis, of the complete phase diagram for the system $PbBr_2$–PbO, together with some observations on the chemical preparation and thermal decomposition of $PbBr_2$–PbO–H_2O (or Pb(OH)Br). Extensive x-ray diffraction data related to this work will be the subject of a forthcoming publication from these Laboratories.

Thermal analysis studies have been reported previously by Sandonnini[1] and Bruni,[2] the former claiming formation of one stable compound, $PbBr_2 \cdot 2PbO$, and two peritectic compounds, $PbBr_2 \cdot PbO$ and $PbBr_2 \cdot 4PbO$; the latter being in agreement except for an indication that the $PbBr_2 \cdot 4PbO$ was more probably $PbBr_2 \cdot 6PbO$. Critical examination of the experimental data of both of these investigators reveals discrepancies and indicates questionable accuracy.

The literature[3] on the chemical preparation of the various lead oxybromides is confused, undoubtedly in some cases as a result of the preparation of lead hydroxybromide, instead of $PbBr_2$, by precipitation from aqueous media.[4] Further evidence for this conclusion is presented herein.

EXPERIMENTAL

Materials

Mallinckrodt Analytical Grade PbO and $PbBr_2$ were tested by chemical and spectrographic means and found to be at least 99.90 percent pure. This source of lead oxide was chosen for its high density and comparatively small volume change on fusion. The lead bromide decreased considerably in volume when it was melted, a disadvantage which was overcome by fusing the salt in a Vycor flask, quenching it on a highly polished copper block, and grinding. This treatment did not in any way affect its chemical purity.

As a material for the crucible, Pyrex, Vycor, zirconia, titania, alumina, titanium, and tantalum were shown to be unsatisfactory. Platinum, gold, and magnesia were sufficiently resistant to attack for contact times of less than 4 to 5 hours, but were also attacked significantly if subjected to prolonged exposure at high temperatures (900°C).

Apparatus and Procedure

A 60-g charge of the desired mixture was placed in a magnesia crucible 30 mm in diameter and 50 mm long. The crucible was inserted into a closed end Sillimanite tube placed in the cavity of a heavily insulated Hoskins crucible type electric furnace. The voltage across the furnace was stabilized with a Sola inductance-type unit, regulated with a 5-ampere Variac autotransformer, and observed with a voltmeter.

When the fusion temperature was reached the melt was first mixed by stirring with a platinum wire. Then, an assembly, which consisted of a 24-gauge bare platinum, platinum-10 percent rhodium thermocouple and a platinum ring stirrer, was fitted onto the mouth of the Sillimanite tube so that the thermocouple and stirrer were centered in the melt. The stirrer wire was attached to a glass rod which was coupled to a Burgess Vibrotool (a vibrator of the type used as a marking tool). By this means, the stirrer could be regulated to give a ripple or a full beating of the melt. The thermocouple wires were each 100 cm long and terminated, with welded copper leads, in an ice bath.

Figure 1 shows a schematic diagram of the electrical circuit used. All components (including the *K*-2 potentiometer and Speedomax recorder) were shielded to ground, in order to prevent amplifier stray-field pickup. The amplifier was a Perkin-Elmer instrument, of the dc breaker type. The arbitrary gain factor of the amplifier, and therefore the recordings, was checked frequently by standardization with the potentiometer. This was important at points near the cooling curve breaks in order that critical thermal values could be determined as accurately as possible (approx ±0.1°C). Background noise and ripple in the recordings were

[1] G. Sandonnini, Atti. accad. nazl. Lincei (5), **23**, 959 (1914).
[2] G. Bruni, Atti. accad. nazl. Lincei (6), **20**, 384 (1934).
[3] G. Andre, Ann. chim. et phys. (6) **3**, 114 (1884); A. J. Balard, *ibid.* (2) **32**, 337 (1826); A. deSchulten, Bull. Soc. Min. **20**, 188 (1897); A. Ditte, Chem. Revs. **94**, 1311 (1882); Karaoglanov and D. Tschawdarov, Z. anorg. u. allgem. Chem. **187**, 273 (1930); Z. Karaoglanov and B. Zagortchev, *ibid.* **211**, 16 (1933); C. Löwig, *Das Brom und seine chemischen Verhältnisse*, Heidelberg (1829); V. P. Shvedor, J. Gen. Chem. (USSR) **17**, 27 (1947); D. Strömholm, Z. anorg. u. allgem. Chem. **38**, 437 (1904); and R. Weinland and F. Paul, *ibid.* **129**, 254 (1923).
[4] L. M. Knowles, J. Am. Chem. Soc. **72**, 4817 (1950).

reduced considerably by negative feedback modifications to the amplifier and by a filtering circuit on the input of the recorder. The Speedomax recorder had a full scale deflection of 0 to 6 mv, with 5-mv steps, for a full range of 0 to 51 mv. Relative placement of the thermocouple, amplifier, power supply, and recorder with respect to the voltage stabilizer, Variac, and ac power lines was critical because of the fields generated by the latter units. The thermocouple was calibrated and standardized periodically by checking against the known melting points of $PbBr_2$ (370.0±0.2°) and $PbCl_2$ (497.0±0.5°).

Chemical analysis for both lead and bromine after each run showed an insignificant change in composition. In no case was volatilization of lead bromide, oxidation by air, or attack of the crucible material sufficient to alter the initial composition weighed out, no change being greater than ±0.3 mole percent PbO.

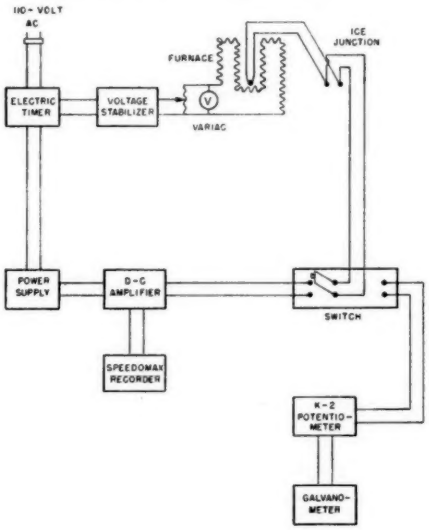

FIG. 1. Schematic circuit diagram.

RESULTS

A typical curve obtained using the apparatus and procedure described above is shown in Fig. 2. The conformity to theoretical curves, the absence of supercooling, and the relatively long breaks are noteworthy. The accuracy of the individual temperatures reported here is estimated to be ±0.5°C for temperatures below approximately 600°C and ±1.0°C for temperatures above 600°C.

The complete thermal data obtained in the study are shown in Table I, and the resulting phase diagram is plotted in Fig. 3. This diagram indicates that four intermediate compounds are formed between $PbBr_2$ and PbO, namely $PbBr_2 \cdot PbO$, $PbBr_2 \cdot 2PbO$, $PbBr_2 \cdot 3PbO$, and $PbBr_2 \cdot 7PbO$. The first intermediate ($PbBr_2 \cdot PbO$) is unstable above 497°C, whereas the others are stable at their melting points. Spot checks by microscopic examination confirmed the presence of the phases indicated by the thermal equilibrium diagram. A dilute solution of ammonium sulfide was used as the etchant.

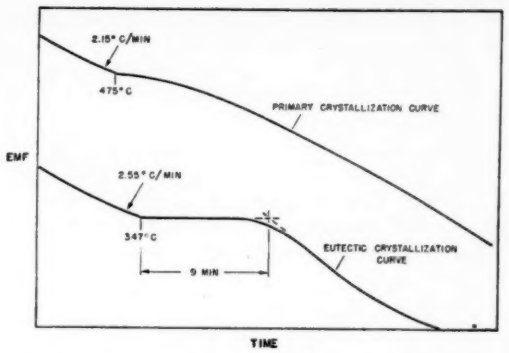

FIG. 2. emf *vs* time for 30 mole percent PbO in $PbBr_2$.

A precipitate of pure $PbBr_2 \cdot PbO \cdot H_2O$ was prepared by the slow addition, with stirring, of 1500 ml of carbon dioxide-free lead acetate solution (containing 67 g of the salt) to two liters of carbon dioxide-free solution

TABLE I. Thermal data observed for the system $PbBr_2$—PbO.

Composition mole percent PbO	Primary break temp, °C	Peritectic break temp, °C	Duration of peritectic break, min	Eutectic break temp, °C	Duration of eutectic break, min
0	370	...	...	...	...
7.00	358	...	...	347	8
12.00	347	...	...	347	17
15.50	380	...	...	347	15
20.00	414	...	...	348	12
25.00	447	...	...	348	9
27.50	461	...	...	348	8
30.00	475	...	...	347	6
32.25	488	...	...	347	5
35.00	495	...	...	347	4
37.50	508	497	...	347	3
40.00	537	497	...	347	3
42.25	567	497	...	347	2
45.00	592	497	11	347	2
50.00	640	497	15	...	...
55.00	676	497	10	...	...
60.00	695	497	5	...	...
62.25	703	497	3	...	...
65.00	707	497	1	...	...
66.67	709	...	...	...	...
68.25	707	...	...	697	3
70.00	704	...	...	697	5
71.36	700	...	...	697	15
72.50	697	...	...	697	24
73.67	703	...	...	697	8
75.00	707	...	...	...	...
77.50	706	...	...	706	16
80.00	713	...	...	704	17
82.50	727	...	...	704	11
85.00	737	...	...	704	4
87.50	741	...	...	...	...
88.20	740	...	...	737	9
90.00	761	...	...	737	10
92.50	800	...	...	737	8
95.00	831	...	...	737	5
100.00	888	...	...	...	...

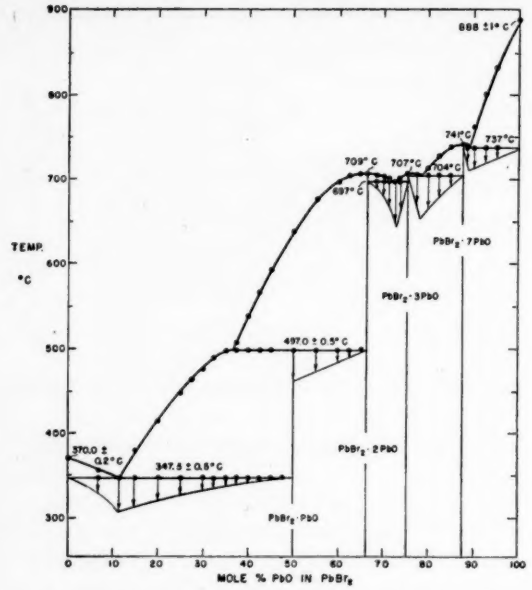

FIG. 3. Phase diagram of the $PbBr_2$–PbO system.

containing 90 g of potassium bromide. This precipitate was heat treated in an open crucible in air to determine the course of its thermal decomposition, with the results shown in Table II.

X-ray diffraction data (to be evaluated in a forthcoming publication from these Laboratories) indicated the existence of three polymorphic forms of the $PbBr_2 \cdot PbO$ formed on dehydration, which are arbitrarily designated as I, II, and III in the table. The thermal decomposition data indicate that above approximately 150°C the $PbBr_2 \cdot PbO \cdot H_2O$ decomposes completely into compositions within the $PbBr_2$-PbO system, all of which show the 497°C $PbBr_2 \cdot PbO$ peritectic transformation temperature. This probably explains why many early investigators report melting points of $PbBr_2$ near 490°C. They had simply prepared the $PbBr_2 \cdot PbO \cdot H_2O$ which decomposed readily at low temperatures, by dehydration, into $PbBr_2 \cdot PbO$. This

TABLE II. Products from the thermal dehydration of $PbBr_2 \cdot PbO \cdot H_2O$.

Heating conditions Duration, hours	Temp, °C	Composition (approximate) after heating as shown by x-ray diffraction[a]
24	128	no change
48	149	a small amount of I formed
64	201	a trace of I, 15 percent of $PbBr_2 \cdot 2PbO$, and the remainder equal amounts of II and III
48	250	75 percent III and 25 percent $PbBr_2 \cdot 2PbO$
48	300	75 percent III and 25 percent $PbBr_2 \cdot 2PbO$
64	355	75 percent III and 25 percent $PbBr_2 \cdot 2PbO$
48	410	75 percent III and 25 percent $PbBr_2 \cdot 2PbO$
48	450	60 percent III and 40 percent $PbBr_2 \cdot 2PbO$

[a] I, II, and III designate polymorphic forms of $PbBr_2 \cdot PbO$.

gives a peritectic transformation temperature on cooling which is easily confused with the curve for the freezing of a pure compound, particularly if the primary crystallization temperature is considerably above the peritectic transition, as it is in this system.

DISCUSSION

The phase diagram reported herein agrees essentially with those of Sandonnini[1] and Bruni[2] up to a composition of 66.7 mole percent PbO. The only major discrepancy in this range is the temperature of peritectic transition which was found to be 497°C and which the earlier investigators reported to be 475°C. Our experience has shown that this value can be depressed as much as 25 to 30° by poor conditions of equilibrium and by rapid cooling rates. It should be noted that these earlier investigators, using 30- and 60-g samples, obtained breaks in the cooling curves of less than 3 minutes for the same melts for which we obtained rests of 20 minutes or longer. The tendency of the melt to supercool, along with poor equilibrium, high cooling rates, attack on contact materials, and volatilization of $PbBr_2$, particularly above 500°C, undoubtedly contributed to the inaccuracy of the earlier data.

Asymptotic Expansion of the Partition Function of the Asymmetric Top

KENNETH F. STRIPP AND JOHN G. KIRKWOOD
*Gates and Crellin Laboratories of Chemistry, California Institute of Technology, Pasadena, California**

(Received June 18, 1951)

Methods developed by Wigner and Kirkwood for the determination of the partition functions of dynamical systems without explicit knowledge of the energy eigenvalues are used to calculate the first two terms of the asymptotic expansion of the partition function of the asymmetric top in powers of Planck's constant. The result is compared with Viney's expansion for the symmetric top and with Gordon's approximate expansion for the asymmetric top.

FOR those systems whose energies are expressible as elementary functions of the quantum numbers, asymptotic expansions of the partition function can be obtained by using summation techniques, such as the Euler-Maclaurin method, on the partition function written as an explicit function of the quantum numbers. In general the energies are not of this form, and such procedures are not applicable. One of the physically simplest cases in point is found in the rotational motion of a rigid molecule with three different moments of inertia, the asymmetric top. An asymptotic expansion of the rotational partition function of such a molecule has not been previously derived, although the corresponding expressions for the symmetric top without[1] and with[2] axial spin, where the energies are of simple form, have been known for some time.

Wigner[3] and Kirkwood[4] have developed direct methods for obtaining asymptotic expansions of the partition function in powers of Planck's constant without explicit knowledge of the eigenvalues of the hamiltonian. In the present article, we shall employ these methods for the calculation of several terms of the asymptotic expansion of the partition function of the asymetric top. The expansion which results proves of course to be symmetrical in the three moments of inertia, and when two of these are set equal it reduces to Viney's expansion for the symmetric top. It is somewhat different in form from the expression proposed by Gordon[5] as a plausible alteration of Viney's formula for use in the asymmetric case.

Kirkwood[4] has demonstrated that the asymptotic expansion can be obtained in the following way. For a system of M degrees of freedom, the partition function may be written as,

$$Z=(2\pi\hbar)^{-M}\int_{-\infty}^{\infty}\int_{\Omega}\Delta_0^{\frac{1}{2}}(q)e^{-(i/\hbar)p\cdot q}\times e^{-\beta H}\Delta_0^{-\frac{1}{2}}(q)e^{(i/\hbar)p\cdot q}dqdp, \quad (1)$$

where $\hbar$ is Planck's constant divided by 2π and

H = hamiltonian operator

$\Delta_0(q)$ = transformation determinant from rectangular to the generalized coordinates, q. (2)

$$p\cdot q=\sum_{k=1}^{M}p_kq_k \qquad \beta=(kT)^{-1}$$

$$dq=\prod_{k=1}^{M}dq_k \qquad dp=\prod_{k=1}^{M}dp_k$$

and q_k and p_k are M canonically conjugate coordinates and momenta. The integral of Eq. (1) is evaluated by determining a function:

$$\omega=e^{-\beta H}\Delta_0^{-\frac{1}{2}}(q)e^{ip\cdot q/\hbar} \quad (3)$$

which satisfies the Bloch equation:

$$H\omega+\partial\omega/\partial\beta=0; \quad \lim_{\beta\to 0}\omega=\Delta_0^{-\frac{1}{2}}(q)e^{ip\cdot q/\hbar}. \quad (4)$$

Attempting a solution of Eq. (4) in the form:

$$\omega=e^{-\beta E}\Delta_0^{-\frac{1}{2}}(q)e^{ip\cdot q/\hbar}g, \quad (5)$$

where E is the classical hamiltonian and

$$g=\sum_{l=0}^{\infty}g_l\hbar^l, \quad (6)$$

one is led by substitution of Eq. (5) into Eq. (4) and the use of the boundary condition on β to the integral equation for g:

$$g=1+i\hbar\int_0^{\beta}e^{\xi E}K_1(ge^{-\xi E})d\xi+\hbar^2\int_0^{\beta}e^{\xi E}K_2(ge^{-\xi E})d\xi, \quad (7)$$

the form K_1 and K_2 depending on H and $\Delta_0(q)$. Insertion of Eq. (6) into Eq. (7) gives the recursion formulas for the g_l:

$$g_0=1 \qquad g_1=i\int_0^{\beta}e^{\xi E}K_1(g_0e^{-\xi E})d\xi$$

$$g_l=i\int_0^{\beta}e^{\xi E}K_1(g_{l-1}e^{-\xi E})d\xi+\int_0^{\beta}e^{\xi E}K_2(g_{l-2}e^{-\xi E})d\xi \quad (8)$$

* Contribution No. 1586.

[1] H. P. Mulholland, Proc. Cambridge Phil. Soc. **24**, 280 (1928).

[2] I. E. Viney, Proc. Cambridge Phil. Soc. **29**, 142 (1933); **29**, 407 (1933); L. S. Kassel, J. Chem. Phys. **1**, 576 (1933).

[3] E. Wigner, Phys. Rev. **40**, 749 (1932).

[4] J. G. Kirkwood, Phys. Rev. **44**, 31 (1933); J. Chem. Phys. **1**, 597 (1933).

[5] A. R. Gordon, J. Chem. Phys. **2**, 65 (1934).

and substitution of these values into Eq. (5) and thence into Eq. (1) produces the desired asymptotic expansion:

$$Z=(2\pi\hbar)^{-M}\int_{-\infty}^{\infty}\int_{\Omega}e^{-\beta E}\sum_{l=0}^{\infty}g_l\hbar^l dqdp. \tag{9}$$

In applying this procedure to the asymmetric top it is convenient to introduce the "momentoids":[6]

$$\begin{aligned}P&=\cos\varphi p_\theta+\sin\varphi\csc\theta(p_\psi-\cos\theta p_\varphi)\\ Q&=-\sin\varphi p_\theta+\cos\varphi\csc\theta(p_\psi-\cos\theta p_\varphi)\\ R&=p_\varphi\end{aligned} \tag{10}$$

where θ, ψ, φ are the eulerian angles and p_θ, p_ψ, p_φ the conjugate momenta. Then the classical energy is:

$$E=\tfrac{1}{2}(P^2/A_x+Q^2/A_y+R^2/A_z), \tag{11}$$

the principal moments of inertia being A_x, A_y, A_z. We now define corresponding operators:

$$\begin{aligned}\mathcal{P}&=\cos\varphi\partial/\partial\theta+\sin\varphi\csc\theta(\partial/\partial\psi-\cos\theta\partial/\partial\varphi)\\ \mathcal{Q}&=-\sin\varphi\partial/\partial\theta+\cos\varphi\csc\theta(\partial/\partial\psi-\cos\theta\partial/\partial\varphi)\\ \mathcal{R}&=\partial/\partial\varphi\end{aligned} \tag{12}$$

in terms of which the hamiltonian operator for the asymmetric top is to be written:

$$H=-\hbar^2/2(\mathcal{P}^2/A_x+\mathcal{Q}^2/A_y+\mathcal{R}^2/A_z) \tag{13}$$

as can be seen by expanding Eq. (13) and comparing the results with Wang's[7] operator. Using Eq. (13) in Eq. (4), Eq. (11) in Eq. (5), and the fact that for the eulerian angles

$$\Delta_0(q)=\sin\theta \tag{14}$$

we find for the asymmetric top:

$$\begin{aligned}2K_1=&1/A_x[2P\mathcal{P}+(\mathcal{P}P)-\cos\varphi\cot\theta P]\\ &+1/A_y[2Q\mathcal{Q}+(\mathcal{Q}Q)+\sin\varphi\cot\theta Q]\\ &+1/A_z[2R\mathcal{R}]\\ 2K_2=&1/A_x[\mathcal{P}^2-\cos\varphi\cot\theta\mathcal{P}+\tfrac{3}{4}\cos^2\varphi\cot^2\theta\\ &+\tfrac{1}{2}-\tfrac{1}{2}\sin^2\varphi\csc^2\theta]+1/A_y[\mathcal{Q}^2+\sin\varphi\cot\theta\mathcal{Q}\\ &+\tfrac{3}{4}\sin^2\varphi\cot^2\theta+\tfrac{1}{2}-\tfrac{1}{2}\cos^2\varphi\csc^2\theta]\\ &+1/A_z[\mathcal{R}^2].\end{aligned} \tag{15}$$

The integration of Eq. (9) is facilitated by keeping the "momentoids" rather than the momenta as variables, the equation becoming then:

$$\begin{aligned}Z=(2\pi\hbar)^{-3}&\int_{-\infty}^{\infty}\int_{-\infty}^{\infty}\int_{-\infty}^{\infty}\int_0^{2\pi}\int_0^{2\pi}\int_0^{\pi}e^{-\beta E}\\ &\times\sum_{l=0}^{\infty}g_l\hbar^l\sin\theta d\theta d\varphi d\psi dPdQdR.\end{aligned} \tag{16}$$

We maintain g as a function of P, Q, R by repeated use of the following relations in working out Eqs. (8), (15):

$$\begin{aligned}\mathcal{P}P&=aP+bQ+cR\\ \mathcal{P}Q&=jP+kQ+lR\\ \mathcal{Q}P&=jP+kQ+mR\\ \mathcal{Q}Q&=eP+fQ-cR\\ \mathcal{R}P&=Q\\ \mathcal{R}Q&=-P\\ \mathcal{P}R&=\mathcal{Q}R=\mathcal{R}R=0\end{aligned} \tag{17}$$

where:

$$\begin{aligned}a&=-\sin^2\varphi\cos\varphi\cot\theta & j&=\sin^3\varphi\cot\theta\\ b&=-\sin\varphi(1+\cos^2\varphi)\cot\theta & k&=-\cos^3\varphi\cot\theta\\ c&=\sin\varphi\cos\varphi & l&=\cos^2\varphi\\ e&=\cos\varphi(1+\sin^2\varphi)\cot\theta & m&=-\sin^2\varphi.\\ f&=\cos^2\varphi\sin\varphi\cot\theta\end{aligned} \tag{18}$$

In this way g_1 and g_2 are evaluated without too much difficulty, and substitution into Eq. (16) and integration gives for the asymptotic expansion of the rotational partition function as far as the first nonclassical term:

$$\begin{aligned}Z=(\pi/\sigma_x\sigma_y\sigma_z)^{\frac{1}{2}}[1+\tfrac{1}{12}(2\sigma_x+2\sigma_y+2\sigma_z-\sigma_x\sigma_y/\sigma_z\\ -\sigma_y\sigma_z/\sigma_x-\sigma_z\sigma_x/\sigma_y)\cdots]\end{aligned} \tag{19}$$

in which:

$$\sigma_u=\hbar^2\beta/2A_u. \tag{20}$$

If two moments of inertia are set equal in this formula, it becomes identical with Viney's result for the symmetric top:

$$\begin{aligned}Z=(\pi^{\frac{1}{2}}/\sigma\sigma_z^{\frac{1}{2}})[1+\tfrac{1}{12}(4\sigma-\sigma^2/\sigma_z)\\ +1/480(32\sigma^2-24\sigma^3/\sigma_z+7\sigma^4/\sigma_z^2)\cdots]\end{aligned} \tag{21}$$

as far as the first quantum term.

The calculation of g_3 and g_4 and thence the next term of the expansion by this method would be straightforward, but quite tedious. We can deduce its probable form, however, from the following considerations. An inspection of the way in which A_z and R would enter

[6] See, for example, J. H. Van Vleck *Electric and Magnetic Susceptibilities* (Oxford University Press, London, 1932), p. 34.
[7] S. C. Wang, Phys. Rev. **34**, 243 (1929).

into the calculation shows that σ_z can next occur in the bracket of Eq. (19) as:

$$\sigma_z^2,\ \sigma_z\sigma_k,\ \sigma_z^2\sigma_k/\sigma_l,\ \sigma_z\sigma_k^2/\sigma_l,\ \sigma_k^2\sigma_l/\sigma_z,\ \sigma_z^2\sigma_k^2/\sigma_l^2,\ \sigma_k^2\sigma_l^2/\sigma_z^2 \quad (22)$$

where the subscripts k, l represent x, y or y, x. Assuming that the equivalent roles of the three σ_u displayed thus far will be continued, we write down a general sum of terms of this kind which includes all interchanges of subscripts and in which each term is multiplied by an arbitrary constant. The symmetry condition we are imposing reduces the number of coefficients to four, and these we then evaluate by requiring that once again Viney's expansion should result when two moments of inertia are set equal. The procedure leads to:

$$1/480\Big\{10(\sigma_x^2+\sigma_y^2+\sigma_z^2)+12(\sigma_x\sigma_y+\sigma_y\sigma_z+\sigma_z\sigma_x) -12\Big(\frac{\sigma_x^2\sigma_y+\sigma_x\sigma_y^2}{\sigma_z}+\frac{\sigma_y^2\sigma_z+\sigma_y\sigma_z^2}{\sigma_x} +\frac{\sigma_z^2\sigma_x+\sigma_z\sigma_x^2}{\sigma_y}\Big)+7\Big(\frac{\sigma_x^2\sigma_y^2}{\sigma_z^2}+\frac{\sigma_y^2\sigma_z^2}{\sigma_x^2}+\frac{\sigma_z^2\sigma_x^2}{\sigma_y^2}\Big)\Big\} \quad (23)$$

as the likely form of the next entry in the bracket of Eq. (19). It may be mentioned that a calculation of this kind leads to the correct result when applied to the first nonclassical term.

THE JOURNAL OF CHEMICAL PHYSICS VOLUME 19, NUMBER 9 SEPTEMBER, 1951

Hydrogen Molecule Energy Calculation by Correlated Molecular Orbitals*

ARTHUR A. FROST AND JERRY BRAUNSTEIN†
Department of Chemistry, Northwestern University, Evanston, Illinois
(Received June 13, 1951)

The electronic energy of the hydrogen molecule was calculated using the correlated molecular orbital wave function

$$\psi=(a_1+b_1)(a_2+b_2)(1+pr_{12}),$$

where a_1, b_1, a_2, and b_2 are $1s$ atomic wave functions of electrons 1 and 2 about nuclei a and b, and r_{12} is the interelectronic distance. The p of the above formula together with z, the effective nuclear charge, used in the explicit definition of the atomic orbitals, are two parameters which are varied in minimizing the energy according to the variation method. The energy minimum was found to be 4.11 ev below the value for complete separation of the nuclei. The minimum occurred at an internuclear distance of 0.71A, and the parameters have the values $z=1.285$ and $p=0.28$ in atomic units. The energy is far better than Coulson's best molecular orbital calculation and better than any other two-parameter calculation except for that of Gurnee and Magee.

IT has previously[1] been shown that the wave function

$$\psi=(a_1+b_1)(a_2+b_2)(1+pr_{12}) \quad (1)$$

for the hydrogen molecule has an advantage over an ordinary molecular orbital wave function in that it will give the correct result for the separated atoms, and also that for normal internuclear distances it introduces explicitly a correlation of the electron distributions which is known to be present. This type of function, a product of molecular orbitals multiplied by a correlating factor involving the interelectronic distance r_{12}, is called a correlated molecular orbital (CMO). Previously, only a crude estimate was made of the energy resulting from this function. The integrals have now all been evaluated for the case where the atomic orbitals a_1, b_1, a_2, and b_2 are $1s$ orbitals with effective nuclear charge z.

The electronic energy may be expressed as

$$E=z^2T^0(\rho, q)+zV^0(\rho, q), \quad (2)$$

where $\rho=zR$ and $q=p/z$ are convenient parameters to use in place of R, the internuclear distance, and p. T^0 and V^0 are the mean kinetic and potential energies if $z=1$:

$$V^0(\rho, q)=V_{a,b}{}^0(\rho, q)+V_{12}{}^0(\rho, q), \quad (3)$$

where the latter terms are electron-nuclei and interelectronic potential energies, respectively. These functions can be separated still further into separate functions of ρ and q:

$$T^0(\rho, q)=\frac{K_0(\rho)+2qK_1(\rho)+q^2K_2(\rho)}{I_0(\rho)+2qI_1(\rho)+q^2I_2(\rho)}, \quad (4)$$

$$V^0a, b(\rho, q)=-\Big(\frac{P_0(\rho)+2qP_1(\rho)+q^2P_2(\rho)}{I_0(\rho)+2qI_1(\rho)+q^2I_2(\rho)}\Big), \quad (5)$$

$$V_{12}{}^0(\rho, q)=\frac{I_{-1}(\rho)+2qI_0(\rho)+q^2I_1(\rho)}{I_0(\rho)+2qI_1(\rho)+q^2I_2(\rho)}. \quad (6)$$

* Presented before the American Chemical Society, Chicago, September, 1950. Abstracted from the Ph.D. thesis of J. Braunstein, Northwestern University.

† Present address: Department of Chemistry and Chemical Engineering, University of Washington, Seattle, Washington.

[1] Frost, Braunstein, and Schwemer, J. Am. Chem. Soc. **70**, 3292 (1948).

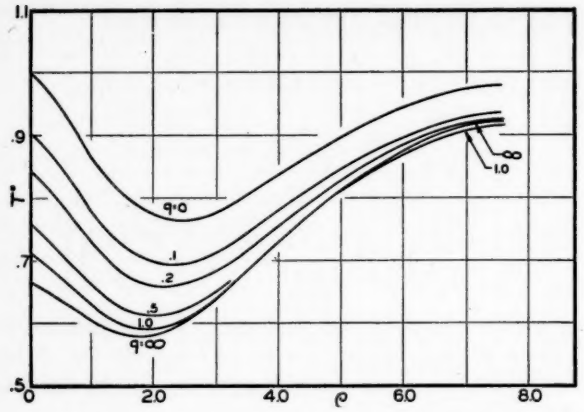

FIG. 1. Kinetic energy at $z=1$ as a function of parameters ρ and q.

The K's, P's, and I's are particular combinations of the integrals which arise on the explicit substitution of Eq. (1) in the variation integral for the energy. The subscript is the exponent of r_{12} in the integrals of the above combinations. Thus, one obtains

$$K_2=-\tfrac{1}{2}\int r_{12}(a_1+b_1)(a_2+b_2)\times\{\nabla_1^2+\nabla_2^2\}r_{12}(a_1+b_1)(a_2+b_2)dv, \quad (7)$$

$$P_1=\int (a_1+b_1)(a_2+b_2)r_{12}\times\left\{\frac{1}{r_{a1}}+\frac{1}{r_{b1}}+\frac{1}{r_{a2}}+\frac{1}{r_{b2}}\right\}(a_1+b_1)(a_2+b_2)dv, \quad (8)$$

$$I_{-1}=\int (a_1+b_1)(a_2+b_2)(1/r_{12})(a_1+b_1)(a_2+b_2)dv, \quad (9)$$

etc.[2] The evaluation of the integrals will be discussed later.

Figures 1, 2, and 3 show T^0, $V_{a,b}{}^0$ and $V_{12}{}^0$ plotted against ρ for various values of q; the curves for $q=0$ are identical with those of the ordinary MO method, while the values of the functions along the ordinate $\rho=0$ are those for the corresponding Hylleraas treatment of the helium atom. It can be seen that at large internuclear distances the T^0's approach the limiting value 1.0 for all q and the $V_{a,b}{}^0$ approach -2.0 for all q; the $V_{12}{}^0$, however, all tend to zero except for the case $q=0$. Thus, the simple MO method implies that even at infinite separation there is a residual repulsion and any degree of correlation whatever reduces this to zero.

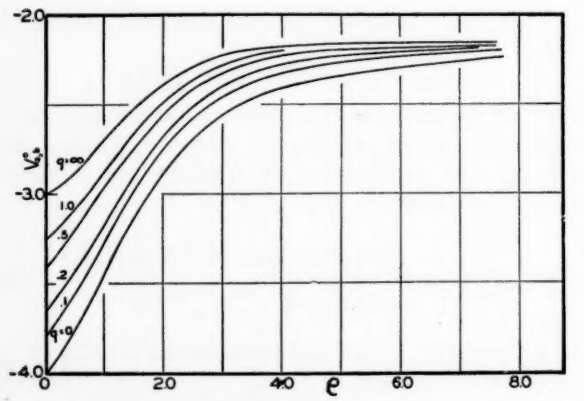

FIG. 2. Electronic-nuclear potential energy at $z=1$ as a function of parameters ρ and q.

[2] Atomic units are used.

The best values of the parameters in the wave function are determined by the usual minimization of the energy. Addition of $1/R$ gives the energy of the hydrogen molecule on the basis of the correlated molecular orbital wave function. This is the CMO curve of Fig. 4; the best values of the parameters z and p (or q) are shown in Figs. 5 and 6. Figure 7 shows a comparison of the CMO results with the results of other methods, in the vicinity of the minimum.

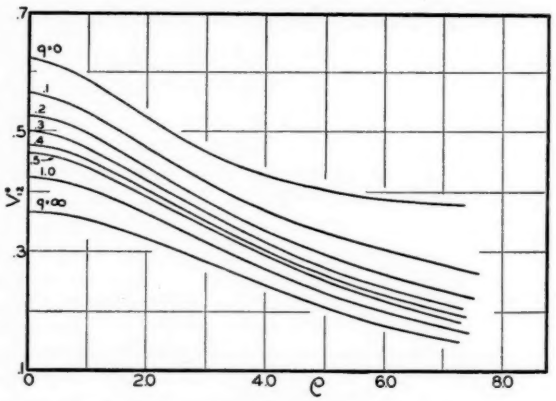

FIG. 3. Interelectronic potential energy at $z=1$ as a function of parameters ρ and q.

RESULTS AND DISCUSSION

The calculated energy of the hydrogen molecule for the CMO wave function is -1.151 atomic units of energy at an internuclear distance of 1.34 atomic units. This corresponds to a binding energy of 4.11 electron volts, the internuclear distance being 0.71A. The calculated energy rises to a maximum of -0.95 au at an internuclear distance of 5.5 au before dropping to the limiting value of -1.0 au at infinite separation of the nuclei. These results are compared with those obtained with other approximate wave functions in Table I and in Fig. 7. The values of the parameters are shown in Figs. 5 and 6.

The energy can be seen to be about the same as that obtained with Weinbaum's three-parameter ionic plus polarization function and is better than that obtained with any of the other two-parameter functions with the exception of that of Gurnee and Magee. Thus, the r_{12} term has the effect of decreasing the weight of the ionic terms of the MO method to the same degree as Weinbaum's ionic function, including, at the same time,

about as much polarization as Rosen's function. The fact that the Gurnee and Magee function, which shifts the undistorted electron clouds into the region between the nuclei, gives a lower energy than the Rosen function, which bulges the electron clouds in both directions along the internuclear axis, indicates that the first type of polarization is a better approximation to the true state of the hydrogen molecule. The CMO function tends to separate the electrons, but this is balanced by the preponderance of ionic terms of the MO function, and the result is that the energy is only 0.04 ev higher than that for the Gurnee and Magee function. Hirschfelder and Linnett's function gives surprisingly good results. In the absence of ionic terms, their three-parameter polarization function gives a binding energy 0.1 ev lower than Rosen's two-parameter function, but the introduction of ionic terms increases the calculated binding energy by 0.33 ev, while Weinbaum's introduction of ionic terms into Rosen's polarization function gave an increase of only 0.19 ev.

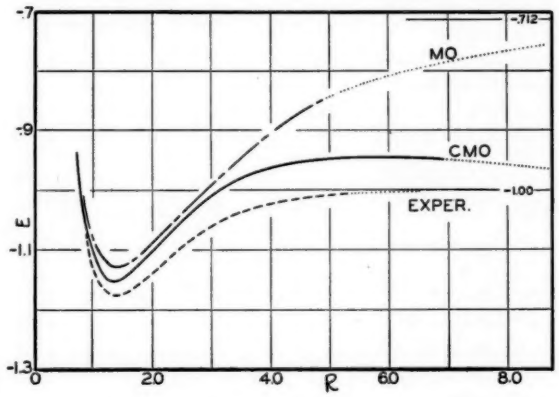

FIG. 4. Energy as a function of internuclear distance.

The binding energy for the CMO function is 0.5 ev greater than that for Coulson's "best" molecular orbital function, which gives a binding energy only 0.13 ev better than does the simple MO function. Furthermore, at large internuclear distances the energy for the CMO function is much closer to the experimental energy than to the energy corresponding to the MO function. The fact that the calculated binding energy is still negative at large separations in Fig. 4 indicates that the function does not provide sufficient correlation, i.e., separation of the electrons at large distances. The additional needed correlation might be obtained by the use of higher powers of r_{12} in the wave function, either in addition to or in place of the term r_{12}.

It would be interesting to observe the behavior of the calculated CMO energy at larger internuclear distances than those in Fig. 7. The form of the function is such that it provides some polarization. If there is an appreciable amount of polarization, then the CMO energy should give a small positive binding energy at these

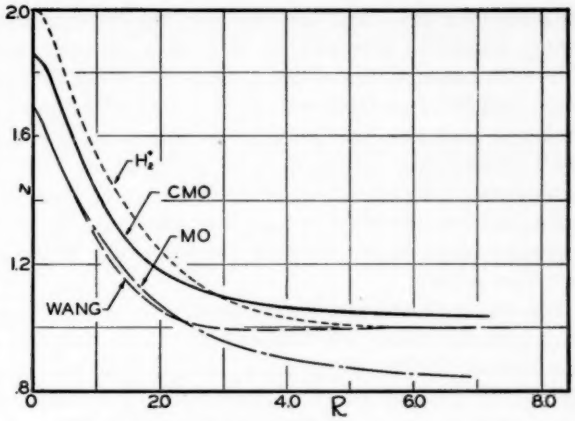

FIG. 5. Effective nuclear charge as a function of internuclear distance.

large distances, and the curve in Fig. 7 would go through another minimum before approaching its limiting value.

It is apparent that the CMO function is a much better approximation for the united atom than for the separated atoms, although the result for the limiting case of infinite separation is correct. Thus, the energy is lowered more at small internuclear distances, and the minimum occurs at a distance smaller than the experimentally observed equilibrium distance; the valence bond functions, on the other hand, give equilibrium distances larger than that observed experimentally because they are better approximations for the separated atoms than for the united atom.

The form of the CMO function appears to be about as good as the corresponding function of Hylleraas for the helium atom from zero internuclear distance to a separation of about 1.5 au, or just beyond the equilibrium distance. Here the difference between the energy

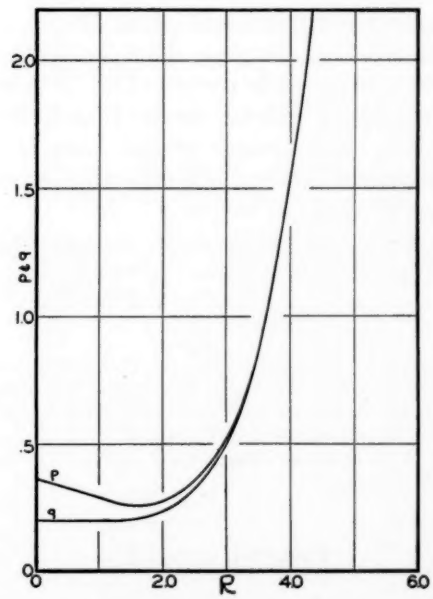

FIG. 6. Parameters p and q as functions of internuclear distance.

calculated for the CMO function and the experimental energy begins to increase. At this same distance, the difference between the effective nuclear charge for the Wang and MO functions and that for the CMO function begins to increase. The behavior of this parameter for small internuclear distances is to be expected. The r_{12} term in the CMO function tends to separate the electrons; and because of this separation, the electrons have a smaller effect on one another than the MO or Wang functions predict.

The value of the correlation parameter p is seen to drop from its value of 0.364 for the helium atom to a minimum of 0.28 at about 1.6 au and then to rise very rapidly. If the dimensionless parameter q is considered, it remains constant at 0.20 from zero internuclear distance to about 1.6 au, where it rises very rapidly. The correlation parameter is extremely large at internuclear distances greater than 5.0 au. This is probably the result of the insufficient amount of correlation provided by the function, as discussed above.

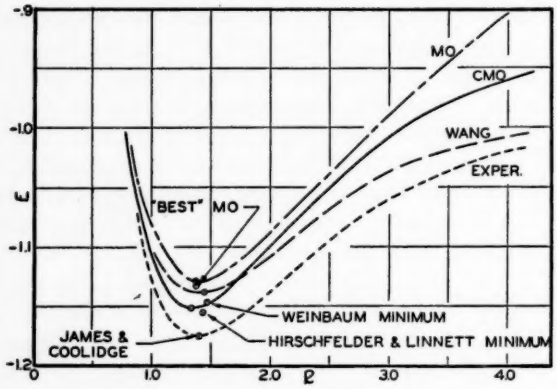

FIG. 7. Energy as a function of internuclear distance.

The extension of CMO-type functions to more complex molecules does not seem feasible at the present time. The new integrals which would be introduced would involve more than two centers if more nuclei were involved and higher atomic orbitals than 1s if more electrons were considered, and their evaluation would be extremely difficult.

This investigation was supported by a grant from the Abbott Fund of Northwestern University.

APPENDIX I

The integrals K_i, P_i, and I_i of Eqs. (4), (5), and (6) break down into separate integrals which may be classified according to the atomic orbitals which are involved, and the functions of the electron-nuclear and interelectronic distances $f(r_{12}, r_{a1}, r_{b1}, r_{a2}, r_{b2})$ which arise in the variation integral for the energy. The three main types which occur are:

coulomb:

$$\int a_1^2 b_2^2 f(r_{12}, r_{a1}, \cdots) dv,$$

$$\int a_1^2 a_2^2 f(r_{12}, r_{a1}, \cdots) dv;$$

TABLE I. Hydrogen molecule calculations.

Wave function	R (A)	D_e ev	D_e kcal/mole	s	p
1.[a] $(a_1+b_1)(a_2+b_2)$ (MO)	0.84	2.65	61.0	(1)	(0)
2.[b] $a_1b_2+b_1a_2$	0.80	3.14	72.0	(1)	
3.[c] $(a_1+b_1)(a_2+b_2)$ (MO)	0.73	3.47	79.8	1.193	(0)
4.[c] $\exp[-\rho(\lambda_1+\lambda_2)]$ $\times f(\mu_1^n, \mu_2^n)$ ("best" MO)	0.73	3.60	82.9		
5.[d] $a_1b_2+b_1a_2$	0.76	3.76	86.7	1.166	
6.[e] $a_1b_2(1+\sigma z_{a1})(1+\sigma z_{b2})$ $+b_1a_2(1+\sigma z_{b1})$ $\times(1+\sigma z_{a2})$	0.77	4.02	92.7	1.190	
7.[f] $a_1b_2+b_1a_2+C\{a_1a_1+b_1b_2\}$	0.77	4.00	92.2	1.193	
8.[f] $a_1b_2(1+\sigma z_{a1})(1+\sigma z_{b2})$ $+b_1a_2(1+\sigma z_{b1})$ $\times(1+\sigma z_{a2})$ $+C\{a_1a_2+b_1b_2\}$	0.77	4.10	94.5	1.190	
9.[g] $(a_1+b_1)(a_2+b_2)(1+pr_{12})$ (CMO)	0.71	4.11	94.6	1.285	0.28
10.[h] $c_1d_2+d_1c_2$; $c_1=Ne^{-sr}c1$ $r_{ac}=r_{bd}=x=0.07$	0.76	4.15	95.7	1.172	
11.[i] $a_1b_2[1+(\alpha z^2)$ $\times(x_{a1}x_{b2}+y_{a1}y_{b2})$ $+(\beta z^2)(z_{a1}z_{b2})]$ $+b_1a_2[1+(\alpha z^2)$ $\times(x_{b1}x_{a2}+y_{b1}y_{a2})$ $+(\beta z^2)(z_{b1}z_{a2})]$ $+c\{a_1a_2+b_1b_2\}$	0.76	4.25	99.0	1.195	
12.[j] $\exp[-\delta(\lambda_1+\lambda_2)]$ $\times\Sigma_{mnjkp}C_{mnjkp}$ $\cdot[\lambda_1^m\lambda_2^n\mu_1^j\mu_2^k$ $\times(2r_{12}/R)^p$ $+\lambda_1^n\lambda_2^m\mu_1^k\mu_2^j$ $\times(2r_{12}/R)^p]$ (thirteen terms)	0.74	4.72 ± 02	108.8		
13.[k] Experiment	0.7395	4.74	109.3		

[a] H. Hellman, *Einführing in die Quantenchemie* (Franz Deuticke, Leipzig, 1937), p. 133.
[b] W. Heitler and F. London, Z. Physik **44**, 455 (1927); Y. Sugiura, Z. Physik **45**, 484 (1927).
[c] C. A. Coulson, Trans. Faraday Soc. **33**, 1479 (1937); C. A. Coulson, Proc. Cambridge Phil. Soc. **34**, 204 (1938).
[d] S. C. Wang, Phys. Rev. **31**, 579 (1928).
[e] N. Rosen, Phys. Rev. **38**, 255, 2099 (1931).
[f] S. Weinbaum, J. Chem. Phys. **1**, 317, 593 (1933).
[g] This paper.
[h] E. F. Gurnee and J. L. Magee, J. Chem. Phys. **18**, 142 (1950).
[i] J. O. Hirschfelder and J. W. Linnett, J. Chem. Phys. **18**, 130 (1950).
[j] Reference 6.
[k] Experiment, see G. Herzberg, *Spectra of Diatomic Molecules* (D. Van Nostrand Company, Inc., New York, 1950), second edition, pp. 99, 351, 532.

exchange:

$$\int a_1b_1a_2b_2 f(r_{12}, r_{a1}, \cdots) dv;$$

mixed:

$$\int a_1^2 a_2 b_2 f(r_{12}, r_{a1}, \cdots) dv.$$

The function $f(r_{12}, r_{a1}, r_{b1}, r_{a2}, r_{b2})$ takes on the following forms:

$$r_{12}^{-1}, r_{12}^n, r_{12}^n/r_{a1}, r_{12}n/r_{b1}, r_{12}n/r_{a2}, r_{12}n/r_{b2},$$

where n has the values 0, 1, and 2. The integrals, after multiplication by a suitable normalization factor, may be thought of as representing average values of $f(r_{12}, \cdots)$ over electronic distributions represented by the products of the atomic orbitals above.

The 64 integrals in the above classification are not all different. In particular, those whose integrands differ only by interchange of

the nuclei a and b or of the electrons 1 and 2, or both, are identical. The integrals in which $n=0$ are separable into integrals over the coordinates of a single electron and easily evaluated in terms of elliptical coordinates. Some of them occur in the hydrogen molecule ion calculations. There remain twenty-five integrals which will be discussed here according to the method of solution. Numerical values of those which have not been published previously have been tabulated in Appendix III.

The following shorthand notation will be used in discussing the integrals. The integrand will be referred to by the letter which identifies the integral: C for the coulombic integrals involving two nuclei, D for the coulombic integrals involving one nucleus, E for the exchange integrals, and M for the mixed integrals. The specific form of the f will be denoted by the superscript and subscript of the letter, the superscript n referring to the exponent of r_{12}, and the subscript being $a1$, $b1$, $a2$, $b2$ for the corresponding coordinates and zero for the function r_{12}^n. Thus, we have

$$\int a_1^2 b_2^2 (r_{12}^2/r_{a1})dv = C_{a1}^2.$$

The general method of solution was to write the integrals in terms of elliptical coordinates. Most of the integrands were then products of exponentials and polynomials in terms of the six variables of integration, and successive ordinary integration could be carried out. This sufficed for the integrals D_{b1}^1, D_{b1}^2, C_0^{-1}, C_0^1, C_0^2, C_{a1}^1, C_{a1}^2, C_{b1}^2, M_0^{-1}, M_0^1, M_0^2, M_{a1}^1, M_{b2}^1, M_{a1}^2, M_{a2}^2, and M_{b2}^2.

The integrals E_0^2, D_{a1}^2, and M_{b1}^2 were solved in the same manner except that, because the coordinates r_{a1}, r_{b1}, r_{a2}, and r_{b2} were all present, r_{12} could not be one of the natural coordinates of the system, but had to be expressed in terms of the other coordinates, using the cosine law. The integration could then be carried out simply, although in practice it was simpler to solve them as well as some of the simpler integrals in terms of the functions defined and tabulated by Kotani, Amemiya, and Simose,[3] Rosen,[4] Zener and Guillemin,[5] and James and Coolidge.[6]

The method used for the seven difficult integrals was that of Kotani *et al.* and is based on the method used by Sugiura to evaluate E_0^{-1}. The integrand is written in terms of elliptical coordinates and defined in terms of r_{a1}, r_{b1}, r_{a2}, and r_{b2}; the term r_{12} in the integrand is expressed as r_{12}^2 in terms of the cosine law multiplied by $1/r_{12}$ expressed as a Neumann expansion in the elliptical coordinates. Except for the case of C_{b1}^1, which involves an infinite series, the series break off after a few terms because of the odd and even properties of the Legendre polynomials and the cosine function in the Neumann expansion. It is then possible to integrate by ordinary methods. The labor has been reduced a great deal by the building up of tables of some of the integrals for different values of one, two, or three variables.

APPENDIX II. LIST OF FORMULAS OF THE CMO INTEGRALS

Separate integrals follow the notation of Kotani, Amemiya, and Simose:[3]

$$\begin{aligned}
D_{b1}^1 &= \rho[A_0(\rho)B_0(\rho) - A_0(2\rho)B_0(2\rho)] \\
&\quad -\tfrac{1}{4}\rho^2[A_1(2\rho)B_0(2\rho)+A_0(2\rho)B_1(2\rho)] \\
&\quad +\tfrac{1}{4}\rho^3[A_2(\rho)B_0(\rho)+A_0(\rho)B_2(\rho)+2A_1(\rho)B_1(\rho)], \\
zD_{b1}^2 &= \tfrac{3}{2}\rho^2[A_1(\rho)B_0(\rho)+A_0(\rho)B_1(\rho)]+\tfrac{1}{8}\rho^4[A_3(\rho)B_0(\rho) \\
&\quad +A_0(\rho)B_3(\rho)+3A_2(\rho)B_1(\rho)+3A_1(\rho)B_2(\rho)], \\
zC_0^1 &= \tfrac{1}{2}\rho^2[A_1(\rho)B_0(\rho)+A_0(\rho)B_1(\rho)]-\rho^2A_1(2\rho) \\
&\quad +\tfrac{1}{8}\rho^4[A_3(\rho)B_0(\rho)+A_0(\rho)B_3(\rho)-A_2(\rho)B_1(\rho) \\
&\quad -A_1(\rho)B_2(\rho)]-(\rho^3/12)[3A_2(2\rho)-A_0(2\rho)], \\
z^2C_0^2 &= 6+\rho^2,
\end{aligned}$$

$$\begin{aligned}
C_{a1}^1 &= \tfrac{1}{4}\rho^2[A_1(\rho)B_0(\rho)+A_0(\rho)B_1(\rho)-2A_1(2\rho)] \\
&\quad +\tfrac{1}{8}\rho^4[A_3(\rho)B_0(\rho)+A_0(\rho)B_3(\rho)-A_2(\rho)B_1(\rho) \\
&\quad -A_1(\rho)B_2(\rho)], \\
C_{b1}^1 &= 1-\tfrac{1}{2}\rho_2A_1(2\rho)+\rho[F_{010}(\rho,-\rho)-F_{001}(\rho,-\rho) \\
&\quad -F_{010}(2\rho,0)+F_{001}(2\rho,0)], \\
zC_{a1}^2 &= (9/2)+\rho^2, \\
zC_{b1}^2 &= \tfrac{3}{2}\rho^2[A_1(\rho)B_0(\rho)+A_0(\rho)B_1(\rho)]+\tfrac{1}{8}\rho^4[A_3(\rho)B_0(\rho) \\
&\quad +A_0(\rho)B_3(\rho)-A_2(\rho)B_1(\rho)-A_1(\rho)B_2(\rho)], \\
zM_0^1 &= \rho^2A_1(\rho)+(\rho^4/12)[3A_3(\rho)-A_1(\rho)]-\tfrac{1}{2}\rho^2[A_1(2\rho)B_0(\rho) \\
&\quad -A_0(2\rho)B_1(\rho)]+\tfrac{1}{8}\rho^3[A_2(2\rho)B_0(\rho)-A_0(2\rho)B_2(\rho)], \\
z^2M_0^2 &= \tfrac{1}{2}\rho^3[3A_2(\rho)-A_0(\rho)]+(\rho^5/40)[5A_4(\rho)-A_0(\rho)], \\
M_{a1}^1 &= \tfrac{1}{4}\rho^2[2A_1(\rho)-A_1(2\rho)B_0(\rho)+A_0(2\rho)B_1(\rho)] \\
&\quad +(\rho^4/12)[3A_3(\rho)-A_1(\rho)], \\
M_{a1}^1+M_{b1}^1 &= (\rho^6/1260)\{21G_0^0(0,\rho)[15W_0^0(4,1,\rho)+15W_0^0(3,2,\rho) \\
&\quad -5W_0^0(3,0,\rho)-30W_0^0(2,1,\rho)+7W_0^0(1,0,\rho)] \\
&\quad +30G_2^0(0,\rho)[-7W_2^0(3,0,\rho)+8W_2^0(1,0,\rho)] \\
&\quad +126G_1^0(1,\rho)[-5W_1^0(3,2,\rho)+3W_1^0(2,1,\rho)] \\
&\quad +105G_0^0(2,\rho)[3W_0^0(2,1,\rho)-W_0^0(1,0,\rho)] \\
&\quad +252G_3^0(1,\rho)W_3^0(2,1,\rho)-210G_2^0(2,\rho)W_2^0(1,0,\rho) \\
&\quad -72G_4^0(0,\rho)W_4^0(1,0,\rho)+63G_1^1(0,\rho)\times[5W_1^1(2,1,\rho) \\
&\quad -W_1^1(1,0,\rho)]-7G_3^1(0,\rho)W_3^1(1,0,\rho)\}, \\
M_{a2}^1 &= \tfrac{1}{4}\rho^3[2A_2(\rho)-\tfrac{2}{3}A_0(\rho)]-\tfrac{1}{4}\rho^2[A_1(2\rho)B_0(\rho) \\
&\quad -A_0(2\rho)B_1(\rho)]+\rho[F_{010}(\rho,0)-F_{001}(\rho,0) \\
&\quad -F_{010}(2\rho,\rho)+F_{001}(2\rho,\rho)], \\
M_{b2}^1 &= \rho[2A_0(\rho)-A_0(2\rho)B_0(\rho)]-\tfrac{1}{4}\rho^2[A_1(2\rho)B_0(\rho) \\
&\quad +A_0(2\rho)B_1(\rho)]+\tfrac{1}{4}\rho^3[2A_2(\rho)+\tfrac{2}{3}A_0(\rho)], \\
zM_{a1}^2 &= (\rho^5/40)[5A_4(\rho)-A_0(\rho)]+\tfrac{1}{4}\rho^3[3A_2(\rho)-A_0(\rho)], \\
zM_{b1}^2 &= (\rho^7/240)\{[A_1(\rho)B_0(\rho)+A_0(\rho)B_1(\rho)][3(5A_4(\rho) \\
&\quad -A_0(\rho))-10(3A_2(\rho)-A_0(\rho))]+5(A_3(\rho)B_0(\rho) \\
&\quad +A_0(\rho)B_3(\rho)+A_2(\rho)B_1(\rho)+A_1(\rho)B_2(\rho)) \\
&\quad \times(3A_2(\rho)-A_0(\rho))\}, \\
zM_{a2}^2 &= 3\rho^2A_1(\rho)+(\rho^4/12)[3A_3(\rho)-A_1(\rho)], \\
zM_{b2}^2 &= 3\rho^2A_1(\rho)+\tfrac{1}{4}\rho^4[A_3(\rho)+A_1(\rho)], \\
zE_0^1 &= (\rho^7/25200)\{6300W_0^0(4,2,\rho)-2100W_0^0(4,0,\rho) \\
&\quad -6300W_0^0(2,2,\rho)+2940W_0^0(2,0,\rho)-280W_0^0(0,0,\rho) \\
&\quad -2100W_1^0(3,3,\rho)+2520W_1^0(3,1,\rho)-756W_1^0(1,1,\rho) \\
&\quad -80W_2^0(0,0,\rho)-144W_2^0(1,1,\rho)+2100W_1^1(2,2,\rho) \\
&\quad -840W_1^1(2,0,\rho)+84W_1^1(0,0,\rho)+16W_3^1(0,0,\rho)\}, \\
z^2E_0^2 &= (\rho^8/360)(3A_2(\rho)-A_0(\rho))[3(5A_4(\rho)-A_0(\rho)) \\
&\quad -5(3A_2(\rho)-A_0(\rho))], \\
2E_{a1}^1 &= (\rho^6/180)\{45W_0^0(4,1,\rho)+45W_0^0(3,2,\rho) \\
&\quad -15W_0^0(3,0,\rho)-75W_0^0(2,1,\rho)+16W_0^0(1,0,\rho) \\
&\quad -30W_1^0(3,2,\rho)+18W_1^0(2,1,\rho)+4W_2^0(1,0,\rho) \\
&\quad +30W_1^1(2,1,\rho)-6W_1^1(1,0,\rho)\}, \\
zE_{b2}^2 &= (\rho^7/360)\{A_1(\rho)[9(5A_4(\rho)-A_0(\rho))-30(3A_2(\rho) \\
&\quad -A_0(\rho))]+5[3A_3(\rho)+A_1(\rho)](3A_2(\rho)-A_0(\rho))\}.
\end{aligned}$$

Numerical values of the various integrals were taken from the work of Rosen[4] and Kotani *et al.*,[3] although certain component integrals had to be evaluated for the first time.

APPENDIX III. TABLES OF VALUES OF THOSE INTEGRALS WHICH HAVE NOT BEEN PUBLISHED PREVIOUSLY

In the following the position of the decimal point is indicated by the number in parentheses, e.g., 4708788(−1) means 0.4708788: 1133604(0) means 1.133604, etc.

ρ	$F_{010}(2\rho,\rho)-F_{001}(2\rho,\rho)$	$F_{010}(\rho,0)-F_{001}(\rho,0)$
1.0	4708788(−1)	1133604(0)
1.5	1951582	5074526(−1)
2.0	8998269(−2)	2492983
2.5	4268694	1286477
3.0	2237792	6843366(−2)
3.5	1168044	3716101
4.0	6217569(−3)	2048250
4.5	3359923	1141775
5.0	1837514	6421306(−3)
6.0	5648848(−4)	2072272
7.0	1784754(−4)	6821857(−4)

[3] Kotani, Amemiya, and Simose, Proc. Phys. Math. Soc. Japan **20**, extra No. 1 (1938); **22**, extra No. (1940).
[4] N. Rosen, Phys. Rev. **38**, 255, 2099 (1931).
[5] C. Zener and V. Guillemin, Phys. Rev. **34**, 999 (1929).
[6] H. M. James and A. S. Coolidge, J. Chem. Phys. **1**, 825 (1933).

ρ	$F_{010}(\rho,-\rho)-F_{001}(\rho,-\rho)$
1.0	8250554(−1)
1.5	3231421
2.0	1473405
2.5	7543480(−2)
3.0	4253858
3.5	2600794
4.0	1698814
4.5	1170247
5.0	8410918(−3)
6.0	4781972
7.0	2982252(−3)

ρ	zC_0^1	zM_0^1	zE_0^1
0	218750(0)	218750(0)	218750(0)
0.5	223908(0)	212501(0)	204022(0)
1.0	238817	195952(0)	167778(0)
1.5	262070	173159(0)	124535(0)
2.0	291949	147769(0)	851544(−1)
2.5	326836	122469(0)	544946(−1)
3.0	365402	990020(−1)	330353(−1)
3.5	406633	783242(−1)	191471(−1)
4.0	449794	608089(−1)	106866(−1)
4.5	494361	464340(−1)	577597(−2)
5.0	539966	349404(−1)	303683(−2)
6.0	633328	190490(−1)	783580(−3)
7.0	728570	995566(−2)	187662(−3)

ρ	$z^2C_0^2$	$z^2M_0^2$	$z^2E_0^2$
0	600000(0)	600000(0)	600000(0)
0.5	625000(0)	587956(0)	564394(0)
1.0	700000(0)	555498	474728(0)
1.5	825000(0)	509155	363765(0)
2.0	100000(1)	454727	258209(0)
2.5	122500(1)	396830	172074(0)
3.0	150000(1)	339050	108793(0)
3.5	182500(1)	284063	657974(−1)
4.0	220000(1)	233708	383156(−1)
4.5	262500(1)	189131(0)	215966(−1)
5.0	310000(1)	150593(0)	118325(−1)
6.0	420000(1)	916147(−1)	330608(−2)
7.0	550000(1)	530806(−1)	853937(−3)

ρ	D_{b1}^1	C_{a1}^1	C_{b1}^1	M_{a1}^1
0	1875000(0)	1.875	1.875	1.875
0.5				
1.0	1451170(0)	2110912(0)	1525007(0)	1705995(0)
1.5	1201925(0)	2375403	1357169	1528913
2.0	9976898(−1)	2706496	1242269	1323669
2.5	8379530(−1)	3084172	1167481	1111898
3.0	7147076	3494112	1119230	9096486(−1)
3.5	6193325	3926358	1087728	7271645
4.0	5446517	4374183	1066664	5696000
4.5	4852417	4833015	1052161	4382657
5.0	4371539	5299872	1041862	3319282
6.0	3645271	6249980	1028663	1828338
7.0	3124898(−1)	7214264(0)	1020871(0)	9628737(−2)

ρ	M_{a2}^1	M_{b2}^1	$M_{a1}^1+M_{b1}^1$	$2E_{a1}^1$
0	1.875	1.875	3.75	3.75
0.5				
1.0	1449023(0)	1387903(0)	2978958(0)	2532360(0)
1.5	1146667	1077034	2446843	1716913
2.0	8754017(−1)	8120732(−1)	1966344	1073895
2.5	6542710	6001952	1555679	6313613(−1)
3.0	4752644	4367331	1214020	3533894
3.5	3413649	3136689	9350691(−1)	1900581
4.0	2420285	2227475	7111410	9889034(−2)
4.5	1697224	1566066	5343155	5004194
5.0	1178958	1091266	3968854	2472901(−2)
6.0	5554673(−2)	5176976(−2)	2122298	5694150(−3)
7.0	2549533(−2)	2392339(−2)	1094049	1231042(−3)

ρ	zD_{b1}^2	zC_{b1}^2	zC_{a1}^2	zM_{a1}^2
0	4.5	4.5	4.5	4.5
0.5			475 (0)	4439048(0)
1.0	3631634(0)	3984988(0)	55 (0)	4267408
1.5	3090572	3858835	675	4003789
2.0	2624514	3899253	85	3667585
2.5	2240654	4065644	1075 (1)	3280836
3.0	1931837	4321352	135	2867734
3.5	1685151	4638624	1675	2451839
4.0	1487611	4998513	205	2053187
4.5	1328081	5388347	2475	1686544
5.0	1197820	5799801	295	1361066
6.0	9996345(−1)	6666607	405	8455024(−1)
7.0	8570469(−1)	7571407(0)	535 (1)	4975229

ρ	zM_{b1}^2	zM_{a2}^2	zM_{b2}^2	zE_{b2}^2
0	4.5	4.5	4.5	4.5
0.5		4207802(0)	4283634(0)	4075029(0)
1.0	3251116(0)	3617481	3862734	3192415
1.5	2475824	2970423	3388790	2263755
2.0	1844728	2368361	2909700	1489076
2.5	1361616	1848625	2447162	9229830(−1)
3.0	1000919	1418932	2016377	5450770
3.5	7335832(−1)	1073895	1628771	3092062
4.0	5357727	8028384(−1)	1291256	1695400
4.5	3895621	5936375	1006059	9029211(−2)
5.0	2817710	4345979	7714958(−1)	4689062
6.0	1448339	2268058	4350212	1186878
7.0	7265843(−2)	1147449(−1)	2338977(−1)	2803237(−3)

The Entropy of Aqueous Solutes

RICHARD E. POWELL AND WENDELL M. LATIMER
Department of Chemistry and Chemical Engineering, University of California, Berkeley, California

(Received May 23, 1951)

The standard partial molal entropies of monatomic ions and of non-electrolytes in aqueous solution can be represented by the empirical expressions,

for monatomic ions: $\bar{S}^0=(3/2)R\ln M+37-270Z/r_e^2$,

for non-electrolytes: $\bar{S}^0=S^{\text{int}}+(3/2)R\ln M+10-0.22V_M$.

Here Z is the absolute value of the charge on the ion, r_e is the effective radius of the ion, and V_M is the molal volume.

These expressions can be interpreted in terms of the smoothed-potential type of partition function for the system.

MONATOMIC IONS

THE theory of the entropy of aqueous ions has received not a little attention.[1–5] The recent measurement of the entropies of several additional +3 ions and of two +4 ions, for which there were no data previously, provides a stringent test of the theoretical formulas.

In Table I a summary is given of the standard partial molal entropies, $\bar{S}^0$, of the monatomic ions.[6] These are conventional ionic entropies, i.e., are based upon $\bar{S}^0=0$ for hydrogen ion. The arguments have been given before[2] for supposing that the true ionic entropy of hydrogen ion is in fact not far from zero. In our subsequent theoretical discussion we shall regard these data as true ionic entropies. From inspection of all the data in Table I, we find it possible to write a general equation for the entropies of the monatomic ions:

$$\bar{S}^0=(3/2)R\ln M+37-270Z/r_e^2, \qquad (1)$$

where M is the atomic weight, Z is the absolute value of the charge of the ion, and r_e is the effective ionic radius. For cations we have taken r_e to be 2.00A greater than the crystal radius and for anions 1.00A greater than the crystal radius, the crystal radii being those given by Pauling.[7] The agreement between Eq. (1) and the experimental data is shown in Fig. 1, in which the function $\bar{S}^0-(3/2)R\ln M$ is plotted against Z/r_e^2. The agreement is remarkably good in view of the large range of variation of the quantities involved: $\bar{S}^0$ from +32 to −83, crystal radius from 0.5A to 2.55A, and charge from −2 to +4.

Some of the points which deviate most widely from the line in Fig. 1 are based upon data which are themselves open to suspicion. For example, if instead of Pauling's crystal radius for Ag^+ we were to use the value derived from Ag_2O, the plotted point for Ag^+ would be shifted to the opposite side of the line. Moreover, the entropies of some of the +3 ions are uncertain by several eu because of uncertainty in the data for the heat of their dilution.

Equation (1) should properly have included a term $R\ln p$, where p is the quantum weight or multiplicity of the ground state. For the majority of the ions considered, the value of p is unity, but for the ions of the transition series and the rare earths this contribution to the entropy may become significant. Thus for Fe^{+++} p is 5 and $R\ln p$ is 3.2 eu.

We can try to interpret these results in terms of a detailed model of the two-component system. A partition function for the smoothed-potential model of the two component system is

$$Q=(n_1+n_2)!/n_1!n_2!\times\left[\frac{(2\pi M_1kT)^{\frac{1}{2}}}{N_0{}^{\frac{1}{3}}h^3}(n_1V_1{}^f+n_2V_2{}^f)Q_1{}^{\text{int}}e^{-\chi_1/kT}\right]^{n_1}\times\left[\frac{(2\pi M_2kT)^{\frac{1}{2}}}{N_0{}^{\frac{1}{3}}h^3}(n_1V_1{}^f+n_2V_2{}^f)Q_2{}^{\text{int}}e^{-\chi_2/kT}\right]^{n_2}. \qquad (2)$$

Here $V_1{}^f$ and $V_2{}^f$ are the contributions per molecule of type 1 and 2 to the free volume of the system. They are

TABLE I. Ionic entropies at 298.15°K.

Cs^+	31.8	Ca^{++}	−13.2	Cr^{+++}	−73.5
Tl^+	30.4	Cd^{++}	−14.6	Al^{+++}	−74.9
Rb^+	29.7	Mn^{++}	−20	Ga^{+++}	−83
K^+	24.5	Cu^{++}	−23.6	U^{++++}	−78
Ag^+	17.67	Zn^{++}	−25.45	Pu^{++++}	−87
Na^+	14.4	Fe^{++}	−27.1	I^-	26.14
Li^+	3.4	Mg^{++}	−28.2	Br^-	19.25
Pb^{++}	5.1	U^{+++}	−36	SH^-	14.9
Ba^{++}	3.0	Pu^{+++}	−39	Cl^-	13.17
Hg^{++}	−5.4	Gd^{+++}	−43	F^-	−2.3
Sn^{++}	−5.9	In^{+++}	−62	OH^-	−2.5
Sr^{++}	−9.4	Fe^{+++}	−70.1	S^{--}	−6.4

[1] W. M. Latimer and C. Kasper, J. Am. Chem. Soc. **51**, 2293 (1929).
[2] Latimer, Pitzer, and Slansky, J. Chem. Phys. **7**, 108 (1939).
[3] H. Ulich, Z. Elektrochem. **36**, 497 (1930).
[4] D. D. Eley and M. G. Evans, Trans. Faraday Soc. **34**, 1093 (1938).
[5] H. S. Frank and M. W. Evans, J. Chem. Phys. **13**, 507 (1945).
[6] See W. M. Latimer, *Oxidation Potentials* (Prentice-Hall, Inc., New York, second edition to be published). Values in general from K. K. Kelley, *Entropies of Inorganic Substances, Revision*, Bureau of Mines Bulletin 477 (1948). Values for Pu^{+3}, Pu^{+4}, U^{+3}, and U^{+4} are based upon unpublished work by R. E. Connick.
[7] L. Pauling, *The Nature of the Chemical Bond* (Cornell University Press, Ithaca, New York, 1939).

to be regarded as partial molecular quantities, and are not necessarily identical with the free volumes of the respective pure liquids. Q^{int} is the internal (rotational, vibrational, and electronic) partition function of the molecule; χ is its potential energy.

We may call species 1 the water and species 2 the solute. Then the partial molal entropy of the solute is, at infinite dilution,

$$\bar{S}_2 = -R\ln N_2 + S_2^{\text{int}} + R\ln\left[\frac{(2\pi M_2 kT)^{\frac{3}{2}}e^{\frac{5}{2}}}{N_0^{\frac{3}{2}}h^3}V_1'\right] + R\frac{V_2'}{V_1'} - \frac{d\chi_2}{dT} + R\frac{d\ln V_1'}{d\ln T} + R\frac{d(V_2'/V_1')}{d\ln T}. \quad (3)$$

The standard partial molal entropy, $\bar{S}_2^0$, is

$$\bar{S}_2^0 = \bar{S}_2 + R\ln N_2 + R\ln 55.5, \quad (4)$$

where N_2 is the mole fraction of solute. This is for a standard state of $1M$. We may write

$$\bar{S}_2^0 - S_2^{\text{int}} - (3/2)R\ln M_2 = \text{const} + R\frac{V_2'}{V_1'} - \frac{d\chi_2}{dT} + R\frac{d(V_2'/V_1')}{d\ln T}, \quad (5)$$

where the constant includes, besides natural constants, only functions of the free volume of pure water. We shall assume that the last term on the right of Eq. (5) is small. We have then to consider the two terms RV_2'/V_1' and $-d\chi_2 dT$. The term RV_2'/V_1' undoubtedly changes as the size of ion changes. However, as we shall find when we come to examine non-electrolyte solutions, the contribution of this term amounts to only a few entropy units. On the other hand, $-d\chi_2/dT$ may become very large, so it appears that most of the variation in entropy from one ion to another arises from this term.

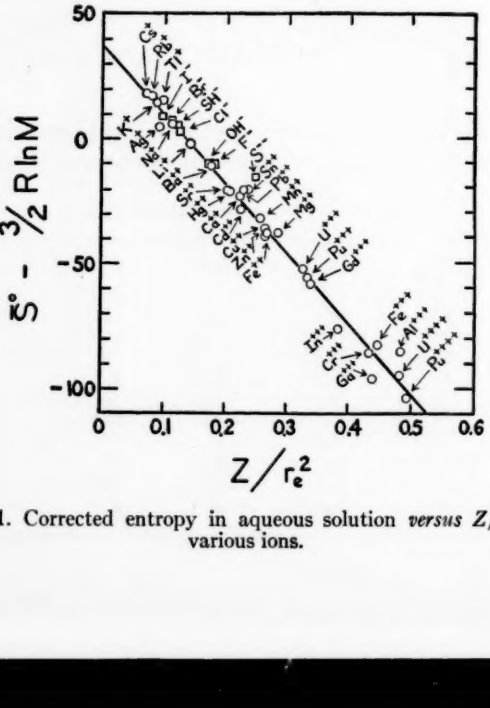

FIG. 1. Corrected entropy in aqueous solution *versus* Z/r^2 for various ions.

For calculation of $-d\chi_2/dT$ we require an explicit expression for the potential energy of the ion immersed in water. Born[8] has proposed that the potential energy is that of a conducting sphere of charge Z and radius r, immersed in a continuum of dielectric constant D. The potential energy would be $\chi_2 = Z^2/2Dr$, and the electrostatic contribution to the entropy would be

$$-d\chi_2/dT = (Z^2/2D^2r)dD/dT. \quad (6)$$

According to Eq. (6) the ionic entropy should be a linearly decreasing function of Z^2/r. A glance at the data will show that the Z-squared dependence required by the Born model is in disagreement with experiment. This disagreement has already been commented upon by several investigators.[2,4]. Coulter and Latimer[9] observed that the ionic entropy decreased more nearly with the first power of Z, and proposed an empirical equation for the entropy of hydration,

$$\Delta S_{\text{hydration}} = B - AZ/r, \quad (7)$$

where B and A are suitable constants. The experimental data can be represented well by Eq. (7), though the agreement is not as good as with Eq. (1).

It is of some interest to inquire what type of physical model could give $-d\chi_2/dT$ proportional to $-Z/r^2$, so as to be consistent with the empirical Eq. (1). Suppose the ion to be a point charge of Z, surrounded at an average distance r by a spherical shell of n water dipoles, each of dipole moment μ, the effective dielectric constant of the intervening space being D. The water dipoles are not free to rotate but are spatially fixed, being held in their positions by their hydrogen-bonding.[10] Such a model for the aqueous ion is quite obviously oversimplified, but we may at least hope it will yield results which are qualitatively correct.

The contribution to the electrostatic potential energy of such an ion would be $\chi_2 = -nZ\mu/Dr^2$, and the contribution to its entropy

$$-d\chi_2/dT = (nZ\mu/Dr^2)[(d\ln n/dT) - d\ln D/dT]. \quad (8)$$

Equation (8) is consistent with Eq. (1) if we can suppose

$$(n\mu/D)[(d\ln n/dT) - d\ln D/dT] \quad (9)$$

to be nearly independent of Z and r. There is very little we can say with assurance about n, μ, D, or the temperature derivatives of n and D. The value of n is probably of the order of 10; its temperature coefficient is expected to be negative, since thermal agitation will decrease the number of molecules effectively oriented about an ion. The value of μ may not be greatly different from its value in the gas, 1.84×10^{-18}. The effective dielectric constant for a dipole in the neighborhood of an ion is not identical with the bulk dielectric constant; we may estimate D to be 10. The temperature coefficient of D

[8] M. Born, Z. Physik **1**, 45 (1920).
[9] L. V. Coulter and W. M. Latimer, J. Am. Chem. Soc. **62**, 2557 (1940).
[10] This model has some, though not all, features in common with the model used by Eley and Evans, reference 4.

is even uncertain as to sign; it would be positive if the predominant effect of increasing temperature were to permit the free rotation of a greater fraction of the locally oriented water dipoles. If we assign the observed value, -270, to the coefficient (9), the temperature coefficient term in brackets takes the value -0.002 deg^{-1}, which is not absurd. The apparent constancy of the coefficient (9) with respect to Z and r may be fortuitous to a certain extent.

NON-ELECTROLYTES

The entropy of inert gases in aqueous solution has been examined from a theoretical point of view by several authors.[5,11–13] We have observed that the entropies of a number of non-electrolytes in aqueous solution can be represented by the expression,

$$\bar{S}^0=(3/2)R\ln M+S^{\text{int}}+10-0.22V_M. \qquad (10)$$

Here $\bar{S}^0$ is the standard partial molal entropy of the solute, the standard state being the hypothetical molal solution; M is its molecular weight; S^{int} is its molal internal (rotational, vibrational, and electronic) entropy, which we have evaluated on the assumption that it is the same as for the gaseous molecule; and V_M is its molal volume in the pure liquid state. The agreement between Eq. (10) and the experimental data is shown in Fig. 2, in which the function $\bar{S}^0-(3/2)R\ln M-S^{\text{int}}$ is plotted against V_M. (This function is most easily evaluated as $26.00-\Delta S^0_{\text{vap}}$.)

It has long been known that the entropies of the rare gases in aqueous solution decrease in the order He, Ne, A, Kr, Xe, Rn. Figure 2 points out that the entropies of a number of other non-electrolytes in aqueous solution, once they have been corrected for internal degrees of freedom, likewise decrease regularly with increasing molal volume. Moreover, the entropies of most solutes lie near to those of the rare gases of the same molal volume, even with solutes which are rather different chemically from the rare gases.

A few solutes which are highly polar (e.g., H_2S, NH_3, SO_2) have entropies more positive by some 5 to 10 eu than those of comparable nonpolar molecules. This is probably related to a local breakdown ("melting") of the water structure, which may even proceed as far as actual compound formation (NH_4OH, H_2SO_3). The entropies of ions, after the effect of charge has been taken into account, are some 20 or 25 eu more positive than those of comparable nonpolar molecules. It is likely that we have here two manifestations of a single phenomenon. Frank and Evans[5] have discussed the point and suggested that the positive increment of entropy arises from a "thawed belt" of water outside of the "frozen patch" of water adjacent to each ion. The high entropy of aqueous N_2 is an anomaly for which we offer no explanation.

Some solutes which are large and nonspherical, especially those (like the alcohols) which can form hydrogen bonds with the water, give points lying below the line on Fig. 2. Probably such molecules are not rotating freely in the solution, so that S^{int} for the solute should properly be taken less than it is in the gas phase. The uncertainty in the internal entropy correction becomes greater for the more complex organic molecules, so we have not attempted to include on Fig. 2 all the organic molecules for which solubility data in water are available. However, such organic solutes generally do give points falling in the neighborhood of the continuation of the line in Fig. 2. Highly polar molecules or those which tend to form loose compounds with water (e.g., formamide, acetone, acetylene) give points lying above the line, and the higher alcohols give points lying below the line.

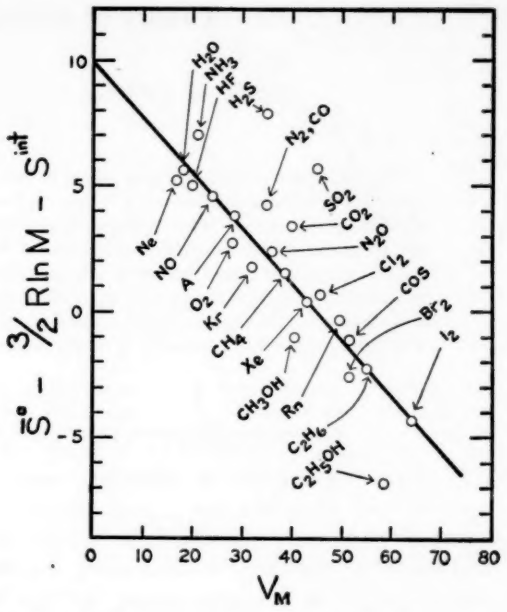

FIG. 2. Corrected entropy in aqueous solution *versus* molal volume for various neutral molecules.

We can recast the empirical Eq. (10) into terms of the smoothed-potential theoretical Eq. (5). If we suppose the term $-d\chi_2/dT$ to be small for these solutes, then Eqs. (10) and (5) are consistent provided

$$RV_2'/V_1'=-0.22V_M. \qquad (11)$$

That is, the partial molal free volume V_2' is negative and proportional to the molecular volume of the solute. A molecule of non-electrolyte added to pure water interacts with the water molecules in such a way that the total free volume of the solution is actually diminished. If one likes, he may interpret this as the "freezing" of water molecules around each solute molecule. In view of the chemical nonspecificity of the effect, it is perhaps more plausible to say that the librational motion of water molecules, which can be considerable in the open lattice of normal water, is more restricted when the molecules are adjacent to a nonpolar solute.

[11] E. Lange and R. Watzel, Z. physik. Chem. **A182**, 1 (1938).
[12] D. D. Eley, Trans. Faraday Soc. **35**, 1281, 1421 (1939).
[13] A. Munster, Trans. Faraday Soc. **46**, 165 (1950).

THE JOURNAL OF CHEMICAL PHYSICS VOLUME 19, NUMBER 9 SEPTEMBER, 1951

Theory of Anisotropic Colloidal Solutions

AKIRA ISIHARA
Department of Physics, Faculty of Science, University of Tokyo, Tokyo, Japan
(Received April 16, 1951)

The appearance of anisotropic phase in the unipolar coacervations of tobacco mosaic virus or bentonite solutions are explained theoretically, and the recent theory of Onsager is confirmed. As has been emphasized already by Langmuir, the repulsive forces between solute molecules and the force arising from thermal agitation are decisive for the occurrence of the anisotropic phase. The critical concentrations where the anisotropic phase starts are explicitly determined for prolate and oblate spheroidal and also cylindrical solute molecules. It is found that the critical concentrations are all inversely proportional to the axial ratios, and therefore, it is explained why these critical concentrations are of the same order of magnitude in spite of the totally different characters of solute molecules.

INTRODUCTION

SOME of the thixotropic or rheopectic sols show coacervations at rather low concentrations. The well-known examples are the cases of tobacco mosaic virus and bentonite particles.[1] In both cases, the second phase solution, which is characterized by the spontaneous birefringence, appears similarly at the concentrations of about 1 to 2 percent in spite of the fact that the respective solute particles have a different appearance—the former are rod shaped, whereas the latter are flat plate-like.

However, they are similar on the point of highly asymmetrical shape, and contrary to the bipolar or the other complex coacervates, the main force between these unipolar coacervates is repulsive. Therefore, it is natural to consider—as Onsager did[2]—that the solute molecules are rigid anisotropic bodies, and the equilibrium in molecular orientation is established between the repulsive force and the one arising from the thermal agitation. If necessary, we can tinge the more precise mean force between the solute molecules with the rigid body potential by enlarging or contracting the molecular shape.

Then, what is the explicit relation between the critical concentration and the molecular shape? We shall give the answer in this paper and shall show that the solution must become anisotropic above the concentration whose magnitude is similar in the two cases mentioned. It must be noted that the present theory does not explain the phenomena of coacervation themselves.

INTEGRAL EQUATION DETERMINING THE MOLECULAR ORIENTATIONS

In the volume V of solution at temperature T, let us consider N solute molecules, N_s of which lie in the solid angle $\Delta\omega$ in the direction specified by the suffix s. Following Onsager,[2] if we take the approximation of imperfect gas theories, the mixing free energy of this system can be expressed by

$$\Delta F = F_0 - kT \log Z, \tag{1}$$

$$Z = N! \prod_s \left[\frac{(\Delta\omega/4\pi)^{N_s}}{N_s!} \right] \int e^{-w/kT} d\tau, \tag{2}$$

where F_0 is the function depending only on temperature, w is the interaction potential between the solute molecules, $d\tau$ is the volume element specifying the positions and the orientations of the molecules:

$$d\tau = \Pi d\tau_s = \Pi dx dy dz \sin\theta d\theta d\varphi / 4\pi. \tag{3}$$

We shall then introduce the distribution function $g(s)$ determining the orientations of the anisotropic solute molecules in space:

$$N_s = N g(s) \Delta\omega(s),$$

$$\int g(s) d\omega(s) = 1. \tag{4}$$

The function $g(s)$ is determined by the minimal condition of the free energy of Eq. (1), and must satisfy the following integral equation:

$$\log 4\pi g(s) = \lambda - c \int \beta(s, t) g(t) d\omega(t), \tag{5}$$

where c represents the number density of the solutes and λ is the parameter determined by the normalizing condition of Eq. (4). As was stated in the first section, the systems we shall deal with are dilute and the higher order of c has been neglected in deriving Eq. (5). The integral kernel $\beta(s, t)$ corresponds to the "irreducible integral" of two solute molecules of orientations s and t, and if we take the approximation of the rigid body potential it is given by the co-volume of the two solute molecules. For a smooth rigid ovaloid, this has been calculated by the present author as the integration over the surface of unit sphere:[3]

[1] L. Langmuir, J. Chem. Phys. **6**, 873 (1938).
[2] L. Onsager, Phys. Rev. **62**, 558 (1942); Ann. N. Y. Acad. Sci. **51**, 627 (1949).
[3] A. Isihara, J. Chem. Phys. **18**, 1446 (1950); A. Isihara and T. Hayashida, J. Phys. Soc. Japan **6**, 40, 46 (1951). With respect to $\beta(s, t)$ for a dumbbell model, see: A. Isihara, J. Chem. Phys. **19**, 397 (1951); A. Isihara and M. Toda, J. Polymer Sci. (to be published).

$$\beta(\gamma)=\frac{1}{6}\int(H+K)(H+K, H+K)d\omega;$$
$$H=H(\alpha,\beta);\quad K=K(\theta',\varphi'),\qquad(6)$$
$$d\omega=\sin\alpha d\alpha d\beta,$$

where γ is the angle between the axes of the two solute molecules A and B having the orientations (θ, φ) and (θ_1, φ_1), respectively (Fig. 1). $H(\alpha, \beta)$ is the length of a perpendicular line drawn from a point of molecule A to the plane of orientation (α, β) which is in contact with the molecule. $K(\theta', \varphi')$ is the corresponding one belonging to the molecule B. $(F, F)\equiv(H+K, H+K)$ is the differential operator for functions H and K on the unit sphere and is defined by the following expressions:

$$(F,F)=2\left[\left(\frac{\partial^2F}{\partial\alpha^2}+F\right)\left(\frac{1}{\sin^2\alpha}\frac{\partial^2F}{\partial\alpha^2}+\frac{\cos\alpha}{\sin\alpha}\frac{\partial F}{\partial\alpha}+F\right)-\left\{\frac{\partial}{\partial\alpha}\left(\frac{1}{\sin\alpha}\frac{\partial F}{\partial\beta}\right)\right\}^2\right].\qquad(7)$$

Geometrically, (H, H) represents twice the product of the principal radii R_1, R_2 corresponding to the direction (α, β):

$$(H,H)=2R_1R_2.\qquad(8)$$

Equation (6) represents the fact that when the molecules A and B are rigid ovaloids, the competent covolume $\beta(\gamma)$ of A and B is also ovaloid shaped; the volume of an ovaloid is given by the formula

$$v=\frac{1}{3}\int HR_1R_2d\omega,\qquad(9)$$

where the integration is to be done, as in the case of Eq. (6), over the surface of unit sphere. Equation (7) can be deduced by combining the property that R_1, R_2, and 0 are the eigenvalues of the matrix (H_{xy}) and the well-known Rodrigues formula defining the principal radius. Here (H_{xy}) is the matrix composed of the second derivatives of the function $H(x, y, z)$ which is connected with $H(\alpha, \beta)$ by the following equation:

$$H(x,y,z)=(x^2+y^2+z^2)^{\frac{1}{2}}\times H\left(\cos^{-1}\frac{z}{(x^2+y^2+z^2)^{\frac{1}{2}}},\frac{\pi}{2}\left(1-\frac{y}{|y|}\right)+\tan^{-1}\frac{y}{x}\right).\qquad(10)$$

As has been demonstrated in the previous paper, it establishes the relation:

$$\int H(K,L)d\omega=\int K(H,L)d\omega,\qquad(11)$$

for the supporting functions H, K, and L on the unit sphere. Therefore, by using Eq. (11), $\beta(\gamma)$ is rewritten as follows:

$$\beta(\gamma)=2v+\frac{1}{2}\int H(K,K)d\omega+\frac{1}{2}\int K(H,H)d\omega,\qquad(12)$$

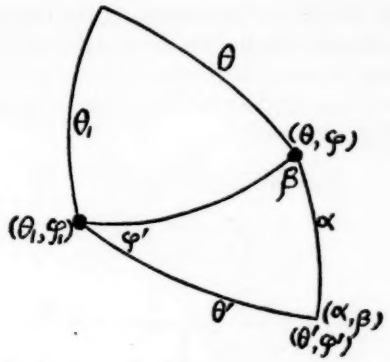

FIG. 1. Configuration of two intersecting anisotropic colloid particles. (θ, φ) and (θ_1, φ_1) represent the axes of molecules A and B, respectively. (α, β) is the direction (measured from the axis of molecule A) of perpendicular line explained in the paper. (θ', φ') is the corresponding one measured from the axis of B.

where v is the volume of a solute molecule and in this equation we have considered that all the molecules have the same shape.

Now, as a typical case, we shall apply Eq. (12) to the ellipsoid of revolution:

$$\left.\begin{aligned}x&=a\sin\alpha\cos\beta,\\ y&=a\sin\alpha\sin\beta,\\ z&=b\cos\alpha.\end{aligned}\right\}\qquad(13)$$

In this case, H is determined as

$$H(\alpha)=(a^2\sin^2\alpha+b^2\cos^2\alpha)^{\frac{1}{2}},\qquad(14)$$

irrespective of β. Introducing the eccentricity ϵ:

$$\begin{aligned}\epsilon^2&=1-a^2/b^2\quad(b\geqq a,\ \text{prolate})\\ &=1-b^2/a^2\quad(b\leqq a,\ \text{oblate}),\end{aligned}\qquad(15)$$

Eq. (14) is rewritten:

$$\begin{aligned}H(\alpha)&=b(1-\epsilon^2\sin^2\alpha)^{\frac{1}{2}}\quad\text{(prolate)}\\ &=a(1-\epsilon^2\cos^2\alpha)^{\frac{1}{2}}\quad\text{(oblate).}\end{aligned}\qquad(16)$$

In the configuration of Fig. 1, K is a function of θ' and has the same functional form as H of Eq. (16). Combining Eqs. (12) and (16) and using Eq. (7) and the property:

$$\int H(K,K)d\omega=\int K(H,H)d\omega,\qquad(17)$$

we can obtain the explicit form of integral kernels corresponding to the configuration of Fig. 1:

$$\begin{aligned}\beta(\gamma)&=2v+2a^2b(1-\epsilon^2)\int_0^{\pi/2}\frac{(1-\epsilon^2\sin^2\alpha)^{\frac{1}{2}}}{(1-\epsilon^2\sin^2\theta')^2}\sin\alpha d\alpha d\beta\quad\text{(prolate),}\\ &=2v+2ab^2\int_0^{\pi/2}\frac{(1-\epsilon^2\cos^2\alpha)^{\frac{1}{2}}}{(1-\epsilon^2\cos^2\theta')^2}\sin\alpha d\alpha d\beta\quad\text{(oblate).}\end{aligned}\qquad(18)$$

As can be seen from the definition, the mean value of $\beta(\gamma)$ is connected with the second virial coefficient A_2 in the equation of osmotic pressure. The calculations of the previous theories[3] show that this is expressed by the following equations:

$$A_2=(4N_0v/M_2^2)f, \tag{19}$$

$$f=\frac{1}{8v}\int_0^{\pi/2}\beta(\gamma)\sin\gamma d\gamma, \tag{20}$$

$$=\frac{1}{4}\left(1+\frac{\rho s}{v}\right), \tag{21}$$

where N_0 is Avogadro's number, M_2 the molecular weight, s the surface area of solute molecule and ρ is the "mean radius" of the solute molecule defined by

$$\rho=(1/4\pi)\int Hd\omega. \tag{22}$$

THE DISTRIBUTION FUNCTION AND THE CONDITION FOR THE APPEARANCE OF ANISOTROPIC PHASE

(a) Prolate Spheroid

To solve the integral equation, it is convenient to expand the kernel in Legendre polynomials:

$$\beta(\gamma)=2v+B_0(\epsilon)-\sum_{l=1}^{\infty}B_l(\epsilon)P_{2l}(\cos\gamma). \tag{23}$$

Then, by a straightforward calculation we obtain

$$B_0(\epsilon)=8\pi a^2b(1-\epsilon^2)\int_0^{\pi/2}(1-\epsilon^2\sin^2\alpha)^{\frac{1}{2}}\sin\alpha d\alpha$$

$$\times\int_0^{\pi/2}(1-\epsilon^2\sin^2\alpha)^{-2}\sin\alpha d\alpha=2s\rho, \tag{24}$$

where s is the surface of the ellipsoid and ρ is the mean radius defined in the previous section. Explicitly, these quantities are given by the following equations

$$s=2\pi ab\left\{(1-\epsilon^2)^{\frac{1}{2}}+\frac{\sin^{-1}\epsilon}{\epsilon}\right\},$$

$$\rho=\frac{b}{2}\left\{1+\frac{1-\epsilon^2}{2\epsilon}\log\frac{1+\epsilon}{1-\epsilon}\right\}. \tag{25}$$

Thus, from Eq. (21), we see that if $\epsilon\ll1$, the numerical factor f of Eq. (20) will be

$$f=1+\frac{\epsilon^4}{15}+\frac{\epsilon^6}{15}+\cdots, \tag{26}$$

whereas if $\epsilon\approx1$ and $b\gg a$,

$$f=\frac{3\pi}{32}\frac{b}{a}. \tag{27}$$

The expression (26) has already appeared in previous papers (see Eq. (21)). The coefficients B_l are expressed by

$$B_l(\epsilon)=9\pi a^2b(1-\epsilon^2)\sum_{n\geqq l}\sum_{m\geqq l}$$

$$\times\frac{a_{nl}a_{ml}}{4l+1}\frac{1\cdot3\cdots(2n-3)}{2^nn!}(m+1)\epsilon^{2(n+m)}, \tag{28}$$

$$a_{nl}=\sum_{r\geqq l}^{n}(-)^r{}_nC_r\frac{2r!(4l+1)}{2^{r-l}(r-l)!1\cdot3\cdots(2r+2l+1)}. \tag{29}$$

Inserting the kernel of Eq. (23) into Eq. (5) and expanding the distribution function which is an even function of θ into the Legendre polynomials:

$$g(\theta)=\sum C_{2n}P_{2n}(\cos\theta), \tag{30}$$

we obtain the following expressions for $g(\theta)$ and its expansion coefficients C_n:

$$g(\theta)=\frac{1}{4\pi}\exp\left\{\mu+c\sum_{l=1}^{\infty}B_l(\epsilon)C_{2l}\frac{4\pi}{4l+1}P_{2l}(\cos\theta)\right\}, \tag{31}$$

$$C_{2n}=\frac{4n+1}{4\pi}\frac{\int_0^{\pi/2}g(\theta)P_{2n}(\cos\theta)\sin\theta d\theta}{\int_0^{\pi/2}g(\theta)\sin\theta d\theta}, \tag{32}$$

where μ is the normalizing constant.

Equations such as (32) are the transcendental equations to determine the expansion coefficients C_n. However, it is somewhat difficult to solve such equations rigorously. Fortunately, the critical concentration of the solution where the phase separation begins, is very low and we shall *a priori* neglect the coefficients C_n for $n>2$, and examine the condition of obtaining the second coefficient C_2.

As is illustrated schematically in Fig. 2, this condition is determined where the curve expressing the right-hand side of Eq. (32) as a function of C_2 intersects the straight line corresponding to the left-hand member of the equation. When the concentration is very low, there is no such intersection other than the one at $C_2=0$, which shows that the solution is isotropic. On the other hand, if the concentration increases until the condition

$$cB_1(\epsilon)>5 \tag{33}$$

is established, the second coefficients C_2 in the equation can be determined definitely. Therefore, Eq. (33) gives the required condition for the occurrence of anisotropic phase.

As a matter of course, this condition coincides with that of free energy minimum. Introducing Eqs. (23)

and (30) into Eq. (1), we find

$$\Delta F=F_0-NkT(1+\log c)+NkTc(v+\rho s)$$
$$+\frac{NkT}{2}\sum\frac{(4\pi)^2C_{2l}^2}{(4l+1)}\left(1-\frac{cB_l}{4l+1}\right), \quad (34)$$

which shows the critical concentration is given by

$$c=\frac{\sum C_{2l}^2/(4l+1)}{\sum C_{2l}^2B_l/(4l+1)^2}\approx\frac{5}{B_1}. \quad (35)$$

Then, what is the explicit form of the critical concentration? The summation of the series of Eq. (28) gives the answer:

$$B_1(\epsilon)=8\pi a^2b(1-\epsilon^2)h_1(\epsilon)h_2(\epsilon), \quad (36)$$

$$h_1(\epsilon)=\frac{5}{16}\left\{-\frac{(1-\epsilon^2)(3+\epsilon^2)}{2\epsilon^2}\log\frac{1+\epsilon}{1-\epsilon}+\frac{3}{\epsilon^2}-1\right\}, \quad (37)$$

$$h_2(\epsilon)=\left\{\frac{4\epsilon^2-3}{4\epsilon^3(1-\epsilon^2)^{\frac{1}{2}}}\tan^{-1}\frac{\epsilon}{(1-\epsilon^2)^{\frac{1}{2}}}+\frac{3-2\epsilon^2}{4\epsilon^2(1-\epsilon^2)}\right\}. \quad (38)$$

For such anisotropic molecules as tobacco mosaic virus or bentonite, ϵ is very nearly 1 and these functions can be approximated simply by

$$h_1(\epsilon)=5/8, \quad (39)$$

$$h_2(\epsilon)=\pi/8(1-\epsilon^2)^{\frac{1}{2}}. \quad (40)$$

Therefore, the critical concentration in volume can be expressed as follows:

$$C_v=\frac{4\pi}{3}a^2bc=\frac{32}{3\pi}\frac{a}{b}=3.4\frac{a}{b}. \quad (41)$$

The dimension of tobacco mosaic viruses has not yet been sharply determined, because it depends upon the purification of the sample and also on the methods of measurements. However, the current data are given by

$$2a=150\text{A}; \quad 2b=2700\text{A}. \quad (42)$$

Mere insertion of these values into Eq. (42) shows that the concentration given by Eq. (41) gives somewhat higher value than the experiments. This deviation may be originated in the electrostatic repulsion between virus molecules, which makes these molecules repel each other before they come into contact. From our standpoint, we must replace such forces by a mean force of rigid body type. Equation (41) indicates that the effective force is of repulsive character, the range of which is equivalent to the ellipsoid of major axis $2b$ and minor axis $2a$. These values correspond to the critical concentration of about 2 percent and seem to be very plausible.

(b) Oblate Spheroid

The same procedure can be applied to the oblate spheroid. The expansion coefficients of the integral kernel are given by

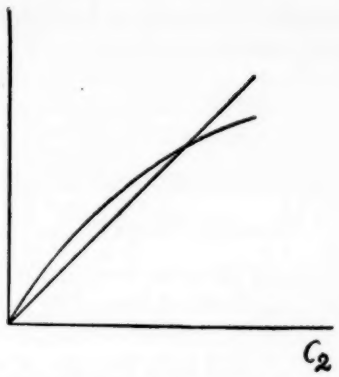

FIG. 2. Schematic representation of both sides of Eq. (32) for C_2. The second expansion coefficient C_2 of the distribution function is determined by the intersection of the two curves in the figure.

$$\beta(\gamma)=2v+B_0(\epsilon)-\sum_{l=1}^{\infty}B_l(\epsilon)P_{2l}(\cos\gamma), \quad (43)$$

$$B_0(\epsilon)=8\pi ab^2\int_0^{\pi/2}(1-\epsilon^2\cos^2\alpha)^{\frac{1}{2}}\sin\alpha d\alpha$$
$$\times\int_0^{\pi/2}\frac{\sin\alpha d\alpha}{(1-\epsilon^2\cos^2\alpha)^2}=2s\rho, \quad (44)$$

where s and ρ are calculated as follows:

$$s=2\pi a^2\left(1+\frac{1-\epsilon^2}{2\epsilon}\log\frac{1+\epsilon}{1-\epsilon}\right),$$
$$\rho=\frac{a}{2}\left\{(1-\epsilon^2)^{\frac{1}{2}}+\frac{\sin^{-1}\epsilon}{\epsilon}\right\}. \quad (45)$$

Therefore, as was noted in the previous papers,[3] the coefficient f of Eq. (19) is the same as the case of the prolate spheroid. (Of course, in Eq. (27) we must replace the axial ratio by its inverse.)

Again, the coefficients $B_l(l\geqq 1)$ are defined by

$$B_l(\epsilon)=8\pi ab^2$$
$$\times\sum_{n\geqq l}\sum_{m\geqq l}\frac{b_{nl}b_{ml}}{4l+1}\frac{1\cdot3\cdots(2n-3)}{2^n n!}(m+1)\epsilon^{2(n+m)}, \quad (46)$$

$$b_{nl}=\frac{2n!(4l+1)}{2^{n-l}(n-l)!1\cdot3\cdots(2n+2l+1)}. \quad (47)$$

Particularly, we have

$$B_1(\epsilon)=8\pi ab^2h_3(\epsilon)h_4(\epsilon), \quad (48)$$

$$h_3(\epsilon)=\frac{1}{4}\left\{\frac{\sin^{-1}\epsilon}{\epsilon}-\frac{3}{4}\frac{\sin^{-1}\epsilon}{\epsilon^3}+\frac{3}{4}\frac{(1-\epsilon^2)^{\frac{1}{2}}}{\epsilon^2}-\frac{(1-\epsilon^2)^{\frac{1}{2}}}{2}\right\}, \quad (49)$$

$$h_4(\epsilon)=\frac{5}{2}\left\{\frac{3}{2\epsilon^2}+1+\frac{\epsilon^2}{1-\epsilon^2}-\frac{1}{4\epsilon}\left(1+\frac{3}{\epsilon^2}\right)\log\frac{1+\epsilon}{1-\epsilon}\right\}. \quad (50)$$

For such thin oblate molecules as bentonite, it is sufficient to replace these functions by

$$h_3(\epsilon)=\pi/32, \tag{51}$$

$$h_4(\epsilon)=5/2(1-\epsilon^2). \tag{52}$$

Thus, the critical concentration in this case is given by

$$C_v=32b/3\pi a=3.4b/a, \tag{53}$$

which is naturally of the same form as Eq. (41). Therefore, since the axial ratio of bentonite is of the same order of magnitude as tobacco mosaic virus,[1] we can expect the experimental fact that the critical concentrations of these molecules are in similar order of magnitude in spite of their totally different characters.

(c) Circular Cylinder

We have hitherto considered the case of the ellipsoid of revolution. Another typical case which is suitable to tobacco mosaic virus is that of the cylindrical model. As has been shown in the previous papers,[3] the H-function for the cylinder of radius a and length $2b$ is given by

$$H(\alpha)=a\sin\alpha+b\cos\alpha, \tag{54}$$

from which the second virial coefficient A_2 has been calculated. In those papers, we have used Eq. (21) in spite of the fact that its applicability for such angular ovaloid was not directly demonstrated. However, from the physical point of view, it is apparent that the formula is true. The right-hand members of it have definite values and meanings if the quantity ρ is determined in this case.

On the other hand, we cannot use the original expressions such as Eq. (7) for the calculation of $\beta(\gamma)$, because they cannot be defined in the cylindrical case. Therefore, we shall utilize the kernel calculated by Onsager:

$$\beta(\gamma)=2v+4\pi a^3\sin\gamma+4\pi a^2b|\cos\gamma|$$
$$+16ab^2\sin\gamma+16a^2b\int_0^{\pi/2}(1-\sin^2\gamma\sin^2\phi)^{\frac{1}{2}}d\phi. \tag{55}$$

Analogous solution of the integral equation is obtained with s and ρ given by[4]

$$s=2\pi a(a+2b), \tag{56}$$

$$\rho=\tfrac{1}{4}(a\pi+2b). \tag{57}$$

The critical concentration is determined by the coefficient:

$$B_1(\epsilon)=\frac{5\pi a}{8}(b-a)(4b-\pi a), \tag{58}$$

as in the previous cases.

[4] We wish here to note that the average value of $\beta(\gamma)$ of Onsager coincide with our previous result. Since his paper was not available to us, we could not cite his result in our papers.

If the axial ratio is very large, this reduces to (in volume concentration):

$$\begin{aligned} C_v&=4a/b \quad \text{(elongated)},\\ &=16b/\pi a=5.1b/a \quad \text{(flat)}, \end{aligned} \tag{59}$$

which are of the same order of magnitude as in the corresponding cases of prolate and oblate spheroids. It is interesting that the coefficient B_1 vanishes at $b=a$. The physical origin of the other zero point $b=\pi a/4$ is not clear.

CONCLUDING REMARKS

In deriving the critical concentrations, we have hitherto totally neglected the contributions from the higher order coefficients B_l. Although, from the definitions of B_l, we can infer the appropriateness of such procedure, we shall here add the expression for B_2 in the case of prolate spheroid:

$$B_2(\epsilon)=8\pi a^2b(1-\epsilon^2)h_5(\epsilon)h_6(\epsilon), \tag{60}$$

$$h_5(\epsilon)=\frac{1}{128}\left\{\frac{1}{2}\left(\log\frac{1+\epsilon}{1-\epsilon}\right)\left(-\frac{35}{\epsilon^5}+\frac{45}{\epsilon^3}-\frac{9}{\epsilon}-\epsilon\right)\right.$$
$$\left.+\left(\frac{35}{\epsilon^4}-\frac{100}{3\epsilon^2}+1\right)\right\}, \tag{61}$$

$$h_6(\epsilon)=\frac{1}{8\epsilon^4}\left\{\frac{-72\epsilon^4+180\epsilon^2-105}{2\epsilon(1-\epsilon^2)^{\frac{1}{2}}}\right.$$
$$\left.\times\tan^{-1}\frac{\epsilon}{(1-\epsilon^2)^{\frac{1}{2}}}+\frac{8\epsilon^4-5\epsilon^2+35}{2(1-\epsilon^2)}+35\right\}. \tag{62}$$

In the limit $\epsilon\to1$, these functions approach to

$$h_5(\epsilon)=1/48, \tag{63}$$

$$h_6(\epsilon)=3\pi/32(1-\epsilon^2)^{\frac{1}{2}}. \tag{64}$$

Therefore, B_2 will assume the form

$$B_2(\epsilon)=\pi^2ab^2/64, \tag{65}$$

and its ratio to $B_1(\epsilon)$ will be

$$B_2/B_1=1/40. \tag{66}$$

Thus, the ratio of the first two members in the denominator of Eq. (35) becomes

$$(C_2^2/C_1^2)(5/9)^2/40, \tag{67}$$

which may be neglected in the first approximation.

To complete the theory, we must of course evaluate the expansion coefficients C_l for $l\geqq2$ as well as the higher irreducible integrals β_l $(l>2)$. These are es-

pecially needed for the discussion of the coacervations explained before.

At any rate, we believe that we have given some enlightenments on the theory of anisotropic colloidal solutions. Some of the origins of analogous phenomena in soap solutions, in disk-shaped tungstic acid sols, or in some lipide systems may be put in the category of our theory. With respect to the role of attractive and repulsive forces in the stability of lyophobic sols and the effect of added salts, the reader should refer to the recent work of Verwey and Overbeek.[5]

[5] E. J. W. Verwey and J. Th. G. Overbeek, *Theory of the stability of Lyophobic Colloids* (Elsevier Publishing Company, Inc., New York, 1948).

THE JOURNAL OF CHEMICAL PHYSICS VOLUME 19, NUMBER 9 SEPTEMBER, 1951

The Infrared Spectra of *N*-Acetylglycine and Diketopiperazine in Polarized Radiation at 25° and at −185°C*

ROGER NEWMAN AND RICHARD M. BADGER
Gates and Crellin Laboratories of Chemistry,† California Institute of Technology, Pasadena, California
(Received April 17, 1951)

The infrared absorption spectra of single crystals of N-acetylglycine and of diketopiperazine have been observed at room temperature, and at −185°C, using polarized radiation. The spectrum of the former substance shows some remarkable changes with temperature. In both cases cooling produces a pronounced narrowing of the broad bands due to the vibration of hydrogen atoms involved in strong hydrogen bonds. The two spectra furnish examples of NH absorption in the two extremes of weak and very strong hydrogen bonding. In diketopiperazine two possible interpretations of the doublet structure in the NH valence band are offered.

INTRODUCTION

THE present paper describes the results of an investigation of the polarized infrared spectra of two crystalline substances related to glycine, N-acetylglycine and diketopiperazine (glycine anhydride). The crystal structures of both these substances have been determined by x-ray methods and are of a particularly simple type. In view of this comparative simplicity it was felt that a study of the infrared spectra of these substances might provide worthwhile information of the relationship between spectrum and structure in amino acids and related compounds.

CRYSTAL STRUCTURES[1,2]

The crystals of both acetylglycine and diketopiperazine are monoclinic and belong to the space group C_{2h}^5. In Fig. 1 we have shown a unit cell diagram for acetylglycine. In Fig. 2 two views of the unit cell of diketopiperazine are shown. For the first substance the essentially planar molecules (exclusive of the hydrogen atoms) lie parallel to (100). The molecules are presumably joined together by a two-dimensional network of hydrogen bonds, as indicated in the figure. For the second substance, the planar molecules (again exclusive of the hydrogen atoms) lie almost parallel to (101). The inclination of the molecular planes to this crystallographic plane is approximately 6°. The molecules are joined together by the system of hydrogen bonds as shown in the figure.

It is worth pointing out the germane features of the hydrogen bonds. In acetylglycine a bond is formed between two oxygen atoms of different molecules. The O—H···O distance is 2.56 au, which is one of the shortest bonding distances of this type so far reported. On the other hand the bond formed between a nitrogen of one molecule and an oxygen of another is rather long

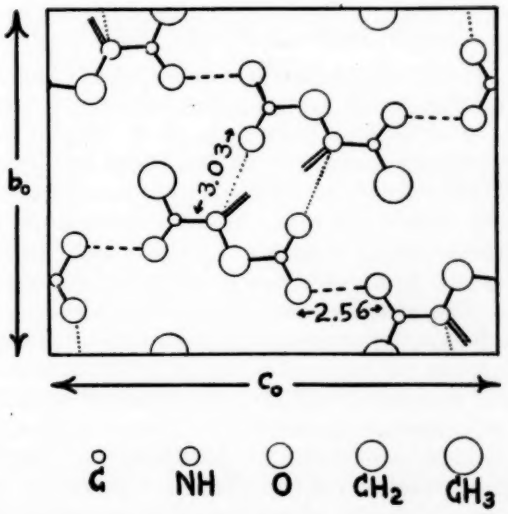

FIG. 1. Unit cell of N-acetylglycine. A view perpendicular to (100). The dashed and dotted lines show the hydrogen bonds. The doubled lines represent the spectroscopically determined directions of the N—H bonds (after Carpenter and Donohue).

* This investigation was supported by the ONR under contract N6-ori-102, VI.
† Contribution No. 1558.
[1] G. B. Carpenter and J. Donohue, J. Am. Chem. Soc. **72**, 2315 (1950).
[2] R. B. Corey, J. Am. Chem. Soc. **60**, 1598 (1938).

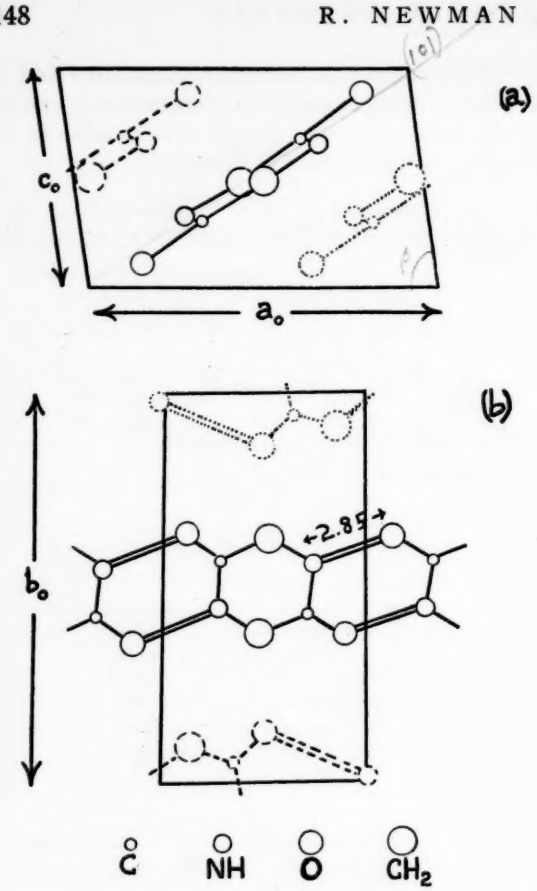

FIG. 2. Unit cell of diketopiperazine (a) View perpendicular to (010). (b) View perpendicular to (101). The doubled lines show the hydrogen bonds (after Corey).

for an N—H···O bond, 3.03 au. In diketopiperazine the N—H···O bonds are in contrast quite short, 2.85 au. These bond lengths and the accompanying implications of bond strengths will be important in our subsequent discussion of the spectra.

SELECTION OF ORIENTATIONS

As was pointed out elsewhere[3] the selection of orientations for the observation of polarized spectra in crystals of the monoclinic system may be a difficult task. Fortunately for the crystals studied in the present work the relative simplicity of the crystal structures considerably reduced this job. In the crystals of both substances the heavy atoms of a given molecule have been shown to be very nearly coplanar. The median planes of all molecules are parallel, and indeed parallel to the **b** axis. To an approximation quite adequate for our purposes we may regard the molecules as having a plane of symmetry, and the normal modes as divided into two classes which are symmetric and antisymmetric with respect to reflection in this plane. Consequently whatever transient electric moment is generated by a given vibration will either be parallel or perpendicular to the symmetry plane. Generalizing to the crystal, it is therefore readily seen that to obtain maximum information, observations should be made with the electric vector of the light beam either parallel to or perpendicular to the parallel symmetry planes, i.e., to the median planes of the molecular skeletons.

For the observation of the in-plane motions a further simplification is possible since the **b** axis lies, in both cases, in the plane paralleling the molecules. Observations of motions in this plane should be made with the electric vector of the light beam parallel or perpendicular to **b**, since the latter is a symmetry-fixed eigenvector of the complex dielectric tensor.

The foregoing arguments of course have meaning only in the case of a plane parallel light beam incident upon the crystal. In the present work this is not the situation. The micro-illuminator used produces a convergent beam incident upon the sample. This in turn has the effect of introducing into the observed spectrum contributions from an unwanted source. That is, one must expect to find the spectrum, which is characteristic for the electric vector vibrating perpendicular to the face of the crystal section being studied, superimposed upon the spectrum of interest. Data are not available for making an accurate calculation of this mixing but an estimate based on very simple considerations indicated that in our apparatus the observed spectrum would consist of about 80 to 90 percent of the desired component. This degree of purity is adequate for qualitative considerations.

EXPERIMENTAL

A. Apparatus

The spectra were taken both with a Beckman IR-2 spectrometer (NaCl optics) and in the region from 4000 to 2800 cm^{-1} with a vacuum grating instrument.[4] The samples, whose preparation is described subsequently were mounted at the focus of an all reflecting infrared microscope or micro-illuminator having an evacuable housing and provided with means for cooling the sample

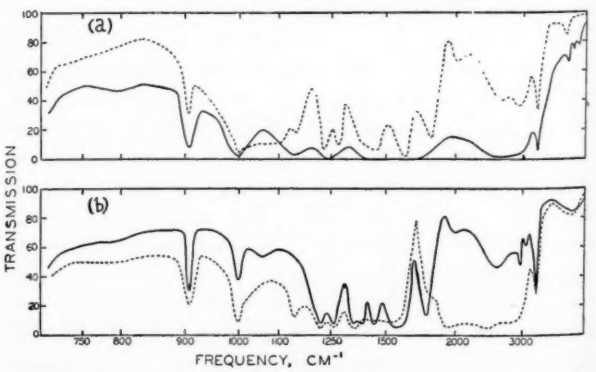

FIG. 3. Spectra of N-acetylglycine at 25°C. (a) Spectra of (011) section about 30μ thick. Solid curve for $E\|$(100), dashed for $E\perp$intersection (100) and (011). (b) Spectra of (100) section about 5 to 10μ thick. Solid curve $E\|$**b**, dashed $E\|$**c**.

[3] R. Newman and R. S. Halford, J. Chem. Phys. **18**, 1276 (1950).

[4] Badger, Zumwalt, and Giguère, Rev. Sci. Instr. **19**, 861 (1948).

holder to liquid air temperature. Polarization was produced by means of a silver chloride polarizer.[5,6]

Our micro-illuminator will be described elsewhere in detail, but a few remarks regarding the construction and operation of the low temperature equipment may be of interest. As in other cells for low temperature work recently described,[7,8] the sample holder projects from the inner thimble of a Dewar vessel, which, in our instrument, extends as a side arm from the casing of the micro-illuminator. The stainless steel Dewar tube is attached with a sylphon bellows, and adjusting screws are provided so that the sample under observation can readily be adjusted in the optical focus without breaking the vacuum.

Using an oil diffusion pump with suitable water-cooled baffle an operating pressure of about 2×10^{-5} mm was obtainable. Even at this pressure, the rate of ice formation on the cooled sample was not negligible. However, spectra could be taken for somewhat over an hour after the initial cooling before an ice band ($\sim3\mu$) of objectionable intensity developed, which, allowed sufficient time for our work. Presumably, if the various gasketed joints were made more permanent than was convenient for us to do, both the operating pressure and the related rate of ice formation would have been considerably reduced. The thermal efficiency of the system is comparatively high. The initial cooling consumed about 50 ml of liquid nitrogen and the subsequent rate of consumption was about 40 ml per hour. The sample reached thermal equilibrium at about −185°C in about 5 minutes after the initial introduction of refrigerant. The temperature was measured on a trial run by imbedding a chromel-alumel thermocouple in a sheet of silver chloride placed in the position normally occupied by the sample.

TABLE I. Frequencies (cm^{-1}) observed for acetylglycine.[a]

b_0		c_0	⊥(100)	Intensity	Tentative assignments
4500		4500		w	2×OH stretch
3340	=	3340		s	N−H stretch
3150				w	2×1600
2980				w	C−H stretch
2500		3000			OH stretch
	≪	to		vs	2×1280
2000		1850			2×1000
1750	>	∼1750		s	C=O stretch (carboxyl)
1600	>	1600			C=O stretch (acetyl)
		to		vs	
1440	>(?)	1400			CH_2, CH_3 bends
1350	<	1350		s	NH_2 bend, CH_2 wagging, twisting
1280	<	1280		s	
1220	<	1220		s	CH_3 bends
		1150		w	
1060				w	
			∼1020	w	
1000	<	1000		s	C−N−C stretch
905	<	905		s	
770		770		w	

[a] The inequalities give the relative intensity in the two orthogonal directions b and c. The symbol ∼ indicates a shoulder. Since our data for the third column were obtained from a crystal section which produced a mixing of the three spectra (b, c, ⊥(100)) we have elected to omit in the third column any frequency which appears in the first two. This would be in accord with the theoretical mutual exclusion of the (100) and ⊥(100) spectra.

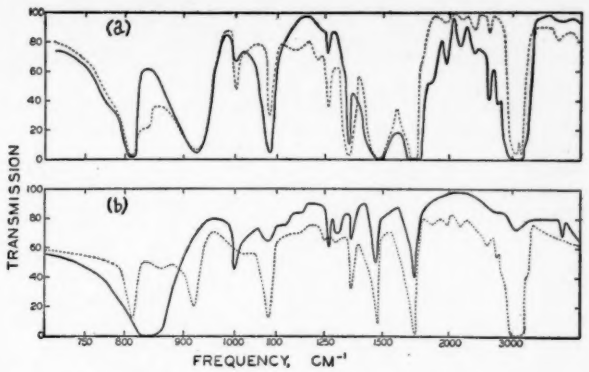

FIG. 4. Spectra of diketopiperazine at 25°C. (a) Spectra of (101) section about 20μ thick. Solid curve $E\|[101]$, dashed $E\|\mathbf{b}$. (b) Spectra of (010) section about 10μ thick. Solid curve $E\perp[101]$, dashed $E\|[101]$.

B. Preparation of Samples

Acetylglycine

Small crystals (several millimeters on an edge) of this substance were grown from aqueous solution at room temperature. For these crystals and for those of diketopiperazine, identification was achieved by reference to their well-described optical, geometrical, and mechanical properties.[1,2] Sections with faces parallel to (100) were obtained by cleaving the crystals parallel to this plane with a razor blade. Sections about 60μ thick could be obtained in this way. These were further thinned by a hand-polishing technique essentially like that previously described.[3] The final product was a section somewhat less than 10μ thick. Some attempts were made to prepare sections using a microtome. The results were not, however, as satisfactory as those of the aforementioned method, although some usable specimens were obtained.

After the sections were prepared they were mounted on a mask of thin copper sheet. As the crystals did not always completely cover the hole in the mask, additional masking was obtained by means of pieces of aluminum foil cemented to the copper sheet. The mask was then attached to a brass strip which could in turn be mounted on a modified goniometer head. The latter allowed the crystal to be carefully placed at the focus of the micro-illuminator. This mounting procedure was employed for all the specimens used.

As was pointed out previously we would have liked to obtain a section of acetylglycine whose faces were perpendicular to the molecular plane (100). However, because of the marked cleavage of the crystals parallel to this latter plane, this ambition was not fulfilled. Sections which were approaching a suitable thickness would invariably fracture and be rendered useless in some stage of the procedure. As an alternative, although not a

[5] R. Newman and R. S. Halford, Rev. Sci. Instr. **19**, 270 (1948).
[6] N. Wright, J. Opt. Soc. Am. **38**, 69 (1948).
[7] E. L. Wagner and D. F. Hornig, J. Chem. Phys. **18**, 296 (1950).
[8] A. Walsh and J. B. Willis, J. Chem. Phys. **18**, 552 (1950).

TABLE II. Frequencies (cm^{-1}) observed for **b** spectrum of acetylglycine at 25° and −185°.[a]

25°	−185°	25°	−185°
3340	3340		1170*
3150	3150	~1150	
2980	2980		1130*
2930	2930		1095*
2500	2500		1065*
	2280*	1060	
	2020*		1005*
2000		1000	
~1950	~1950		995*
1820	1820	905	910
1750	1750		
1600 to 1500	1600 to 1500		
1440	1440		
1400			
1380	1380		
1300 to 1220	1320*		
	1280*		
	1230*		
	1205*		

[a] The symbol ~ indicates a shoulder. The starred frequencies are those which are manifest only at the low temperature. This table refers to spectra taken from a sample about twice as thick as that to which the spectra of Table I belong. Consequently certain weak bands are listed here which do not appear in that table.

completely satisfactory one, it was found possible to prepare sections with faces parallel to (011). This plane makes an angle of about 45° with (100). Although the same difficulty was encountered as before, by occasional good fortune a usable specimen was obtained.

Diketopiperazine

Crystals of this substance were grown from aqueous solution at 50°C. At this temperature fairly large thin plates formed whose faces were parallel to (010). By further polishing of these plates suitable specimens about 10μ thick were produced. From other more symmetrically formed crystals, sections with faces parallel to (101) were obtained. For this purpose, due to the poor solubility of this substance, a slight departure from the conventional technique was employed. The innovation was simply the use of a microtome to plane the crystals down parallel to (101). In the final thinning operation the hand-polishing technique was again employed. Sections about 20μ thick were obtained in this way.

RESULTS AND DISCUSSION

The spectra of acetylglycine at room temperature are shown in Fig. 3, those of diketopiperazine in Fig. 4. A listing of the observed frequencies, their intensity-orientation relationships and assignments are given in Tables I, II and III. In these tables a number of bands are given several alternative assignments or none at all. The frequencies and polarization data provided insufficient information to allow for unambiguous assignments in these cases.

No particular purpose would be served by discussing the complete spectra in detail. Both the molecules and their spectra are too complex for such a treatment. However, it does seem worth while to study those features of the spectra which are not overwhelmingly complex or obscure and which perhaps can yield additional information concerning the crystal structures and dynamics. The discussion which follows points out what we believe to be the more important results in this connection.

A. Acetylglycine

Two strong hydrogen stretching fundamentals would be expected to appear in the spectrum of this substance, one due to the N−H bond and the other to the O−H bond.[9] For reasons that will become apparent from the subsequent discussion we ascribe the sharp band at 3340 cm^{-1} to the N−H stretching vibration and the broad intense band extending from 1850 to 3000 cm^{-1} to the O−H stretching. The relatively weak C−H stretching band appears at 2980 cm^{-1}.

The band at 3340 (N−H) is of only moderate intensity and is quite narr , (half-width approximately 40 cm^{-1}). A study of the polarization behavior of the band for several samples seemed to indicate that the change in electric moment of the individual molecule projected in the (100) plane is directed at 45±10° to the **c** axis.‡ For reasons given it was not possible to obtain data that would conclusively demonstrate that the component in a direction perpendicular to the (100) plane is zero. However, structural considerations would indicate that in all probability the N−H bond is very nearly parallel to this plane, a conclusion supported by our limited data. We can consequently infer that the angle between the N−H bond and the bond joining the nitrogen and central carbon atom is approximately 100°. The error in this estimate may be as large as 10°, but is not so large as to admit the possibility that the hydrogen atom lies on a line connecting nitrogen and oxygen atoms, (i.e., the dotted lines of Fig. 1) which requires an angle of 132°.

All these observations strongly support the conclusion that the N−H···O hydrogen bond is very weak, as was indicated by the long N−O distance of 3.03A. The sharpness of the band indicates very weak coupling of the N−H vibration with lattice modes as contrasted with the O−H vibration to be discussed. The position of the hydrogen atom relative to the oxygen is rather unfavorable for the formation of a strong hydrogen bond and the H−N−C angle is roughly that to be expected in the absence of any hydrogen bond. The observed angle is 100°±10°, whereas in the isolated molecule it

[9] G. Herzberg, *Infrared and Raman Spectra of Polyatomic Molecules* (D. Van Nostrand Company, Inc., New York, 1945), p. 195.

‡ This angle was obtained by the usual Lambert's law calculation on the band center. The I_0 used was taken to be the mean of the transmission values on the apparent edges of the band.

might be expected to lie between the limits 109° and 120°.

The frequency of the N—H band is of considerable interest since if the relation between frequency shift and strength of hydrogen bond can be quantitatively understood, it should be of great assistance in elucidating the structure of crystalline polypeptides and proteins. This frequency in acetylglycine differs by only about 10 cm^{-1} from that found in some fibrous proteins[10,11] and in some synthetic polypeptides[12] where, furthermore, the bands are also relatively sharp. However, on the basis of these facts one would probably not be quite justified at this time in asserting that the N—H···O bonds in these substances are as weak as in acetylglycine, since the N—H frequency is dependent on other factors not as yet completely understood.

The absorption region extending from about 1850 to 3000 cm^{-1} is very remarkable both for its great breadth and for its high intensity. We are not aware that any band quite similar to it has previously been reported. For reasons discussed subsequently we ascribe it to the OH valence vibration with frequency greatly shifted by the extremely strong hydrogen bonding, and greatly broadened as a consequence of the unusually strong coupling with lattice vibrations.

The band is strongly polarized and appears with maximum intensity when the electric vector is parallel to the **c** axis of the crystal. Of all the hydrogen valence vibrations this behavior is to be expected only in the case of the O—H vibration, as one may see by reference to Fig. 1. From considerations regarding bond angles and the extremely short O—O distance of 2.56A, it seems highly probable that the hydrogen atom lies at least very nearly on the line connecting the two oxygen atoms which it links. Changes in dipole moment arising from its vibration should consequently be very nearly parallel to the **c** axis.

The band is extremely broad and its mean frequency is extremely low for an O—H vibration. This is undoubtedly a consequence of the strong hydrogen bonding and possibly might have been anticipated by an extrapolation of the observations on the lower fatty acids. The acetic acid dimer, for example, in which the O—H···O distance is 2.76A,[13] exhibits an absorption extending over about 1200 cm^{-1} with a maximum shifted about 600 cm^{-1} from the normal frequency of unbounded OH.[14]

As a check on the above interpretation we have made observations on KH_2PO_4 in which an O—H···O distance of 2.54A has been shown to exist.[15] In a single crystal of this substance we found a broad, intense absorption covering essentially the same region as in acetylglycine. The polarization behavior was consistent with its assignment to an O—H valence vibration. While the character of the O—H···O bonds cannot be expected to be entirely equivalent in the two compounds, nevertheless they are probably sufficiently similar so that the comparison of the two spectra is valid.

In the hope of throwing further light on the nature of the broad O—H absorption an investigation of the low temperature spectrum was undertaken. In Fig. 5 the **b** spectra of a single crystal taken at both room temperature and −185°C are shown. A number of rather surprising differences between the two spectra is exhibited.

First, there would appear to be a slight decrease in the intensity of the 3340 N—H band. Next, it would appear that there is some decrease in the intensity of the residual O—H band, particularly on the high frequency side. This is perhaps indicative of a narrowing of the band as the temperature is lowered (see subsequent discussion for diketopiperazine). The apparent narrowing of several other bands and accompanying general increases in transmission throughout the spectrum are also to be noted.

A number of apparently new bands make their appearance in the low temperature spectrum. These

TABLE III. Frequencies (cm^{-1}) observed for diketopiperazine.[a]

b_0		[101]		⊥ b_0 and [101] (out of plane)	Intensity	Tentative assignments
		~3450			w	
3280	<	3300 to 2940	≫	3000	vs	N—H stretch +2×1700, 3×1070
3000						
		2800			w	2×1470, 2×1070+810
		2750			w	
2550	<	2550			w	2×1340, 1340+1260, 2×915+810
2300	>	2300			w	1340+1000, 3×810
2130	<	2130			w	2×1070
2000	<	2000			w	2×1000
~1800	<	~1800			w	2×915, 1000+815
1720 to 1660	<	1740 to 1640	>	1710	vs	C=O stretch
~1520		~1520			w	
1490 to 1450	<	1490 to 1450	>	1470	vs	CH_2 scissors
1340	>	1340	>	1340	s	N—H in plane bend[b]
		~1290	<	1290	w	
1260	>	1260		1260	w	
1220	>	~1220			w	
1180				~1180	w	Ring stretchings, CH_2 bendings except for 840 which is an out of plane bending, probably of C=O
				~1150	w	
1070	<	1070	>	1070	s	
1000	>	1000		1000	w	
915		915			vs	
~840			<	840	vs	
810	<	810			s	
~780					w	

[a] The inequalities signs give the relative intensities in the three mutually orthogonal directions. The symbol ~ indicates a shoulder.
[b] Suggested by deuteration experiments.

[10] Ambrose, Elliott, and Temple, Nature **163**, 859 (1949).
[11] M. Goldstein and R. S. Halford, J. Am. Chem. Soc. **71**, 3584 (1949).
[12] E. S. Ambrose and A. Elliott, Proc. Roy. Soc. (London) **A205**, 47 (1951).
[13] J. Karle and L. O. Brockway, J. Am. Chem. Soc. **66**, 574 (1944).
[14] Buswell, Rodebush, and Roy, J. Am. Chem. Soc. **60**, 2239 (1938).
[15] J. West, Z. Krist. **74**, 306 (1930).

either have no counterpart in the room temperature spectrum or at best appear there in a very weak and diffuse form. Particularly surprising is the presence of two fairly intense bands at 2020 and 2280 cm^{-1}. Strong absorption is usually not to be expected in this region for substances of the type being investigated here. The set of new frequencies are listed in Table II.

It was first thought that these new absorptions were spurious and resulted from the condensation of water vapor, carbon dioxide, or even diffusion pump oil on the cooled samples. However, unlike the behavior of condensation bands the intensity of these new absorptions in the acetylglycine spectrum were constant over a period of more than an hour and a half. Furthermore, a blank specimen of AgCl produced no trace of such bands when subjected to the normal cooling procedure. Not even after two and a half hours had passed after the initial cooling and the ice band at 3μ had become quite intense was there any evidence for these absorptions. The spectra of other crystals (e.g., diketopiperazine, glycine) that have been examined under comparable conditions likewise gave no evidence of these bands. It would therefore seem that the new low temperature bands are indeed real.

In some cases, notably in the 1250 cm^{-1} region and perhaps the 1000 cm^{-1} band, it appears as if the low temperature bands were better resolved versions of the room temperature band envelopes. In these instances the explanation may lie in the sort of band narrowing that has been observed in the case of diketopiperazine (see Sec. B).

It is a little difficult to understand the possible origin of some of the other bands. The fact that the single crystals survive cooling and reheating seems to rule against a first-order transition at some intervening temperature which would in any pronounced way alter the crystal structure. However, it is possible that some minor modification (e.g., "freezing in" of the motions of the methyl groups, small changes in lattice dimensions) could produce rather large changes in the intensity pattern. In the absence of further information, however, it would not seem profitable to prolong the discussion at this time.

B. Diketopiperazine

In the region from 3300 to 2940 cm^{-1} we have observed a band of extreme intensity, and breadth of around 300 cm^{-1} at half-height. In those views of the crystal for which the absorption is not overwhelmingly intense the band is resolved into two components. The major of these appears at 3000 cm^{-1} and its somewhat less intense companion at 3280 cm^{-1}. This apparent doubling of the band has been observed before.[16–18] Both components appear to exhibit the same polarization behavior. Several much weaker bands observed only as shoulders are also found. The intensity of the lower frequency component and the frequency of its companion seem to preclude the possibility that the band is due in any large part to the C—H stretching vibration. (The 2980 C—H band of acetylglycine serves as a suitable comparison.) We therefore feel quite confident that at least the greatest contribution to this band must come from the N—H stretching vibration, a view which is in accord with its polarization behavior. In the (010) view of the crystal the N—H absorption should be almost entirely confined to the orientation in which the electric vector is parallel to [101]. For the (101) view of the crystal the intensity ($E||[101]$) should be greater than the intensity ($E||b$). These expectations are borne out by the data.

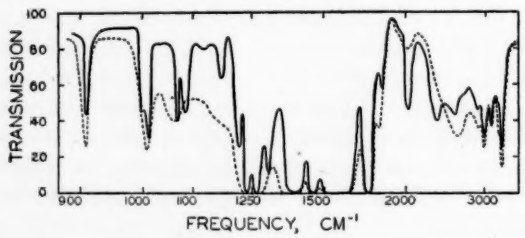

FIG. 5. Spectra of N-acetylglycine for $E||b$ at 25°C (dashed curve) and −185°C (solid curve). Sample about 10 to 15μ thick.

The presence of structure in the region of N—H absorption has previously been observed in several cases. It has been the subject of considerable discussion and has been variously interpreted. In the case under discussion it is reasonable to attribute the major component of the band to the one active N—H valence vibration. For its companion two reasonable explanations are suggested.

The individual molecules of diketopiperazine have centers of symmetry in the crystal. This should be expected to result in an exclusion rule which in first approximation prohibits the appearance of the overtones and combinations of even parity derived solely from infrared active fundamentals. However, the possibility of combination of active and inactive fundamentals is in no way restricted. Indeed in the region 2000–3000 cm^{-1} a number of weak bands appear which can be comfortably attributed to combinations of an active and an inactive fundamental, wherein the inactive frequencies are assumed to be virtually identical with the active ones. This assumption seems completely reasonable and could presumably be verified by a Raman spectrum. If the foregoing arguments are valid then from the observational viewpoint there is no selection rule and any combination band could be expected.

For the 3280 cm^{-1} band we have chosen two such combinations as being most probable. The first possibility is that the band is derived from the combination of the active and inactive C=O frequencies.

The second possibility is the assignment of 3280 cm^{-1} to the third overtone of 1070 cm^{-1}. The latter we ascribe

[16] Buswell, Downing, and Rodebush, J. Am. Chem. Soc. **62**, 2759 (1940).
[17] H. Lenormant, Ann. Chim. **5**, 459 (1950).
[18] L. Kellner, Proc. Roy Soc. (London) **A177**, 447 (1941).

to a ring vibration involving chiefly the C−N bonds having partially double bond character. Since this vibration might be expected to interact strongly with the N−H stretching vibration a resonance of 3×1070 cm^{-1} with the NH band could give intensity to the former. The 1070 cm^{-1} band is presumably a fundamental because of its rather high intensity. It is rather unlikely that it is a hydrogen bending fundamental since only the CH_2 wagging vibration would have the correct polarization behavior, and in other molecules the frequency of this mode is considerably higher. Furthermore, the intensity is rather too great. The assignment of 1070 cm^{-1} to the ring vibration mentioned seems reasonable both on the basis of frequency and regarding the presumed interaction with the N−H valence vibration. From observations on other molecules it is evident that the N−H linkage is very sensitive to the character of the bonding of the nitrogen atom to other atoms.

The band at 1470 presents some problems. It has the frequency to be expected for a CH_2 scissors vibration but has, in part, the wrong polarization behavior and also a rather high intensity. These effects are perhaps due in part to an overlay of some other bands (the corresponding region in glycine, for example, shows fine structure) and in part to some interaction with the C=O vibration.

The effect on the N−H band of cooling the sample to −185°C is particularly marked. In Fig. 6 two sets of spectra taken under different conditions of polarization are shown. The second set (Fig. 6(b)) is perhaps the more striking. It is seen that the lower frequency component seems to shrink more or less symmetrically about its band center as the sample is cooled from 25° to −185°. Such band narrowing, when observed, is usually attributed to a decrease in the anharmonic coupling between molecular modes and lattice modes, as the population numbers of the higher states of the latter decrease with temperature. More simply, the classical amplitude of the lattice oscillations decreases with temperature producing a smaller broadening. That the effect is so marked in the present case is perhaps best explained by the existence of large interactions between the N−H molecular mode and the lattice through the mechanism of the strong N−H···O bond. In the opposite sense the breadth of the N−H band at room temperature is of course attributed to the strong hydrogen bond.

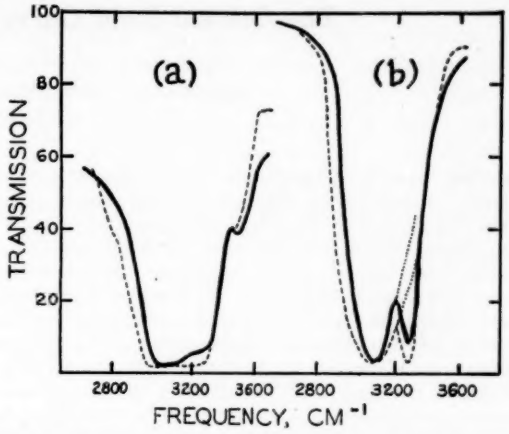

FIG. 6. N−H band of diketopiperazine at 25°C (dashed curve) and −185°C (solid curve). (a) $E||[101]$. (b) $E||b$.

The higher frequency component seems to show decreased intensity on cooling. However, it would seem that this effect results more from the position of this band as a satellite to the other more intense band than to any intrinsic modification in the former. The dotted lines in Fig. 6(b), representing the probable course of the spectral curves in the absence of the satellite, point out the basis for our view.

The two spectra of Fig. 4**b** (the (010) view) would presumably be mutually exclusive if the molecular planes accurately lay in the (101) plane and if observations had been made in parallel light. A certain amount of overlapping is observed, however, more than can be accounted for by the slight tipping (6°) of the molecular planes out of (101). This is perhaps in large part due to our use of strongly convergent light to whose disadvantages we have referred before.

ACKNOWLEDGMENT

We should like to express our thanks to Dr. R. B. Corey for several helpful discussions and to Dr. J. A. Berson (University of Southern California) who prepared some of the diketopiperazine used in this work.

The Critical Field Curve in an Antiferromagnetic Crystal

C. G. B. GARRETT
Department of Physics, Harvard University, Cambridge, Massachusetts
(Received June 13, 1951)

Van Vleck's theoretical model for the antiferromagnetic state is extended to describe the effect of applying magnetic fields so large that the Zeeman splitting is of the same order of magnitude as the exchange interaction. The intensity of magnetization, entropy, and Gibbs free energy are calculated. It is concluded that, when the field is applied parallel to the direction of the antiferromagnetic chains, the antiferromagnetic configuration (that in which there are two sublattices in the crystal possessing unequal magnetizations) is energetically favored for all values of H and T at which it is mathematically permissible. The boundary of the antiferromagnetic solution is a certain critical field curve in the H, T plane, ending at the Curie temperature T_C on the T axis, and at a critical field H_C on the H axis, related to T_C by $\mu H_C/kT_C=1$. The case of perpendicular field, and the influence of next-to-nearest neighbor interaction, are also discussed. Comparison is made between the predictions of the theory and the results of recent experiments by the writer on critical field phenomena in cobalt ammonium sulfate at temperatures below 1°K. This theoretical treatment of exchange antiferromagnetism is contrasted with the theory of Sauer and Temperley on dipole-dipole interaction cooperative effects, which also predicts the existence of a critical curve. The possibility of observing critical field effects in other materials at much higher or much lower temperatures is also discussed.

1. INTRODUCTION

EXPERIMENTS by the writer[1] on a single crystal of cobalt ammonium sulfate at temperatures below 1°K indicate that, if a magnetic field is applied along that crystal magnetic axis which is most nearly parallel to the direction of easy magnetization of the ions in the crystal, the region on the H, T diagram in which the material shows antiferromagnetic properties appears to be bounded by a fairly well-defined "critical field" curve. Outside this curve the crystal behaves very much as would be expected on the simple Brillouin theory for a one-spin paramagnetic; inside the curve the properties are anomalous. One feature of the critical field phenomenon is that the ac magnetic susceptibility rises to a sharp peak at or near the critical curve. The cooperative phenomena in cobalt ammonium sulfate and similar materials may be due to exhange forces between the ions, as for antiferromagnetic materials with transition points at much higher temperatures, or they may be due to dipole-dipole interaction between the ions. At present there is no adequate theory to describe any possible cooperative phenomena produced by dipole-dipole interaction alone, although a start has been made by Sauer and Temperley[2] and by Luttinger and Tisza.[3] On the other hand, there exists for an exchange antiferromagnet a simple Weiss-type theory due to Néel, to Bitter, and to Van Vleck,[4] which has been successful in accounting for many of the low field properties of antiferromagnetic materials. Sauer and Temperley consider immediately the case of arbitrarily large fields and arbitrarily low temperatures, and their theory predicts (for the dipole-dipole problem) the existence of critical field phenomena. The purpose of the present paper is to extend Van Vleck's model for an exchange antiferromagnet to describe the effect of applying very strong fields, and to show that in this case also one would expect critical field effects. First it will be as well to set side by side the two different approaches adopted by Sauer and Temperley and by Van Vleck, to illustrate the differences between the two problems.

For the problem of dipole-dipole interaction it has not been found possible to give any sort of rigorous treatment based on the idea of an "effective field." It is possible to work out more or less unambiguously the relative energies of various possible configurations of the ions at the absolute zero (Sauer,[5] Luttinger and Tisza.[3]) In order to take into account the effect of nonzero temperature and magnetic field, the simplest possible assumption that one can make is that of the Bragg-Williams approximation, and it is on this basis that Sauer and Temperley deduce that the appearance of the ordered (antiparallel) state is bounded by a critical field curve. Of course, this assumption of the validity of the Bragg-Williams method is a pure guess; but the dipole-dipole problem is so intractible that so far no other model has been found which gives even approximately the observed type of behavior. On the other hand, the exchange problem can be treated much more easily. The forces are short-range, so that we need consider interaction only between neighbors or next-to-nearest neighbors; and if further we make the classic assumption of replacing the matrix expressions for the spins by their (spatially and quantum-mechanically) averaged values, we are able at once to take account of the interactions between the ions by thinking of each ion as sitting in an "effective field" caused by the orientation of its neighbors. When the exchange integral is negative (antiferromagnetism), it is necessary to consider several sublattices: the simplest case is that considered by Van Vleck,[4] in which the number of sublattices is 2, and the present discussion will be restricted to this. More recently Anderson[6] has ex-

[1] C. G. B. Garrett, Proc. Roy. Soc. (London) **206A**, 242 (1951).
[2] J. A. Sauer and H. N. V. Temperley, Proc. Roy. Soc. (London) **176A**, 203 (1940).
[3] J. M. Luttinger and L. Tisza, Phys. Rev. **70**, 954 (1946).
[4] J. H. Van Vleck, J. Chem. Phys. **9**, 85 (1941); L. Néel, Ann. phys. **5**, 256 (1936); F. Bitter, Phys. Rev. **54**, 79 (1937).
[5] J. A. Sauer, Phys. Rev. **57**, 142 (1940).
[6] P. W. Anderson, Phys. Rev. **79**, 705 (1950).

tended the model to take account of break-up into 4 sublattices.

Following Van Vleck, it will be assumed that (i) the crystal is cubic in structure, and (ii) the exchange is isotropic. It connot be pretended that this model will be applicable to any actual material, but for purposes of comparison it will be convenient to refer from time to time to the experimental results for cobalt ammonium sulfate. The outstanding difference is, of course, that in cobalt ammonium sulfate one direction is clearly marked out as that along which alignment is likely to occur, so that the differences in behavior under the influence of parallel or perpendicular field are the results of chief interest; whereas in the model there are three equivalent cubic axes, and there is no reason to prefer one rather than another. It is however possible to distinguish between the behavior of the crystal when the field is applied parallel or perpendicular to the direction along which alignment has already taken place in zero field. If the field be applied parallel to this direction, we shall show that there is indeed a critical field curve, within which the configuration containing a certain amount of spontaneous antiferromagnetism is energetically favored. If the point at which this curve hits the T axis be called T_C (the Curie point), and that at which it hits the H axis be called H_C (the critical field at the absolute zero), then the ratio $\mu H_C/kT_C$ (where $\mu=\frac{1}{2}g\beta$ is the ionic magnetic moment) is found to be unity, irrespective of how large the exchange integrals may be. What the theory cannot do, however, is to take account of the possibility of the formation of domains, within which the direction of spontaneous antiferromagnetism need not be either parallel or antiparallel to the applied field.

2. EXTENSION OF VAN VLECK'S MODEL TO ARBITRARILY LARGE FIELDS

We consider a cubic crystal, and divide the magnetic ions up into two sets, the i set and the j set, in such a way that every i ion is surrounded by six j ions and vice versa: and for the moment we take into account only the exchange between nearest neighbors. Now because of the particular form of the exchange coupling perturbation term in the hamiltonian, then (if we replace each i and j spin by their respective average values) the interaction is formally equivalent to the addition to the external magnetic field acting on any one spin of a term proportional to the mean magnetization of the spins in the neighboring set. Thus the effective field acting on an ion in the i set is equal to the vector sum of the externally applied field and a field whose magnitude and direction are determined by the average spin of the j set. The fields are (see Van Vleck[4])

$$\mathbf{H}_i=\mathbf{H}+(2zJ/g\beta)\mathbf{s}_j,$$
$$\mathbf{H}_j=\mathbf{H}+(2zJ/g\beta)\mathbf{s}_i, \qquad (1)$$

where $\mathbf{s}_i$ and $\mathbf{s}_j$ represent the average spins of the ions in the two sublattices; $\mathbf{H}_i$ and $\mathbf{H}_j$ are the respective "effective" fields, z is the number or exchanging neighbors, J the exchange integral, and β the Bohr magneton. Now $\mathbf{s}_i$ and $\mathbf{s}_j$ must be related to the fields $\mathbf{H}_i$ and $\mathbf{H}_j$ by Brillouin functions; and evidently, $\mathbf{s}_i$ must be parallel to $\mathbf{H}_i$ and $\mathbf{s}_j$ to $\mathbf{H}_j$. For simplicity, we consider the case of one spin, since in most practical examples all the spin degeneracy will have been removed at higher temperatures by crystal fields (Stark effect), except for the twofold Kramers degeneracy. Thus, the magnitudes of $\mathbf{s}_i$ and $\mathbf{s}_j$ are given by

$$s_i=\tfrac{1}{2}\tanh(g\beta H_i/2kT),$$
$$s_j=\tfrac{1}{2}\tanh(g\beta H_j/2kT). \qquad (2)$$

First we shall consider what happens when the field is always parallel to the direction of magnetization of the spins in both sublattices, deferring until paragraph 5 the discussion of the case of "field perpendicular to the direction of spontaneous antiferromagnetism." For parallel field Eqs. (1) reduce to scalar relations between the four unknowns s_i, s_j, H_i, and H_j. Now it is always possible to find a solution of Eqs. (1) and (2) such that $s_i=s_j$; this leads to a Curie-Weiss law for low field-strengths, and in general gives rise to something like Brillouin behavior. Configurations of this type will be called the "B" state (for Brillouin). But, as will be seen in a moment, at sufficiently low temperatures and magnetic fields it is also possible to find solutions of Eqs. (1) and (2) such that s_i and s_j are unequal—a state of affairs which in zero field corresponds to Van Vleck's "spontaneous antiferromagnetism." This state will be called the "A" state (for antiferromagnetic); and in order to decide whether at any particular field and temperature this or the B state will be stable, it is necessary to evaluate the (magnetic) Gibbs free energy for each: the state with the lower G being of course the more stable.

To simplify the notation, it is convenient to introduce a characteristic temperature T_C equal to $(-zJ/2k)$, and a characteristic field H_C equal to $(-zJ/g\beta)$: the implication of these quantities will become clear in a moment. For simplicity we shall introduce "reduced" fields and temperatures $h=H/H_C$ and $t=T/T_C$, and further write $\sigma_i=2s_i$ and $\sigma_j=2s_j$. The net magnetization of the crystal is clearly $M=\frac{1}{4}g\beta N(\sigma_i+\sigma_j)$. With this notation we find from Eqs. (1) and (2)

$$\sigma_i=\tanh[(h-\sigma_j)/t],$$
$$\sigma_j=\tanh[(h-\sigma_i)/t]. \qquad (3)$$

For the B state in zero field, σ_i and σ_j are zero at all temperatures, while for the A state

$$\sigma_0=\tanh(\sigma_0/t). \qquad (4)$$

Now in zero field the state with the lower entropy (here clearly the A state, since it is partially ordered and the B state is not) must be preferred, since this means that it has the lower free energy. Thus, the A state is stable at all temperatures (still in zero field) at which a solution of Eq. (4) is possible with $\sigma_0\neq 0$, i.e.,

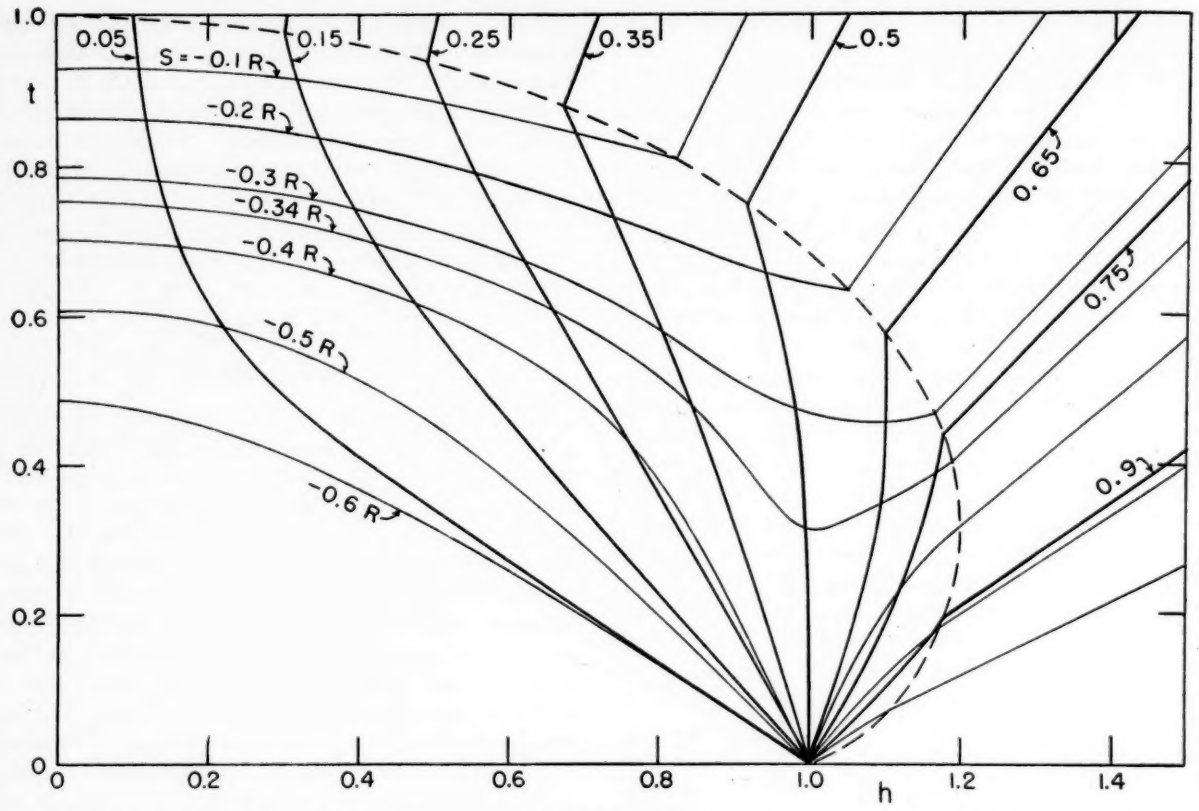

FIG. 1. h, t phase diagram for the antiferromagnetic model. The critical curve (limit of the A state) is shown dotted. The thicker lines are isochores; the thinner, isentropes.

up to $t=1$. Hence T_C is the "Curie point" of the material. Consider next the process of magnetization at the absolute zero. In zero field the two values of σ are 1 and -1, and we make the convention that the j sublattice is that for which in zero field the magnetization is parallel to the positive sense of the field to be applied. Thus H_i is negative in zero field and for all fields up to $H=(-zJ/g\beta)$ (i.e., up to $h=1$), at which point it changes sign. Now since in Eqs. (3) the tanh term must be either 1 or -1, depending on the sign of the operand, the magnetization of the i sublattice changes abruptly at this point from saturation antiparallel to the field to saturation parallel to the field, so that the magnetization of the crystal as a whole changes from zero to saturation. Thus the magnetization curve of the crystal at the absolute zero is a simple step function, and H_C is the value of the field at which the step occurs.

When neither H nor T is zero Eqs. (3) give:

B state—

$$h=\sigma+t\tanh^{-1}\sigma, \tag{5}$$

A state—

$$h=(\sigma_j\tanh^{-1}\sigma_j-\sigma_i\tanh^{-1}\sigma_i)/(\tanh^{-1}\sigma_j-\tanh^{-1}\sigma_i), \tag{6}$$

$$t=(\sigma_j-\sigma_i)/(\tanh^{-1}\sigma_j-\tanh^{-1}\sigma_i). \tag{7}$$

To show the properties of the model graphically it is instructive to construct an H, T diagram, in which we are interested in computing lines of constant magnetization (which it will be convenient to call "isochores," since magnetization, like volume in conventional thermodynamics, is the extensive quantity) and lines of constant entropy (isentropes). Isochores may be calculated from Eqs. (6) and (7) directly, taking σ_i and σ_j as independent variables and finding h and t for each pair of values. The calculation of entropy is given in the next paragraph. Now it will be noticed that the A state is mathematically possible only for low fields and temperatures. The limiting curve bounding the region in the H, T diagram within which the A solution is possible can be determined by finding the limits of the expressions (7) for h and t as the difference $\sigma_j-\sigma_i$ is made to approach zero, the sum $\sigma_j+\sigma_i$ being kept constant. We find

$$h=t\tanh^{-1}[(1-t)^{\frac{1}{2}}]+(1-t)^{\frac{1}{2}}. \tag{8}$$

On this limiting curve the value of the average spin $\frac{1}{2}\sigma$ is given by

$$\sigma^2=1-t. \tag{9}$$

The calculated H, T diagram is shown in Fig. 1. The isochores are shown thicker than the isentropes: the numbers attached to the isochores represent the ratio of the magnetization to the saturation value. The mathematical limit of the A state is shown dotted, and in order to avoid confusion, the B isochores are not

continued inside this dotted curve. It remains to be seen, however, whether or not the A state is the more stable throughout the region within which it is mathematically possible.

3. ENTROPY AND FREE ENERGY

We now turn to the calculation of the other thermodynamical functions for the exchange antiferromagnet in a parallel field. Since there is one direction of quantization, we may calculate the entropy statistically by thinking of the magnetization as being due to $\frac{1}{2}N(1+\sigma)$ spins aligned parallel to the field, and $\frac{1}{2}N(1-\sigma)$ spins antiparallel to it. The entropy per gram-ion is

$$\frac{S}{k}=\log C^{N}_{\frac{1}{2}N(1+\sigma)}=\log\frac{N!}{\{\frac{1}{2}N(1+\sigma)\}!\{\frac{1}{2}N(1-\sigma)\}!} \quad (10)$$

or, using Stirling's formula,

$$S/k=N\log 2 -\tfrac{1}{2}N[(1+\sigma)\log(1+\sigma)+(1-\sigma)\log(1-\sigma)], \quad (11)$$

a result which may easily be confirmed by starting from the Brillouin function for the magnetization and working out the entropy thermodynamically. Hence, for an antiferromagnetic assembly of two sublattices with average spins $\frac{1}{2}\sigma_i$ and $\frac{1}{2}\sigma_j$, we have

$$S/k=N\log 2-\tfrac{1}{4}N[(1+\sigma_j)\log(1+\sigma_j) +(1-\sigma_j)\log(1-\sigma_j)+(1+\sigma_i)\log(1+\sigma_i) +(1-\sigma_i)\log(1-\sigma_i)]. \quad (12)$$

Numerical values for the entropy of the A and B states may be found from Eqs. (11) and (12). Figure 2 shows the variation in entropy along several isochores. plotted as a function of the reduced temperature t, Notice that for the B state isentropes coincide with isochores, as is obvious from the fact that the sole ordering parameter is the unique average spin for every ion in the lattice. From Fig. 2 isentropes have been drawn on Fig. 1 (the thinner lines). The figures attached to the lines are the differences between the entropy along the isentrope and the entropy at infinite temperature ($R\log 2$).

We turn now to the important question of the balance of Gibbs free energy between the two competing states. The Gibbs free energy is defined in differential form as follows:

$$dG=-SdT-MdH. \quad (13)$$

(i) *Zero field: B state—*

We have at once

$$G_B{}^0=-RT\log 2+G_0, \quad (14)$$

since the entropy remains constant at $R\log 2$ at all temperatures down to the absolute zero. (In order to satisfy the third law, it is sufficient to suppose that the degeneracy is removed at a temperature very low in comparison with T_C. If the degeneracy temperature be sufficiently low, the free energy will not be appreciably affected.)

(ii) *Zero field: A state—*

From Eq. (11), writing σ_0 for σ,

$$G_A{}^0=-\int_0^T SdT=-RT\log 2 +R\int_0^T[\sigma_0\tanh^{-1}\sigma_0+\tfrac{1}{2}\log(1-\sigma_0{}^2)]dT. \quad (15)$$

The integral may be evaluated by substituting $x=\tanh^{-1}\sigma_0$. We find

$$G_A{}^0=-RT\log 2+RT_C\frac{\sigma_0\log(1-\sigma_0{}^2)}{2\tanh^{-1}\sigma_0} +\tfrac{1}{2}RT_C\sigma_0{}^2+G_0'. \quad (16)$$

From Eqs. (14) and (16), adjusting the constants so that the free energies of the A state and the B state are equal at the Curie point, the difference in G becomes

$$G_B{}^0-G_A{}^0=-RT_C\left[\tfrac{1}{2}\sigma_0{}^2+\sigma_0\frac{\log(1+\sigma_0)+\log(1-\sigma_0)}{\log(1+\sigma_0)-\log(1-\sigma_0)}\right], \quad (17)$$

from which it appears that the A state has a free energy lower than that of the B state by an amount which increases from zero at the Curie point to $\frac{1}{2}RT_C$ at the absolute zero.

(iii) *Nonzero field: B state—*

We evaluate $-\int MdH$ using Eq. (5). The change in G, in terms of the parameter σ, is

$$G_B{}^H-G_B{}^0=-\tfrac{1}{2}g\beta NH_C\int_0^\sigma(\sigma+\sigma t/(1-\sigma^2)d\sigma =-\tfrac{1}{2}RT_C[\sigma^2-\log(1-\sigma^2)], \quad (18)$$

since $\frac{1}{2}g\beta H_C=kT_C$.

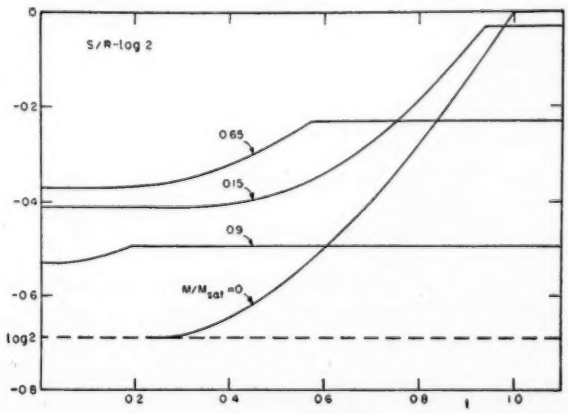

FIG. 2. Variation of the entropy along several isochores, plotted as a function of the reduced temperature.

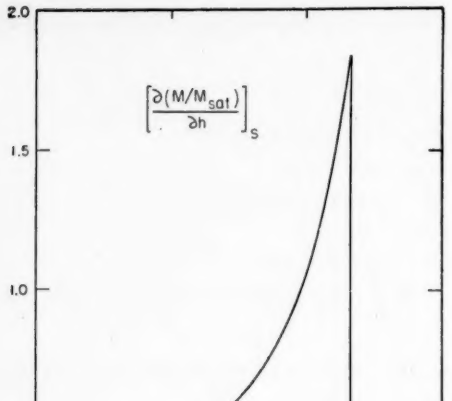

FIG. 3. Differential susceptibility during isentropic magnetization. $S/R=\log 2-0.3$.

(iv) *Nonzero field: A state*—

Since we are interested in isothermal magnetization, only one parameter is needed to specify the state of the system. It is convenient to take as this parameter $\xi=\sigma_j-\sigma_i$, and further to introduce the quantity $m=\sigma_j+\sigma_i$. From Eqs. (7) and (6) we get, after considerable reduction,

$$m=[\xi^2-4\xi\coth(\xi/t)+4]^{\frac{1}{2}}, \tag{19}$$

$$h=t\tanh^{-1}\{\tfrac{1}{2}[\xi^2-4\xi\coth(\xi/t)+4]^{\frac{1}{2}}-\tfrac{1}{2}\xi\} +\tfrac{1}{2}\xi+\tfrac{1}{2}[\xi^2-4\xi\coth(\xi/t)+4]^{\frac{1}{2}}. \tag{20}$$

The change in G is now proportional to

$$\int m(\partial h/\partial\xi)_t d\xi=\int[(\xi/t)\operatorname{csch}^2(\xi/t)-(t/\xi)]d\xi.$$

Integrating, and noticing that in zero field $\xi=2\sigma_0$, we obtain

$$G_A{}^H-G_A{}^0=-\tfrac{1}{2}RT_C\Big[t\log\{\sinh[(\sigma_j-\sigma_i)/t]/(\sigma_j-\sigma_i)\} -(\sigma_j-\sigma_i)\coth[(\sigma_j-\sigma_i)/t] +2\sigma_0\frac{\log(1+\sigma_0)+\log(1-\sigma_0)}{\log(1+\sigma_0)-\log(1-\sigma_0)}+\sigma_0{}^2+1\Big], \tag{21}$$

so that (using Eqs. (17) and (18)) the difference between the Gibbs free energy of the two states in a magnetic field is

$$G_B{}^H-G_A{}^H=-\tfrac{1}{2}RT_C\{\sigma^2-t\log(1-\sigma^2) -t\log\{\sinh[(\sigma_j-\sigma_i)/t]/(\sigma_j-\sigma_i)\} +(\sigma_j-\sigma_i)\coth[(\sigma_j-\sigma_i)/t]-1\}. \tag{22}$$

At the mathematical limit of the A state we have $\sigma_j-\sigma_i=0$, so that the third and fourth terms on the right-hand side of Eq. (22) become $t\log t$ and t, respectively. Further, from Eq. (9), the first term is $1-t$, and the second is $-t\log t$. Thus the difference in Gibbs free energy between the two states vanishes at the mathematical limit of the A state. But, if this be so, G_A must be less than G_B for all points within the limiting curve, for since along any isotherm M_A is at any point less than M_B, as may be seen from inspection of Fig. 1 (note that the isochores for the B state are rectilinear right down to the absolute zero), and since M is just $(\partial G/\partial H)_T$, it follows that $(\partial\Delta G/\partial H)_T$ is always greater than zero for all strengths between zero and the critical curve. Therefore the A state is thermodynamically the more stable at all points in the H, T plane at which it is mathematically permissible. This means that the transition is continuous in M (but not in $(\partial M/\partial H)_T$) at all temperatures. The transition is second order and therefore involves no latent heat at any temperature.

The following points are of interest in connection with the properties of this model for an antiferromagnet, as illustrated in Fig. 1:

(a) Since for the B state isochores are also isentropes, we should expect (if we may apply this model to some paramagnetic salt as used in a magnetic cooling experiment) that during adiabatic demagnetization the magnetization will remain constant down to fields of the order of a few hundred gauss, i.e., until the system crosses the critical curve. Throughout this region the differential susceptibility should be zero. Figure 3 shows the predicted behavior of the differential susceptibility for a typical isentrope ($S/R=\log 2-0.3$) right down to zero field. Notice that the differential susceptibility should be quite small in small fields, thereafter increasing to a maximum as the system crosses the critical curve, and then falling discontinuously to zero. The figure should be compared with Fig. 8 of Garrett,[1] which shows the observed behavior of an actual material along a direction more or less parallel to the spontaneous antiferromagnetic chains. The peak in a field of a few hundred gauss is indeed found, but there is no discontinuity in the observed susceptibility. The suggestion was made by Garrett[1] that the observed smearing-out of the transition might be the result of some sort of intermediate state, caused by local field effects; but it should be remembered that in saying this, it is by no means obvious that one is not correcting for the same physical effect twice over, using two different types of approximation. A more plausible explanation (valid either for dipole-dipole or for exchange coupling) would be that the internal fields due to alignment effects will in reality cover a whole range of values, a fact which cannot be taken into account in any theory which replaces spins by their mean values in calculating the "effective fields."

(b) Outside the critical curve the specific heat at constant magnetization should be zero, and this should

be true in particular for magnetization zero (zero field). Actually, it is found that there is a $1/T^2$ tail to the specific heat at temperatures above the critical point, in agreement with the theoretical expectations on a rigorous quantum-mechanical model (Van Vleck[7]) and with the observation of a certain amount of short-range order remaining at temperatures considerably in excess of the Curie temperature, as indicated by experiments on neutron diffraction (Shull and Smart[8]).

(c) The application of a magnetic field shifts the position of the maximum in the specific heat to lower and lower temperatures. So long as we consider the specific heat at constant magnetization, there remains only one peak in the specific heat curve; but for fields near H_C the specific heat at constant field-strength develops a double peak, as is shown in Fig. 4. Physically, this is because one sublattice loses its entropy quite near the critical temperature, while (because the internal field and the external field nearly cancel) the other remains ordered to a much lower temperature. Whether this would appear in a rigorous model designed to take into account a distribution of internal fields cannot be predicted. The only example in the literature of a double peak in a one-spin paramagnetic at low temperatures is that of copper sulfate (Ashmead,[9] Geballe,[10] and this is in *zero* field.

(d) All the isentropes for $S/R>\frac{1}{2}\log 2$ pass through a point very near the absolute zero, at a field-strength H_C. (The point would be *at* the absolute zero were it not for remaining lattice entropy, nuclear spin degeneracy, etc.) This again is due to the assumption of replacing spins by their mean values in calculating the effective fields, since in the actual case, although the mean value of H_i vanishes at H_e when $T=0$, the mean square value will not. Of course, if this model were exact, one would only have to apply at 1°K a magnetic field large enough to remove more than half the spin degeneracy entropy (a task easily within the range of existing techniques) in order, on demagnetizing to a field H_C, to reach a temperature many times lower than the Curie point of the material.

(e) It is interesting to note that the present model gives no first-order transition at any temperature, whereas Sauer and Temperley's model predicts a first-order transition at all temperatures below $2T_C/3$. Physically there seems to be no good reason for this. The experiments on cobalt ammonium sulfate indicate that, in practice, the transition is not even as sharp as second order. Even in zero field, the gradient of the entropy curve seems to be continuous within the accuracy of present measurements, while the low field susceptibility certainly passes through a smooth maximum rather than a cusp.

[7] J. H. Van Vleck, J. Chem. Phys. **5**, 320 (1937).
[8] C. G. Shull and J. S. Smart, Phys. Rev. **76**, 1256 (1949).
[9] J. Ashmead, Nature **143**, 853 (1939).
[10] T. H. Geballe, Report of Conference on Very Low Temperatures held at M.I.T. (1950).

4. NEXT-TO-NEAREST NEIGHBOR INTERACTION

It is easy to generalize the problem to include exchange between next-to-nearest neighbors. The "effective field" acting on a spin in the i sublattice now contains a term proportional to the average magnetization of next-to-nearest neighbors, i.e., to the average spin of the i sublattice itself. Thus, in terms of reduced quantities, we have

$$h_i=h-\sigma_j-\alpha\sigma_i;\quad \sigma_i=\tanh(h_i/t),$$
$$h_j=h-\sigma_i-\alpha\sigma_j;\quad \sigma_j=\tanh(h_j/t) \qquad (23)$$

(see Néel[11]). It is easily seen that, corresponding to Eqs. (5), (6), (7), and (8), we have

B state—

$$h=(1+\alpha)\sigma+t\tanh^{-1}\sigma,$$

A state—

$$t=(1-\alpha)(\sigma_j-\sigma_i)/(\tanh^{-1}\sigma_j-\tanh^{-1}\sigma_i),$$

$$h=[(\tanh^{-1}\sigma_j)(\sigma_j+\alpha\sigma_i)-(\tanh^{-1}\sigma_i)(\sigma_i+\alpha\sigma_j)]/(\tanh^{-1}\sigma_j-\tanh^{-1}\sigma_i),$$

limit of the A state—

$$h=t\tanh^{-1}\{[1-t/(1-\alpha)]^{\frac{1}{2}}\}+(1+\alpha)[1-t/(1-\alpha)]^{\frac{1}{2}}. \qquad (24)$$

The factor α will usually be a number between 0 and 1; Eqs. (24) reduce to the case of nearest-neighbor-only exchange for $\alpha=0$. Without working out in detail the consequences of nonzero α, several features may be noted. In the first place, the Curie point, for a given value of the exchange integral J, is reduced to $(1-\alpha)$ of its value for $\alpha=0$. From Eqs. (11) for the entropy in zero field it may easily be seen that the difference in free energy for the A and B states at the absolute zero is also reduced in the same ratio as the Curie temperature, i.e., to $\frac{1}{2}RT_C(1-\alpha)$.

We consider the process of magnetization at the absolute zero. In zero field the stable state has $\sigma_j=1$, $\sigma_i=-1$. This configuration satisfies Eqs. (23) up to a field $h=1-\alpha$, while the configuration $\sigma_j=\sigma_i=1$ satisfies them for fields greater than $h=(1+\alpha)$. But in the

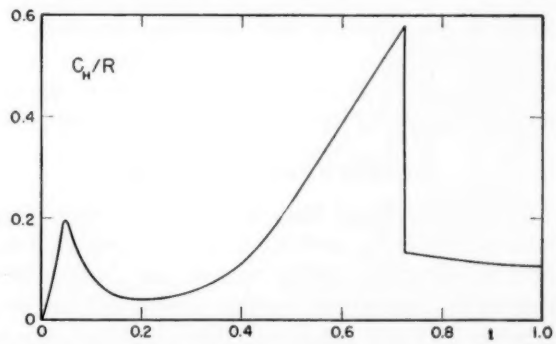

FIG. 4. Specific heat at constant field-strength ($h=0.95$) plotted against reduced temperature.

[11] L. Néel, Ann. phys. **3**, 137 (1948).

intermediate region it is impossible to find a solution of Eq. (23) possessing perfect order (zero entropy). We can satisfy Eq. (23) only by arranging that h_i shall vanish, so that σ_i can have any value between -1 and 1. In this region, we have

$$M=\tfrac{1}{4}g\beta N(\sigma_i+\sigma_j)=\tfrac{1}{4}g\beta(h+\alpha-1)/\alpha, \qquad (25)$$

so that the net magnetization should increase linearly from zero to saturation between $h=1-\alpha$ and $h=1+\alpha$. Unfortunately, this solution is invalidated by the third law; in practice, this means that the assumption that it is possible to find a configuration of spins such that the effective field acting on either sublattice vanishes is an oversimplification, consequent on the replacement of spins by their mean values.

For the B state with next-to-nearest neighbor exchange the magnetization curve at $T=0$ is given by $\sigma_i=\sigma_j$ and $h_i=h_j=0$. It may easily be seen that the Gibbs free energies again become equal at the limit of the A state, which at the absolute zero occurs at $h=(1+\alpha)$.

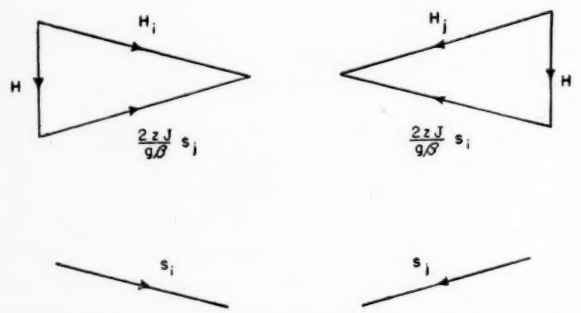

FIG. 5. Vector composition of effective fields for "perpendicular" orientation of the external field. The isolated arrows represent the directions of the average spins.

We may summarize the results of introducing next-to-nearest neighbor exchange thus: (a) the Curie point is lowered; (b) the critical field is increased; (c) the magnetization curve at the absolute zero is changed from a simple step function into a form in which the change from zero to saturation occurs, not over an indefinitely small range of field-strengths, but linearly over a range which is the greater, the greater is the coupling between next-to-nearest spins: but (d) the difficulties in reconciling the model with the third law are even greater with next-to-nearest neighbor exchange than without it.

5. PERPENDICULAR FIELD

It has been assumed from the start that the crystal is cubic in structure, and we have been studying the process of alignment along one of the crystal axes. Supposing that the crystal has been cooled to a temperature below its Curie point, and that alignment has set in along one such axis, we next inquire what will be the result of applying a field along a direction perpendicular to this axis. So long as the field is small in comparison with H_C, there is no difficulty in answering this question; but once a field has been applied so large that the spins have been dragged into parallelism with it, there ceases to be any distinction between the existing situation and that holding for the case of strong *parallel* field. In order to fit the theory to materials in which, for one reason or another, one axis is clearly marked out as that along which alignment takes place in the absence of disturbing influences, we introduce the fiction that for magnetization and demagnetization alike the spins get as near as they can (compatible with Eq. (1)) to parallelism with this direction. The problem is now solved directly from Eq. (1). The vector triangles representing the composition of $\mathbf{H}_i$ and $\mathbf{H}_j$ must be congruent, since $\mathbf{H}_i$ must be parallel to $\mathbf{s}_i$ and $\mathbf{H}_j$ to $\mathbf{s}_j$, while the external field $\mathbf{H}$ is common to both. Further, since from Eq. (2) the ave age spins s_i and s_j are not linearly related to the fields H_i and H_j, the only possible solution is that in which the two triangles are isoscles. (See Fig. 5.) It, therefore, follows that the magnitudes of the vectors $\mathbf{s}_i$, $\mathbf{s}_j$, $\mathbf{H}_i$, and $\mathbf{H}_j$ are unchanged by the application of a perpendicular field, so that the magnitude of the average spin in both sets continues to be given by Eq. (4). The component of magnetization in the direction parallel to the applied field is

$$-\tfrac{1}{2}g\beta N\sigma_0[\tfrac{1}{2}H/(zJ\sigma_0/g\beta)]=\tfrac{1}{4}g\beta N(H/H_C), \qquad (26)$$

where H_C is the quantity $-zJ/g\beta$ as before. Equation (26) holds up to the point at which the triangles in Fig. 5 degenerate into straight lines, i.e., until the spins have been dragged into parallelism with the applied field. The subsequent history of the magnetization curve will be given by Eqs. (3), since the arrangement is now identical with that for parallel field. The change-over occurs at a field $2H_C\sigma_0$: for fields less than this the magnetization given by Eq. (26) is linear in H, and independent of the temperature, as already found by Van Vleck[4] for fields very small in comparison with H_C. At the absolute zero it will require a field $2H_C$ to bring the crystal up to saturation. From Eq. (4) we see that the limiting curve to the region of linear susceptibility is given by

$$2t\tanh^{-1}(\tfrac{1}{2}h)=h. \qquad (27)$$

Inside this curve it follows from Eq. (26) that isochores will be vertical straight lines; and, since $(\partial T/\partial H)_S=-(\partial M/\partial S)_H=0$, the isentropes will be horizontal straight lines. Experimentally, this means that there should be no magnetothermal effects along the perpendicular direction, and no field-dependence of the susceptibility. In experimental language, the quantities Ξ and ψ/χ (see Garrett[12]) ought to be zero at all temperatures below the Curie point for fields up to the limit given in Eq. (27), when the field is applied at right angles to the alignment direction. Again to compare with the experimental results for cobalt ammonium

[12] C. G. B. Garrett, Proc. Roy. Soc. (London) **203A**, 375 (1950).

sulfate,[1] one finds that along the K_2 axis, which is perpendicular to the directions of "easy magnetization" for both the nonequivalent sets of ions in the crystal: (a) the susceptibility is remarkably constant with temperature, in agreement with Eq. (26), and (b) the field-dependence of the susceptibility is small, although not exactly zero.

6. CONCLUSION

The remarkable feature of the work described here is that although the theoretical model is quite different from that adopted by Sauer and Temperley for the description of dipole-dipole cooperative effects, both theories give rise to the appearance of a critical curve of very roughly the same type, and in both theories the quantities $\mu H_C/kT_C$ are of the same order of magnitude. Neither theory gives any account of hysteresis effects, although it is easy to see how the model outlined here could lead to the existence of several configurations at any one field and temperature, each located at a local minimal value of the Gibbs free energy, and separated by configurations of higher Gibbs free energy. In any case, one would expect that hysteresis effects will be confined to the A state of the material, and so should be confined to the region of the phase diagram within the critical curve.

Since both approaches lead to a critical curve with $\mu H_C \sim kT_C$, we may have some confidence that this is a general feature of the antiferromagnetic state. For paramagnetic salts of the sort used in magnetic cooling experiments the Curie temperatures are of the order of tens of millidegrees, so that the critical fields will be a few hundred gauss. Thus, for cobalt ammonium sulfate[1] the critical field, defined by finding the locus of the minima in the isochores and isentropes and extrapolating to the absolute zero, was found to be such as to make the ratio $\mu H_C/kT_C$ about 1.4. Actually, Fig. 1 shows that at about half the Curie temperature—the lowest temperature attainable during the experiments—the minima are occurring at a field slightly greater than H_C, so that the discrepancy is in the right direction. More recently, similar behavior has been reported for cupric chloride (Gorter *et al.*[13]), for which the Curie point appears to be at about 4°K, and the critical field at the lowest temperatures about 7000 gauss. Here again, one finds that the ratio $\mu H_C/kT_C$ is of the order of unity. Manganese oxide and selenide have Curie points at about 150°K (Squire[14]); but the critical field must now be of the order of 10^6 gauss, that is, well outside the range of contemporary magnets. Squire[14] has reported that the Curie point of MnSe is lowered by about 6° on applying a field of 10 gauss, and it has already been suggested (Yin Yuang Li[15]) that this might be due to a change in the type of ordering. Now inspection of Eq. (8) shows that near the Curie point the critical curve is given by $h \sim 2(1-t)^{\frac{1}{2}}$, so that a field of 10 gauss should lower the Curie point by only about 10^{-8} degree. It seems however possible that if one took into account the existence of four sublattices, as in the theory of Anderson,[6] one might find a change-over between two different kinds of antiferromagnetic ordering at a very much lower field-strength than that required to abolish the antiferromagnetic ordering altogether. Finally, it should be pointed out that there is a possibility that a material containing only nuclear paramagnetism, like lithium fluoride, might become antiferromagnetic at temperatures of the order of the microwave line width, i.e., at about 10^{-6} °K. If so, one would expect critical field effects for these materials also; and it is easily seen that the critical field at the absolute zero should be something like 1 gauss. Even if these nuclear paramagnetic salts turn out to be ferromagnetic at very low temperatures, there remains the possibility that one might, on cooling the spin system to a very small *negative* temperature (Purcell and Pound[16]) achieve an antiparallel configuration, for which the critical field should again be of the order of 1 gauss.

In conclusion, I should like to thank Professor Van Vleck for very helpful discussions on the work described in this paper, and Mr. H. N. V. Temperley for various remarks on the methods used in the calculations for the theory of Sauer and Temperley.[2]

[13] Poulis, van den Handel, Ubbink, Poulis, and Gorter, Phys. Rev. **82**, 552 (1951).
[14] C. F. Squire, Phys. Rev. **56**, 922 (1939).
[15] Yin Yuang Li, Phys. Rev. **80**, 457 (1950).
[16] E. M. Purcell and R. V Pound, Phys. Rev. **81**, 279 (1951).

THE JOURNAL OF CHEMICAL PHYSICS VOLUME 19, NUMBER 9 SEPTEMBER, 1951

The Parallel Vibrations of Linear Triatomic Molecules

W. J. Orville Thomas
The Edward Davies Chemical Laboratories, University College of Wales, Aberystwyth, Wales
(Received March 22, 1951)

The possible solutions of the valence force potential constants occurring in the potential function for the stretching modes of some triatomic molecules are found; these are found as functions of a parameter p related to the coordinates describing the parallel modes of vibration.

The form of the normal modes and the potential energy distribution corresponding to a particular set of constants for each molecule is obtained.

(1) INTRODUCTION

THE general linear triatomic molecule has the point group $C_{\infty v}$. The two parallel vibrations belong to the same symmetry class, Σ^+. In general, one mode of vibration is localized to a certain extent in one of the bonds, the second in the other bond. In the following treatment an attempt is made to consider one vibration, ν_1, as derived from a pseudo-antisymmetrical mode of vibration; the other, ν_2, to arise from a pseudo-symmetrical form. Torkington[1] in his treatment of the secular equation of second degree suggested the use of coordinates of the form,

$$\left.\begin{aligned}\Delta_1&=\Delta_1'+p_1\Delta_2',\\ \Delta_2&=\Delta_2'+p_2\Delta_1',\end{aligned}\right\} \quad (1)$$

where the p's are so chosen that Δ_1 and Δ_2 become the normal (unnormalized) coordinates for the problem.

For the problem under discussion Eqs. (1) will be written as

$$\left.\begin{aligned}\Delta_1&=\Delta_1'-p\Delta_2',\\ \Delta_2&=\Delta_2'+p\Delta_1',\end{aligned}\right\} \quad (2)$$

where $\Delta_1'=\Delta r_1$, $\Delta_2'=\Delta r_2$, and $-1\leq p\leq+1$; this range being chosen to make the limits hold for the symmetrical linear triatomic molecule.

When p is positive, Δ_1 is pseudo-antisymmetrical, and Δ_2 is pseudo-symmetrical; p negative gives the opposite results. Δ_1 will be taken as the coordinate associated with ν_1, the higher frequency, while Δ_2 is associated with ν_2. By varying the value of p from $+1$ to -1, we can show the effect of considering first one vibration and then the other as the pseudo-antisymmetrical one. p may be regarded as a "mixing" factor which takes account of the fact that although ν_1 may be primarily associated with changes in r_1, r_2 is not entirely unaffected. It is to be noted that coordinates (2) are symmetry coordinates for the class Σ^+ vibrations of the linear XYZ systems for all values of p.

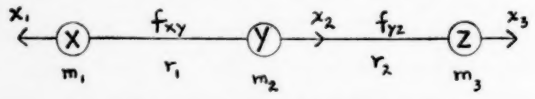

FIG. 1. The general linear triatomic molecule.

[1] P. Torkington, J. Chem. Phys. **17**, 357 (1949).

(2) MATHEMATICAL FORMULATION OF THE PROBLEM

In the general solution of the secular equation of second degree Torkington[1] derives a solution (VII) in which d_{22} (the potential constant associated with Δ_2) takes a minimum value; the (unnormalized) normal coordinate for the higher frequency being identical with Δ_1. This particular solution leads rapidly to a solution of the secular equation, with a minimum of calculation.

When this solution is used with coordinates of the form (2), the force constants d are obtained as functions of p.

Taking coordinates (2) as the valence force symmetry coordinates for the problem, and defining the system in its displaced position by the cartesian displacement coordinates x_i, as shown in Fig. 1, we have, using Torkington's procedure,[1] the following $[a]$ matrix,

$$[\mathbf{a}]\equiv\left[\begin{array}{c|c|c}1 & p+1 & -p\\ p & p-1 & 1\end{array}\right]$$
$$\text{Associated mass } m_1 \quad m_2 \quad m_3.$$

With $M=m_2$, the matrix **A** is found to be as follows:

$$\begin{bmatrix}p^2(1+\mu_3)+2p+1+\mu_1 & p^2+p(\mu_1-\mu_3)-1\\ p^2+p(\mu_1-\mu_3)-1 & p^2(1+\mu_1)-2p+1+\mu_3\end{bmatrix},$$

where $\mu_i=m_2/m_i$.

The solution for the force constants for solution (VII) is

$$d_{11}=\lambda_1/A_{11}+A_{12}^2\lambda_2/A_{11}\cdot D,$$
$$d_{22}=A_{11}\lambda_2/D,$$
$$d_{12}=-A_{12}\lambda_2/D,$$

TABLE I. The parallel vibration frequencies of some linear triatomic molecules.

Molecule	HCN	ClCN	BrCN	ICN	NNO	OCS
Frequencies cm^{-1}	3312.9 2089.0	2201 729	2187 580	2158 470	2223.5 1285.0	2050.5 863.4
Reference	a	a	a	a	b	c

[a] G. Herzberg, *Molecular Spectra and Molecular Structure* (D. Van Nostrand Company, Inc., New York, 1945), Vol. II.
[b] E. K. Plyler and E. F. Barker, Phys. Rev. **38**, 1827 (1931).
[c] See reference 3.

TABLE II. Solutions for the force constants.

Molecule	Force constant	Value of p 1.000	0.750	0.500	0.250	0.000	−0.250	−0.500	−0.750	−1.000
HCN	f_{CH}	5.285	5.522	5.754	5.956	6.116	6.240	6.281	6.256	6.159
	f_{CN}	20.129	19.031	18.155	17.528	17.348	17.527	18.293	19.440	21.011
	f_{12}	−1.444	−0.926	−0.283	0.476	1.343	2.273	3.326	4.159	5.007
ClCN	f_{CCl}	10.577	8.873	7.078	5.482	4.691	6.027	11.095	20.152	30.204
	f_{CN}	9.253	10.806	12.943	15.884	19.816	24.555	28.981	30.844	28.896
	f_{12}	−3.353	−3.045	−2.254	−0.598	2.526	7.817	15.327	23.120	28.038
BrCN	f_{CBr}	10.170	8.302	6.390	4.693	3.885	5.270	10.760	21.540	35.131
	f_{CN}	8.690	10.258	12.411	15.349	19.348	24.400	29.873	33.706	33.647
	f_{12}	−4.190	−3.804	−3.020	−1.151	2.092	7.586	15.828	25.563	33.333
ICN	f_{CI}	9.141	7.253	5.316	3.619	2.810	4.193	9.746	20.945	35.773
	f_{CN}	7.991	9.551	11.681	14.586	18.555	23.664	29.403	33.873	34.621
	f_{12}	−4.829	−4.413	−3.497	−1.725	1.513	7.012	15.386	25.674	34.477
NNO	f_{NN}	13.912	15.252	17.120	19.659	22.869	26.070	27.777	26.747	23.815
	f_{NO}	14.506	13.250	11.858	10.550	9.899	10.953	14.522	19.840	24.443
	f_{12}	0.319	0.471	1.030	2.344	4.949	9.137	14.196	17.994	19.377
OCS	f_{CO}	9.893	11.193	12.984	15.572	19.067	23.335	27.373	28.854	26.743
	f_{CS}	11.309	9.971	8.520	7.203	6.549	7.676	12.105	19.897	28.159
	f_{12}	−1.041	−0.832	−0.182	1.120	3.730	8.265	14.850	21.517	25.341

where $\lambda=4\pi^2\nu^2c^2m_2$, ν being a vibration frequency in cm^{-1}, c the velocity of light in $cm\cdot sec^{-1}$. $D=A_{11}A_{22}-A_{12}^2$.

For the system under discussion the second degree potential function is

$$2V=d_{11}\Delta_1^2+d_{22}\Delta_2^2+2d_{12}\Delta_1\Delta_2. \quad (3)$$

On substitution for the Δ's this can be shown to be equivalent to

$$2V=(d_{11}+p^2d_{22}+2pd_{12})\Delta r_1^2+(d_{22}+p^2d_{11}-2pd_{12})\Delta r_2^2 +2\{p(d_{22}-d_{11})+(1-p^2)d_{12}\}\Delta r_1\Delta r_2. \quad (4)$$

The valence force potential function for the parallel vibrations of the system may be written as

$$2V=f_{xy}\Delta r_1^2+f_{yz}\Delta r_2^2+2f_{12}\Delta r_1\Delta r_2. \quad (5)$$

Comparison of (4) and (5) leads to the relations,

$$\left.\begin{aligned} f_{xy}&=d_{11}+p^2d_{22}+2pd_{12},\\ f_{yz}&=d_{22}+p^2d_{11}-2pd_{12},\\ f_{12}&=p(d_{22}-d_{11})+(1-p^2)d_{12}.\end{aligned}\right\} \quad (6)$$

From these relations f may be obtained for various values of p. Curves of f against p may then be drawn and the most reasonable set of constants chosen on an empirical basis or otherwise. These curves represent the possible sets of values (with the restriction here that $-1\leq p\leq+1$), hitherto obtained by varying the interaction constant f_{12} and solving for f_{xy} and f_{yz} at each value of f_{12}.[2-4]

[2] J. Duchesne, Mem. soc. roy. sci. Liège Sér. I, 429 (1943).
[3] T. Y. Wu, *Vibrational Spectra and Structure of Polyatomic Molecules* (Edwards Brothers, Inc., Ann Arbor, Michigan, 1946), pp. 151, 156.
[4] Coulson, Duchesne, and Manneback, *Contribution a l'etude de la structure moleculaire* (Liège, 1948), p. 33.

The transformation to (unnormalized) normal coordinates given by Torkington's solution (VII) is,

$$\eta_1=\Delta_1',$$
$$\eta_2=-A_{12}'\Delta_1'+A_{11}'\Delta_2',$$

where the elements A_{ij} refer to the matrix $\mathbf{A}$ with $p=0$. The description of the form of the normal vibrations is,[1] in terms of the simple set of coordinates $\Delta_1'=\Delta r_1$, $\Delta_2'=\Delta r_2$,

$$\left.\begin{aligned} \rho_1&=(\Delta_1'/\Delta_2')(\nu_1)=-[1+\mu_1+p]/[1+p(1+\mu_3)],\\ \rho_2&=(\Delta_2'/\Delta_1')(\nu_2)=1/p.\end{aligned}\right\} \quad (7)$$

Torkington[1] has obtained expressions for the relative contributions to the potential energy from the terms of the potential function (3), in each normal mode. For the particular solution (VII) of the secular equation used here these expressions are

$$V_{11}(\nu_1)=1+A\mu_1;\quad V_{11}(\nu_2)=0;$$
$$V_{22}(\nu_1)=A\mu_1;\quad V_{22}(\nu_2)=1;$$
$$V_{12}(\nu_1)=-2A\mu_1;\quad V_{12}(\nu_2)=0;$$

so that $V_{11}+V_{22}+V_{12}=1$, $A=A_{12}^2/D$, and $\mu_1=\lambda_2/\lambda_1$.

(3) SOLUTION FOR THE FORCE CONSTANTS

Values for the frequencies of the stretching modes of linear triatomic molecules have been allocated in most cases. Some of these are listed in Table I. Using these values for the frequencies the values of the valence force potential constants for the various p values were obtained. They are given in Table II, in units of 10^{-5} dyne/cm. In HCN, $r_1=r(CH)$; in the XCN series, $r_1=r(CN)$; in NNO and OCS, r_1 is $r(NN)$ and $r(CO)$

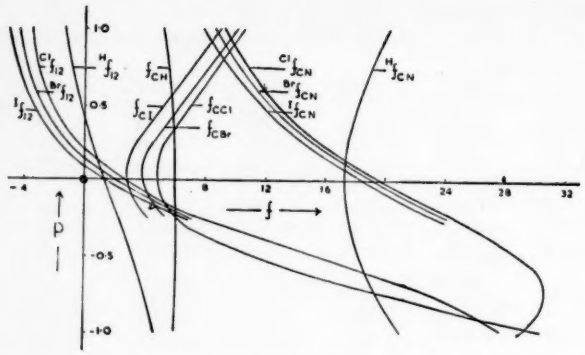

FIG. 2. Variation of the force constants with p in the XCN series.

respectively. Curves of f against p were drawn for the XCN series, Fig. 2, and for NNO and OCS, Fig. 3.

(4) AN EMPIRICAL METHOD OF DETERMINING p

Isotopic frequencies are known for the two molecules HCN[5] and NNO.[6,7] The values of the valence force constants occurring in the potential function (5) are then unambiguously defined for these systems. The p values giving these sets of constants may be obtained from Figs. 2 and 3.

The precise value of f_{CN} is determined in hydrogen cyanide from the data for HCN and DCN; it is $f_{CN}=18.065\times10^5$ dynes/cm.[4] The small changes in the XCN bond lengths shown in Table V which run parallel to the electronegativities of X, suggest slight variations in this force constant from one molecule to another. To arrive at "best values" we have used Gordy's relations,[8,9] for the CN link they are

$$N=(6.48/r^2)-2.00, \qquad \text{(i)}$$

$$f=1.67N(7.599/r^2)^{\frac{3}{4}}+0.30. \qquad \text{(ii)}$$

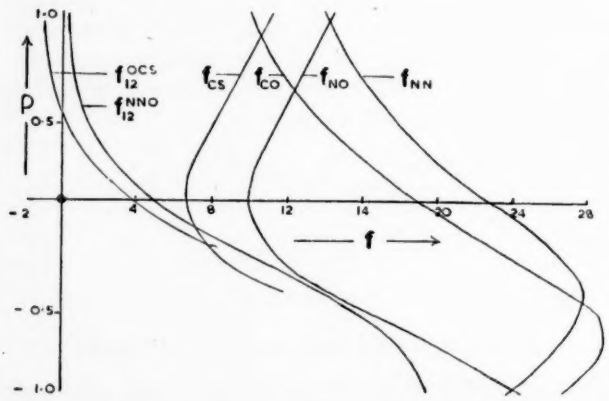

FIG. 3. Variation of the force constants with p in NNO and OCS.

[5] A. Dadieu and H. Kopper, Wien. Anz. 92 (1935). P. F. Bartunek and E. F. Barker, Phys. Rev. 48, 516 (1935).
[6] W. S. Richardson and E. B. Wilson, J. Chem. Phys. 18, 694 (1950).
[7] J. Bigeleisen and L. Friedman, J. Chem. Phys. 18, 1656 (1950).
[8] W. Gordy, J. Chem. Phys. 15, 305 (1947).
[9] W. Gordy, J. Chem. Phys. 14, 305 (1946).

N is the *bond order* and r the CN bond length in angstom units.

From Table V and (i) the relative *bond orders* in HCN:ICN:BrCN:ClCN are 1:0.995:0.991:0.982. The relation (ii) gives $N=2.89$ for HCN and from this and the other N values defined by the ratios, the f_{CN} values in the other molecules may be obtained. They are given in Table IV together with the corresponding values for the other force constants. The values of p corresponding to these f_{CN} values are given in Table III.

On plotting these values of p against the ratio ν_2/ν_1 a smooth curve is obtained, Fig. 4, which may be used in interpolating for unknown p values in other molecules with known vibration frequencies.

For the X·CN series a plot of p against the atomic weight of X is a smooth curve, Fig. 5; this curve might be used to interpolate for CH_3CN, treating the methyl group as a single particle.

In order to test the above empirical method the $f-p$ curves for OCS were obtained and p determined from the ratio of the frequencies. The results are given in Table IV together with data on the related molecules CO_2 and CS_2.

TABLE III. Geometrical form and potential energy distribution.

Molecule	HCN	ClCN	BrCN	ICN	NNO	OCS
p	0.485	0.140	0.088	0.027	0.422	0.242
ρ_1	−7.050	−1.682	−1.767	−1.829	−1.352	−1.499
ρ_2	2.062	7.143	11.364	37.037	2.370	4.132
$V_{11}(\nu_1)$	1.240	1.058	1.053	1.042	1.052	1.080
$V_{22}(\nu_1)$	0.240	0.058	0.053	0.042	0.052	0.080
$V_{12}(\nu_1)$	−0.480	−0.116	−0.106	−0.084	−0.104	−0.160

$V_{11}(\nu_2)=0.000$; $V_{22}(\nu_2)=1.000$; $V_{12}(\nu_2)=0.000$.

(5) THE GEOMETRICAL FORM OF THE VIBRATIONS AND THE DISTRIBUTION OF POTENTIAL ENERGY IN THE TWO MODES

From the expressions given in Sec. (3), it is seen that for ρ_1, in the range of p considered here, the numerator is always positive, (or taking the negative sign inside the bracket always negative). The sign of ρ_1 depends, then, on the sign of the denominator. ρ_1 will be negative and ρ_2 positive for positive p. It is clear, however, that for a certain range of p, ρ_1 will be negative for a negative p and so also will ρ_2; i.e., both ν_1 and ν_2 will be pseudo-antisymmetrical.

This range of p is given by,

$$0>p>-\frac{1}{1+\mu_3}.$$

Thus ρ_1 is negative, corresponding to ν_1 being a pseudo-antisymmetrical vibration, for $1>p>-(1+\mu_3)^{-1}$; therefore, for small μ_3, ν_1 is a pseudo-antisymmetrical vibration over almost the entire range of p considered here. Finally, ρ_2 is positive for positive p and negative for negative p.

The two stretching vibrations of a linear triatomic

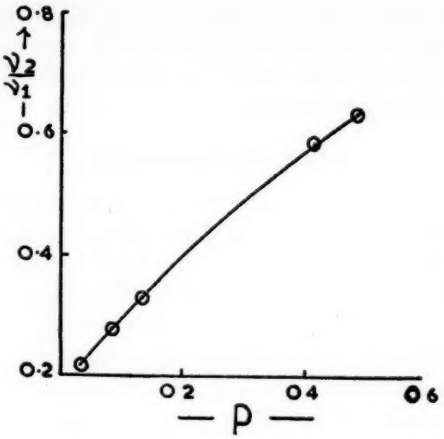

FIG. 4. Plot of frequency ratio against p.

molecule can thus be either (i) one pseudo-symmetrical and the other pseudo-antisymmetrical or (ii) both pseudo-antisymmetrical. They are never both pseudo-symmetrical. Taking valency considerations into account, the first possibility is the more probable; and in the systems treated in this paper it is found that alternative (i) holds in each case.

Using Torkington's[1] description of the form of the normal vibrations, the values of ρ for the two parallel normal modes of vibration are found. They are given in Table III together with the values of p and the relative energy components V_{ij} expressed as fractions of the total potential energy of the system.

(6) DISCUSSION

The force constants found for the systems discussed together with those already in the literature are given in Table IV.

Glockler and Tung[10] developed an empirical method for obtaining valence force potential constants which they applied to the OCS molecule. Their method gave unsatisfactory values for the constants in OCS and they obtained a set of force constants by assuming a value for the interaction constant f_{12}. They consider the following set to be the most satisfactory,

$$f_{CO}=15.216, \quad f_{CS}=7.401,$$

$$f_{12}(\text{assumed})=0.602\times10^5 \text{ dynes/cm}.$$

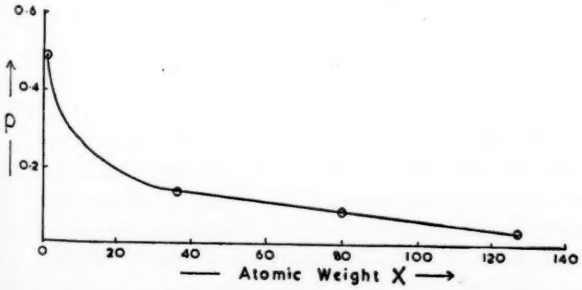

FIG. 5. Plot of atomic weight of X against p in the X·CN series.

[10] G. Glockler and J.-Y. Tung, J. Chem. Phys. **13**, 388 (1945).

TABLE IV. Force constants.

Molecule	f_{xy}	f_{yy}	f_{13}	Reference
HCN	5.70	18.07	−0.30	a
ClCN	17.61	5.01	0.50	···
BrCN	17.80	4.10	0.70	···
ICN	17.94	2.92	1.06	···
NNO	17.88	11.39	1.36	b
OCS	15.68	7.20	1.15	···
CO_2	15.5	···	1.29	c
CS_2	7.5	···	0.60	c

[a] See reference 4. [b] See reference 8. [c] See reference 5.

The set of constants given for OCS in Table IV is a reasonable one. These indicate that the CO link in OCS is a little stronger and the CS link a little weaker than the comparable links in CO_2 and CS_2. This might be expected from the electronegativity values for oxygen and sulfur. The indications are then, that the bond lengths in these molecules would differ as follows,

$$r_{CO}(OCS)<r_{CO}(CO_2) \quad \text{and} \quad r_{CS}(OCS)>r_{CS}(CS_2).$$

The force constant value of Glockler and Tung[10] gives the opposite indication for the CO link.

Recent spectroscopic work, including the microwave region, has yielded the bond lengths given in Table V. It is seen that the force constant values of Glockler and Tung are not in as good accord with the spectroscopic values for the bond lengths as those given in Table IV.

An interesting feature is that the value of f_{12} for OCS lies between the values for f_{12} in CO_2 and CS_2 as is to be expected on simple grounds.

Gordy's relation[9] connecting the force constant, bond length, and *bond order* may be used to obtain estimates of *bond order*. Using the force constant values

TABLE V. Bond lengths and bond orders in linear triatomic molecules.

Molecule	Link	Bond length A	Bond order N
CO_2	CO	1.163[a]	2.24
CS_2	CS	1.554[a]	2.06
OCS	CO	1.161[b]	2.32
	CS	1.560	1.95
NNO	NN	1.126[c]	2.45
	NO	1.191	1.51
HCN	CH	1.059[d]	0.99
	CN	1.157	2.89
ClCN	CCl	1.630[e]	1.27
	CN	1.163	2.92
BrCN	CBr	1.789[e]	1.26
	CN	1.160	2.90
ICN	CI	1.995[e]	1.11
	CN	1.159	2.90

[a] Reference 9, p. 398.
[b] Townes, Holden, and Merrit, Phys. Rev. **74**, 113 (1948).
[c] Coles, Elyash, and Gorman, Phys. Rev. **72**, 973 (1947).
[d] Gordy, Revs. Modern Phys. **20**, 668 (1948).
[e] Smith, Ring, Smith, and Gordy, Phys. Rev. **74**, 370 (1948). Townes, Holden, and Merrit, Phys. Rev. **74**, 113 (1948).

given in Table IV, and the bond lengths given in Table V, the values of the *bond orders* in the various links were obtained. They are given in Table V.

The values obtained for the *bond orders* for the CX links in the XCN series show the same trend as do the values for the electronegativities of the X atoms,[9] i.e.,

$$N_{CCl} > N_{CBr} > N_{CI} > N_{CH}.$$

It might be noted also that there is an appreciable change in the value of N as the electronegativity value of X goes from a value larger than for the carbon atom to one smaller, $N_{CBr}=1.26$, $N_{CI}=1.11$.

The values given for f_{CX} indicate an appreciable stiffening in the CX links when compared with the values usually quoted (reference 5, p. 193); this behavior is mirrored in the values obtained for the bond orders in the CX links.

It is worthwhile pointing out that the values obtained for the interaction constant f_{12} for the XCN series in this paper show the opposite trend to the stretching force constants f_{CX}.

ACKNOWLEDGMENTS

It is a pleasure to express my sincere thanks to Dr. P. Torkington for very helpful correspondence during which he pointed out many irrelevances and clarified some ambiguities in this paper. My thanks are also due to Dr. Mansel Davies and to Professor C. A. Coulson for much useful criticism and discussion.

Acknowledgment is made to the University of Wales for a Research Fellowship and to the Grants Committee of the Royal Society for providing a calculating machine.

THE JOURNAL OF CHEMICAL PHYSICS VOLUME 19, NUMBER 9 SEPTEMBER, 1951

Gaseous Detonation.* I. Initiation of Detonation†

A. J. MOORADIAN‡ AND W. E. GORDON§
Department of Chemistry, University of Missouri, Columbia, Missouri
(Received August 28, 1950)

By means of piezoelectric gauges, a study has been made of the development of detonation from a shock wave propagated into a mixture. With a sufficiently strong shock, detonation above the stable velocity is immediately established which decays smoothly to the steady state. When the shock is weaker than required for detonation the phenomena which ensue depend upon the strength of the shock wave and the nature of the medium. A zone of combustion, accompanied by a build-up of the pressure, develops in the wake of the shock front. This may lead to a smooth acceleration of the latter until detonation is established; shock waves may be formed which overtake the front and cause detonation; or the initial shock may decay without detonation. The hydrodynamic properties of the medium are particularly important in determining the sequence of events. Composition and pressure limits are observed beyond which detonation cannot be initiated in any case. Near these limits there is always "spin" in the detonation, which appears on the pressure records as a periodic oscillation of the pressure for some distance behind the wave front. In these experiments the initiating shock wave was produced by a detonating mixture such as $2H_2$-O_2 contained behind a Cellophane diaphragm. The strength of the shock wave was very much increased when this mixture was diluted with hydrogen.

INTRODUCTION

In a recent work Berets, Greene, and Kistiakowsky[1] have made a study of the initiation of detonation by shock waves. In the introduction to their paper there is a brief review of the subject with a list of references. The work described here supplements that in reference 1 by obtaining the pressure contours of the shock waves as they pass into detonation. This grew out of an investigation of the detonation limits in hydrogen-oxygen mixtures with various diluents.[2] In order to decide whether a given mixture was detonable or not, it was necessary to insure that a sufficiently strong initiation had been supplied, and hence a means was devised whereby the strength of the initiation could be changed and the effect of this studied. From the many detonations performed, it was possible to pick out examples which demonstrated certain regularities in the initiation phenomena.

EXPERIMENTAL

Most of the experiments were performed in a straight copper tube with a 20-mm inside diameter, which had a mirror-like interior surface. The tube consisted of two sections: the first, 2 m in length, contained the initiating mixture; and the second, 10 m in length, contained the mixture under investigation. Provision was made for the insertion of a Cellophane diaphragm between the two sections. For this purpose an ordinary pipe union (nominally for $\frac{1}{2}$-inch pipe) was bored to remove the internal threads and to provide a slip-fit over the ends

* This work has been supported by the ONR under Contract N7onr-292, Task Order I.

† This constitutes part of the work for the dissertation submitted by A. J. Mooradian in partial fulfillment of the requirements for the degree of Doctor of Philosophy at the University of Missouri.

‡ Present address: National Research Council, Chalk River, Ontario, Canada.

§ Present address: Arthur D. Little, Inc., Cambridge, Massachusetts.

[1] Berets, Greene, and Kistiakowsky, J. Am. Chem. Soc. **72**, 1086 (1950).

[2] To be presented in a later paper in this series.

of the copper tubes. When the union was tightened the ends of the tubes were almost butted, so that the smoothness of the internal surface was effectively preserved. (This appeared to be of considerable importance.) The opposing faces of the union were machined flat, and thin rubber gaskets were cemented to them to provide a seal around the diaphragm.

Earlier some experiments were made in an iron tube, 6 m long with a 21-mm inside diameter. The surface of the tube in this case was quite rough. The construction was similar to the copper tube.

Provision was made at the extremities of the two sections for evacuating them separately and admitting the gas mixtures. The latter were made up from gases supplied in commercial cylinders. With each mixture composition a series of experiments was performed in which the initial pressure was varied through the range from about 0.125 atmos to 3.0 atmos. Since the pressure of the initiating mixture could be adjusted independently, it was possible to provide a wide range of strengths of ignition by varying the "initiator ratio," the ratio of the pressure of the initiator to that of the experimental mixture.

After each shot the tube was dried by a current of dry air. Then the union was broken and the Cellophane fragments swept out of each compartment by closing the open end with a rubber stopper, allowing the air pressure to build up to three or four atmospheres, and suddenly removing the stopper. This was repeated until there was no more dust in the blast from the end of the tube. When the fragments were allowed to accumulate they produced marked effects on the detonation wave.

The wave was detected by six tourmaline piezoelectric gauges connected in parallel to a cathode-ray oscillograph. In addition to indicating the time of arrival of the wave, the gauges also recorded the pressure-time contour of the wave at each point. They were spaced far enough apart that the overlapping of the signals provided no serious problem in interpreting the records. The polarity of the crystals in alternate gauges was reversed so that the oscillograph beam would remain near the center of the screen. This also aided in the identification of the signals with the corresponding gauges. No attempt was made in this investigation to measure the pressures accurately, but relative values were estimated from the deflections. The time constant of the amplifier circuit was sufficiently long (about 10 milliseconds) that the decay of the signals did not seriously affect the shape of the pressure contours.

The construction of the gauges is shown in Fig. 1. The crystal elements, of irregular shapes, were cut from slabs of tourmaline about 0.5 mm thick. These varied in size, but all were less than 1 cm on the greatest dimension. The crystal faces were coated with silver and soldered on the mounting. The crystals were mounted in the gauge tube with the top edge about 1 mm below the brim of the tube, and the crystal faces parallel to

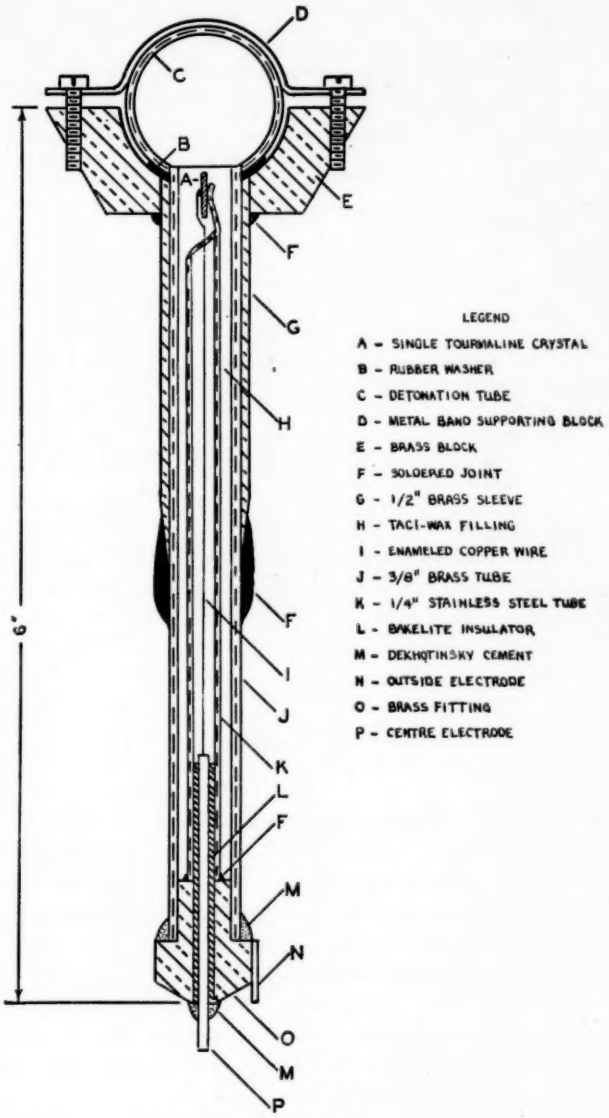

FIG. 1. Piezoelectric gauge.

the tube axis. In this way the crystal was edge-on to the shock wave which was transmitted down the gauge tube when the detonation wave passed over the mouth. The mounting was constructed so as to minimize obstructions which would cause reflections of the shock wave.

The gauge tube was filled with Cenco Taci-Wax. There is evidence from work in this laboratory that gauges of this construction, but filled with Vaseline, record quite faithfully the pressure contours of shock and detonation waves. However, the Vaseline proved troublesome and Taci-Wax was substituted. This reduced the sensitivity of the gauges to about one-half of that with the Vaseline, but the contours of the waves were very similar with the two fillings.

The oscillograph beam was photographed with a rotating drum camera, which held a strip of 35-mm film, 25 cm long. A simultaneous time base was pro-

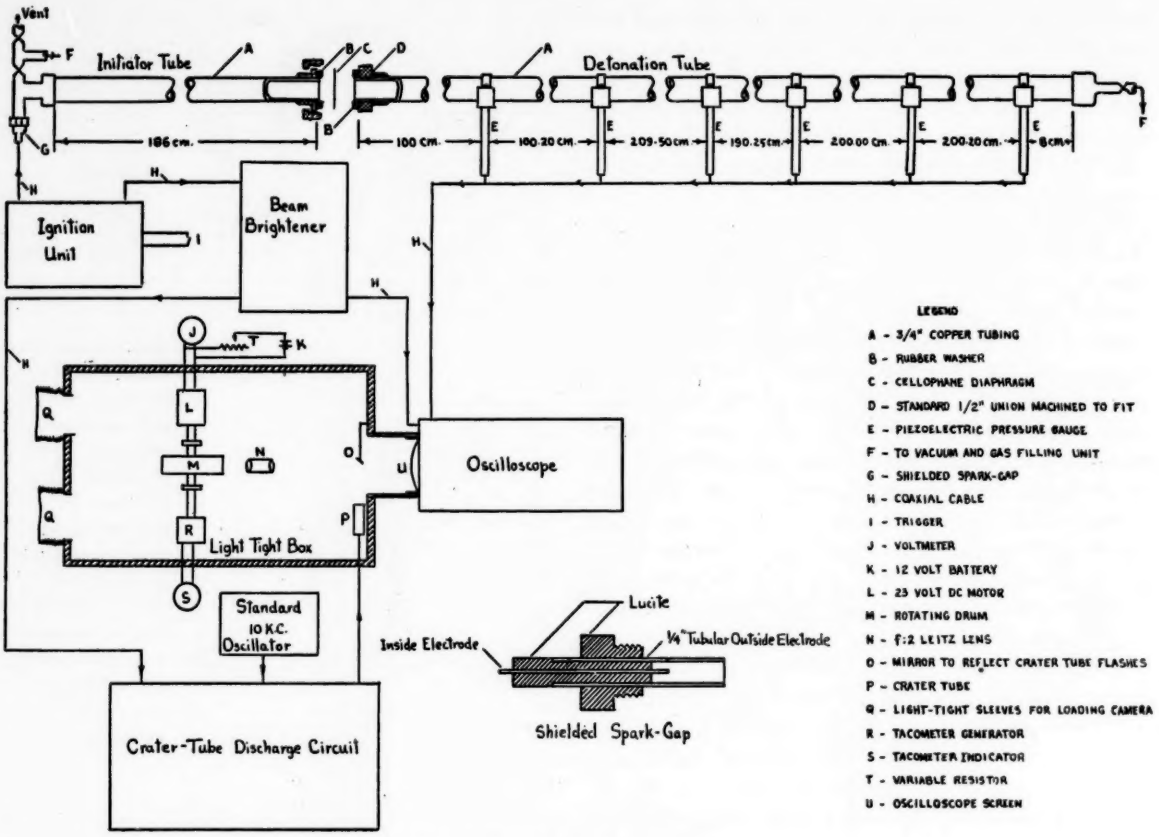

FIG. 2. Experimental arrangement.

vided on the film by a carefully calibrated 10-kc crystal-monitored oscillator, which flashed a crater-type gas discharge tube, Sylvania Type R1130B. A signal from the circuit used to spark the detonation simultaneously actuated the oscillograph beam brightener and the crater tube circuit. A schematic diagram of the arrangement is shown in Fig. 2.

A representative record in Fig. 3 shows the signals from five of the gauges and, above the oscillograph trace, the 10-kc time base.

Earlier in the investigation a method employing a number of spark gaps was used to obtain the detonation velocities. The gaps were charged just below the sparking potential, and were discharged by the passage of the detonation wave. Through a suitable circuit the discharges were made to produce flashes in a crater tube. Although this method worked well with rich mixtures, in more dilute mixtures the discharges were erratic or did not occur at all. It possessed the advantage over the piezoelectric method of allowing closer spacing of the detecting elements. Thus with this method it was possible to measure the rapidly changing velocity of the wave just after the bursting of the diaphragm (see Figs. 4 and 5).

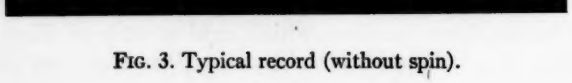

FIG. 3. Typical record (without spin).

RESULTS AND DISCUSSION

In some of the early experiments the two tube compartments were filled to a pressure slightly above atmospheric, the union was broken, the diaphragm removed quickly, and the tube reconnected. Under these conditions, without the diaphragm, it was found that the detonation wave from the rich initiating mixture fell rapidly in velocity upon crossing the boundary into the dilute mixture and assumed the stable detonation velocity in the latter. The situation is represented in Fig. 4. This is quite similar to the results of the experiments of Campbell and Woodhead.[3] From this it is seen that the influence of the initiator is exerted for only a short time, after which the manner of propagation is solely dependent upon the properties of the mixture itself. This is, of course, to be expected theoretically. A slight oscillation of the velocity as in the 20 percent hydrogen-air mixture, was sometimes observed in the weaker mixtures. The points in Fig. 4 are average velocities plotted at the middle of the intervals. The scatter of the points near the division line is thought to be due largely to the very short intervals and the consequent lack of precision in the measurements.

[3] Campbell and Woodhead, J. Chem. Soc. 3010 (1926).

The introduction of the Cellophane diaphragm had a drastic effect on the transmission of detonation. This is illustrated in Fig. 5, which shows this effect when the whole tube was filled with the knallgas mixture, $2H_2$-O_2. Apparently the shock wave transmitted across the diaphragm is unable to sustain detonation, the velocity falls abruptly, but rises rapidly again to the stable value as the shock wave develops into a detonation. Although it would appear from Fig. 5 that the diaphragm was detrimental to the initiation, subsequent experiments showed that with weaker mixtures, initiation was just as effective with the diaphragm as without. Also, by using the diaphragm, it was possible to obtain a much stronger initiation by raising the pressure of the initiator above that of the mixture.

The influence of the initiator ratio in this experimental arrangement is shown by the results in Table I. For any given initial pressure of the mixture there is a critical initiator ratio below which stable detonation does not

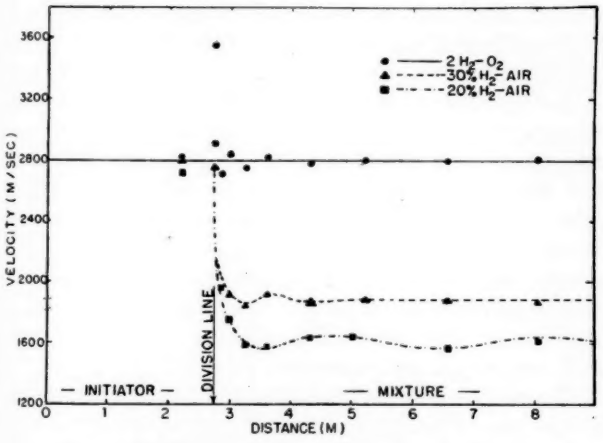

FIG. 4. Stabilization of the detonation wave passing from the initiator into a dilute mixture.

occur. This critical ratio increases as the pressure of the mixture is lowered, until a limiting pressure is reached below which stable detonation cannot be obtained, even with a very high pressure of the initiating mixture. This will be referred to as the low pressure detonation limit. For the mixture in Table I, 18 percent hydrogen in air, the limit lies somewhere between 190 and 95 mm Hg.

The composition of the initiating mixture had an important and, at first sight, a paradoxical effect. Mixtures of low density were always difficult to initiate with the knallgas mixture. For example, the mixture 7 percent oxygen in hydrogen at an initial pressure of 2 atmos did not detonate with knallgas at an initiator ratio of 1.7, the highest obtainable in our apparatus. However, this same mixture was actually over-initiated when the knallgas was diluted fifty percent with hydrogen, and at an initiator ratio of 1.5. (See Figs. 8 (a) and (b).) In further experiments it was always found that

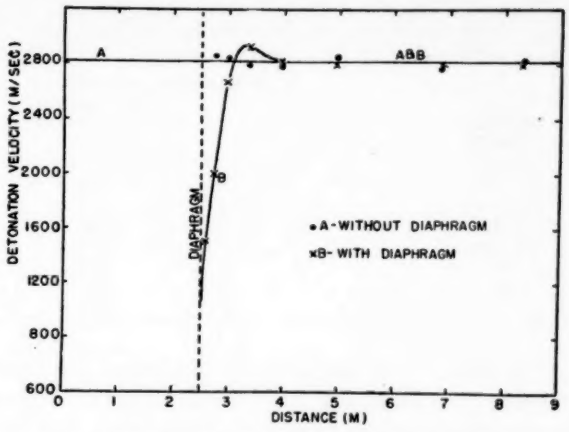

FIG. 5. Effect of a Cellophane diaphragm on the transmission of a detonation wave in $2H_2$-O_2.

this dilute mixture gave a stronger initiation than knallgas itself, and that the critical initiator ratio with it was lower. One might expect that since the theoretical pressure and temperature in the detonation wave are lower in the dilute mixture that the initiation would not be as good. However, it will be seen that when the mechanism of the initiation with this arrangement is examined, the difference in densities of the two mixtures is of much greater importance than the changes in pressure and temperature.

In Fig. 5 it is noted that the velocity of the wave decreases abruptly at the diaphragm. This phenomenon may be pictured in the following manner: When the detonation front reaches the relatively dense diaphragm, there is a momentary reflection of the shock wave. Following the rupture of the diaphragm the situation is similar to that in the "shock tube" treated by Pay-

TABLE I. Effect of initiator ratio with 18 percent H_2-air mixture using $2H_2$-O_2 initiator.

Press. of mixture (mm Hg)	Press. of initiator (mm Hg)	Initiator ratio	Final condition of detonation wave
2290	1140	0.50	unstable
1520	1140	0.75	stable
760	760	1.00	unstable
760	1140	1.50	stable
570	570	1.00	unstable
570	855	1.50	stable
380	380	1.00	unstable
380	570	1.50	unstable
380	760	2.00	stable
190	380	2.00	unstable
190	570	3.00	stable
95	285	3.00	unstable
95	380	4.00	unstable
95	570	6.00	unstable
95	760	8.00	unstable
95	1140	12.00	unstable

TABLE II. Example of theoretical calculations on the shock tube with air in the expansion chamber.

Shock wave intensity	Required compression ratio: Argon in compression chamber	Hydrogen in compression chamber
2.0	5.7	2.4
3.0	17	4.1
4.0	52	6.0
5.0		8.4
10		23
20		78

man,[4] in which a compressed gas is separated from gas at a lower pressure in the "expansion chamber." Under these conditions a shock wave is transmitted into the expansion chamber, and a rarefaction spreads back into the compression chamber, the flow of gas from the high pressure region supporting the shock front. For small compression ratios this flow velocity is proportional to a quantity u, given by $u=RT/\gamma M$, where the quantities on the left have their usual significance. Hence, as was discovered by Payman and Shepherd[4] the flow velocity is higher and the shock wave is stronger, the lower the average molecular weight of the compressed gas. The magnitude of the effect is illustrated by the theoretical calculations in Table II.||

Table II also illustrates the exponential nature of the dependence of shock wave intensity on the compression ratio in the shock tube. With this conception of the mechanism for the initiation in our experiments, the values of the initiator ratios of Table I become more meaningful. Referring to Table I, it will be noted that when the initial pressure of the mixture is reduced from 2.0 to 0.25 atmos, the required initiator ratio increases from 0.75 to 3.0. This does not mean then a corresponding fourfold increase in the shock wave intensity required for initiation; a rough estimate based on shock tube theory gives an increase in the strength of the shock wave something less than twofold.

From the results with several different mixtures and with various initiating conditions, it has been possible to distinguish five different types of initiation phenomena. These are outlined below:

Detonable: (a) over-initiation leading to stable detonation.
(b) under-initiation developing to stable detonation.
(c) under-initiation with no detonation.

Non-detonable: (d) over-initiation giving unstable detonation.
(e) under-initiation with no detonation.

Before proceeding with a description of these initiation effects it is necessary to mention a characteristic phenomenon which was observed in all of the dilute mixtures near the detonation limits. This was the so-called "spinning detonation" which has been the subject of much previous investigation.[5-7] In our experiments the spin appeared as a periodic (but nonsinusoidal) oscillation of the pressure in the wake of the detonation front. The period was characteristic of the mixture composition. These vibrations were always found when the detonation had reached a steady state (except in some richer mixtures) and were also observed as a transient phenomenon when an over-initiated detonation wave in a nondetonable mixture reached a velocity close to the theoretical value for the mixture. The observations on spin will be the subject of a later paper—they are of interest here because they aided the interpretation of the records.

A typical succession of pressure-time contours at the six gauges for case (a) above, is shown in Fig. 6. The contours in this and the following figures are free representations, not scaled drawings.

The interpretation of the record in Fig. 6, aside from the presence of the spin phenomenon, seems quite apparent. A high intensity shock wave, sent into the mixture by the initiator, supports detonation corresponding to a point on the Hugoniot curve above the Chapman-Jouget point (for stable detonation). The rarefaction, propagating with a velocity higher than the detonation front, gradually lowers the pressure until the Chapman-Jouget condition is reached. From this point the wave, now stable, travels with a sensibly constant velocity over the remainder of the tube.

Case (b), with under-initiation developing into detonation, is particularly interesting. The upper part of Fig. 7 shows a typical progression of piezoelectric records for this situation. Below this in Fig. 7, the average velocities in the intervals are plotted graphically, and a smooth curve is drawn to represent the instantaneous velocity.

In the experiment represented in Fig. 7 the wave entered from the initiator as a low amplitude shock wave with a speed less than half of the stable detonation

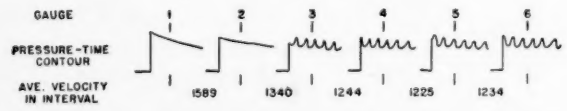

FIG. 6. (Case a); Over-initiation in $2H_2$-O_2-17A at initial pressure 0.25 atmos; with $2H_2$-O_2 initiator; initiator ratio, 6:1.

[4] Payman and Shepherd, Proc. Roy. Soc. (London) **A186**, 293 (1946). See also, Courant and Friedrichs, *Supersonic Flow and Shock Waves* (Interscience Publishers, Inc., New York, 1948), p. 181. A full application of the theory has been made by G. N. Patterson, in Memo. No. 9903, Naval Ordnance Laboratory, Silver Springs, Maryland.

|| The theoretical predictions in Table II have been confirmed in shock tube experiments in this laboratory.

[5] Campbell and Finch, J. Chem. Soc. 2094 (1928).
[6] Bone and Fraser, Trans. Roy. Soc. (London) **A230**, 373 (1931).
[7] Bone, Fraser and Wheeler, Trans. Roy. Soc. (London) **A235**, 29 (1935).

velocity. At the first gauge position there is a slight "hump" in the pressure behind the initial shock front. At the second gauge small secondary shocks appear behind the first. Between the second and third gauge positions, the velocity rose steeply, the shock amplitude increased several-fold, and a very high broad pressure region developed behind the front. Following this the phenomenon was quite similar to the over-initiated detonation in Fig. 6.

The velocity curve in Fig. 7 is very similar to the results obtained by Berets, Greene, and Kistiakowsky.[1] As in this case, they quite frequently observed the "overshoot" of the velocity above the final stable value.

There can be little doubt that the pressure rise behind the shock front is due to combustion of the gases in this region. Flames situated some distance behind a shock front have often been observed photographically.[7] The gas, compressed and heated in the shock front, begins to react slowly, and the reaction accelerates from self-heating. Accompanying the rise in pressure due to the combustion, there will be a flow of gas out of the burning region. This gas flow will serve to reinforce the shock wave, which, thus intensified, will initiate a still more rapid combustion in the fresh gas. Thus the effect can be rapidly accumulative, until at some point, presumably when the shock wave is sufficiently strong, the phenomenon takes on the characteristics of a detonation.

In this "building up" period, just prior to detonation, pressures considerably higher than the stable detonation pressure sometimes appear, as at the third gauge position in Fig. 7. Such observations have been made by Rimarski and Konschak[8] and by Henderson.[9] It is interesting to note in this connection an observation by Campbell and Woodhead[3] that glass tubes which would support the stable detonation wave invariably broke when the detonation was *initiated* in them. This is perhaps not difficult to understand. The pressure which is developed in any element of the gas will depend upon a number of factors: the extent to which the gas is compressed before the combustion begins, the rate of burning, and the simultaneous rate of expansion. Here we may imagine a homogeneous reaction commencing almost at the same instant throughout a broad region of gas which has been precompressed in the shock front. In the middle of this region the limiting condition of a constant volume explosion may be approached. In the steady-state detonation wave, on the other hand, the gas expands at a rate which more than compensates for the rise in temperature due to combustion, and the reaction is actually accompanied by a decrease in pressure.[10]

It seems altogether likely that the mechanism which

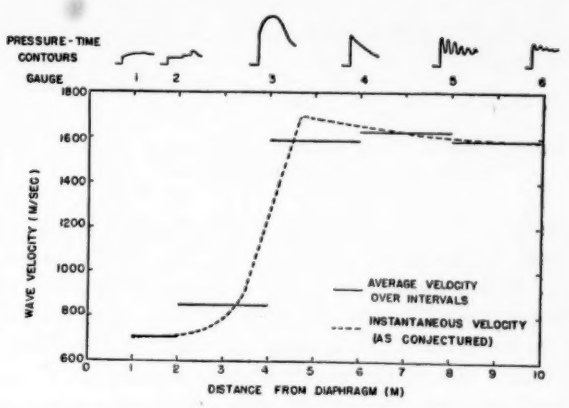

FIG. 7. (Case b); Under-initiation developing into detonation; 18 percent H_2-air, initial pressure 2 atmos; initiator $2H_2$-O_2; initiator ratio, 3:4.

we have pictured for the experiment in Fig. 7 is also the sort of thing that occurs in the development of detonation from a flame. One can understand in these terms, for example, the production of the so-called "retonation" wave, discovered by Dixon.[11] When a region of high pressure develops at some point in the tube, shock waves will travel out in both directions, to the rear (into the burned gas) as well as forward. Previous work by one of the authors[12] has shown that the retonation is in fact a simple shock wave which is rapidly attenuated. The high luminosity which it shows in photographs probably arises from the fact that it is travelling in the hot combustion products left by the flame.

Figure 8(a) illustrates the third case, under-initiation in a detonable mixture, in which the shock wave dies out without developing into detonation. Figure 8(b) shows the remarkable effect of diluting the initiator with hydrogen: even with a smaller initiator ratio, the same mixture is over-initiated.

It is interesting to note in Fig. 8(a) that the second gauge recorded a pressure "hump" behind the shock front, and that this was accompanied by an acceleration of the wave. However, in contrast to Fig. 7, detonation did not develop here. This is even more remarkable

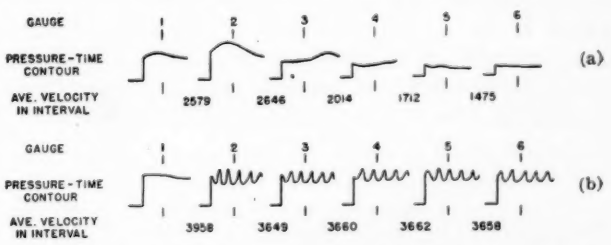

FIG. 8(a) (Case c); Under-initiation without detonation; 7 percent O_2 in H_2, initial pressure 2 atmos; initiator $2H_2$-O_2; initiator ratio 1.7:1. 8(b) Over-initiation in same mixture as in Fig. 8a at 2 atmos initial pressure; initiator $5H_2$-O_2; initiator ratio 1.5:1.

[8] Rimarski and Konschak, Autogene Metallbearbeit. **27**, 209 (1934).

[9] Henderson, Proc. Pacific Coast Gas Association, 32 (1941).

[10] von Neuman, OSRD Report No. 549 (1942). See also Courant and Friedrichs, reference 4.

[11] Dixon, Trans. Roy. Soc. (London) **A200**, 315 (1903).

[12] Gordon, NavOrd Report No. 99-46 from the Woods Hole Oceanographic Institution (1946).

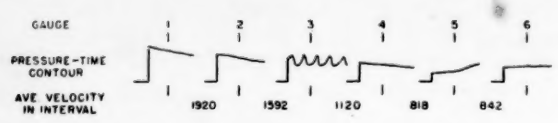

FIG. 9. (Case d); Over-initiation in 18 percent H_2-air below the low pressure limit; initiator ratio, 12:1.

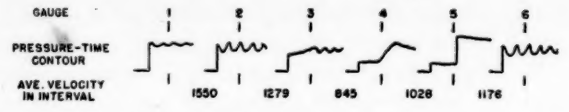

FIG. 10. Recurrent detonation in 14 percent hydrogen-/air (below the composition limit) initial pressure 1 atmos; initiator $2H_2$-O_2; initiator ratio 2.6:1.

when it is noted that the shock wave intensity initially is much higher in Fig. 8(a) than in Fig. 7 (Mach number, 2.80, corresponding to the velocity 2579 m/sec cf. 1.86 corresponding to the velocity 707 m/sec.). The reason for this may lie in what we might call an "over-reaching" effect; the shock front accelerated by the flow of gas from the burning zone gets too far ahead of the latter to be further supported, and consequently degenerates. Such an effect should be most pronounced in mixtures which have a high acoustic velocity, that is in mixtures of low molecular weight. In fact, the development of detonation from under-initiation was never observed with hydrogen-diluted mixtures in our experiments.

A brief description will serve to indicate the results in nondetonable mixtures. With sufficiently strong initiation it was possible to produce waves which had, initially, a velocity higher than the theoretically stable detonation velocity. The ensuing phenomena entirely resembled those for over-initiation in detonable mixtures (Fig. 6), except that the detonation did not remain stable in the latter part of the tube. There was every indication in such cases that detonation did occur in the beginning, and the usual spin phenomenon developed as the velocity approached the Chapman-Jouget value. This case is illustrated in Fig. 9.

In Fig. 9 there is an increase in velocity near the end of the tube and, as usual in such cases, there is a rise in pressure behind the shock front on the fifth gauge. Again, this is probably due to the development of a zone of combustion. This can result in building up to detonation a second time, and the process can presumably repeat over and over again in a long tube, the wave being re-initiated in each cycle, and subsequently decaying because of the inability of the mixture to support a stable detonation. This sort of thing is illustrated in Fig. 10. (The theoretical velocity for the 14 percent hydrogen-air mixture in Fig. 10 is 1482 m/sec, but by extrapolation of the observed velocities in more concentrated hydrogen-air mixtures, the stable velocity expected would be about 1390 m/sec.) In the case in Fig. 10 the pressure "hump" actually developed into a very strong shock or detonation front behind the initial shock (fifth gauge).

It is interesting to note that the phenomena of over-initiation, development of spin at or near the theoretical velocity, and acceleration of the shock front associated with the appearance of a pressure "hump" behind the front, were observed even for mixtures considerably below the detonation limits, e.g., 10 percent hydrogen-air (limit between 14 and 15 percent hydrogen).

SUMMARY

It is evident that shock waves play an important role in the initiation of detonation in gases. The actual manner in which these build up to detonation is a rather complicated process, the nature of which depends as much upon the hydrodynamic properties as the chemical nature of the medium. A weak shock wave initiates slow combustion which by self-heating gives rise to an explosion in the rear of the wave. Such explosions may act either to increase the shock wave intensity smoothly, and accelerate it into detonation; or, may give rise to shock waves in the rear of the initial front which overtake the latter and lead to a discontinuous acceleration. One is inclined to believe that this sequence of events is not unique to the particular experimental arrangement used here, but is quite general for other sources of ignition.

It is possible to initiate short-lived detonation even in mixtures which will not maintain a stable wave under the conditions of the experiment, and in some mixtures there is a recurrent cycle of initiation and of subsequent decay of detonation. The prerequisite for detonation appears to be the establishment of a sufficiently intense shock wave to maintain rapid combustion immediately behind itself. In a later paper data will be presented on the limits of detonation, and the criteria for stable detonation will be discussed.

THE JOURNAL OF CHEMICAL PHYSICS VOLUME 19, NUMBER 9 SEPTEMBER, 1951

The Statistical Mechanical Theory of Transport Processes. V. Quantum Hydrodynamics*

J. H. IRVING† AND ROBERT W. ZWANZIG
Gates and Crellin Laboratories of Chemistry, California Institute of Technology, Pasadena, California
(Received June 1, 1951)

This paper is concerned with certain extensions of a formal technique devised by Wigner for handling problems in quantum-statistical mechanics, especially to problems in quantum-mechanical transport processes. The approach is to find the closest possible analogy between classical and quantum-statistical mechanics, so that the extensive work in classical statistical mechanics can be utilized. This analogy is attained with the Wigner distribution function, with which averages of dynamical variables in quantum mechanics may be calculated by integrations in phase space. We will first state some basic properties of distribution functions in classical statistical mechanics, and then state the corresponding properties of the density matrix in quantum mechanics. We will define and discuss the Wigner distribution function, show that it has the desired averaging properties, and obtain the analog of the Liouville equation satisfied by this function. We will derive the analog of the Liouville equation in reduced phase space, and then obtain the equations of hydrodynamics from quantum-statistical mechanics.

I. DISTRIBUTION FUNCTIONS IN CLASSICAL STATISTICAL MECHANICS

GIBBSIAN statistical mechanics is based on the concept of a distribution of systems in phase space. His "density-in-phase" is now usually called the distribution function. (Hereafter, we will abbreviate this to d.f.) When normalized over the entire volume accessible to the system, it becomes the probability d.f., and gives the probability that the coordinates and momenta of a system of N particles will have the values $\mathbf{R}_1, \mathbf{R}_2, \cdots \mathbf{R}_N$, and $\mathbf{p}_1, \mathbf{p}_2, \cdots \mathbf{p}_N$. (When no confusion will result, we will refer to the sets of coordinates and momenta with single symbols $\mathbf{R}$, $\mathbf{p}$.) In equilibrium, for a canonical ensemble, the probability d.f. has the form,

$$f^{(N)}(\mathbf{R}, \mathbf{p}) = \exp[\beta(A - H^{(N)})], \tag{1.1}$$

where A is the free energy of the system, and $H^{(N)}$ is the hamiltonian function,

$$H^{(N)} = \sum_{k=1}^{N} \frac{p_k^2}{2m_k} + U(\mathbf{R}_1, \mathbf{R}_2, \cdots \mathbf{R}_N). \tag{1.2}$$

In a nonequilibrium state, the time behavior of the d.f. is given by Liouville's equation,

$$\frac{\partial f^{(N)}}{\partial t} + \sum_{k=1}^{N} \frac{\mathbf{p}_k}{m_k} \cdot \nabla_{\mathbf{R}_k} f^{(N)} + \sum_{k=1}^{N} (\nabla_{\mathbf{R}_k} U) \cdot \nabla_{\mathbf{p}_k} f^{(N)} = 0. \tag{1.3}$$

Usually the potential is simplified to a sum of terms which refer to interactions between single particles and an external field, and other terms which refer to interactions between pairs of particles:

$$U(\mathbf{R}_1, \cdots \mathbf{R}_N) = \sum_{k=1}^{N} \phi_k(\mathbf{R}_k) + \tfrac{1}{2} \sum_{j \neq k}^{N} \sum_{k}^{N} V_{jk}(\mathbf{R}_j, \mathbf{R}_k). \tag{1.4}$$

When this is done, reduced d.f.'s, and in particular the singlet and pair d.f. become useful. The reduced d.f.'s are defined by

$$f^{(m)}(\mathbf{R}_1, \cdots \mathbf{R}_m, \mathbf{p}_1, \cdots \mathbf{p}_m; t) = \int \cdots \int f^{(N)} \prod_{m+1}^{N} d\mathbf{R}_k d\mathbf{p}_k \tag{1.5}$$

and are called specific d.f.'s because they refer to the precise specification of each particle. Also used are the generic d.f.'s, which refer to the probability of finding any particle of the required type at a point in phase space. With the assumption of pair potentials many thermodynamic and transport properties of fluids can be expressed in terms of the singlet and pair d.f. alone. An excellent discussion on the use of these d.f.'s in equilibrium statistical mechanics may be found in an article by DeBoer.[1]

II. TRANSITION TO QUANTUM MECHANICS

It is not immediately clear how one should go about setting up the quantum-mechanical analog of classical Gibbsian statistical mechanics. The difficulty lies in the fact that the uncertainty principle prohibits the precise specification of the location of a system in phase space. Several approaches are possible in defining quantum mechanical d.f.'s. One of them is to use instead of the phase space technique, the matrix formulation of quantum mechanics, in which the analog of the d.f. is the density matrix. A second possibility is to construct a d.f. which has no simple interpretation in terms of probability concepts, but which can be used for calculating averages over phase space in a way which is formally identical with the classical one. This is the procedure that was followed by Wigner and which will be utilized later in this paper.‡

* This work was supported by the ONR under Contract N6onr-244 with the California Institute of Technology. The paper is one of a series of articles on the statistical mechanical theory of transport processes by John G. Kirkwood and collaborators.

† Present address, Hughes Aircraft Company, Culver City, California.

[1] J. DeBoer, *Reports on Progress in Physics* XII, 1948–9, pp. 305–374.

‡ Another possibility may be to use some kind of coarse-graining in phase space, so that one may talk about the probability of finding a system in a certain cell, possibly of volume h^{3N}, in phase space. This approach has not yet been used successfully.

The density matrix method can be developed in a very general way;[2] however, it is usually used in the "coordinate" representation. This has been studied in great detail by Husimi[3] and by Born and Green.[4] The density matrix is defined for a pure state as

$$\rho(\mathbf{R}, \mathbf{R}'; t)=\Psi^*(\mathbf{R}'; t)\Psi(\mathbf{R}; t), \tag{2.1}$$

where $\Psi(\mathbf{R}; t)$ is the wave function for the state of the system. When we deal with an ensemble of systems, or a mixed state, the density matrix has the form,

$$\rho(\mathbf{R}, \mathbf{R}'; t)=\sum_j A_j\Psi_j^*(\mathbf{R}'; t)\Psi_j(\mathbf{R}; t), \tag{2.2}$$

where Ψ_j is the wave function and A_j is the statistical weight of the j'th state in the ensemble. The space d.f. is given by $\rho(\mathbf{R}, \mathbf{R}'; t)$ and reduced d.f.'s are defined in the usual way. Averages of dynamical variables are calculated as traces of matrix products: if $\alpha(\mathbf{R}, \mathbf{R}')$ is the matrix associated with the variable α, then the average value of α is the trace of the matrix product of α and ρ,

$$\langle\alpha\rangle_{Av}=\int\int\alpha(\mathbf{R}, \mathbf{R}')\rho(\mathbf{R}', \mathbf{R})d\mathbf{R}'d\mathbf{R}. \tag{2.3}$$

This is the average over a state, if the system is in a pure state; or it is the ensemble average of the pure state averages, if the system is in a mixed state. Matrices are assigned to the basic variables in the following way—

coordinates:

$$\alpha(\mathbf{R}_1, \cdots \mathbf{R}_N)\rightarrow\alpha(\mathbf{R}_1, \cdots \mathbf{R}_N)\prod_k\delta(\mathbf{R}_k-\mathbf{R}_k')$$

momenta: $$\mathbf{p}_j\rightarrow-i\hbar\nabla_{\mathbf{R}_j}\cdots\prod_k\delta(\mathbf{R}_k-\mathbf{R}_k'). \tag{2.4}$$

For example, the hamiltonian operator is

$$H^{(N)}(\mathbf{R}, \mathbf{R}')$$

$$=\left\{-\sum_j\frac{\hbar^2}{2m_j}\nabla_{\mathbf{R}_j}^2+U(\mathbf{R})\right\}\prod_k\delta(\mathbf{R}_k-\mathbf{R}_k') \tag{2.5}$$

and Schrödinger's time dependent equation is

$$\frac{\partial\rho^{(N)}}{\partial t}=-\frac{i}{\hbar}\left\{\sum_k\frac{-\hbar^2}{2m_k}\nabla_{\mathbf{R}_k}^2\rho^{(N)}+\sum_k\frac{\hbar^2}{2m_k}\nabla_{\mathbf{R}'k}^2\rho^{(N)}\right.$$

$$\left.+U(\mathbf{R})\rho^{(N)}-U(\mathbf{R}')\rho^{(N)}\right\}. \tag{2.6}$$

(The superscript on ρ refers to the number of particles in the system.) This equation is the quantum-mechanical analog of the classical Liouville equation in the density matrix formalism. Born and Green[4] have made use of this in their method for setting up a quantum-mechanical theory of transport processes.

In 1932, Wigner[5] showed how a phase space d.f. could be constructed and used for simple evaluations of averages. This function is defined most conveniently in terms of the density matrix,

$$f^{(N)}(\mathbf{R}, \mathbf{p}; t)=\left(\frac{1}{\pi\hbar}\right)^{3N}\int\cdots\int_{-\infty}^{+\infty}\exp\left(\frac{2i}{\hbar}\mathbf{p}\cdot\mathbf{Y}\right)$$

$$\times\rho^{(N)}(\mathbf{R}-\mathbf{Y}; \mathbf{R}+\mathbf{Y}; t)d\mathbf{Y}. \tag{2.7}$$

Some of the more important properties of the Wigner d.f. are as follows:

(1) $f^{(N)}$ is everywhere real, although not necessarily positive.

(2) $$\int f^{(N)}d\mathbf{p}=\rho^{(N)}(\mathbf{R}, \mathbf{R}; t) \tag{2.8}$$

so that the integral of the d.f. over momentum space *does* give the probability density in configuration space.

(3) $$\int f^{(N)}d\mathbf{R}=\sigma^{(N)}(\mathbf{p}, \mathbf{p}; t), \tag{2.9}$$

where $\sigma^{(N)}(\mathbf{p}, \mathbf{p}'; t)$ is the momentum representation of the density matrix.§ Therefore, the integral of the d.f. over configuration space gives the probability density in momentum space.

(4) $$\frac{1}{m_j}\int\mathbf{p}_jf^{(N)}d\mathbf{p}=\frac{\hbar}{2im_j}\{\Psi^*\nabla_{\mathbf{R}_j}\Psi-\Psi\nabla_{\mathbf{R}_j}\Psi^*\} \tag{2.10}$$

when $f^{(N)}$ represents the pure state Ψ. The right side is recognized as the standard expression for the probability current density in configuration space.

(5) $f^{(N)}(\mathbf{R}, \mathbf{p}; t)$

$$=\left(\frac{1}{\pi h}\right)^{3N}\int\cdots\int_{-\infty}^{+\infty}\exp\left[-\frac{2i}{\hbar}\mathbf{R}\cdot\mathbf{p}'\right]$$

$$\times\sigma^{(N)}(\mathbf{p}-\mathbf{p}', \mathbf{p}+\mathbf{p}'; t)d\mathbf{p}', \tag{2.11}$$

which is an expression for $f^{(N)}$ dual to Eq. (2.7) where the roles of coordinates and momenta are changed, and i is replaced by $-i$.

(6) Since the Wigner d.f. is a bilinear form in Ψ, it is symmetric for both symmetric and antisymmetric

[2] J. Von Neumann, *Mathematische Grundlage der Quantenmechanik* (Dover Publications, New York, 1943).

[3] K. Husimi, Proc. Phys.-Math. Soc. Japan **22**. 264 (1940).

[4] M. Born and H. S. Green, *A General Kinetic Theory of Liquids* (Cambridge University Press, London, 1949).

[5] E. Wigner, Phys. Rev. **40**, 749 (1932).

§ $\sigma^{(N)}$ is not independent of $\rho^{(N)}$ because of the fourier transform relation between coordinate and momentum representations of the wave function. This is a point of major difference between quantum mechanics and classical mechanics, where the probability densities in configuration and momentum space may be specified independently. This independence permits, for example, a factorization of the classical d.f. for a canonical ensemble.

wave functions. However, it is possible to determine whether any particular d.f. corresponds to a Bose-Einstein or a Fermi-Dirac system in this way: take the inverse fourier transform of $f^{(N)}$ to obtain $\rho^{(N)}$ $(\mathbf{R}, \mathbf{R}')$ and then examine the symmetry of this function by interchanging either the primed or the unprimed quantities, but not both.

(7) The great values of the Wigner d.f. is that it is possible to calculate averages of dynamical variables by direct integration over phase space, without using operator technique. Although Wigner showed this only for some special kinds of variables, it gives the correct average for any function of coordinates and momenta, if the Weyl correspondence[6,7] for quantum mechanical operators is used. This assignment of operators is made in the following way: if $g(\mathbf{p}, \mathbf{q})$ is the classical variable whose operator is desired, we obtain its fourier expansion ξ,

$$g(\mathbf{p}, \mathbf{q}) = \int\int \exp[i(\boldsymbol{\sigma}\cdot\mathbf{p} + \boldsymbol{\tau}\cdot\mathbf{q})]\xi(\boldsymbol{\sigma}, \boldsymbol{\tau})d\boldsymbol{\sigma}d\boldsymbol{\tau}. \quad (2.12)$$

Then, the quantum-mechanical operator is defined as

$$G(\mathbf{x}, \mathbf{x}') = \int\int \exp[i(\boldsymbol{\sigma}\cdot\mathbf{P} + \boldsymbol{\tau}\cdot\mathbf{Q})]\xi(\boldsymbol{\sigma}, \boldsymbol{\tau})d\boldsymbol{\sigma}d\boldsymbol{\tau}, \quad (2.13)$$

where $\mathbf{P}(\mathbf{x}, \mathbf{x}')$ and $\mathbf{Q}(\mathbf{x}, \mathbf{x}')$ are the operators corresponding to momentum and position. We will now derive this averaging property of the Wigner d.f., using the coordinate representation of the density matrix. For simplicity in notation, only one dimension will be considered—the generalization is obvious. The operators P and Q are now

$$P = -ih\frac{d}{dx}\delta(x-x'), \qquad P^n = \left(-ih\frac{d}{dx}\right)^n \delta(x-x')$$

$$Q = x\delta(x-x'), \qquad Q^n = x^n\delta(x-x')$$

and the average value of g is

$$\langle g\rangle_{Av} = \int\int\left\{\int G(x, x')\rho(x,'x'')dx'\right\}\delta(x-x'')dxdx''.$$

Substitute the expression for g into the integral, and use the following property[7] of the exponential operator

$$e^{i(\sigma P+\tau Q)} = \exp\left(i\frac{\sigma\hbar}{2}\tau\right)e^{i\tau Q}e^{i\sigma P}$$

to get

$$\langle g\rangle_{Av} = \int\left[\exp\left(i\frac{\sigma\hbar}{2}\tau\right)e^{i\tau Q}e^{i\sigma P}\rho(x', x'')\right] \times \xi(\sigma, \tau)\delta(x-x'')dxdx'dx''d\sigma d\tau.$$

[6] H. Weyl, *The Theory of Groups and Quantum Mechanics* (London), p. 274.
[7] N. H. McCoy, Proc. Nat. Acad. Sci. **18**, 674 (1932).

Then, the Taylor's series expansion property

$$e^{i\sigma P(x,x')}\rho(x', x'') = \rho(x'+\sigma\hbar, x'')\delta(x-x')$$

leads to

$$\langle g\rangle_{Av} = \int\left[\exp\left(i\frac{\sigma\hbar}{2}\tau\right)e^{i\tau Q(x,x')}\rho(x'+\sigma\hbar, x'')\right]\xi(\sigma, \tau) \times \delta(x-x')\delta(x-x'')dxdx'dx''d\sigma d\tau$$

and integration over x' and x'' gives

$$\langle g\rangle_{Av} = \int\exp\left(i\frac{\sigma\hbar}{2}\tau\right)e^{i\tau x}\rho(x+\sigma\hbar, x)\xi(\sigma, \tau)dxd\sigma d\tau.$$

Now replace $\xi(\sigma, \tau)$ by its expansion $g(p, q)$:

$$\langle g\rangle_{Av} = \left(\frac{1}{2\pi}\right)^2\int\exp\left(i\frac{\sigma\hbar}{2}\tau\right)e^{i\tau x}\rho(x+\sigma\hbar, x) \times g(p, q)e^{-i(\sigma p+\tau q)}dxd\sigma d\tau dpdq.$$

Integrate over τ and then over x, using the fourier theorem to get

$$\langle g\rangle_{Av} = \frac{1}{2\pi}\int e^{-i\sigma p}g(p, q)\rho\left(q+\frac{\hbar\sigma}{2}, \quad q-\frac{\hbar\sigma}{2}\right)d\sigma dpdq.$$

Now, take $\hbar\sigma/2 = -Y$, and

$$\langle g\rangle_{Av} = \frac{1}{\hbar\pi}\int\exp\left(\frac{2i}{\hbar}pY\right) \times g(p, q)\rho(q-Y, q+Y)dpdqdY \quad (2.14)$$

or

$$\langle g\rangle_{Av} = \int g(p, q)f(p, q)dpdq \quad (2.15)$$

$$f(p, q) = \frac{1}{\hbar\pi}\int\exp\left(\frac{2i}{\hbar}pY\right)\rho(q-Y, q+Y)dY,$$

where f is the Wigner d.f. for one dimension.

With this theorem, it should be possible to carry large parts of classical statistical mechanics into quantum-mechanical language merely by changing the definition of the d.f. This will be illustrated in this paper by deriving the equations of hydrodynamics.

The starting point for a statistical mechanical theory of transport processes in quantum mechanics is the analog of the Liouville equation. The quantum-mechanical equation of motion has already been given in the density matrix formalism, and can be used to get the equation of motion for Wigner's d.f. Although this is described in detail by Wigner[5] we will outline the derivation here. We replace $\mathbf{R}$ by $\mathbf{R}-\mathbf{Y}$ and $\mathbf{R}'$ by $\mathbf{R}+\mathbf{Y}$ in Eq. (2.6), multiply through by $(1/\hbar\pi)^{3N}\exp(2i\mathbf{p}\cdot\mathbf{Y}/\hbar)$

and integrate over $\mathbf{Y}$: This gives

$$\frac{\partial f^{(N)}}{\partial t}=-\frac{i}{\hbar}\left(\frac{1}{\hbar\pi}\right)^{3N}\sum_{k=1}^{N}\frac{\hbar^2}{2m_k}\int\exp\left(\frac{2i\mathbf{p}\cdot\mathbf{Y}}{\hbar}\right)$$
$$\times[\nabla_{\mathbf{R}_k+\mathbf{Y}_k}{}^2\rho^{(N)}(\mathbf{R}-\mathbf{Y},\,\mathbf{R}+\mathbf{Y})$$
$$-\nabla_{\mathbf{R}_k-\mathbf{Y}_k}{}^2\rho^{(N)}(\mathbf{R}-\mathbf{Y},\,\mathbf{R}+\mathbf{Y})]d\mathbf{Y}$$
$$-\frac{i}{\hbar}\left(\frac{1}{\hbar\pi}\right)^{3N}\int\exp\left(\frac{2i\mathbf{p}\cdot\mathbf{Y}}{\hbar}\right)$$
$$\times[U(\mathbf{R}-\mathbf{Y})-U(\mathbf{R}+\mathbf{Y})]\rho^{(N)}(\mathbf{R}-\mathbf{Y},\,\mathbf{R}+\mathbf{Y})d\mathbf{Y}.$$

The kinetic energy contributions can be integrated by parts,

$$\sum_{k=1}^{N}\frac{\hbar^2}{2m_k}\frac{i}{\hbar}\left(\frac{1}{\hbar\pi}\right)^{3N}\int\exp\left(\frac{2i\mathbf{p}\cdot\mathbf{Y}}{\hbar}\right)$$
$$\times[\nabla_{\mathbf{R}_k+\mathbf{Y}_k}{}^2\rho^{(N)}(\mathbf{R}-\mathbf{Y},\,\mathbf{R}+\mathbf{Y};\,t)$$
$$-\nabla_{\mathbf{R}_k-\mathbf{Y}_k}{}^2\rho^{(N)}(\mathbf{R}-\mathbf{Y},\,\mathbf{R}+\mathbf{Y};\,t)]d\mathbf{Y}$$
$$=\sum_{k=1}^{N}\frac{\mathbf{p}_k}{m_k}\cdot\nabla_{\mathbf{R}_k}f^{(N)}(\mathbf{R},\,\mathbf{p};\,t),\quad(2.16)$$

which is identical in form with the classical result. The potential energy contribution is

$$\boldsymbol{\theta}\cdot f^{(N)}=\frac{i}{\hbar}\left(\frac{1}{\hbar\pi}\right)^{3N}\int[U(\mathbf{R}-\mathbf{Y})-U(\mathbf{R}+\mathbf{Y})]$$
$$\times\exp\left(\frac{2i}{\hbar}\mathbf{p}\cdot\mathbf{Y}\right)\rho^{(N)}(\mathbf{R}-\mathbf{Y},\,\mathbf{R}+\mathbf{Y})d\mathbf{Y},\quad(2.17)$$

and the equation of motion can be written

$$\frac{\partial f^{(N)}}{\partial t}+\sum_{k=1}^{N}\frac{\mathbf{p}_k}{m_k}\cdot\nabla_{\mathbf{R}_k}f^{(N)}+\boldsymbol{\theta}\cdot f^{(N)}=0.\quad(2.18)$$

The potential dependent term can be put into several different forms, involving integral or differential operators. If we define the kernel

$$K(\mathbf{R},\,\mathbf{p}-\mathbf{p}')=\frac{i}{\hbar}\left(\frac{1}{\hbar\pi}\right)^{3N}$$
$$\times\int_{-\infty}^{+\infty}[U(\mathbf{R}-\mathbf{x})-U(\mathbf{R}+\mathbf{x})]$$
$$\times\exp\left[\frac{2i}{\hbar}(\mathbf{p}-\mathbf{p}')\cdot\mathbf{x}\right]d\mathbf{x}\quad(2.19)$$

then this term is

$$\boldsymbol{\theta}\cdot f^{(N)}=\int_{-\infty}^{+\infty}K(\mathbf{R},\,\mathbf{p}-\mathbf{p}')f^{(N)}(\mathbf{R},\,\mathbf{p}')d\mathbf{p}'.\quad(2.20)$$

Another possible form is

$$\boldsymbol{\theta}\cdot f^{(N)}=\frac{i}{\hbar}\left(\frac{1}{\hbar\pi}\right)^{3N}$$
$$\times\int\int[f^{(N)}(\mathbf{R},\,\mathbf{p}-\mathbf{p}')-f^{(N)}(\mathbf{R},\,\mathbf{p}+\mathbf{p}')]$$
$$\times\exp\left[\frac{2i}{\hbar}(\mathbf{R}-\mathbf{x})\cdot\mathbf{p}'\right]U(\mathbf{x})d\mathbf{x}d\mathbf{p}'.\quad(2.21)$$

The corresponding differential operator forms are

$$\boldsymbol{\theta}\cdot f^{(N)}=\frac{i}{\hbar}\left[U\left(\mathbf{R}-\frac{\hbar}{2i}\nabla_{\mathbf{p}}\right)\right.$$
$$\left.-U\left(\mathbf{R}+\frac{\hbar}{2i}\nabla_{\mathbf{p}}\right)\right]f^{(N)}(\mathbf{R},\,\mathbf{p}),\quad(2.22)$$

$$\boldsymbol{\theta}\cdot f^{(N)}=\frac{i}{\hbar}\left[f^{(N)}\left(\mathbf{R},\,\mathbf{p}-\frac{\hbar}{2i}\nabla_{\mathbf{R}}\right)\right.$$
$$\left.-f^{(N)}\left(\mathbf{R},\,\mathbf{p}+\frac{\hbar}{2i}\nabla_{\mathbf{R}}\right)\right]U(\mathbf{R}),\quad(2.23)$$

and may be summarized in a convenient formal way:

$$\boldsymbol{\theta}\cdot f^{(N)}=-\frac{2}{\hbar}\sin\left[\frac{\hbar}{2}\nabla_{\mathbf{R}}\nabla_{\mathbf{p}}\right]U(\mathbf{R})f^{(N)}(\mathbf{R},\,\mathbf{p}),\quad(2.24)$$

where $\nabla_{\mathbf{R}}$ must operate on the potential only. The series expansion of this is the form that Wigner obtained originally. It shows that the quantum-mechanical equation of motion differs from the classical one only in second and higher powers of $\hbar$. For a system of harmonic oscillators the quantum-mechanical and classical equations are identical.

If the potential can be expressed as a sum of pair potentials and an external part,

$$U=\sum_{i=1}^{N}\phi_i(\mathbf{R}_i)+\tfrac{1}{2}\sum_{i\neq j}^{N}\sum^{N}V_{ij}(\mathbf{R}_i,\,\mathbf{R}_j)\quad(1.4)$$

then the operator forms can be written in the same way,

$$\boldsymbol{\theta}\cdot f^{(N)}=\sum_i\boldsymbol{\theta}_i{}^{(e)}\cdot f^{(N)}+\tfrac{1}{2}\sum_{i\neq j}\sum\boldsymbol{\theta}_{ij}\cdot f^{(N)},\quad(2.25)$$

where $\boldsymbol{\theta}_i{}^{(e)}$ is the operator corresponding to the i'th part of the external potential and $\boldsymbol{\theta}_{ij}$ is the operator corresponding to the pair potential, V_{ij}.

The reduced equations of motion are analogous to the classical ones, with the correspondence of $\boldsymbol{\theta}_i$ in quantum mechanics to $-(\nabla_{\mathbf{R}_i}U)\cdot\nabla_{\mathbf{p}_i}$ in the classical case. The equation of motion for the set of particles $\mathbf{n}$ is obtained by integrating the equation of motion for the entire set $\mathbf{N}$ over the coordinates and momenta of the set $\mathbf{N}-\mathbf{n}$. We restrict the discussion to the distributions

for which the surface integrals of the currents vanish on the boundary of the phase space accessible to the system, so that Green's theorem may be used:

$$f^{(n)}(\mathbf{r},\mathbf{p})=\int\int f^{(N)}(\mathbf{r},\mathbf{p};\mathbf{R},\mathbf{P})d\mathbf{R}d\mathbf{P} \tag{2.26}$$

$$\frac{\partial f^{(n)}}{\partial t}+\sum_{i=1}^{n}\frac{\mathbf{p}_i}{m_i}\cdot\nabla_{\mathbf{r}_i}f^{(n)}+\sum_{i=1}^{n}\boldsymbol{\theta}_i^{(e)}\cdot f^{(n)}=-X^{(n)}$$

$$X^{(n)}=\int\int\left\{\sum_{i=n+1}^{N}\boldsymbol{\theta}_i^{(e)}\cdot f^{(N)}+\tfrac{1}{2}\sum_{i\neq j}^{N}\sum^{N}\boldsymbol{\theta}_{ij}\cdot f^{(N)}\right\}d\mathbf{R}d\mathbf{P},$$

where $\mathbf{r}$, $\mathbf{p}$ refer to the set $\mathbf{n}$ and $\mathbf{R}$, $\mathbf{P}$ refer to the set $\mathbf{N}-\mathbf{n}$. The first part of the integral vanishes by integration over $\mathbf{P}$. The second part can be split up into three groups of terms, one containing terms referring to pair interactions for which both particles are in the set $\mathbf{n}$, another in which one particle is in set $\mathbf{n}$ and the other is in set $\mathbf{N}-\mathbf{n}$, and the third in which both particles are in set $\mathbf{N}-\mathbf{n}$:

$$X^{(n)}=\tfrac{1}{2}\sum_{\substack{i=1\\ i\neq j}}^{n}\sum_{j=1}^{n}\int\int\boldsymbol{\theta}_{ij}\cdot f^{(N)}d\mathbf{R}d\mathbf{P}$$

$$+\sum_{i=1}^{n}\sum_{j=n+1}^{N}\int\int\boldsymbol{\theta}_{ij}\cdot f^{(N)}d\mathbf{R}d\mathbf{P}$$

$$+\tfrac{1}{2}\sum_{\substack{i=n+1\\ i\neq j}}^{N}\sum_{j=n+1}^{N}\int\int\boldsymbol{\theta}_{ij}\cdot f^{(N)}d\mathbf{R}d\mathbf{P}.$$

The third group of terms vanish by integration over $\mathbf{P}$, the first group integrates obviously, and the second group leads to integrals involving $f^{(n+1)}$:

$$X^{(n)}=\tfrac{1}{2}\sum_{\substack{i=1\\ i\neq j}}^{n}\sum_{j=1}^{n}\boldsymbol{\theta}_{ij}\cdot f^{(n)}+\sum_{i=1}^{n}\sum_{j=n+1}^{N}X_{ij}{}^{(n)}, \tag{2.27}$$

$$X_{ij}{}^{(n)}=\int\int\boldsymbol{\theta}_{ij}\cdot f^{(n+1)}(\mathbf{r},\mathbf{p};\mathbf{R}_j,\mathbf{P}_j)d\mathbf{R}_jd\mathbf{P}_j.$$

Equations (2.26) and (2.27) contain the reduced Liouville equation in quantum-statistical mechanics. The specialization to the equation for the singlet d.f. is given here as an illustration:

$$\frac{\partial f^{(1)}}{\partial t}+\frac{\mathbf{p}_1}{m_1}\cdot\nabla_{\mathbf{R}_1}f^{(1)}+\boldsymbol{\theta}_1^{(e)}\cdot f^{(1)}$$

$$=-\sum_{j=2}^{N}\int\int\boldsymbol{\theta}_{1j}\cdot f^{(2)}(\mathbf{R}_1,\mathbf{R}_j,p_1,p_j;t)d\mathbf{R}_jd\mathbf{p}_j. \tag{2.28}$$

III. THE EQUATIONS OF HYDRODYNAMICS

In this section, we will show how the equations of hydrodynamics can be derived in quantum-statistical mechanics. In particular, we will show that the derivations and results are formally identical with those obtained by Irving and Kirkwood.[8] Their derivations have been given in great detail, and there is no need to duplicate them here. The goal of the following discussion is a statement of the equations of hydrodynamics in a form which involves all N particles in the system. The remainder of the derivation consists in reducing these equations to a form which involves singlet and pair d.f.'s, and may be found in the paper of Irving and Kirkwood. The notation used here will be the same as their's.

The equations of hydrodynamics are obtained by calculating the time derivatives at a point of the fluid of the mass density, the momentum density, and the energy density. For this purpose, the following results are useful. If $\alpha(\mathbf{R},\mathbf{p})$ is a dynamical variable, the average of α is

$$\langle\alpha\rangle_{\text{Av}}\equiv\langle\alpha(\mathbf{R},\mathbf{p});f^{(N)}(\mathbf{R},\mathbf{p};t)\rangle$$

$$=\int\int\alpha(\mathbf{R},\mathbf{p})f^{(N)}(\mathbf{R},\mathbf{p};t)d\mathbf{R}d\mathbf{p} \tag{3.1}$$

and if α is not an explicit function of the time,

$$\frac{\partial\langle\alpha\rangle_{\text{Av}}}{\partial t}=\left\langle\alpha(\mathbf{R},\mathbf{p});\frac{\partial f^{(N)}(\mathbf{R},\mathbf{p};t)}{\partial t}\right\rangle. \tag{3.2}$$

When we use the analog of Liouville's theorem in this expression, we get

$$\frac{\partial\langle\alpha\rangle_{\text{Av}}}{\partial t}=-\left\langle\alpha;\sum_{k=1}^{N}\frac{\mathbf{p}_k}{m_k}\cdot\nabla_{\mathbf{R}_k}f^{(N)}\right\rangle-\langle\alpha;\boldsymbol{\theta}\cdot f^{(N)}\rangle. \tag{3.3}$$

The first term is identical with the classical one, and can be transformed with Green's theorem to

$$\left\langle\alpha;-\sum_{k=1}^{N}\frac{\mathbf{p}_k}{m_k}\cdot\nabla_{\mathbf{R}_k}f^{(N)}\right\rangle=\left\langle\sum_{k=1}^{N}\frac{\mathbf{p}_k}{m_k}\cdot\nabla_{\mathbf{R}_k}\alpha;f^{(N)}\right\rangle. \tag{3.4}$$

The other term is (using Eq. (2.21))

$$\langle\alpha;\boldsymbol{\theta}\cdot f^{(N)}\rangle=\frac{i}{\hbar}\left(\frac{1}{\hbar\pi}\right)^{3N}$$

$$\times\int\int\alpha(\mathbf{R},\mathbf{p})\{f^{(N)}(\mathbf{R},\mathbf{p}-\mathbf{p}')-f^{(N)}(\mathbf{R},\mathbf{p}+\mathbf{p}')\}$$

$$\times\exp\left[\frac{2i}{\hbar}(\mathbf{R}-\mathbf{R}')\cdot\mathbf{p}'\right]U(\mathbf{R}')d\mathbf{R}'d\mathbf{p}'d\mathbf{R}d\mathbf{p},$$

and when $\mathbf{p}-\mathbf{p}'$ is replaced by $\mathbf{p}$ in the first term of the integral, and $\mathbf{p}+\mathbf{p}'$ is replaced by $\mathbf{p}$ in the second term (the limits remaining from minus infinity to plus in-

[8] J. H. Irving and J. G. Kirkwood, J. Chem. Phys. **18**, 817 (1950).

finity), we get

$$\langle \alpha; \theta \cdot f^{(N)} \rangle = \langle A; f^{(N)} \rangle \tag{3.5}$$

$$A = \frac{i}{\hbar}\left(\frac{1}{h\pi}\right)^{3N} \int\int \{\alpha(\mathbf{R}, \mathbf{p}+\mathbf{p}') - \alpha(\mathbf{R}, \mathbf{p}-\mathbf{p}')\} \times \exp\left[\frac{2i}{\hbar}(\mathbf{R}-\mathbf{R}')\cdot\mathbf{p}'\right] U(\mathbf{R}')\, d\mathbf{R}'\, d\mathbf{p}'.$$

This can also be put into operator form,

$$A = \frac{i}{\hbar}\left\{\alpha\left(\mathbf{R}, \mathbf{p}+\frac{\hbar}{2i}\nabla_{\mathbf{R}}\right) - \alpha\left(\mathbf{R}, \mathbf{p}-\frac{\hbar}{2i}\nabla_{\mathbf{R}}\right)\right\} U(\mathbf{R}). \tag{3.6}$$

If we expand this as a series in $\hbar$ and take the limit as $\hbar$ approaches zero, the classical result is obtained. A more useful result is this: if α is of the form,

$$\alpha = \alpha_1(\mathbf{R}) + \sum_{k=1}^{N} \alpha_{2k}(\mathbf{R})\mathbf{p}_k + \sum_{j=1}^{N}\sum_{k=1}^{N} \alpha_{3jk}(\mathbf{R})\mathbf{p}_j\cdot\mathbf{p}_k, \tag{3.7}$$

this leads by a simple substitution to the equation for the rate of change of the average value of this special α:

$$\begin{aligned}\frac{\partial\langle\alpha\rangle_{N}}{\partial t} &= \sum_{1=k}^{N}\left\langle \frac{\mathbf{p}_k}{m_k}\cdot\nabla_{\mathbf{R}_k}\alpha_1; f^{(N)}\right\rangle \\ &+ \sum_{j=1}^{N}\sum_{k=1}^{N}\left\langle \frac{\mathbf{p}_j\mathbf{p}_k}{m_k}\cdot\nabla_{\mathbf{R}_k}\alpha_{2j}; f^{(N)}\right\rangle \\ &+ \sum_{k=1}^{N}\langle \alpha_{2k}(\nabla_{\mathbf{R}_k}U); f^{(N)}\rangle \qquad (3.7') \\ &+ \sum_{i}\sum_{j}\sum_{k}\left\langle \mathbf{p}_i\cdot\mathbf{p}_j\frac{\mathbf{p}_k}{m_k}\cdot\nabla_{\mathbf{R}_k}\alpha_{3ij}; f^{(N)}\right\rangle \\ &+ \sum_{j}\sum_{k}\langle \alpha_{3jk}(\mathbf{p}_j\cdot\nabla_{\mathbf{R}_k}U + \mathbf{p}_k\cdot\nabla_{\mathbf{R}_j}U); f^{(N)}\rangle,\end{aligned}$$

which differs from the corresponding classical equation only in the definition of the d.f. It can also be shown that higher terms in the expansion of α in powers of $\mathbf{p}$ will lead to expressions differing in form from the classical ones.

As a special case of this theorem, take the following values of α

$$\begin{aligned}\alpha_d &= \sum_{k=1}^{N} m_k\delta(\mathbf{R}_k-\mathbf{r}) \\ \boldsymbol{\alpha}_m &= \sum_{k=1}^{N}\mathbf{p}_k\delta(\mathbf{R}_k-\mathbf{r}) \qquad (3.8) \\ \alpha_E &= \sum_{k=1}^{N}\left\{\frac{p_k^2}{2m_k} + \phi_k(\mathbf{R}_k) + \tfrac{1}{2}\sum_{\substack{i=1\\ \neq k}}^{N} V_{ik}(\mathbf{R}_i, \mathbf{R}_k)\right\}\delta(\mathbf{R}_k-\mathbf{r}).\end{aligned}$$

These quantities define the mass density, the momentum density, and the energy density:

$$\rho(\mathbf{r}; t) = \langle \alpha_d; f^{(N)}\rangle \tag{3.9}$$

$$\rho(\mathbf{r}; t)\mathbf{u}(\mathbf{r}; t) = \langle \boldsymbol{\alpha}_m; f^{(N)}\rangle \tag{3.10}$$

$$E(\mathbf{r}; t) = \langle \alpha_E; f^{(N)}\rangle \tag{3.11}$$

and lead to the equations of continuity, momentum transport, and energy transport, respectively:

$$\frac{\partial\rho(\mathbf{r}; t)}{\partial t} = -\nabla_{\mathbf{r}}\cdot[\rho(\mathbf{r}; t)\mathbf{u}(\mathbf{r}; t)] \tag{3.12}$$

$$\begin{aligned}\frac{\partial[\rho(\mathbf{r}; t)\mathbf{u}(\mathbf{r}; t)]}{\partial t} &= -\nabla_{\mathbf{r}}\cdot\sum_{k=1}^{N}\left\langle \frac{\mathbf{p}_k\mathbf{p}_k}{m_k}\delta(\mathbf{R}_k-\mathbf{r}); f^{(N)}\right\rangle \\ &- \sum_{j\neq k}^{N}\sum^{N}\langle(\nabla_{\mathbf{R}_k}V_{jk})\delta(\mathbf{R}_k-\mathbf{r}); f^{(N)}\rangle \\ &- \sum_{k=1}^{N}[\nabla_{\mathbf{r}}\phi_k(\mathbf{r})]\langle\delta(\mathbf{R}_k-\mathbf{r}); f^{(N)}\rangle \qquad (3.13)\end{aligned}$$

$$\begin{aligned}\frac{\partial E(\mathbf{r}; t)}{\partial t} &= -\nabla_{\mathbf{r}}\cdot\left[\sum_{k=1}^{N}\left\langle\frac{p_k^2}{2m_k}\frac{\mathbf{p}_k}{m_k}\delta(\mathbf{R}_k-\mathbf{r}); f^{(N)}\right\rangle\right. \\ &+ \sum_{k=1}^{N}\phi_k(\mathbf{r})\left\langle\frac{\mathbf{p}_k}{m_k}\delta(\mathbf{R}_k-\mathbf{r}); f^{(N)}\right\rangle \\ &\left.+ \tfrac{1}{2}\sum_{j\neq k}^{N}\sum^{N}\left\langle V_{jk}\frac{\mathbf{p}_k}{m_k}\delta(\mathbf{R}_k-\mathbf{r}); f^{(N)}\right\rangle\right] \\ &+ \tfrac{1}{2}\sum_{j\neq k}^{N}\sum^{N}\left\langle(\nabla_{\mathbf{R}_k}V_{jk})\cdot\frac{\mathbf{p}_k}{m_k}\right. \\ &\left.\times[\delta(\mathbf{R}_j-\mathbf{r}) - \delta(\mathbf{R}_k-\mathbf{r})]; f^{(N)}\right\rangle. \qquad (3.14)\end{aligned}$$

These results have the same form as the classical ones, as obtained by Irving and Kirkwood, although the d.f. is of course determined by the laws of quantum mechanics. The remainder of their derivation consists in transforming these equations into the form in which the stress tensor and heat current density are given in terms of singlet and pair d.f.'s and the potential of intermolecular force. Since these transformations are identical with those of the classical case, they will not be repeated here. We will now state the results of these calculations. The microscopically correct hydrodynamical equations are the continuity equation:

$$\frac{\partial}{\partial t}\rho(\mathbf{r}; t) = -\nabla_{\mathbf{r}}\cdot[\rho(\mathbf{r}; t)\mathbf{u}(\mathbf{r}; t)] \tag{3.12}$$

the equation of motion (momentum transport equa-

tion):

$$\frac{\partial}{\partial t}[\rho\mathbf{u}]+\nabla_{\mathbf{r}}\cdot[\rho\mathbf{u}\mathbf{u}]=\mathbf{X}+\nabla_{\mathbf{r}}\cdot\boldsymbol{\sigma} \tag{3.13'}$$

and the energy transport equation,

$$\frac{\partial E}{\partial t}+\nabla_{\mathbf{r}}\cdot[E\mathbf{u}+\mathbf{q}-\mathbf{u}\cdot\boldsymbol{\sigma}]=0. \tag{3.14'}$$

The quantities appearing in the above equations are defined as follows:‖

$$\rho(\mathbf{r};t)=\sum_{k=1}^{N}\langle m_k\delta(\mathbf{R}_k-\mathbf{r});f^{(N)}\rangle \tag{3.9}$$

=mass density at $\mathbf{r}$.

$$\mathbf{u}(\mathbf{r};t)=\frac{1}{\rho(\mathbf{r};t)}\sum_{k=1}^{N}\langle\mathbf{p}_k\delta(\mathbf{R}_k-\mathbf{r});f^{(N)}\rangle \tag{3.10}$$

=mean molecular velocity (fluid velocity) at $\mathbf{r}$.

$$\mathbf{X}(\mathbf{r};t)=-\sum_{k=1}^{N}[\nabla_{\mathbf{r}}\phi_k(\mathbf{r})]\langle\delta(\mathbf{R}_k-\mathbf{r});f^{(N)}\rangle \tag{3.15}$$

=body force per unit volume due to external fields at $\mathbf{r}$.

$$E(\mathbf{r};t)=E_K+E_\phi+E_V \tag{3.16}$$

=internal energy density at $\mathbf{r}$, where

$$E_K(\mathbf{r};t)=\sum_{k=1}^{N}\left\langle\frac{p_k^2}{2m_k}\delta(\mathbf{R}_k-\mathbf{r});f^{(N)}\right\rangle \tag{3.17}$$

=kinetic energy density,

$$E_\phi(\mathbf{r};t)=\sum_{k=1}^{N}\phi_k(\mathbf{r})\langle\delta(\mathbf{R}_k-\mathbf{r});f^{(N)}\rangle \tag{3.18}$$

=potential energy density associated with external fields, and

$$E_V(\mathbf{r};t)=\tfrac{1}{2}\sum\sum_{j\neq k}\langle V_{jk}\delta(\mathbf{R}_k-\mathbf{r});f^{(N)}\rangle \tag{3.19}$$

=potential energy density caused by molecular interaction. (In defining E_V it is assumed that the potential energy of interaction between two molecules is localized half at each molecule.)

These definitions are completely general. The other quantities, however, appearing in the above hydrodynamical equations, $\boldsymbol{\sigma}$ and $\mathbf{q}$, have been defined only for a single component, single phase system in which the intermolecular force is central, depending on range only. Their definitions follow.

$$\boldsymbol{\sigma}(\mathbf{r};t)=\boldsymbol{\sigma}_K+\boldsymbol{\sigma}_V \tag{3.20}$$

=stress tensor at $\mathbf{r}$, where

$$\boldsymbol{\sigma}_K=-\sum_{k=1}^{N}m\left\langle\left(\frac{\mathbf{p}_k}{m}-\mathbf{u}\right)\left(\frac{\mathbf{p}_k}{m}-\mathbf{u}\right)\delta(\mathbf{R}_k-\mathbf{r});f^{(N)}\right\rangle \tag{3.21}$$

=kinetic contribution to stress tensor.

$$\boldsymbol{\sigma}_V(\mathbf{r};t)=\frac{1}{2}\int\frac{\mathbf{R}\mathbf{R}}{R}V'(R)\left\{1-\tfrac{1}{2}\mathbf{R}\cdot\nabla_{\mathbf{r}}+\cdots+\frac{1}{n!}(-\mathbf{R}\cdot\nabla_{\mathbf{r}})^{n-1}+\cdots\right\}\rho^{(2)}(\mathbf{r},\mathbf{r}+\mathbf{R};t)d\mathbf{R} \tag{3.22}$$

=intermolecular force contribution to stress tensor.

$$\mathbf{q}(\mathbf{r};t)=\mathbf{q}_K+\mathbf{q}_V \tag{3.23}$$

=heat current density at $\mathbf{r}$, where

$$\mathbf{q}_K(\mathbf{r};t)=\sum_{k=1}^{N}\left\langle\frac{m}{2}\left|\frac{\mathbf{p}_k}{m}-\mathbf{u}\right|^2\times\left(\frac{\mathbf{p}_k}{m}-\mathbf{u}\right)\delta(\mathbf{R}_k-\mathbf{r});f^{(N)}\right\rangle \tag{3.24}$$

=heat current due to transport of thermal kinetic energy, and

$$\mathbf{q}_V(\mathbf{r};t)=-\tfrac{1}{2}\mathbf{u}(\mathbf{r};t)\cdot\int\left[V(R)\mathbf{1}-\frac{\mathbf{R}\mathbf{R}}{R}V'(R)\times\{1-\tfrac{1}{2}\mathbf{R}\cdot\nabla_{\mathbf{r}}+\cdots\}\right]\times\rho^{(2)}(\mathbf{r},\mathbf{r}+\mathbf{R};t)d\mathbf{R}+\frac{1}{2}\int\left[V(R)\mathbf{1}-\frac{\mathbf{R}\mathbf{R}}{R}V'(R)\times\{1-\tfrac{1}{2}\mathbf{R}\cdot\nabla_{\mathbf{r}}+\cdots\}\right]\cdot\mathbf{j}_1^{(2)}(\mathbf{r},\mathbf{r}+\mathbf{R};t)d\mathbf{R} \tag{3.25}$$

=contribution to heat current density by molecular interaction.

In the definitions of $\boldsymbol{\sigma}_V$ and $\mathbf{q}_V$ the following quantities appear,

$$\rho^{(2)}(\mathbf{r},\mathbf{r}';t)=\sum\sum_{j\neq k}\langle\delta(\mathbf{R}_j-\mathbf{r})\delta(\mathbf{R}_k-\mathbf{r}');f^{(N)}\rangle \tag{3.26}$$

=pair density at $\mathbf{r}$ and $\mathbf{r}'$, the probability per (unit volume)^2 that one particle (any particle) will be at $\mathbf{r}$ and another at $\mathbf{r}'$.

$$\mathbf{j}_1^{(2)}(\mathbf{r},\mathbf{r}';t)=\sum\sum_{j\neq k}\left\langle\frac{\mathbf{p}_k}{m_k}\delta(\mathbf{R}_k-\mathbf{r})\delta(\mathbf{R}_j-\mathbf{r}');f^{(N)}\right\rangle \tag{3.27}$$

‖ The bracket notation $\langle;f\rangle$ means the expectation value of the quantity appearing to the left of the semicolon over an ensemble having a probability distribution function, $f(\mathbf{R}_1,\cdots,\mathbf{R}_N;\mathbf{p}_1,\cdots\mathbf{p}_N;t)$.

$=$projection onto the space of $\mathbf{r}$ of the particle current density at $\mathbf{r}$, $\mathbf{r}'$ in pair space, $=$particle current density at $\mathbf{r}$ if another particle is at $\mathbf{r}'$ multiplied by the particle density at $\mathbf{r}'$.

The differential operator, $\nabla_{\mathbf{r}}$, occurring in the definitions of $\boldsymbol{\sigma}_V$ and $\mathbf{q}_V$ operate on $\rho^{(2)}(\mathbf{r}, \mathbf{r}+\mathbf{R}; t)$ and $\mathbf{j}_1^{(2)}(\mathbf{r}, \mathbf{r}+\mathbf{R}; t)$ with $\mathbf{R}$ held fixed. Since in the interior of a fluid $\rho^{(2)}$ and $\mathbf{j}_1^{(2)}$ are slow functions of $\mathbf{r}$ (holding $\mathbf{R}$ fixed), changing negligibly for $\mathbf{r}$ varying by a displacement whose length is of the order of the "range" of intermolecular forces, all terms beyond the first may be neglected in the brace appearing in the definitions of $\boldsymbol{\sigma}_V$ and $\mathbf{q}_V$. This yields the simplified expressions:

$$\boldsymbol{\sigma}_V(\mathbf{r}; t)=\frac{1}{2m^2}[\rho(\mathbf{r}; t)]^2 \times \int \frac{\mathbf{RR}}{R} V'(R) g^{(2)}(\mathbf{r}, \mathbf{R}; t) d\mathbf{R} \quad (3.28)$$

$$\mathbf{q}_V(\mathbf{r}; t)=\frac{1}{2}\int\left[V(R)\mathbf{1}-\frac{\mathbf{RR}}{R}V'(R)\right] \cdot[\mathbf{j}_1^{(2)}(\mathbf{r}, \mathbf{r}+\mathbf{R}; t)-\mathbf{u}(\mathbf{r}; t)\rho^{(2)}(\mathbf{r}, \mathbf{R}+\mathbf{r}; t)]d\mathbf{R} \quad (3.29)$$

where the correlation function $g^{(2)}$ is defined by

$$\rho^{(2)}(\mathbf{r}, \mathbf{r}+\mathbf{R}; t) = (1/m^2)\rho(\mathbf{r}; t)\rho(\mathbf{r}+\mathbf{R}; t)g^{(2)}(\mathbf{r}, \mathbf{R}; t). \quad (3.30)$$

The pressure is defined by

$$P(\mathbf{r}; t)=-\tfrac{1}{3}\ \text{Trace}\ \boldsymbol{\sigma}(\mathbf{r}; t). \quad (3.31)$$

In an ensemble which is in equilibrium, the pressure is

$$P=\tfrac{2}{3}\sum_{k=1}^{N}\left\langle\frac{p_k^2}{2m}\delta(\mathbf{R}_k-\mathbf{r}); f^{(N)}\right\rangle -\frac{2\pi}{3}\left(\frac{\rho}{m}\right)^2\int_0^\infty R^3V'(R)g^{(2)}(R)dR. \quad (3.32)$$

(In deriving the stress tensor, it is assumed that $\mathbf{R}\cdot\nabla_{\mathbf{R}}\rho^{(2)}$ is negligible. In the absence of external forces, and with the neglect of surface effects, this assumption is justified.) We cannot replace the average kinetic energy by $3kT/2$, because this is now a quantum-mechanical system. Thus, the temperature enters into the equation in an implicit way. This is the quantum-mechanical equation of state that has been obtained by Born and Green[4] using the virial theorem and by DeBoer[1] using statistical thermodynamics. There is some ambiguity in the derivation presented here, for the following reason: the stress tensor obtained by this method is undetermined up to an arbitrary tensor of vanishing divergence. This arbitrary tensor may not necessarily have a vanishing trace, and may therefore contribute to the pressure. In the classical case, Irving and Kirkwood showed that the definition used here in terms of the d.f. is consistent with the physical picture involving the force "acting across" a unit area. This definition may be used in the quantum-mechanical case, but is still arbitrary.

CONCLUSIONS

The equations of hydrodynamics have been derived from quantum-statistical mechanics, and contain microscopically correct expressions for the stress tensor and heat current density of a quantum fluid. These expressions are identical with the classical ones, except in the specification of the d.f., which must be obtained using some quantum-mechanical theory. Born and Green have obtained similar expressions in the density matrix formalism. Their efforts to apply these expressions to the problem of liquid helium II have not been entirely successful. What is needed is a logical procedure for terminating the chain of reduced equations of motion, so that $f^{(2)}$ can be evaluated with fair accuracy. This may take the form of a quantum-mechanical analog of the theory of Brownian motion developed by Kirkwood, or some other way of introducing the irreversibility of hydrodynamic effects. When such a theory is available, it should be possible to construct a rigorous molecular theory of quantum superfluids.

ACKNOWLEDGMENT

The authors are grateful to Professor J. G. Kirkwood and to Professor E. Wigner for suggesting various aspects of the problem and for many helpful discussions.

Note added in proof: E. Moyal [Proc. Cambridge Phil. Soc. 45, 99 (1949)] has made a similar discussion of some of the properties of the Wigner d.f., and H. S. Green [J. Chem. Phys. 19, 955 (1951)] has shown how an approximate Wigner d.f. may be obtained using quantum corrections to the classical d.f.

Paramagnetic Resonance Absorption of Microwaves*

FORREST W. LANCASTER† AND WALTER GORDY
Department of Physics, Duke University, Durham, North Carolina
(Received April 3, 1951)

Paramagnetic resonance absorption in approximately a hundred salts in the powder form, containing atoms of the iron and rare earth groups and organic as well as inorganic radicals, has been investigated. The frequencies employed range from 9000 to 50,000 Mc/sec. Exchange interaction which affects markedly the line widths and shape was found to be of wide occurrence even in ions separated by large organic radicals. The results indicate that paramagnetic resonance is a promising new method of investigating the orbital properties of these organic radicals. Evidence has been found in copper acetate for the simultaneous transition of electrons in neighboring ions with the absorption of a single quantum.

PARAMAGNETIC absorption in the microwave region was first observed by Zavoisky,[1] and it has subsequently been observed by Cummerow and Halliday[2] and by others.[3] It has been treated theoretically by Gorter and Van Vleck[4] and by others.[5] In these experiments the paramagnetic substance is placed in a magnetic field. The resulting Larmor precession of the electron spin gives rise to absorption of radiation. The resonant frequencies are given by the simple formula,

$$\nu = g\beta H/h, \tag{1}$$

where g is the gyromagnetic ratio, β is the Bohr magneton, h is Planck's constant, and H represents the magnetic field strength. For a free electron spin the g factor would be 2. The values usually obtained are close to, but not exactly, 2. The deviation from 2 arises from the spin orbit coupling in the ion. In a crystalline solid the "quenching" of the orbital momentum by the internal electrical field may cause a splitting of the lines which depends upon the orientation of the crystal in the external field. The latter effect, first observed by Bagguley and Griffiths,[3] provides a new method for studying crystal structures.

The widths and shapes of the absorption lines offer a means of studying the magnetic coupling and exchange interaction within the substance. It appears that exchange interaction,[4] particularly that involving organic radicals, is of considerable significance.

Paramagnetic resonance may also be used to investigate nuclear moments and nuclear couplings in paramagnetic substances. Nuclear hyperfine structure in paramagnetic substances, detected first by Penrose in copper sulfate,[6] has now been observed in cobalt[7] and manganese[8] salts.

The present work represents a preliminary survey of the paramagnetic resonance absorption of millimeter waves by a number of salts in the powder form. Some salts were included which have been studied recently by others in the longer wave region. The survey published

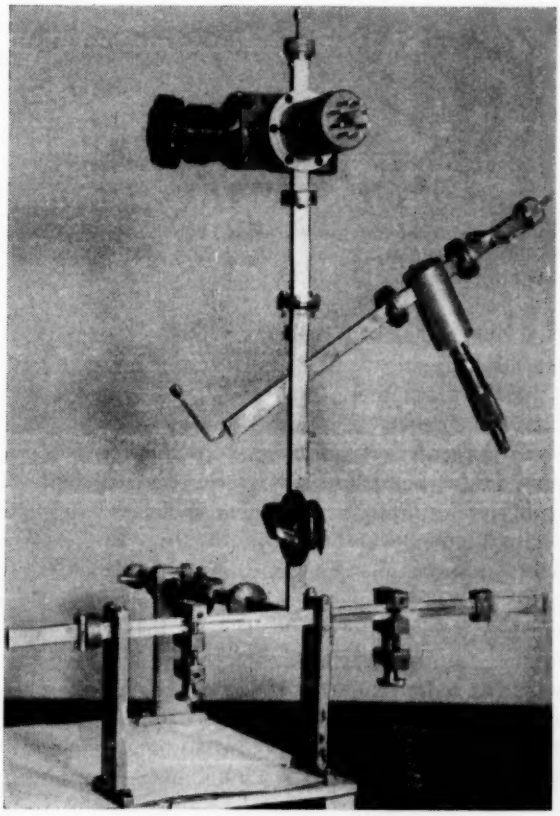

FIG. 1. Magic tee bridge used in detection of paramagnetic resonance.

* The research reported in this document has been made possible through support and sponsorship extended by the Geophysical Research Directorate of the Air Force Cambridge Research Laboratories under Contract No. W19-122-ac-35. It was submitted by Forrest W. Lancaster in partial fulfillment for the requirements of the Ph.D. degree.

† Present address: Department of Physics, North Carolina State College, Raleigh, North Carolina.

[1] E. Zavoisky, J. Phys. (U.S.S.R.) **9**, 211, 245, 447 (1945); **10**, 170, 197 (1946).

[2] R. L. Cummerow and D. Halliday, Phys. Rev. **70**, 443 (1946).

[3] D. M. S. Bagguley and J. H. E. Griffiths, Nature **160**, 532 (1947); Weiss, Whitmer, Torrey, and Hsiang, Phys. Rev. **72**, 975 (1947); Whitmer, Weidner, and Weiss, Phys. Rev. **73**, 470 (1948); D. Halliday and J. Wheatley, Phys. Rev. **74**, 1210(A) (1948).

[4] J. C. Gorter and J. H. Van Vleck, Phys. Rev. **72**, 1128 (1947); J. H. Van Vleck, Phys. Rev. **74**, 1168 (1948).

[5] C. Kittel and J. M. Luttinger, Phys. Rev. **73**, 162 (1948); P. R. Weiss, Phys. Rev. **73**, 470 (1948).

[6] R. B. Penrose, Nature **163**, 992 (1949).

[7] Bleaney, Ingram, and Pryce, Nature **164**, 116 (1949).

[8] T. S. England and E. S. Schneider, Nature **166**, 437 (1950).

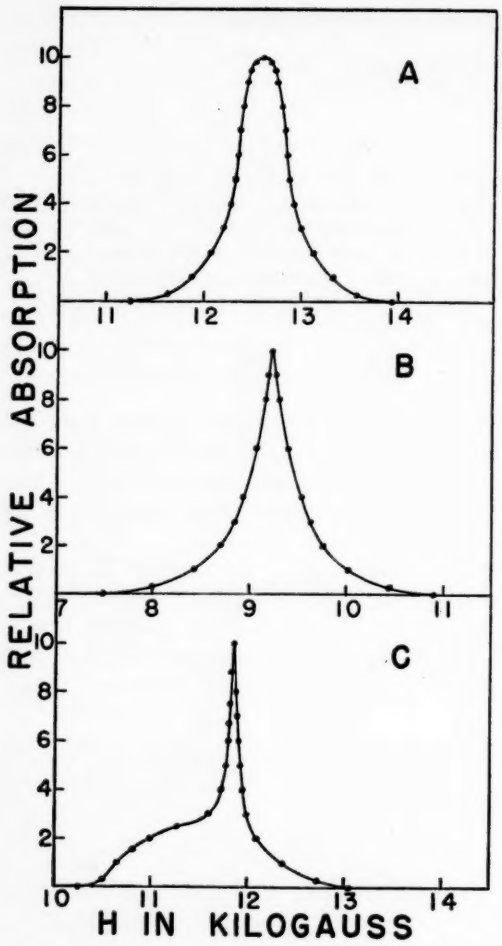

FIG. 2. Paramagnetic resonance of (A) copper acetyl acetonate at 35390 Mc/sec; (B) copper formate at 28400 Mc/sec; and (C) copper oxalate at 34040 Mc/sec.

earlier by the Oxford group[9] included several of the same salts. In most cases, however, the latter paper simply stated whether absorption was detected and did not list the observed g factors or line widths. The greater part of the previous work has been done in the 3-cm region. Since the absorption increases with frequency, we found it desirable to make most of our measurements in the millimeter wave region.

More information can be obtained from individual crystals than from powders. Also, it is frequently of advantage to make the observations at low temperature. Nevertheless, we have chosen to make our studies on powders at room temperature in order to survey a large number of compounds in a reasonable time. Such a survey makes possible a more advantageous choice of subjects for detailed study. Although in the powder form the crystalline axes are oriented at random, it is still possible in some instances to resolve lines caused by Stark splitting by the crystalline field. The analysis, however, is somewhat more complex than it is for individual crystals. The anisotropy in the g factor caused by the crystalline splitting of the orbital levels broadens the line of a powder where the crystalline axes are oriented in all directions. Nevertheless, as is demonstrated in the present work, it is possible to obtain much information about exchange interaction with the powder method.

[9] Bagguley, Bleaney, Griffiths, Penrose, and Plumpton, Proc. Phys. Soc. (London) 111, 542 (1948).

EXPERIMENTAL METHOD

Figure 1 shows the microwave bridge used in the measurements. It consists of a "magic tee" with two balanced arms containing line squeezers for adjusting the phase of the radiation, terminated with two equivalent cells which are of the order of a half-centimeter in length. So far, the bridge has been used to study salts in a powder form only. As nearly as possible, an equal amount of salt is placed in each cell so that the losses in each arm are approximately equivalent. The phases are then adjusted with the line squeezers so that a minimum amount of energy is reflected into the fourth arm, which contains the crystal detector. One of the cells is then placed in the magnetic field. The occurrence of a paramagnetic absorption produces an unbalance which is detected by the crystal. This unbalance is due to two effects: (1) the actual energy absorbed in the medium and (2) the changing of wavelength in the medium, caused by the anomalous dispersion in the region of the absorption line. With this bridge each of these effects

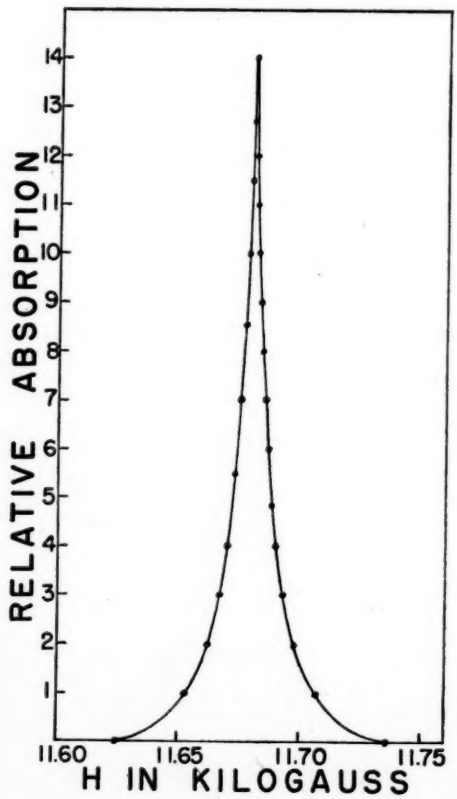

FIG. 3. Paramagnetic resonance of diphenyl trinitrophenyl hydrazyl at 32710 Mc/sec.

can be observed separately by adjustment of the phase for minimum indicator reading at each setting of the magnetic field. The remaining unbalance is then due to energy loss only, and the amount of phase adjustment needed gives a measure of the change in wavelength in the medium. The results given here represent the combined absorption and dispersion effects. The bridge was balanced with no magnetic field on the sample.

To reduce dielectric losses and to obtain a better impedance match the samples of weak absorbers were placed in a polystyrene cell made in the form of a wedge so that the sample was concentrated near the cell walls where the magnetic field component of the radiation is strongest and the electric component weakest. Because the attenuation of wave guide is a function of its width, the line squeezers make possible, in addition to phase adjustments, the compensation of small differences in dielectric losses in the two arms, since for any given setting of one of the squeezers the other one can be used to balance the phase. This makes unnecessary the use of attenuators or the exact matching of the two cells in order to obtain a good balance.

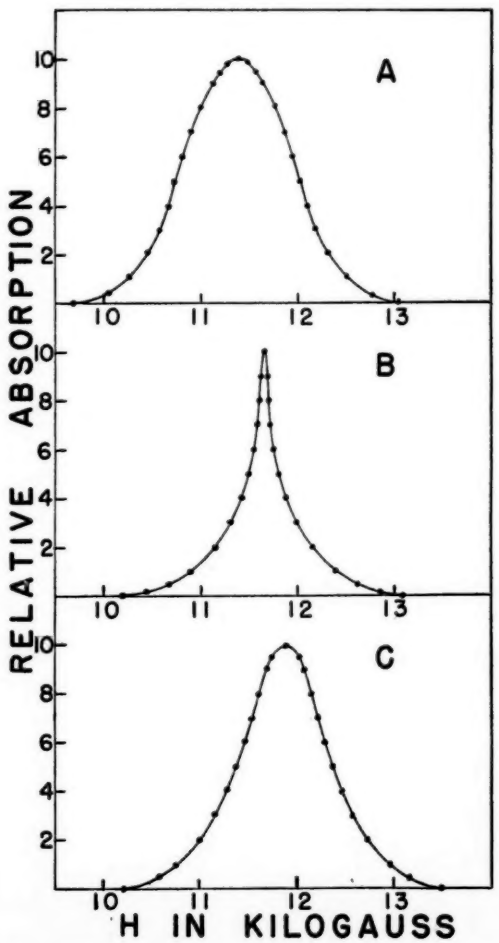

FIG. 4. Paramagnetic resonance of (A) copper bromide at 35290 Mc/sec; (B) copper chloride at $f=35440$ Mc/sec; and (C) copper fluoride at 35680 Mc/sec.

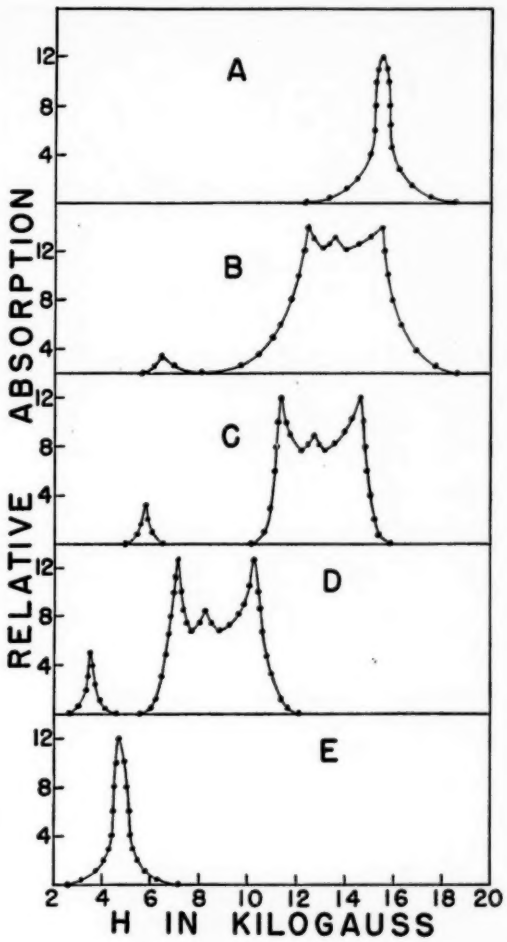

FIG. 5. Paramagnetic resonance of copper acetate at different frequencies. (A) 50,160 Mc/sec; (B) 39,030 Mc/sec; (C) 29,845 Mc/sec; (D) 23,890 Mc/sec; (E) 9785 Mc/sec.

Because the two arms of the bridge are relatively short and of approximately the same length, the balance does not depend critically on the oscillator frequency. This method does not, therefore, require high frequency stability of the microwave oscillator as do the methods which employ a high Q cavity to contain the sample. Another advantage over the cylindrical cell is that much smaller gaps are required between the magnetic pole pieces. Because one dimension of rectangular wave guide is not critical, it is possible to reduce the gap between the pole pieces to the order of a millimeter. This makes it possible to obtain high fields and hence to work at high microwave frequencies.

The balanced bridge method employed allows the use of relatively high power levels without the generation of excessive crystal noise because only the unbalanced power falls on the crystal. Best sensitivity is obtained with a superheterodyne receiver. Also, one can increase the sensitivity greatly by employing a phase-sensitive, lock-in amplifier combined with a modulation of the absorption line by a low frequency ac magnetic field superimposed upon the dc field. The latter method

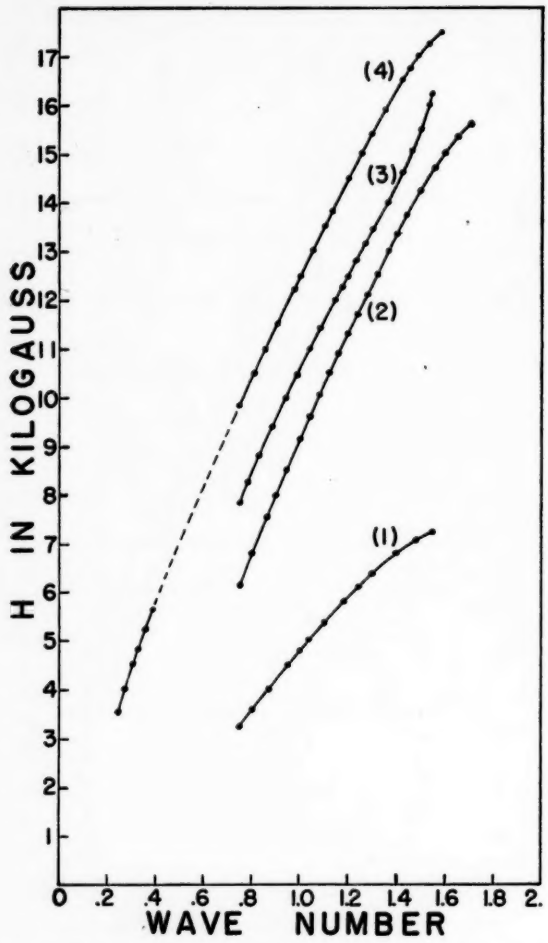

FIG. 6. Plot of paramagnetic resonance frequencies of copper acetate against resonance field strength.

will be used in later experiments in which the paramagnetic substance will be studied in diluted form.

Except for Fig. 3 the magnetic field was read with a flip coil at each setting. Because of its sharpness, special methods were required to obtain the curve in Fig. 3. In most instances readings were taken at points of equal absorption on either side of the point of maximum absorption.

RESULTS

The principal results are summarized in Tables I, II, and III. Some typical absorption curves are shown in Figs. 2–12. For most substances we have observed only a single symmetrical peak with a corresponding g factor near 2. In some instances an asymmetry apparently caused by crystalline field splitting or anisotropy in the g factor was observed, and, in a lesser number, multiple peaks were found. Several resonance curves were obtained which have sharply peaked nongaussian shapes like that of diphenyl trinitrophenyl hydrazyl, Fig. 3, which is known to have exchange interaction.[10]

[10] Holden, Kittel, Merritt, and Yager, Phys. Rev. **77**, 147 (1950); C. H. Townes and J. Turkevitch, Phys. Rev. **77**, 148 (1950).

Van Vleck[4] has shown that isotropic exchange interaction between like ions contributes to the fourth moment of the absorption line, $\langle(\Delta\nu)^4\rangle_{Av}$, but not to the second moment, $\langle(\Delta\nu)^2\rangle_{Av}$. As a result, the lines are more sharply peaked than would be expected for a purely gaussian curve. He has shown that, in contrast, spin-spin interaction has the opposite tendency—that is, to blunt the absorption line rather than to peak it as does exchange interaction. Other factors, such as unresolved hyperfine structure and crystalline field interaction, which affect line shapes would not tend to produce a sharp symmetrical peaking of the absorption line, as does exchange narrowing; but they might blunt its shape, as does spin-spin interaction, or might produce unsymmetrical distortions because of unresolved components. Thus, even in the complex polycrystalline materials employed in the present study, where a detailed quantitative analysis is not possible, qualitative evidence for exchange interaction can be obtained from the line shapes.

For all those substances which showed reasonably symmetric absorption curves we have given in the last column of Table I the ratio of the root mean fourth

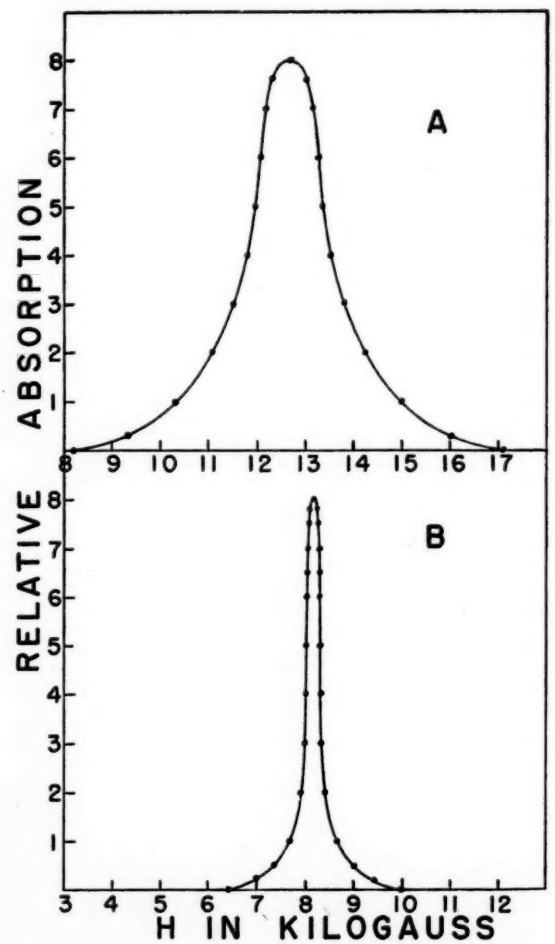

FIG. 7. Paramagnetic resonance of (A) ferric acetyl acetonate at 34490 Mc/sec and (B) ferric fluoride at 23060 Mc/sec.

to the root mean square moment evaluated numerically from the absorption curve with the relation

$$\langle \Delta H^n \rangle_{Av}^{1/n} = [\sum_{-\infty}^{\infty} A(H)(H_{res}-H)^n \Delta H / \sum_{-\infty}^{\infty} A(H)\Delta H]^{1/n}, \quad (2)$$

where $A(H)$ is the intensity of absorption for a given field value H, and H_{res} is the field strength for maximum absorption. For a gaussian shape this ratio is 1.32, while for a rectangular shape it is 1.18. Although most of the curves which we obtained gave ratios near the gaussian value of 1.32, several gave ratios which are appreciably larger than 1.32. Since spin-spin interaction would tend to reduce the ratios below 1.32, and probably any unresolved structure would also tend to do so, it appears fairly probable that there is significant exchange interaction in those substances in which a ratio of about 1.40 or greater is obtained. It does not necessarily follow that there is no such interaction when a ratio of near 1.32 is obtained, since the effects of exchange narrowing could be counterbalanced by other factors already mentioned. Also, exchange interaction between atoms which have different Larmor frequencies in the same field would broaden rather than sharpen the lines. This is illustrated by the broadening of the $CuSO_4 \cdot 5H_2O$ resonant line for certain crystal orientations where the two ions in unit cell have different

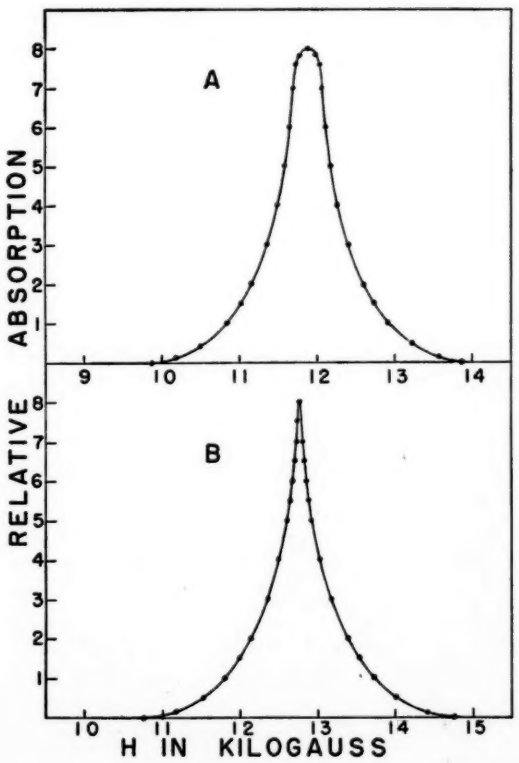

FIG. 8. Paramagnetic resonance of (A) manganese carbonate at 33145 Mc/sec and (B) manganese sulfate at 35570 Mc/sec.

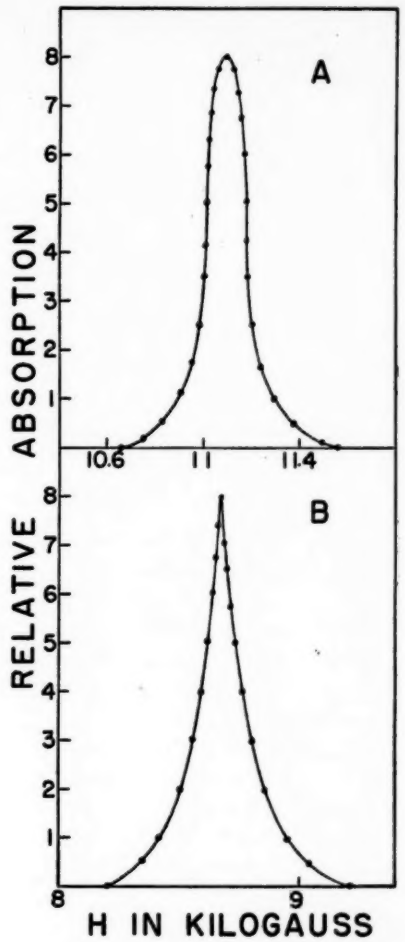

FIG. 9. Paramagnetic resonance of (A) vanadium complex at 30895 Mc/sec and (B) vanadyl chloride at 24138 Mc/sec.

Zeeman energies.[11] Although our method of detection does not give a true line shape, because of dispersion effects, it does not seem probable that the marked differences in the shapes of the individual curves are caused by the method of detection.

Copper

The doubly ionized copper of cupric salts has a single unpaired electron which is in a $3d$ orbit. The ground state of Cu^{++} is $^2D_{5/2}$. In a cubic field the orbital levels are split into a doublet and a triplet. The lowest of the levels is the doublet, which is nonmagnetic.[9] In a tetragonal field the orbital levels are split into a doublet and three singlets, with the level of one of the singlets, $T=3$, lying lowest;[12] and in a rhombic field the orbital degeneracy is completely lifted. The spin degeneracy is a Kramers doublet which is split only by the external magnetic field. The paramagnetic resonance absorption is thus caused essentially by the flipping of the electron

[11] D. M. S. Bagguley and J. H. E. Griffiths, Proc. Roy. Soc. (London) **A201**, 366 (1950). See also R. Arnold and A. Kipp, Phys. Rev. **75**, 1119 (1949).
[12] D. Poulder, Physica **9**, 709 (1942).

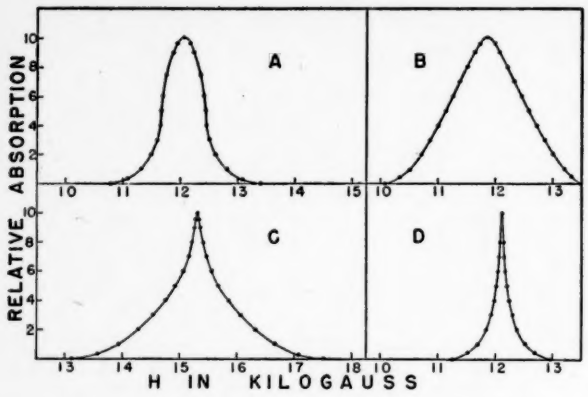

FIG. 10. Paramagnetic resonance of (A) chromium hexammine chloride at 33130 Mc/sec; (b) chromic dirhodanato diethylene diammine rhodanate at 32830 Mc/sec; (C) chromium salicylate at 44220 Mc/sec; and (D) chromium dichloro tetra aqua chloride at 33040 Mc/sec.

spin vector. There is considerable spin orbit coupling,[9] however, which with the crystalline field usually makes the g factor anisotropic and different from 2. The simpler inorganic cupric salts have been studied extensively[13] and will not be discussed in detail here. The results on the more complicated salts containing organic groups are more difficult to interpret because of their complex and uncertain crystalline structures. Nevertheless, they are of interest because of the large amount of exchange interaction which occurs in some types.

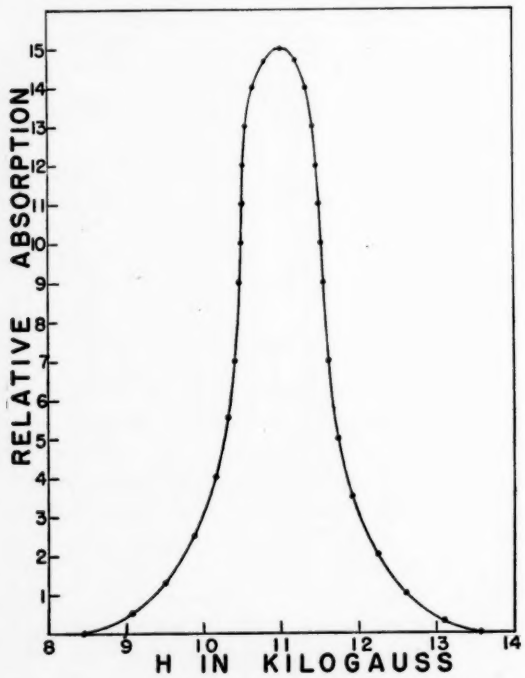

FIG. 11. Paramagnetic resonance of nickelous hexammine dibromide at 32845 Mc/sec.

[13] D. M. S. Bagguley and J. H. E. Griffiths, Nature **162**, 538 (1948); J. Wheatley and D. Halliday, Phys. Rev. **75**, 1412 (1949); R. Arnold and A. Kipp, reference 11; Bleaney, Penrose, and Plumpton, Proc. Roy. Soc. (London) **198**, 406 (1949).

The ratios of the root mean fourth to the root mean square moments of the field deviation defined by Eq. (2) and listed in Table I indicates appreciable exchange interaction in copper chloride, copper formate, copper 2,2 dimethyl decanedione 3,5, and copper tetrapyridine nitrate. Because of other complexities which make their resonance curves asymmetric, this ratio was not calculated for copper oxalate and copper phthalocyanine. Nevertheless, their resonance curves have sharp peaks on the high field sides, which suggests exchange effects. The curve for copper oxalate is shown in Fig. 2.

It is of interest to consider the chemical formulas of certain of these molecules in connection with these results. The immediate surrounding of the Cu in copper

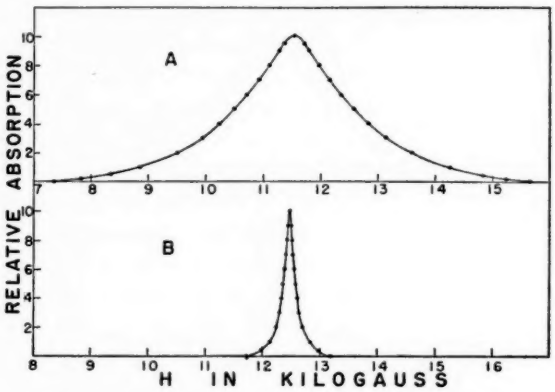

FIG. 12. Paramagnetic resonance of (A) gadolinium chloride at 32500 Mc/sec and (B) cerium oxalate at 33800 Mc/sec.

2,2 dimethyl decanedione 3,5,

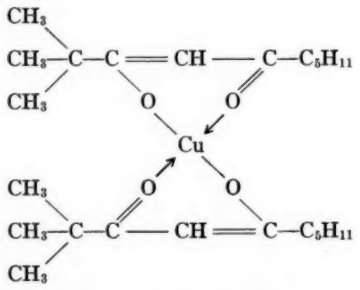

for which there is evidence for exchange narrowing, is similar to those of copper 1-phenyl hexanedione, 3,5,

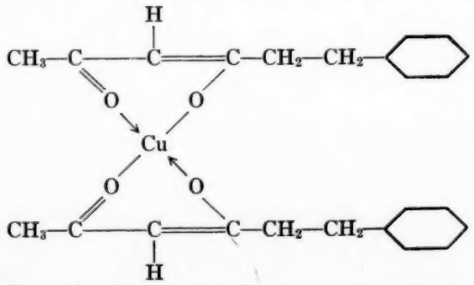

for which a gaussian type resonance curve was obtained.

TABLE I. Compounds showing paramagnetic resonance lines at room temperature.

Ion	Compound	Chemical formula	Mc/sec	Resonance field strength (gauss)	g factor	Line width (gauss)[a]	$\langle(\Delta H)^4\rangle_{Av}^{\frac{1}{4}}/\langle(\Delta H)^2\rangle_{Av}^{\frac{1}{2}}$
Ce^{++++}	Cerium oxalate	$Ce(C_2O_4)_2\cdot 4H_2O$	33800	12860	1.95	180	1.44
Cr^{+++}	Chromium hydroxide	$Cr(OH)_3\cdot 2H_2O$	27530	9875	2.00	535	1.41
	Chromium nitrate	$Cr(NO_3)_3\cdot 9H_2O$	36575	11590	2.26	375	1.33
	Chromium sulfate	$Cr_2(SO_4)_3\cdot 18H_2O$	23595	8460	2.00	350	1.42
	Chromium salicylate	$Cr(C_7H_5O_3)\cdot H_2O$	44220	15270	2.07	700	1.40
	Chromium diaqua dihydroxi dipyridine chloride	$Cr(C_5H_5N)_2(OH)_2(H_2O)_2Cl$	34050	12260	1.99	440	1.41
	Chromium III pentammine chloride	$[Cr(NH_3)_5Cl]Cl_2$	33130	12040	1.97	400	1.33
	Chromium III hexammine chloride	$[Cr(NH_3)_6]Cl_3\cdot H_2O$	34280	12600	1.97	720	1.32
	Chromium dichloro tetra aqua chloride	$[Cr(H_2O)_4Cl_2]Cl$	33040	12130	1.95	180	1.44
	Chromium III hexammine nitrate	$[Cr(NH_3)_6](NO_3)_3\cdot H_2O$	33160	12160	1.95	700	1.32
	Chromium potassium hexacyanide	$K_3Cr(CN)_6$	30670	11220	1.96	570	1.32
	Chromic dirhodanato diethylene diammine rhodanate	$(CH_2)(NH_3)_2Cr\{N(CS)(CO)SCN_2\}_3$	32830	11870	1.98	1540	1.29
Cu^{++}	Copper benzoate	$Cu(C_7H_5O_2)_2\cdot 2H_2O$	44280	14610	1.97	570	1.33
	Copper fluoride	CuF_2	35678	11870	2.15	995	1.29
	Copper chloride	$CuCl_2\cdot 2H_2O$	35440	11650	2.14	540	1.42
	Copper bromide	$CuBr_2$	35290	11360	2.23	1300	1.29
	Copper formate	$Cu(CHO_2)_2\cdot 4H_2O$	28400	9210	2.21	500	1.40
	Copper lactate	$Cu(C_3H_5O_3)_2\cdot 2H_2O$	23000	7860	2.09		Asym.
	Copper acetate	$Cu(C_2H_3O_2)_2\cdot H_2O$	See special summary, Table III.				
	Copper oxalate	$2CuC_2O_4\cdot H_2O$	34040	11790	2.07	120	Asym.
	Copper tartrate	$CuC_4H_4O_6\cdot 3H_2O$	44280	14610	1.97	890	Asym.
	Copper phthalocyanine	$Cu(C_6H_4)_4(CN)_8$	29650	10410	2.02	250	Asym.
	Copper acetyl acetonate	$Cu(C_5H_7O_2)_2$	35390	12590	2.01	620	1.32
	Copper ammonium chloride	$CuCl_2\cdot 2NH_4Cl\cdot 2H_2O$	24160	7840	2.21	210	1.40
	Copper ammonium sulfate	$Cu(NH_4)_2(SO_4)_2\cdot 6H_2O$	32450	10480	2.22	720	1.32
	Copper tungstate	$CuWO_4\cdot 2H_2O$	34570	11450	2.17	1000	1.32
	Copper tetrapyridine nitrate	$[Cu(C_5H_5N)_4](NO_3)_2\cdot H_2O$	32800	11540	2.04	620	1.41
	Copper 2,2 dimethyl decanedione 3,5	$Cu[(CH_3)_3C(CO)_2CH_2C_5H_{11}]_2$	31600	11100	2.04	170	1.41
	Copper 1-phenyl hexanedione 3,5	$Cu[C_6H_5(CH_2)_3(CO)_2CH_3]_2$	30680	10880	2.02	525	1.30
	Copper tetrammine sulfate	$[Cu(NH_3)_4]SO_4\cdot H_2O$	32380	11180 11410	2.07 2.03		Asym.
Fe^{+++}	Ferric ammonium citrate	$Fe(NH_4)_3(C_6H_5O_7)_2\cdot 2H_2O$	35750	12930	1.98	1700	1.33
	Ferric acetyl acetonate	$Fe(C_5H_7O_2)_3$	34490	12680	1.95	1580	1.32
	Ferric fluoride	$(FeF_3)_2\cdot 9H_2O$	23060	8160	2.02	300	1.32
	Ferric sulfate	$Fe_2(SO_4)_3\cdot 9H_2O$	23925	8530	2.01	820	1.32
	Ferric ammonium sulfate	$Fe(NH_4)(SO_4)_2\cdot 12H_2O$	30820	11100	1.99	1200	Asym.
Gd^{+++}	Gadolinium chloride	$GdCl_3\cdot 6H_2O$	32500	11500	2.02	2070	1.32
	Gadolinium chloride	$GdCl_3\cdot 6H_2O$	46610	16140	2.07	3000	
	Gadolinium chloride	$GdCl_3\cdot 6H_2O$	49500	16740	2.12	3200	
	Gadolinium chloride	$GdCl_3\cdot 6H_2O$	51640	17325	2.13	3300	
Mn^{++}	Manganese borate	$Mn(BO_2)_2$	30890	10965	2.01	975	1.44
	Manganese carbonate	$MnCO_3$	33145	11875	2.00	650	1.32
	Manganese chloride	$MnCl_2\cdot 4H_2O$	24120	8650	2.00	700	1.44
	Manganese sulfate	$MnSO_4\cdot 4H_2O$	35570	12760	2.00	450	1.44
Mn^{+6}	Manganese trioxide	MnO_3	28550	10430	1.96	575	1.33
Ni^{++}	Nickel hexammine dibromide	$NiBr_2(NH_3)_6$	32845	11000	2.14	1200	1.32
V^{++++}	Vanadium complex	$VO_3(C_6H_4)_3N_2(CH)_2$	30895	11090	2.02	170	1.33
	Vanadyl chloride	$VOCl_2$	24138	8660	2.00	125	1.38
	Diphenyl trinitrophenyl hydrazyl	$(C_6H_5)_2(NO_2)_3N_2C_6H_2$	32710	11715	2.00	9.5	1.44

[a] Line width between points of half-maximum absorption.

TABLE II. Paramagnetic substances for which absorption peaks could not be observed at room temperature with magnetic fields up to 15000 gauss.

Compound	Chemical formula	Frequency Mc/sec
Cupric carbonate	$2CuCO_3 \cdot Cu(OH)_2$	46210
Cupric thiocyanate	$Cu(SCN)_2$	46205
Cupric ferrocyanide	$Cu_2Fe(CN)_6 \cdot 7H_2O$	46205
Cupric arsenate	$Cu_3(AsO_4)_2 \cdot 4H_2O$	46190
Cupric borate	$Cu(BO_2)_2$	36187
Cupric nitrite	$Cu(NO_2)_2 \cdot 3Cu(OH)_2$	36200
Cupric manganate	$CuMnO_4$	36205
Cupric chromate	$CuCr_2O_7 \cdot 2H_2O$	36810
Cupric phosphate	$Cu_3(PO_4)_2 \cdot 3H_2O$	36208
Cupric cyanide	$Cu(CN)_2$	46210
Cupric oxide	CuO	45780
Cupric sulfide	CuS	45785
Cobaltous acetate	$Co(C_2H_3O_2)_2 \cdot 4H_2O$	46300
Cobaltous carbonate	$Co(CO_3)$	46310
Cobaltous chloride	$CoCl_2 \cdot 6H_2O$	46250
Cobaltous hydroxide	$Co(OH)_2$	45830
Cobaltous nitrate	$Co(NO_3)_2 \cdot 6H_2O$	45825
Cobaltous sulfate	$Co(SO_4) \cdot 7H_2O$	43755
Cobalt complex	$Co(CHO)_2O_2(C_6H_4)_2 \cdot 2H_2O$	46280
Potassium dichromate	$K_2Cr_2O_7$	36128
Potassium chromate	K_2CrO_4	37210
Chromic oxide	Cr_2O_3	46350
Chromium salicylate	$Cr(C_7H_5O_2)_2$	23640
Cerous sulfate	$Ce_2(SO_4)_3 \cdot 4H_2O$	46200
Ceric sulfate	$Ce(SO_4)_2 \cdot 4H_2O$	46215
Cerium acetyl acetonate	$Ce(C_5H_7O_2) \cdot 3H_2O$	46350
Ferrous chloride	$FeCl_2$	37210
Ferric oxide	Fe_2O_3	35865
Ferrous sulfate	$FeSO_4 \cdot 7H_2O$	34675
Ferrous oxalate	$FeC_2O_4 \cdot 2H_2O$	34650
Ferrous ammonium sulfate	$Fe(NH_4)_2(SO_4)_2 \cdot 6H_2O$	34610
Ferric chloride	$FeCl_3,6H_2O$	35790
Manganese dioxide	MnO_2	35285
Nickelic oxide	Ni_2O_3	35290
Nickelous oxide	NiO	34385
Nickelous fluoride	NiF_2	34792
Nickel nitrate	$Ni(NO_3)_2 \cdot 6H_2O$	34798
Nickel chloride	$NiCl_2 \cdot 6H_2O$	35452
Nickel sulfate	$NiSO_4 \cdot 7H_2O$	35478
Nickel acetyl acetonate	$Ni(C_5H_7O_2) \cdot 3H_2O$	46225
Nickel tetrammine sulfite	$Ni(SO_3)_2 \cdot 4NH_3$	45285
Nickel hexammine sulfate	$Ni(SO_4)_2 \cdot 6NH_3$	44324
Nickel ammonium sulfate	$Ni(NH_4)_2(SO_4)_2 \cdot 8H_2O$	46208
Nickel phosphate	$Ni_3(PO_4)_2 \cdot 7H_2O$	43515
Potassium nickel sulfate	$K_2Ni(SO_4)_2 \cdot 6H_2O$	46305
Lanthanum oxide	La_2O_3	51200
Lanthanum chloride	$LaCl_3 \cdot 7H_2O$	46500
Lanthanum nitrate	$La(NO_3) \cdot 6H_2O$	48322
Neodymium chloride	$NdCl_3 \cdot 6H_2O$	46700
Neodymium nitrate	$Nd(NO_3)_3 \cdot 6H_2O$	46650
Praseodymium nitrate	$Pr(NO_3)_3$	51115
Praseodymium chloride	$PrCl_3$	50230
Samarium chloride	$SmCl_3 \cdot 6H_2O$	47320
Samarium nitrate	$Sm(NO_3)_3 \cdot 6H_2O$	46800
Yttrium chloride	$YtCl_3 \cdot 6H_2O$	45602
Yttrium sulfate	$Yt_2(SO_4)_3 \cdot 8H_2O$	45715

Note: The majority of the above compounds were also checked in the 20,000- and 30,000-Mc/s range.

In copper phthalocyanine, the paramagnetic Cu is

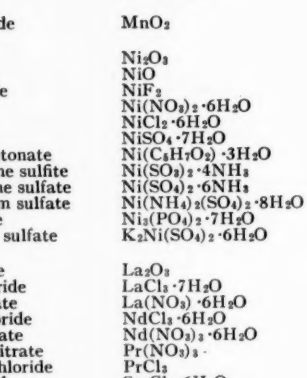

attached to four nitrogens and is at the center of a complex ring structure which has a large number of multiple bonds.

The curves for copper oxalate, tartrate, lactate, and phthalocyanine are similar in that they all have a strong peak on the high field side with a broad shoulder of lower intensity on the low field side. This type of curve would be expected if the crystalline field around the Cu has an axis of symmetry along which g has a maximum value. The strong peak on the high field side (low g) would then correspond to the orientation of the axis perpendicular to the external field, $g_\perp$, for which there would be a greater geometrical probability for the randomly orientated axes in the powder. The curve for copper tetrammine sulfate has two well-defined peaks with the one on the high field side much sharper but slightly weaker than the other. The broader peak has on its low field side a broad shoulder which appears to be a third unresolved peak. These complexities probably arise from the presence of more than one ion in unit cell.

Copper fluoride and copper chloride offer an interesting comparison. It has been demonstrated by Van Vleck[4] that the theoretical line width in copper chloride ($CuCl_2 \cdot 2H_2O$) produced by the spin-spin interaction alone, assuming gaussian shape, is several times that measured in the pure crystal at 200 Mc/sec by Zavoisky. He attributes this extra narrowing primarily to exchange interaction. Although the anisotropic g factor makes the line broader at the high frequencies of the present investigation, the exchange narrowing is revealed by the peaked shape of the absorption curve. The ratio $\langle(\Delta H)^4\rangle_{Av}^{\frac{1}{4}}/\langle(\Delta H)^2\rangle_{Av}^{\frac{1}{2}}$ is 1.42, compared with 1.32 for the gaussian shape. Since in CuF_2 the Cu ions are closer than those in $CuCl_2 \cdot 2H_2O$, the spin-spin broadening would be greater in the former crystal. However, the direct exchange interaction should increase more rapidly with decreasing separation than does the spin-spin interaction, and one might for this reason expect the resonance for CuF_2 to be even more sharply peaked than that of $CuCl_2 \cdot 2H_2O$. Actually, the line shapes, see Fig. 4 and the moment ratios in Table I, indicate significantly less exchange coupling in both CuF_2 and $CuBr_2$ than in $CuCl_2 \cdot 2H_2O$. This greater exchange in the latter salt should not result from the water of crystallization since this would increase the separation of the Cu ions and would tend to decrease the direct exchange.[4] A possible cause of the extra narrowing of the chloride is that the $3d$ orbital of the Cl provides a low energy path for the migration of the electrons between the copper ions in the crystal. This would augment the exchange interaction which sharpens the lines. Such exchange would not be as important in CuF_2 because F has no unused orbital in the valence shell, and it would probably be of less significance for $CuBr_2$ because the unfilled d orbitals of Br are higher energetically than those of Cl. Other chlorides investigated show appreciable exchange narrowing.

TABLE III. Copper acetate summary.

Frequency in Mc/sec	g_1	B_1 gauss	g_2 gauss	B_2 gauss	g_3	B_3 gauss	g_4	B_4 gauss
7575							1.470	3690
8940							1.480	4330
11300							1.490	5430
22600	4.930	3280	2.63	6150	2.070	7820	1.640	9875
26432	4.675	4080	2.400	7950	2.016	9420	1.682	11260
30375	4.520	4820	2.338	9320	2.022	10740	1.722	12620
35150	4.415	5720	2.290	11000	2.056	12275	1.759	14330
39030	4.390	6375	2.254	12420	2.067	13520	1.806	15500
47440			2.280	14910				
50770			2.340	15580				

The marked difference of the paramagnetic resonance of copper acetate $Cu(C_2H_3O_2)_2 \cdot H_2O$ from that of the other copper salts is surprising. Figure 5 shows the absorption curves at several different frequencies, and Fig. 6 shows a plot of resonant frequency against magnetic field. At the lowest frequency and also at the highest frequency used, only a single resonant line was observed, whereas at intermediate frequencies a complex structure was found. At high fields where only one line is obtained, the g factor is greater than 2 and approximately that observed for the copper esters, while at the lowest field the single line observed has a g factor less than 2. Since in a crystal of this type the lowest orbital level is probably a singlet, and since $S=\frac{1}{2}$, it is difficult to account for the number of lines found. It is possible that a strong coupling of adjacent ions through exchange forces causes the complexity. Some type of coupling appears to be breaking down with increasing field. The line observed for the lowest field, line 1, decreases in intensity with increase of frequency (and hence of magnetic field) and is too weak to be detected at the highest frequency employed. It is perhaps not without significance that the g factor obtained from this line is approximately twice that from line 2. A possible origin of line 1 is the simultaneous transition of the electron spin vectors of two neighboring Cu^{++} ions with the absorption of a single quantum.‡ The simultaneous flipping of the spin vectors would be made possible by a strong coupling of the electrons. Evidence for this is that the line in question decreases rapidly with increasing field strength. Transitions of this type have been predicted by Temperley.[14] Evidence for a somewhat similar phenomenon, a double jump in a single atom has been reported recently by Ubbink, Poulis, and Gorter.[15]

Iron

The ground state of Fe^{+++} is ${}^6S_{5/2}$. Since $L=0$, the expected Stark splitting is either zero or extremely small. Because there are five unpaired electrons, a strong resonance absorption with a g factor of nearly 2 is expected. This is in agreement with observation for the three ferric salts studied. The observed lines are symmetric and fairly broad, see Fig. 7.

Manganese

Several salts containing Mn^{++} ions were included. Like Fe^{+++}, the Mn^{++} ion has an S ground state. All except one of the manganese salts investigated gave strong resonance lines with g factors of approximately 2. Two of these are shown in Fig. 8. Note that manganese carbonate has a typical gaussian curve, while that for manganese sulfate has a cusped shape, characteristic of compounds with exchange coupling of the electrons. The moment ratios of the last column in Table I also show exchange narrowing in manganese sulfate, borate, and chloride.

Vanadium

The two tetravalent vanadium salts observed gave sharp resonance peaks with g factors of approximately 2. The line shape of the vanadium complex showed little

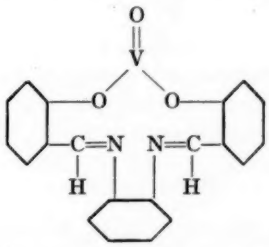

or no evidence for exchange narrowing, $\langle(\Delta H)^4\rangle_{Av}^{\frac{1}{4}}/\langle(\Delta H)^2\rangle_{Av}^{\frac{1}{2}}=1.33$ in contrast to vanadyl chloride, for which this ratio is 1.38. The absorption curves for these two compounds are shown in Fig. 9. The Oxford group,[9] who examined one divalent vanadium salt, the sulfate, reported a narrow line with a g factor of 2.

Chromium

The chromium alums have been studied in detail by other investigators[16] using individual crystals and were found to have crystalline Stark splittings of the order of 0.15 cm^{-1} for zero H. Several of the chromium salts

‡ This possibility was suggested to us by Dr. Harold Ring.

[14] H. N. V. Temperley, Proc. Cambridge Phil. Soc. **35**, 256 (1939).

[15] Ubbink, Poulis, and Gorter, Physica **16**, 570 (1950).

[16] Whitmer, Weidner, Hsiang, and Weiss, Phys. Rev. **74**, 1478 (1948); D. Halliday and J. Wheatley, Phys. Rev. **74**, 1712 (1948).

included in the present study showed the characteristic exchange narrowing. (See the last column of Table I.) This is particularly true of dichloro-tetra-aqua-chromic chloride. Note the shape and width of the resonance curve for this compound as contrasted with that of dirhodanato diethylene diammine chromium rhodanate in Fig. 10. The curve for the latter salt is broad and gaussian in shape, indicating little exchange interaction.

Nickel

Of the thirteen nickel salts investigated only one, $NiBr_2(NH_3)_6$, gave a detectable resonance absorption. (See Fig. 11.) The line is broad, with a g factor of 2.14. The lowest level of most of the nickel salts has zero field splitting of the spin levels sufficient to prevent detection of resonance centimeter waves.[9]

Cobalt

No absorption could be detected for any of the cobalt compounds investigated. (See Table II.) This is in agreement with the results of the Oxford researchers,[9] who could not detect absorption in any of the several cobalt salts they studied at room temperature. At 90° absolute they were able to detect broad lines in some of these. The weak absorption of the Co^{++} ion is caused by the short spin lattice relaxation time which makes the lines extremely broad. One complex organic ring,

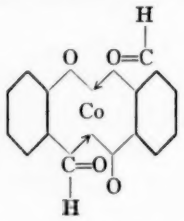

was included in the present study. The absence of detectable resonance probably indicates that the unpaired electrons remain on the Co and that the exchange narrowing is not significant.

Rare Earths

A number of rare earth salts, as listed in Tables I and II, were examined. Resonance peaks were observed for cerium oxalate and gadolinium chloride only. These are shown in Fig. 12. The failure to observe resonance absorption in most of the rare earth salts at room temperature is caused by the failure of the crystalline electric field to break down effectively the spin orbit coupling.[9] As a result of the strong spin orbit coupling, the spin lattice relaxation time is short and the resonance lines so broad that they cannot be detected except at low temperature, or the g factor is so small that it is difficult to obtain a sufficiently high field to observe the resonance with centimeter waves. One of the rare earth ions, Ga^{+++}, has no resultant orbital momentum; its ground state is $^8S_{7/2}$, and for this reason the resonance absorption of its salts can be observed at room temperature. Both the g factor and the line width of gadolinium chloride were found to increase with frequency.

The ground state of Ce^{+++} is $^2F_{5/2}$. Of the four cerium salts examined in the present study, only one showed detectable absorption. The Oxford group[9] examined several cerium salts, but could detect resonance absorption only at low temperature. It is therefore of significance that the one cerium salt showing absorption, $Ce(C_2O_4)\cdot 4H_2O$, has a sharp resonance peak, 170 gauss in width, with a g factor only slightly less than 2. A plausible explanation of the sharpness of this line is that the unpaired $4f$ electron couples through the oxalate ion in some manner with the electrons in other Ce ions. The interaction not only peaks the absorption sharply, but apparently also assists the crystalline field in "quenching" the orbital momentum, so that the g factor obtained is nearly that for a free electron spin.

Discussion of Exchange Effects

Evidence for exchange narrowing has been found for a large number of organic as well as inorganic salts. In most of these salts the paramagnetic atoms or ions are too widely separated by intervening nonparamagnetic atoms or organic radicals for the exchange interaction to be caused by a direct overlapping of the atomic wave functions of the paramagnetic ions. The exchange coupling therefore appears to result from contributions —small perhaps but significant—of wave functions of the neighboring nonparamagnetic atoms or groups to the orbital occupied by the unpaired electron. The unpaired electron would then occupy a semimolecular type orbital rather than a purely atomic orbital, but with the atomic orbital of the paramagnetic element usually making the predominent contribution. It is significant that the organic salts in which exchange narrowing has been found all have unsaturated groups—i.e., organic groups containing double bonds.

The tendency toward large exchange coupling in certain chlorides, sulfates, and the one borate investigated probably results from contributions of the unused $3d$ valence shell orbitals of Cl and S or the incompletely occupied $2p$ valence shell orbitals of B to the composite wave function of the unshared electron. These orbitals provide, so to speak, a low energy path for the exchange of electrons between the paramagnetic ions. This property of Cl and S is in harmony with the special tendency of the second row elements to use the $3d$ orbital to form coordinate, covalent bonds.[17]

The Ce^{+4} ions of cerium oxalate are too far apart for direct spin-spin coupling to be of great significance. For the $4f$ electron which is deep within a subvalence shell there should be little chance of migration. A possible mechanism for the strong coupling of the electrons in different Ce ions is an indirect coupling similar

[17] J. Sheridan and W. Gordy, J. Chem. Phys. **19**, 965 (1951).

to that proposed by Zener[18] for the interaction among the d shell electrons in metals. In this type of interaction the spin of the unpaired d electron couples strongly to those of the conduction electrons. This coupling then tends to align the spins of the d electrons. In the present example it appears that the $4f$ electrons may interact with migrating electrons in the organic radical in a similar way. The wave functions of electrons migrating in the organic radicals are in some respects similar to those of the conducting electrons in a metal. It is these spread-out orbitals or "limited conducting bands" of organic salts which may make possible the exchange narrowing of widely separated paramagnetic ions.

From these observations it appears that paramagnetic resonance will provide a new means of investigating conjugation or resonance in various chemical groups. The ability of an electron to "pass through" a group is closely related to the chemical properties of the group. A related phenomenon in organic chemistry is that substitution at one point in a large organic group frequently affects markedly the reactivity at a point in the group far removed from the point of substitution.

We wish to thank Dr. P. O. Lowdin and Dr. Harold Ring for helpful discussion of this paper, Mr. W. A. Parker for assistance with some of the measurements, and Professors D. G. Hill, W. C. Vosburgh, and C. R. Hauser for some of the chemicals. We are indebted particularly to Dr. Ralph Trambarulo, who not only prepared some of the chemicals but gave valuable suggestions in the course of the experiments.

[18] C. Zener, Phys. Rev. **81**, 440 (1951).

THE JOURNAL OF CHEMICAL PHYSICS VOLUME 19, NUMBER 9 SEPTEMBER, 1951

Bond-Bond Interactions in Linear and Angular Molecules

JULES DUCHESNE AND LOUIS BURNELLE
Faculty of Science, University of Liège, Belgium

(Received May 5, 1951)

The vibration potential function of several molecules is studied with special emphasis on the bond-bond interaction terms. It is shown that in the case of molecules with localized bonds a satisfactory correlation of the results cannot be obtained without assuming the existence of a maximum in the bond-bond energy curve. This maximum presumably arises from the electrostatic interactions between the bond orbitals. As a result, the bond-bond interaction terms may be either positive or negative, according to the position of the point which represents the equilibrium position of the molecule on the curve. However, this sign seems generally positive, except for molecules with hydrogenated bonds. On the other hand, for molecules with delocalized bonds (resonance), a general law may be formulated for the behavior of these terms when they refer to nonadjacent as well as to adjacent bonds. In those cases, the part played by the electrostatic interactions seems to be dominated by the resonance effects.

IT is well known that the potential function for molecular vibrations contains, among others, coefficients in the terms $\Delta r_i \Delta r_j$, which may be called bond-bond interaction terms, as they measure the influence on one bond of a change in another one. In this note, we have especially the aim of extending the previous work[1] on the behavior of the sign of these terms by studying appropriate molecules. The molecules here examined may be classified into two groups respectively characterized by localized bonding electrons (ClHgBr, BrHgI, H_2O, H_2S, F_2O) and by delocalized ones (C_2N_2). The need for a systematization of the cross-terms is very great indeed, and it was therefore of interest to take into account whether their sign follows such a classification or not. C_2N_2 is furthermore a suitable system for discussing the interaction forces between nonadjacent bonds.

Let us first consider the linear triatomic molecules XYZ (ClHgBr, BrHgI). If r_1 and r_2 are the bond lengths XY and YZ, the most general potential function for the parallel vibrations may be written

$$2V = f_1 \Delta r_1^2 + f_2 \Delta r_2^2 + 2 f_{12} \Delta r_1 \Delta r_2.$$

The assigned frequencies, the substances being in the dissolved state, are 232 and 345 cm^{-1} for ClHgBr, and 168 and 233 cm^{-1} for BrHgI.[2] However, two frequencies are not sufficient to fix the exact value of the three force constants f_1, f_2, and f_{12} appearing in the above potential. For this reason, we have plotted f_1 and f_2 against f_{12} according to a method which has proved itself very valuable.[3] The ellipses which are thus obtained and which represent the real values of f_1 and f_2, are shown in Figs. 1–4. From an inspection of these

[1] J. Duchesne, Mém. soc. roy. sci. Liège **11**, 429 (1943); Coulson, Duchesne, and Manneback, *V. Henri Mém. Vol.*(Desoer, Liège, 1948), p. 33.

[2] F. François and M-L. Delwaulle, J. chim. phys. **46**, 80 (1949).

[3] J. Duchesne, Physica **9**, 249 (1942); G. Glockler and J. Y. Tung, J. Chem. Phys. **13**, 388 (1945); P. Torkington, J. Chem. Phys. **17**, 357 (1949).

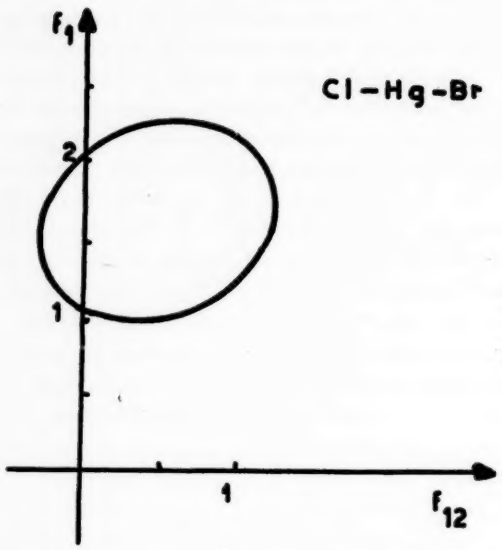

FIG. 1. Allowed solutions for f_1 plotted against f_{12}.

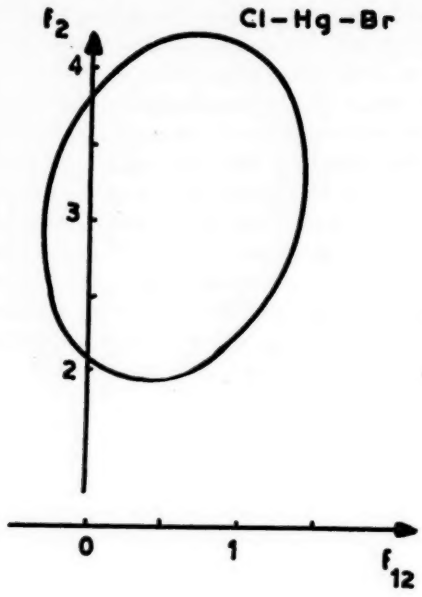

FIG. 2. Allowed solutions for f_2 plotted against f_{12}.

ellipses, it appears that $f_{12}>0$ in both molecules. It is, however, to be pointed out that for ClHgBr this result depends on the reasonable assumption that $f_1>f_2$.

We will now turn our attention to the angular molecules H_2S and F_2O. It is only very recently that the fundamental frequencies of these compounds have been determined with sufficient accuracy to permit an evaluation of the cross terms. For H_2S, the values are[4] 2635, 2651, 1189 cm^{-1}, and for F_2O, they are[5] 929, 461, and 828 cm^{-1}. For the angles, we have adopted 92°16′ and 101°30′, respectively. If r_1, r_2, θ, are the bond lengths and angle, the general potential function is

$$2V=f_1(\Delta r_1^2+\Delta r_2^2)+f_\theta r_1^2\Delta\theta^2+2f_{12}\Delta r_1\Delta r_2 +2g_c r_1\Delta\theta(\Delta r_1+\Delta r_2).$$

As we again meet with a difficulty resulting from the fact that we have only three frequencies available for each molecule, for the calculation of four parameters, we have plotted f_{12} against g_c for both cases in Figs. 5 and 6. From the curve shown in Fig. 5, it is apparent that for H_2S, just as has been found[1] for H_2O,

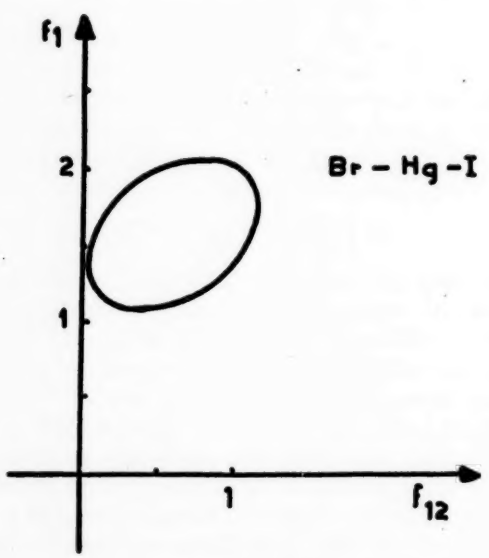

FIG. 3. Allowed solutions for f_1 plotted against f_{12}.

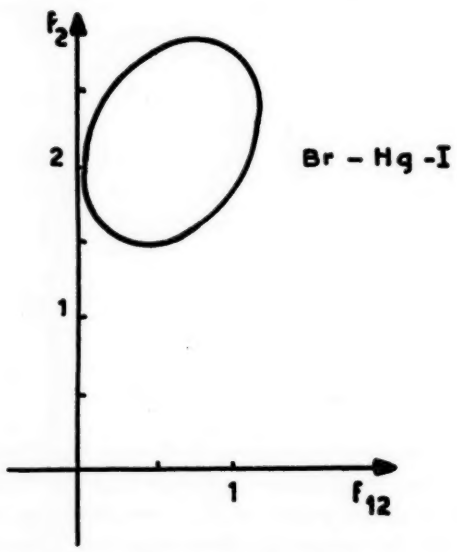

FIG. 4. Allowed solutions for f_2 plotted against f_{12}.

[4] Allen, Cross, and King, J. Chem. Phys. 18, 1412 (1950).
[5] H. J. Bernstein and J. Powling, J. Chem. Phys. 18, 685 (1950).

$f_{12}<0$. The F_2O curve is less self-explanatory, but it can be deduced that within the range of negative values of f_{12}, f_1 and f_2 take inacceptable values. Therefore, it can be asserted that when fluorine is substituted for hydrogen in water, the cross-term changes sign $f_{12}>0$. It follows from the present analysis that no reliable evidence exists to warrant the supposition that the sign of the bond-bond interaction is always negative in the case of molecules with localized bonding electrons. This result does not confirm Linnett and Hoare's rule,[6] according to which a negative sign is expected under these conditions. As the hybridization factor always gives a positive sign,[1] the changing in sign according to the molecule considered must be regarded as arising essentially from the variations of the mutual electrostatic effects resulting from the localized orbitals in the bonds. In another paper it has been shown by Duchesne and Monfils,[7] that negative signs may be explained only by assuming that the curve of the bond-bond energy interaction, in terms of the distance between the nonbonded atoms, gives rise to a maximum. In that case, negative signs should appear between the maximum and the inflection point of the curve, whereas positive signs should be expected beyond the inflection point. More recently, Pople[8] has studied, by quantum mechanics, the variation of this energy in the particular case of H_2O and, in this connection, has demonstrated the great part played by electrostatic repulsions between the bond orbitals. According to the results of this author the curve obtained has a maximum near $\theta=100°$, which is fairly close to the observed equilibrium angle of 104°. It is still difficult to deduce even an approximate value for f_{12}, as the curve cannot yet be drawn with sufficient exactitude. But the appearance of a maximum, if it is real,* would interpret the negative sign. The only assumption would be that the point corresponding to the equilibrium position of the molecule lies somewhere between the maximum and the inflection point of the potential curve. This supports the previous views[7] according to which the presence of a maximum must be a general property of the potential curves determining f_{12}. It seems now possible to assert that, in the case of localized bonding electrons, f_{12}, which depends to a large extent on the electrostatic interactions between the bonds to which it refers, may be either positive or negative. The data seem to indicate that a negative sign is to be expected when the bond contains hydrogen atoms and a positive sign in the other cases.[7,9] It is to be pointed out that for $HgCl_2$ Linnett and Hoare[6] find a negative sign. However, this sign still seems uncertain, as it is obtained from too approximate a value for the antisymmetric frequency, which was deduced by Wehrli[10] from the ultraviolet spectrum. Recent infrared measurements by E. K. Plyler (private communication) locate this vibration at 377 cm^{-1}, the substance being in the solid state. On account of large discrepancies in the frequencies according to the state of aggregation of the compound, any conclusion concerned with the sign of the cross-term seems premature until frequencies for the gaseous state are known.

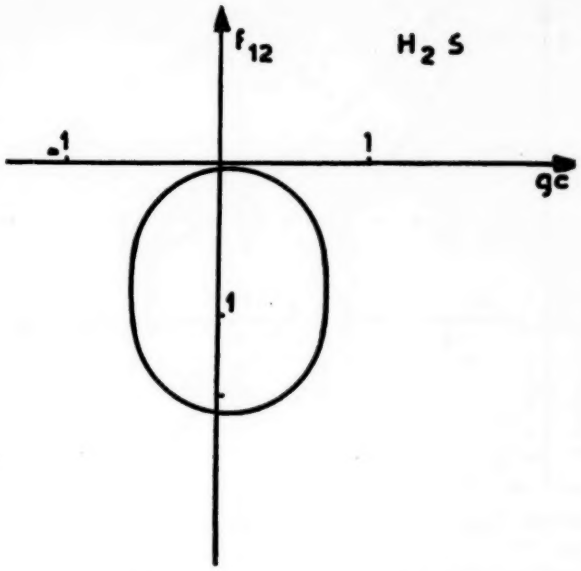

FIG. 5. Allowed solutions for f_{12} plotted against g_c.

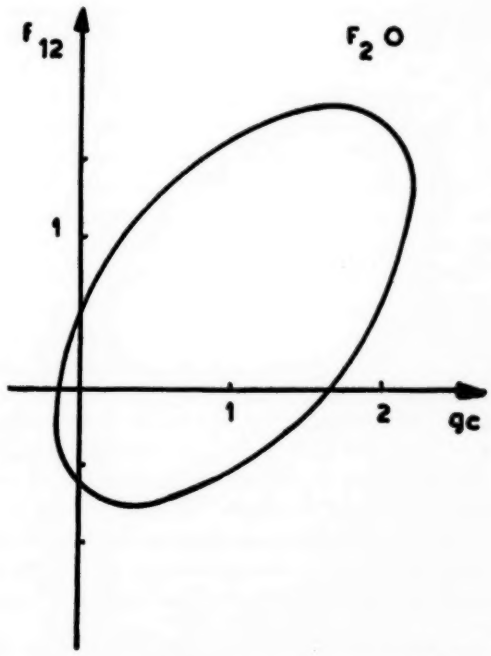

FIG. 6. Allowed solutions for f_{12} plotted against g_c.

[6] H. W. Linnett and M. F. Hoare, Trans. Faraday Soc. **45**, 844 (1949).

[7] J. Duchesne and A. Monfils, J. Chem. Phys. **17**, 586 (1949).

[8] J. A. Pople, Proc. Roy. Soc. (London) **A202**, 323 (1950).

* A correspondence on this point with Dr. J. A. Pople must be acknowledged.

[9] J. Duchesne and I. Ottelet, J. Chem. Phys. **17**, 1354 (1949), and J. phys. et radium **T11**, 119 (1950).

[10] W. Wehrli, Helv. Phys. Acta **11**, 339 (1938).

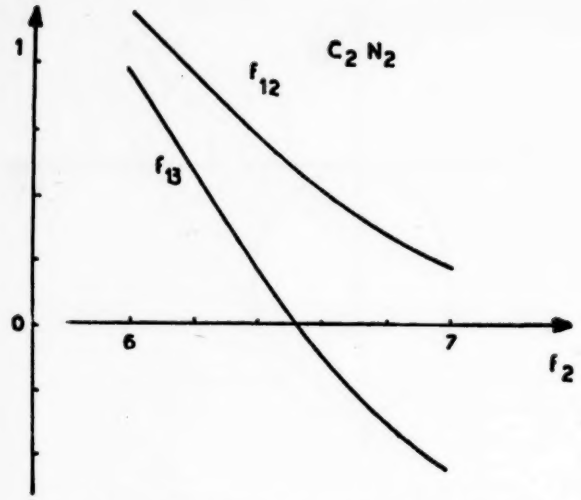

FIG. 7. Allowed solutions for f_{12} and f_{13} plotted against f_2.

Cyanogen (C_2N_2), which has delocalized bonding electrons, has now to be taken into account. This linear and symmetrical molecule gives rise to three parallel vibrations, 2328.5, 850.6, and 2149 cm^{-1}.[11] If r_1, r_3 are the CN bond lengths and if r_2 is the C−C bond length, the general potential function may be written

$$2V=f_1(\Delta r_1^2+\Delta r_3^2)+f_2\Delta r_2^2+2f_{12}\Delta r_2(\Delta r_1+\Delta r_3)+2f_{13}\Delta r_1\Delta r_3.$$

Following the same method as before, we have plotted f_{12} and f_{13} against f_2 in Fig. 7.

It is to be pointed out that f_2 is at least equal to 5.5×10^5 dynes/cm, as smaller values lead to imaginary numbers for f_{12} and f_{13}. As a consequence, it must be admitted that the CC bond is stronger than a single bond for which the force constant is 4.5×10^5 dynes/cm. On the other hand, f_{12}, the bond-bond interaction CC/CN, is certainly positive, as f_2 cannot be supposed to be much greater than 7×10^5 dynes/cm. As regards f_{13}, the bond-bond interaction CN/CN, this is more difficult to locate from the present diagram. In order to carry this question further, we have made use of a fundamental frequency[11] at 2298.4 cm^{-1} which has been assigned to the ν_1-vibration of the isotopic molecule $N\equiv C^{12}-C^{13}\equiv N$. On account of this additional data, it may be presumed that $f_{13}<0$.

In fact, the isotopic shift of ν_1 is rather insensitive to the value of f_{13}, so that no precise value could be calculated. Another way to solve the problem would consist in computing one of the force constants of the normal C_2N_2 molecule by an independent method. This can be performed for the CC force constant f_2. Coulson and Longuet-Higgins[12] have shown how the force constant of a bond i in conjugated hydrocarbons depends on its mobile bond order and its self-polarizability. Using their formula, it is found that

$$f_2=7\times10^5 \text{ dynes/cm.}$$

It is to be noticed that according to a curve due to Coulson,[13] it has been possible to deduce the CC mobile order of C_2N_2 from the CC bond distance, which is equal to 1.38A.[11] The value obtained for f_2 is certainly an upper limit because we have neglected in the calculation a negative term which results from the self-polarizability of the bond. It is, however, practically certain that the self-polarizability is very small, and this would not alter very much the value for f_2. If we adopt $f_2=6.75\times10^5$ dynes/cm, we again obtain different signs for f_{12} and f_{13}. The increase of the C−C bond force constant is due in part to the resonance between structures such as

$$N\equiv C-C\equiv N$$

$$N^+=C=C=N^-.$$

As a matter of fact, such a representation is in agreement with $f_{12}>0$, since it has been found[1] that resonance (delocalized bonding electrons) gives rise to a positive sign for a bond-bond cross term between adjacent bonds. For nonadjacent bonds, it is easy to generalize the earlier interpretation, with the result that, in any conjugated system, f_{ij} must be positive or negative according to whether i and j are separated by an even or odd number of bonds. According to this law, f_{13} must be negative, in agreement with experiment. As a conclusion, it can be stated that the generality of the law derived above results from the fact that the σ-bonds are taken into account as well as the π-bonds for determining the sign of f_{ij}.

TABLE I.

	f_1	f_2	f_θ	f_{12}	f_{13}	g_e
ClHgBr	2.13	1.90		+0.2		
BrHgI	1.78	1.51		+0.2		
H_2O	8.43[a]		0.77	−0.10		+0.25
H_2S	4.01		0.43	−0.03		+0.20
F_2O	4.26		0.69	+1.1		+0.38
C_2N_2	17.29	6.75		+0.40	−0.30	

[a] D. M. Dennison, Revs. Modern Phys. **12**, 175 (1940).

In the Table I, we show how the force constants (expressed in 10^5 dynes/cm) are associated in the different molecules here studied.

An extended account of this work, including the study of the bond-angle interactions, is now in preparation.

We are grateful to Dr. E. K. Plyler for the infrared results for $HgCl_2$.

[11] A. Langseth and C. K. Møller, Acta Chem. Scand. **4**, 725 (1950).

[12] C. A. Coulson and H. C. Longuet-Higgins, Proc. Roy. Soc. (London) **A193**, 456 (1948).

[13] C. A. Coulson, *V. Henri Mém. Vol.* (Desoer, Liège, 1948), p. 15.

Metal-Solution Potentials of Nickel in Foreign Ion Solutions*

D. MacGillavry, J. J. Singer, Jr.,†‡ and J. H. Rosenbaum§||
Department of Chemistry of Clark University, Worcester, Massachusetts

(Received May 21, 1951)

Metal-solution potentials of nickel in foreign ion solutions were investigated. It was found that nickel may show stationary potentials in potassium hydroxide and phosphate buffer solutions, if oxygen was excluded. The stable potentials were reversible with respect to a change of pH. It was noted that nickel was unable to displace hydrogen from a 0.1 M phosphoric acid solution; nickel dissolved only on admission of air. The possibilities of interpreting the observed potentials are discussed.

AN investigation is in progress concerning the phase boundary potentials of inert metals in contact with electrolyte solutions initially free from common ions. In case a solution cannot be kept entirely free from common ions of the electrode metal, the conditions of interest in this work are those where the common ion concentration remains insignificantly small. In view of the marked corrosion resistance of nickel in alkaline media, it was considered probable that stable foreign ion half cells of this type could be realized with nickel, provided suitable precautions are taken and proper experimental techniques are used.

In connection with corrosion research, potential measurements have been published for nickel and other metals brought in contact with solutions of foreign ion salts. During an actual corrosion process, measurable concentrations of common ions go into solution. Many measurements refer to such systems where this may have occurred to a considerable extent. Various theories have been proposed for the behavior of the potentials observed under the rather diverse experimental conditions used. Gatty and Spooner[1] give a list of many electro-chemical equilibria which must be considered and which *a priori* could lead to the establishment of the observed electrode potentials.

The aim of this investigation is a potentiometric study under very carefully controlled conditions of the very early stages of corrosion in order to find ways if possible of preventing its onset. This approach led to the question whether, for a foreign ion system of a relatively inert metal like nickel, conditions might be found under which the solution would remain practically free from common ions over more extended periods.

The literature on potential measurements of such foreign ion systems where all disturbance is avoided to the utmost is not very extensive. The behavior of mercury was subjected to a thorough investigation by Erdey-Gruz and Szarvas.[2] They measured the mercury potentials in many electrolyte solutions at several concentrations in the range 0.001 N to 5.0 N. Their investigation is outstanding on account of their very careful and refined techniques. In a recent investigation by El Wakkad and Salem[3] mercury was brought in contact with a number of buffer solutions covering a wide pH range. Their findings show an interesting dependence of the mercury potentials on the pH of the buffers; this dependence consists of two linear sections with somewhat different slopes separated by a peculiar break at about pH=5.

About solid metals in foreign ion solutions, the literature is more scattered. In 1930 Schmid and Winkelmann[4] published measurements for several inert metals. They claimed that foreign ion systems of solid metals may possess definite and reproducible potentials, and that the anions are absorbed at the boundary. Since then, several other investigations[5] have been published. Tourky and El Wakkad[6] studied the potentials of copper in a set of buffer solutions. Colombier[7] published data for nickel in solutions containing nickel and sodium sulfate.

* This paper was presented in part before the General Meeting of the Division of Physical and Inorganic Chemistry of the American Chemical Society, Chicago Meeting, September, 1950.

† The apparatus described here is fully explained in the dissertation submitted in partial fulfillment of the requirements for the degree of Doctor of Philosophy, Clark University, 1949.

‡ Present address: Bersworth Chemical Company, Framingham, Massachusetts.

§ The major part of the experimental work is taken from the dissertation submitted in partial fulfillment of the requirements for the degree of Doctor of Philosophy, Clark University, 1950.

|| Present address: Naval Powder Factory, Indian Head, Maryland.

[1] O. Gatty and E. C. R. Spooner, *The Electrode Potential Behaviour of Corroding Metals in Aqueous Solutions* (Oxford University Press, Oxford, England, 1938), p. 56.

[2] T. Erdey-Gruz and P. Szarvas, Z. physik. Chem. **177A**, 277 (1936).

[3] S. E. S. El Wakkad and T. M. Salem, J. Phys. and Coll. Chem. **54**, 1371 (1950).

[4] A. Schmid and W. Winkelmann, Helv. Chim. Acta, **13**, 304 (1930).

[5] S. Bodforss, Z. physik. Chem. **160**, 141 (1932); O. Essin and M. Lozmanova, Z. physik. Chem. **167**, 209 (1933); O. Essin and T. Beklemyschewa, J. Phys. Chem. **39**, 371 (1935); I. L. Orestov, J. Phys. Chem. U.S.S.R. **9**, 283 (1937), J. Phys. Chem. U.S.S.R. **11**, 871 (1938), Nature **136**, 442 (1935), Bull. univ. état Asie centrale, No. **22**, 177 (1938); I. M. Kolthoff and C. Wang, J. Phys. Chem. **41**, 539 (1937); Y. A. Boltunov, J. Gen. Chem. U.S.S.R. **7**, 2831 (1937); M. Loshkarev, J. Phys. Chem. (U.S.S.R.) **12**, 156 (1938); I. P. Markovko and E. W. Zmacinsky, Compt. rend. acad. sci. U.R.S.S. **17**, 211, 213 (1937); R. Rius and R. de Castro, Anales real Soc. espan. fis. y quim. Ser. B. **44**, 1157 (1948).

[6] A. R. Tourky and S. E. S. El Wakkad, J. Chem. Soc. 740, 749 (1948).

[7] L. Colombier, Compt. rend. **199**, 273, 408 (1934); "Étude de la passivité du nickel," Publications scientifiques et techniques du Ministère de l'Air (Gauthier Villars, Paris, France, 1935).

CONSIDERATIONS OF EXPERIMENTAL TECHNIQUE

In order to realize stable foreign ion systems with nickel, it appeared advisable to eliminate oxygen from the half cells. By itself, nickel shows little tendency at room temperature to send its ions into solution. This may be deduced from the apparent failure to measure and reproduce the standard potential of nickel. Summarizing the literature, Latimer[8] has stated: "A truly reversible equilibrium appears to be practically unattainable." This would be attainable if nickel had a measurable solution pressure, not inhibited by some retarding mechanism.

In the presence of oxygen, nickel might easily become oxidized at the surface. It is to be feared that surface oxides, once formed, would interact with the electrolyte solution and in this way would dissolve. Thus, this mechanism would provide another way by which common ions of nickel might go into solution, even though nickel has no measurable solution pressure. Then, the formation of surface oxides was found by us to shift the measured potentials very rapidly in the more positive direction up to several decivolts.

To prevent this or any other interference by oxygen, the nickel samples were freed from oxygen and oxides by heating with high frequency induction in pure hydrogen. This treatment was followed by a complete degassing by heating in a high vacuum. The solutions were freed from oxygen before making contact with the nickel. Since the internal resistance of the more concentrated foreign ion half cells was relatively low, it is easily seen, that the use of a galvanometer as a null point instrument would be inadvisable for measuring the potentials for the following reason. Any current passing through such cells would not merely cause concentration polarization to a varying degree, but could have more disturbing effects as well, especially in case of anodic polarization. In the first place, nickel ions might dissolve and in the second place oxygen might be evolved or surface oxides might be formed.

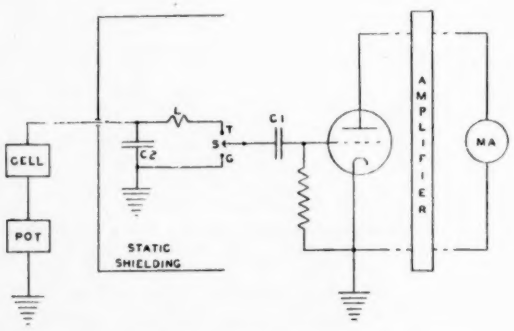

FIG. 1. Principle of the Coleman electrometer employing capacitive input coupling.

As mentioned, this would shift the potentials very markedly. In any event the passage of a continuous current would cause a measurable degree of electrolysis and the products so formed would unavoidably change the nature of an otherwise stable foreign ion cell. This type of polarization would most probably be irreversible.

In order to prevent any irreversible chemical polarization, a vacuum tube electrometer with capacitive input coupling was selected as the null point instrument. Capacitive input coupling was preferred for the study of foreign ion half cells, since a condenser effectively blocks any continuous current that might otherwise flow through the cell. Erdey-Gruz[2] used a binant electrometer for measuring the potentials of mercury-foreign ion cells.

APPARATUS AND EXPERIMENTAL PROCEDURE

The electric potentials were measured with a Leeds and Northrup type K-2 potentiometer and a Coleman Model 3-A electrometer as a null point indicator. The principle of the electrometer employing capactitive input coupling is shown in Fig. 1. The nickel electrodes were always connected directly to the high impedance input terminal of the electrometer. Thus, only this lead had to be highly insulated, the calomel cell and the potentiometer being on the ground side. Shielded cable was used for long connections. The reference electrode was a 1 N KCl calomel electrode, its potential at 30.0°C as taken from Glasstone[9] is +0.2798 volt.

With later runs the potentials were measured with a Philips electrometer. This instrument was described by van Hengel and Oosterkamp[10] and employs a dynamic condenser for coupling the input. The very small apparent input capacity is of the order of 40 pF. The measurements gave the same values using either instrument as null point indicator.

Two series of foreign ion systems of nickel were investigated, one series with potassium hydroxide solutions and another series with potassium phosphate buffers. The solutions were prepared by dissolving reagent grade chemicals of highest available purity in water redistilled from acid permanganate solution. The solutions were freshly prepared before each run. Samples, taken from the cell on completion of a set of measurements, were analyzed as soon as possible after removal.

The main cell, shown in Fig. 2, was constructed using two 500-ml round bottom flasks connected by a capillary syphon. One flask carried the electrode holders and served as the measuring compartment. The other flask served to introduce and mix electrolyte solutions and then to displace all dissolved oxygen by bubbling through a stream of highly purified nitrogen.

[8] W. M. Latimer, *The Oxidation States of the Elements and their Potentials in Aqueous Solutions* (Prentice-Hall, Inc., New York, 1938), p. 187.

[9] S. Glasstone, *The Electrochemistry of Solutions* (Methuen & Company, Ltd., London, England, 1937), p. 327.

[10] J. van Hengel and W. J. Oosterkamp, Philips Technical Review **10**, 338 (1949).

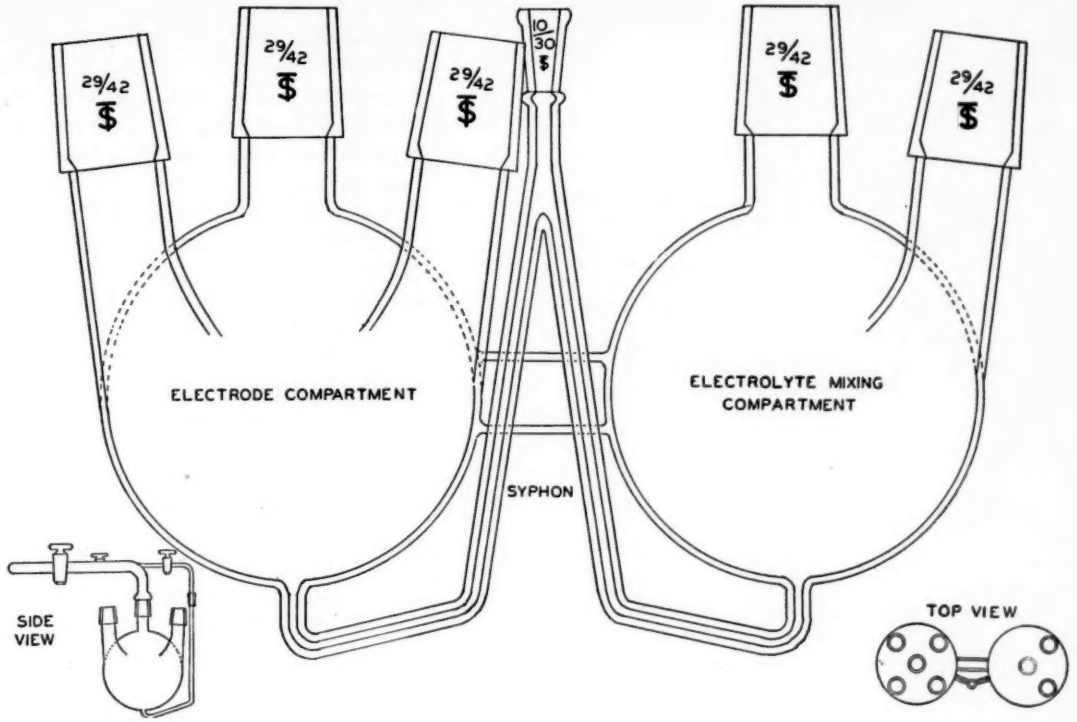

FIG. 2. Main cell.

The nickel samples were 9-cm lengths cut from wire (14 gauge B & S) of highest available purity. The samples were abraded with 2/0 emery cloth, washed with redistilled water, wiped clean with fresh filter paper, mounted in the electrode holders (Fig. 3), and washed successively with redistilled water, redistilled acetone, and redistilled methanol.

After the methanol had evaporated, the electrode holders were mounted on the measuring compartment and the entire system was pumped flat. Next, the system was filled with purified hydrogen and the electrodes were heated to 800–900° for 30 minutes each, while hydrogen continued to flow through the cell, and then the system was pumped flat overnight. After this, the electrodes were heated in a high vacuum at about 1100°C for 30 minutes each, and this was repeated once more. The pressures observed with the induction heater on fell to less than 10^{-5} mm Hg. During the heating in vacuum some of the nickel metal evaporated off, depositing a shiny film on the inside wall of the electrode holder. The various methods for outgassing a metal sample are discussed in detail by Dushman.[11] It appears that the method used here is the best possible one for a solid metal. In several of the runs, one or more of the electrodes were reduced and outgassed longer than the others. The potentials obtained with these electrodes did not differ significantly. The intense heating by induction also insured that the nickel samples were thoroughly annealed and that variations in potential due to inner stresses and strains were improbable.

After the degassing was completed, the vacuum was broken with a stream of purified argon or nitrogen, which entered the main cell through the measuring compartment, flowed through the capillary syphon and left the cell through the mixing compartment. The electrolyte solution was then introduced into the mixing compartment and there thoroughly freed from dissolved oxygen. The gas flow through the syphon effectively prevented any oxygen from diffusing back to the electrodes. When the removal of oxygen was completed, the vent was closed and the solution was syphoned into the measuring compartment. The wire samples were then lowered and partly submerged in the solution. Potential measurements were started immediately after immersion of each sample.

EXPERIMENTAL RESULTS

A first series of measurements was carried out with potassium hydroxide solutions in a pure nitrogen atmosphere. The potentials became steady after several hours, more quickly in the more concentrated solutions and more slowly in the more dilute solutions; in the most dilute solution, 0.00143 M KOH, it took 25 hours. The potential-time curves are represented in Fig. 4.

The measurements were started with the most dilute solution. After the potentials in a solution had remained steady for at least ten hours, the concentration was increased again and measurements resumed. When steady potentials had been obtained for 0.0288 M KOH, hydrogen gas was passed over the solution for 12½ hours. The electrodes became almost 300 mv more negative.

[11] S. Dushman, *Scientific Foundations of Vacuum Technique* (John Wiley and Sons, Inc., New York, 1949).

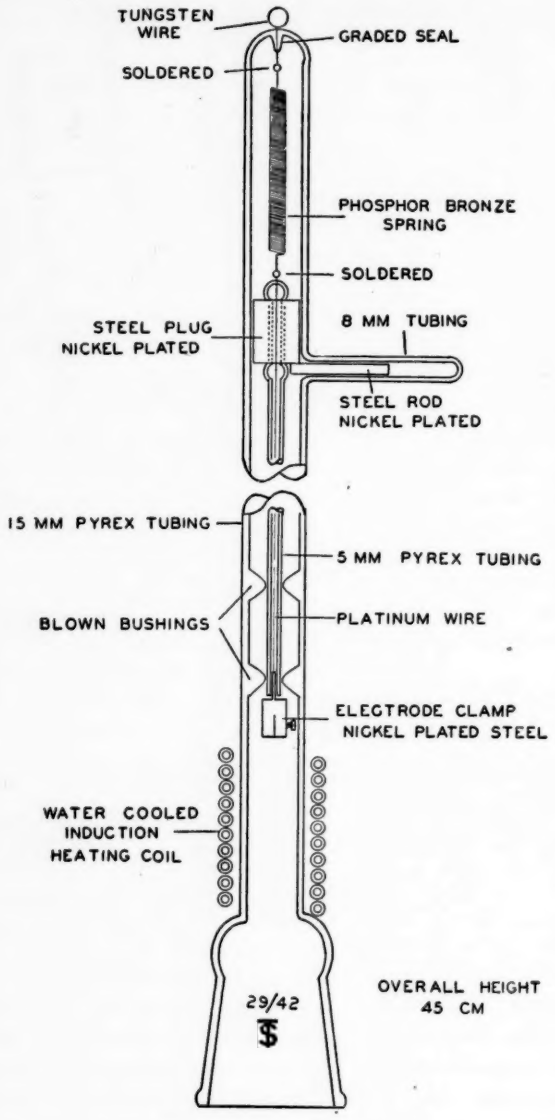

FIG. 3. Electrode holder.

Their last measured values were only 23 mv more positive than the reversible hydrogen potential (−0.745 v). Complete saturation of the solution with hydrogen may not have been obtained, since it was not possible to bubble gas through the solution without some gas entering into the connection to the reference calomel electrode. On account of this, it was not attempted to ascertain whether the last measured potentials would remain stationary or whether the reversible hydrogen potential could be established accurately. Displacing the hydrogen atmosphere with nitrogen did not return the potentials to the initial values observed in nitrogen. The potentials drifted slowly a long time and possibly did not become steady.

The electrodes were cleaned, pretreated, and degassed anew before the next solution, 0.103 M KOH, was measured. Measurements of electrode 2 were started only after 23 hours of immersion. The fact that the final potential became steady and differed by only 10 mv from the final potential of the other electrode is an indication that the electric measuring technique is sufficiently refined and causes no disturbance in the system. After the last solution had been measured, air was admitted to the cell. The potentials rapidly became more positive.

The steady values are plotted against the pH in Fig. 6. The plot¶ approaches a straight line but curves slightly at the highest concentration. The straight portion can be fitted by the equation,

$$E_{\mathrm{KOH/Ni}} = -0.502 - 0.385 \log a_{\mathrm{KOH}} \text{ volt.}$$

The slope 38.5 mv/pH is not in agreement with a behavior according to the Nernst theory. It may be noted also that the intercept of the plot does not correspond to the standard nickel hydroxide potential, −0.660 v, nor to the standard hydrogen-hydroxide potential, −0.828 v (see Latimer[12]).

The second set of measurements was done with a more extended series of phosphate buffer solutions. The phosphate solutions were made up by mixing various volumes of four stock solutions: (a) 0.100 M K_3PO_4, (b) 0.103 M K_2HPO_4, (c) 0.100 M KH_2PO_4, and (d) 0.100 M H_3PO_4. It was possible in this way to change the pH of the phosphate solutions over a wide range and to keep the total phosphate concentration constant at 0.100 M. Purified argon was used as the inert gas atmosphere and in two cases pure nitrogen was used also.

A few typical potential-time curves are shown in Fig. 5. It is seen that during the first few hours, the potentials are drifting. After a while the drifting comes to a stop; the potentials attain steady values or may fluctuate slightly about final values. The initial drifting is quite marked with the alkaline solutions. In the acid solutions the initial potentials are already quite close to the final steady potentials.

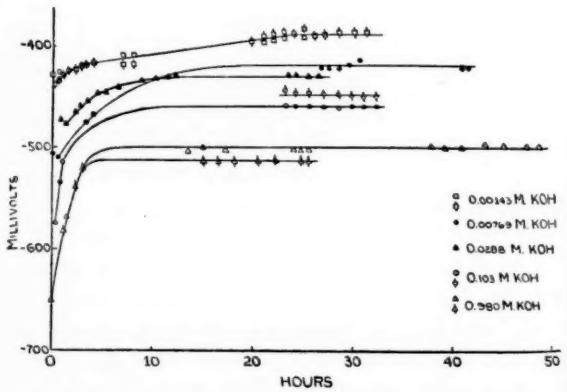

FIG. 4. Potential-time curves of nickel in KOH solutions.

¶ The pH values were taken equal to $14 - \log a_{\mathrm{KOH}}$. No distinction was made between the activities of the OH^- ions and the mean activities (see reference 16) for KOH. It was considered that the differences would be smaller than the experimental errors even for the fairly concentrated solutions.

[12] See reference 13, p. 28.

The stationary potentials of the systems, 0.100 M phosphate/Ni in argon, are plotted against the pH in Fig. 6 together with the steady potentials for the half cells KOH/Ni in nitrogen. The curve of the phosphate potentials is divided into three sections. On the acid side, the plot approaches a straight line with a slope of 44 mv/pH. In the slightly alkaline region the curve appears to be very flat, but is less well defined because of the poorer reproducibility of the electrode potentials in that region (see Fig. 5). On the highly alkaline side, the points appear to fall again on a straight line. The slope of this section is about the same as on the acid side, but may prove to be not identical. The slope is not as precisely known since the range of the highly alkaline solutions was not very extended. It is noteworthy that in any case the slopes of the apparently straight portions do not correspond to the slopes possible for systems obeying the Nernst theory, but rather lie in between the values of RT/nF for $n=1$ and $n=2$.

In order to demonstrate that this complex behavior is real and not illusory, three individual series of measurements were taken. In Table I, all the steady potentials of the individual electrodes of the three runs are tabulated in chronological order as measured. The results of the three runs are mutually consistent. Neither the order nor the direction, whether from high to low pH or from low to high pH, appears to have any influence on the results. Therefore, it seems that the stationary potentials may be considered to be stable potentials which are not subject to further variations, unless the nature of the half cells is changed by drastic means.

After the potentials of the nickel electrodes in the pH 7.15 phosphate solution had become constant in the argon atmosphere, nitrogen was bubbled through the solution for ten hours. The potentials became slightly less negative; these values are listed in the table between brackets. Next the solution was changed to a new pH 6.50. When the steady values in nitrogen had been

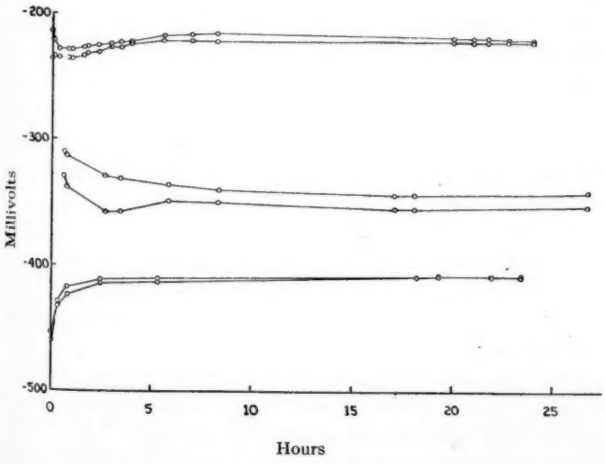

FIG. 5. Potential-time curves of nickel in 0.100 M phosphate solutions. *A*, pH 4.40, 0.100 M KH_2PO_4; *B*, pH 7.15, 0.020 M KH_2PO_4+0.080 M K_2HPO_4; *C*, pH 12.4, 0.100 M K_3PO_4.

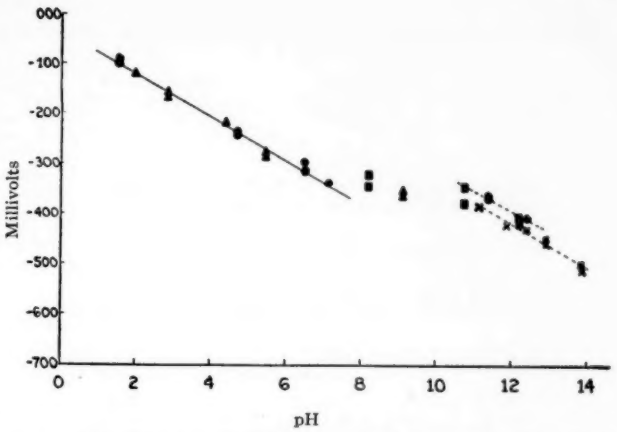

FIG. 6. Stationary potentials of nickel in potassium hydroxide and in 0.100 M phosphate solutions as a function of pH.

○ Run XI
□ Run XII } with 0.100 M phosphate solution
△ Run XIV
× Run 4 and 5 with KOH solutions.

reached, nitrogen was displaced by argon. The potentials became 15–20 mv more negative. Thus, there seems to be a significant difference between the potentials in nitrogen and in argon, just larger than the experimental error, argon giving values which are 10–20 mv more negative. Krueger and Kahlenberg,[13] using nitrogen and argon atmospheres, measured the potentials of nickel and found differences of 66 and 52 mv in 1 N KCl and 1 N KOH respectively.

At the end of Run XI, when the nickel potentials in 0.10 M H_3PO_4 had become constant, air was admitted to the cell. The potentials rose rapidly to more positive values and became unsteady. It was noticed that corrosion took place, as evidenced by a blackening and roughening of the surface, and that it proceeded from the solution-air interface a short distance downward. There was also some pitting on the surface of the nickel electrodes. A considerable nickel ion concentration was found in solution after two days exposure to air. This behavior is evidence that oxygen is necessary for the corrosion of nickel to take place in acid solution. That this corrosion does take place in aerated acid solutions, including KH_2PO_4 solutions, was reported in the literature cited in Uhlig's *Corrosion Handbook*[14] and by Swenson.[15]

DISCUSSION

The results confirm the expectations that with proper precautions stable foreign ion half cells of nickel can be realized and that steady metal-solution potentials can be attained. This proved true not only for combina-

[13] A. C. Krueger and L. Kahlenberg, Trans. Am. Electrochem. Soc. **58**, 107 (1930).

[14] H. H. Uhlig, *Corrosion Handbook* (John Wiley and Sons, Inc., New York, 1948), p. 258.

[15] R. W. Swenson, thesis, Clark University, Worcester, Massachusetts (1949).

TABLE I.

Composition	pH	Stationary potentials of nickel samples 1	2	3	4
Run XI ○ ($R-D$, 97)					
0.100 M K_3PO_4	12.4			−0.408	−0.409
0.068 M K_2HPO_4, 0.033 M K_3PO_4	11.35			−0.365	−0.371
0.020 M KH_2PO_4, 0.080 M K_2HPO_4	7.15			−0.352	−0.341
				(−0.339)	(−0.339)
0.057 M KH_2PO_4, 0.043 M K_2HPO_4	6.50		(−0.278)	(−0.296)	(−0.300)
			−0.298	−0.315	−0.318
0.098 M KH_2PO_4, 0.002 M K_2HPO_4	4.70		−0.236	−0.238	−0.247
0.085 M H_3PO_4, 0.015 M KH_2PO_4	1.55	−0.088	−0.1016	−0.091	−0.089
Run XII □ ($R-D$, 111)					
0.100 M K_3PO_4	12.2	−0.422	−0.409		
0.092 M K_2HPO_4, 0.012 M K_3PO_4	10.75	−0.381	−0.350		
0.003 M KH_2PO_4, 0.097 M K_2HPO_4	8.22	−0.346	−0.323		
0.100 M K_3PO_4	12.2	−0.424	−0.407		
Run XIV △ ($R-D$, 132)					
0.100 M KH_2PO_4	4.40	−0.223		−0.221	
0.050 M H_3PO_4, 0.050 M KH_2PO_4	2.00	−0.120		−0.120	
0.009 M H_3PO_4, 0.091 M KH_2PO_4	2.85	−0.166		−0.160	
0.093 M KH_2PO_4, 0.007 M K_2HPO_4	5.46	−0.286		−0.280	
0.104 M K_2HPO_4	9.10	−0.364	−0.347	−0.357	

tions with alkaline phosphate solutions as anticipated, but also in acid phosphate solutions, if air was excluded at all times. Under these conditions the tests for the presence of nickel in solution always gave negative results. All this lends further support to the view, that at ordinary temperatures the solution pressure of nickel is not operative. Thus, nickel by itself under the conditions of the experiment was unable to displace hydrogen from the solutions used. This was true even for the 0.1 M phosphoric acid solution, although the probable place for nickel in the electromotive force series is below hydrogen.[8]

The measurements of duplicate samples showed the degree of reproducibility obtainable. It was mentioned also that the nickel potentials were reversible with respect to a change of pH. The same potentials could be obtained either from the higher pH side or from the lower pH side. Thus, the question arises by which mechanisms these potentials are established, if the equilibrium $Ni \rightleftharpoons Ni^{++} + 2e$ is inhibited.

An interpretation of the nickel potentials in terms of an oxygen electrode is improbable. Everything possible was done to keep oxygen out. Only water itself could have been a source of oxygen. If this had been so, then even small amounts set free would have made the potentials much more positive.

Redox potentials, which would be dependent on two kinds of potential determining ions, an oxidized form and a reduced form, are not very probable in case of nickel in contact with hydroxide or phosphate solutions.

For the KOH/Ni systems, Table II shows data allowing a quantitative discussion of the various possible equilibria involving Ni^{++}, H^+, or OH^- ions. The reversible $Ni(OH)_2$ potentials and the reversible H_2 potentials for a pressure of 1 atmos are calculated from the KOH activities. Mean ionic activity coefficients were taken from MacDougall,[16] and the standard potentials were taken from Latimer. Obviously, the calculated potentials do not correspond to the ones observed.

A comparison of the observed potentials with those of the standard nickel and standard hydrogen electrode permitted the calculation of the nickel ion concentrations and hydrogen pressures respectively, that should be expected according to the Nernst theory. The former vary from $10^{-4.7}$ to $10^{-8.8}$ gram atoms/liter, while the latter vary from $10^{-9.4}$ to $10^{-11.2}$ atmosphere. It is noteworthy that the nickel ion concentrations calculated in this way came out larger than the nickel hydroxide solubility product would permit for the respective solutions, and that they also reach the lower limit of the dimethyl-glyoxime test (10^{-5} molar), which was negative in all cases. An interpretation in terms of a reversible nickel electrode thus would lead to serious contradictions. The calculated hydrogen pressures are insignificantly small, and even if real would not well be potential determining, as Haber[17] explained.

In Table III various potentials and concentrations are calculated for the 0.1 M phosphate/Ni systems of Run XI with the aid of the observed values and the reversible standard potentials taken from Latimer. The calculated hydrogen pressures vary widely, while the nickel ion concentrations reach values which are impossible ($10^{5.3}$ gram atoms/liter), especially since no nickel ions were actually found in solution.

[16] F. H. MacDougall, *Thermodynamics and Chemistry* (John Wiley and Sons, Inc., New York, 1939), p. 404.
[17] F. Haber, Z. Elektrochem. **10**, 433, 773 (1904).

TABLE II. Nickel in KOH solutions.

[KOH] M	Log a_{KOH}	Potentials in nitrogen observed volts	Analysis $Ni(OH)_2/Ni$ electrode calculated volts	Hydrogen electrode calculated volts	Log [Ni^{++}] calculated	Log $P(H_2)_{atmos}$ calculated
0.00143	−2.862	−0.386	−0.488	−0.670	−4.6	−9.4
0.00769	−2.156	−0.422	−0.530	−0.712	−5.7	−9.7
0.0288	−1.608	−0.430	−0.563	−0.745	−6.0	−10.5
0.103	−1.080	−0.455	−0.595	−0.775	−6.8	−10.6
0.980	−0.138	−0.506	−0.652	−0.833	−8.6	−11.0

In order to arrive at an interpretation of the potentials observed under the carefully controlled conditions, it may be noted that the dependence on pH shows several aspects of interest. The curve for the phosphate potentials is seen to have two breaks. The section between the two breaks shows poorer reproducibility and thus seems to be less well defined. Then, the slopes of the well defined sections, which appear to be very straight, do not agree with the slopes possible for reversible, unpolarizable electrodes obeying the Nernst theory. The values of the slopes of 30°C are in between the values of $RT/F=0.060$ and $RT/2F=0.030$ volt/pH. The pH values were checked with a Beckman pH meter.

Although there is a strong dependence of the potentials on the pH values of the solutions, enough measurements are available to indicate that the other anions in solution also contribute to the observed potentials. For the same pH values on the alkaline side, the differences between the potentials for the hydroxide and for the phosphate cells is about 20 mv, which is definitely larger than the experimental error in this range. Hence, our results are an indication that other ionic species besides the hydroxyl ions may also influence the potentials.

The well-known unpolarizable electrodes could not give these peculiar results. It appears, therefore, that another interpretation must be sought. The alternative appears to call for the consideration of some form or forms of polarizable electrodes. An analysis of the properties of both types of electrodes will be given in another publication. Mercury-solution systems often behave like completely polarizable electrodes. The factors favoring complete electric polarizability of the mercury-solution interphase have been examined by Craxford.[18] He concluded that "the interphase between mercury and a solution containing no mercurous ions approximates to the completely polarizable interphase over the potential range $E_{N-cal.}=0.0$ to -1.3 volt." As is evident from the theory explaining the electrocapillarity of mercury, as given by Koenig[19] and developed further by Grahame,[20] adsorption phenomena play an important role at a mercury-solution interphase under the conditions that it is electrically polarizable.

In so far as the scope of the data here presented is limited, further work is being planned in order to obtain a better understanding, of the factors influencing the potentials. A few more remarks may perhaps be added with respect to some of the conclusions presented in the literature cited.

Erdey-Gruz and Szarvas,[2] from their investigation of mercury, concluded that the anions are preferentially adsorbed. They apparently took into consideration only physical adsorption in the outer Helmholtz layers. In a recent article El Wakkad and Salem[3] discuss the potentials of mercury in contact with solutions initially free from mercury ions. They used a series of buffer solutions covering a wide pH range. The graphs of the potentials plotted against the pH of the buffers are analogous to a curve found for copper by Tourky and El Wakkad.[6] In every case there are two breaks. The midportion of the mercury curves is narrow and also the midportion of the curve for copper is fairly narrow.

It is claimed that under certain conditions cuprous oxide is formed on the copper. The formation of mercury oxides is taken into consideration in the case of mercury. In the case of nickel, oxide formation in the absence of oxygen is not indicated, since atmospheric oxygen getting into nickel half cells has such a marked effect on the potentials.

In this connection the analysis of Grahame[20] is of interest. Grahame discusses the chemisorption of anions in the inner Helmholtz layer at a mercury surface. This effect is pronounced on the positive side of the electro-capillary maximum.

Although it is not yet possible to offer a detailed

TABLE III. Nickel in 0.100 M phosphate buffers.

	Analysis of Run XI				
pH	Potentials in argon observed volts	$Ni(OH)_2/Ni$ electrode calculated volts	Hydrogen electrode calculated volts	Log [Ni^{++}] calculated	Log $P(H_2)_{atmos}$ calculated
12.4	−0.409	−0.564	−0.745	−5.3	−11.2
11.35	−0.368	−0.501	−0.682	−3.9	−10.5
7.15	−0.345	−0.248	−0.430	−3.0	−3.0
6.50	−0.316	−0.209	−0.391	−2.5	−2.5
4.70	−0.242	−0.101	−0.282	+0.3	−1.4
1.55	−0.090	+0.089	−0.093	+5.3	−0.1

[18] S. R. Craxford, Trans. Faraday Soc. **36**, 85 (1940).
[19] O. Koenig, J. Phys. Chem. **38**, 111, 339 (1934).
[20] D. C. Grahame, Chem. Revs. **41**, 441 (1947).

explanation for the measured nickel potentials, it is of interest that on the highly alkaline side the curves for the phosphate and for the hydroxide solutions are close together, although they are not identical. This could be an indication that chemisorption of hydroxyl ions is a major factor not only in the hydroxide solutions but as well in the alkaline phosphate solutions. Grahame pointed out that the properties of the hydroxyl ions at the mercury-solution interphase are different from those of the other anions. However, this picture is very tentative and work in this field will be continued.

ACKNOWLEDGMENTS

The authors wish to express their sincere appreciation to the ONR for the support of this investigation under contract N7onr-464, T.O.I.

The authors are grateful to Dr. R. C. Gunter, Jr., for arranging the loan of the induction heating apparatus and for his help in adapting it for use in this research.

They wish to thank also Mr. F. W. Grant, Jr., and Mr. P. R. Skogstrom for assisting with the tests of the phosphate solutions.

Placement Register

The American Institute of Physics will conduct a Placement Service Register in connection with its 20th Anniversary Meeting in Chicago, Illinois, October 23–27, 1951, at the Hotel Sherman. Records of physicists seeking positions and descriptions of open positions will be available for inspection. Interviews will be arranged between registants and employer representatives who are present. Employers should send to the Institute descriptions of openings which they wish to have posted on $8\frac{1}{2}\times 11$ paper in multiple copies (15 required), or post them upon arrival at the meeting. Registrants seeking jobs should apply to the Institute for registration forms and further information by mail. In order to insure its inclusion at this Register, all material must be received at the Institute office, 57 East 55th Street, New York 22, New York, by October 1, 1951.

Letters to the Editor

THIS section will accept reports of new work, provided these are terse and contain few figures, and especially few half-tone cuts. The Editorial Board will not hold itself responsible for opinions expressed by the correspondents. Contributions to this section should not exceed 600 words in length and must reach the office of the Editor not later than the 15th of the second month preceding that of the issue in which the Letter is to appear. No proof will be sent to the authors. A publication charge of $10.00 per Letter is made which, when honored, will entitle the Institution to 100 free reprints.

On Gibbs' Theory of Surface Tension

TERRELL L. HILL
Naval Medical Research Institute, Bethesda, Maryland
(Received March 6, 1951)

IT would appear that the objections of Guggenheim[1] to Gibbs' discussion of curved surfaces can be removed by *starting* with *macroscopic* independent variables only, avoiding Gibbs' immediate introduction of a dividing surface. Consider a one-component, two-phase system (in complete equilibrium) with N molecules in the region $ABCD$ (Fig. 1) of a spherical cone of solid angle ω. Then, it follows that

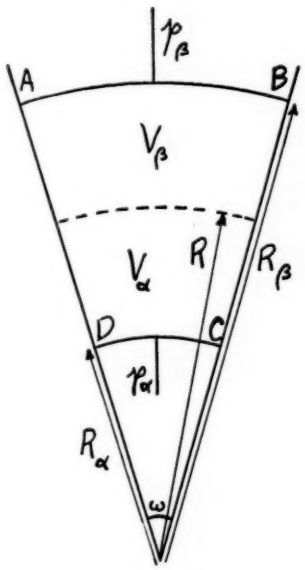

FIG. 1. One-component, two-phase equilibrium in the region $ABCD$ of a spherical cone. The inside and outside pressures are p_α and p_β, respectively.

$$dA=-SdT-p_\beta\omega R_\beta^2dR_\beta+p_\alpha\omega R_\alpha^2dR_\alpha+\sigma d\omega+\mu dN, \qquad \sigma\equiv(\partial A/\partial\omega)_{T,R_\alpha,R_\beta,N}. \tag{1}$$

On integration we obtain

$$\sigma\omega=A-\mu N. \tag{2}$$

Now a dividing surface is introduced at R, defining V_α, V_β (Fig. 1), and an area $\mathfrak{A}$:

$$V_\alpha=\omega(R^3-R_\alpha^3)/3, \tag{3}$$
$$V_\beta=\omega(R_\beta^3-R^3)/3, \tag{4}$$
$$\mathfrak{A}=\omega R^2. \tag{5}$$

On taking differentials of both sides of Eqs. (3)–(5), solving for dR_α, dR_β, and $d\omega$ in terms of dV_α, dV_β, $d\mathfrak{A}$, and dR, and substituting these expressions into Eq. (1), we find, using Eq. (2),

$$dA=-SdT-p_\alpha dV_\alpha-p_\beta dV_\beta+\gamma d\mathfrak{A}+CdR+\mu dN, \tag{6}$$

where the symbols γ and C represent the expressions

$$\gamma\equiv(p_\alpha V_\alpha+p_\beta V_\beta-\mu N+A)/\mathfrak{A}, \tag{7}$$
$$C\equiv\omega R^2(p_\alpha-p_\beta)-2\omega\gamma R. \tag{8}$$

Gibbs starts essentially with Eq. (6) (and must impose an *additional* condition of mechanical equilibrium already taken care of here by Eq. (8)).

In Eqs. (6)–(8), S, p_α, p_β, A, and μ are of course determined by given values of T, R_α, R_β, ω, and N, but V_α, V_β, and $\mathfrak{A}$, and hence also, γ and C, depend in addition on the choice of dividing surface, (R).

For a fixed dividing surface condition or recipe, R may be regarded as a function of T, V_α, V_β, $\mathfrak{A}$, and N; and hence, the term CdR in Eq. (6) can be eliminated, giving

$$dA=-(S-C\partial R/\partial T)dT-(p_\alpha-C\partial R/\partial V_\alpha)dV_\alpha -(p_\beta-C\partial R/\partial V_\beta)dV_\beta+(\gamma+C\partial R/\partial\mathfrak{A})d\mathfrak{A}+(\mu+C\partial R/\partial N)dN,$$

which is valid for *any* dividing surface condition. Alternatively, Gibbs eliminates CdR by choosing the *particular* condition $C=0$, calling the dividing surface so obtained the "surface of tension"; that is, from Eq. (8),

$$2\gamma/R=p_\alpha-p_\beta \quad (C=0) \tag{9}$$

can be used as a condition for locating the surface of tension.

Introducing the surface excess N^s with respect to the dividing surface, Eq. (6) becomes in the usual way

$$\mathfrak{A}d\gamma=-N^sd\mu+CdR \quad (T \text{ const}) \tag{10}$$
$$=-N^sd\mu \quad (T \text{ const}, C=0), \tag{11}$$

where C in Eq. (10) is of course given by Eq. (8). Equation (11) is an alternative condition for locating the surface of tension.

Tolman[2] has published a quasi-thermodynamic condition for locating the surface of tension, his Eq. (12.7), to which there are objections. First, his "local pressure" should be replaced[3] by $\rho(\mu-A)$, where ρ is the local mean density and A is the local mean Helmholtz free energy per molecule. Second, the dependence of p_α, p_β, and $\rho(\mu-A)$, ~~where ρ is the local mean density and A is the local mean Helmholtz free energy per molecule. Second, the dependence of p_α, p_β, and $\rho(\mu-A)$~~ on R was neglected by Tolman. Actually, it is easy to show that Tolman's condition, corrected, reduces to Eq. (11).

Details will be published later in the first of a series of papers[4] on the thermodynamics and (approximate) statistical mechanics of the transition region between two phases, with plane (including $p_\alpha\neq p_\beta$) and curved (including very small drops and bubbles) interfaces, and one or more components.

Note added in proof: Professor Frank P. Buff has kindly pointed out to the writer that he has discussed the thermodynamics and statistical mechanics of curved interfaces in a paper presented at the American Physical Society meeting in Pittsburgh (March 8–10, 1951), and which is to be published. In particular, by a different method, he obtained Eqs. (8) and (10). These equations were originally utilized to obtain the important special case of Eq. (10), $\Gamma=0$, in a note published by Buff and Kirkwood, J. Chem. Phys. **18**, 991 (1950).

[1] E. A. Guggenheim, *Thermodynamics* (North Holland Publishing Company, Amsterdam, 1949).
[2] R. C. Tolman, J. Chem. Phys. **16**, 758 (1948).
[3] This change should be made throughout Tolman's paper, including his expressions for γ for plane and curved surfaces.
[4] The present note is a condensation of the paper submitted. The full paper will be published in J. Phys. and Colloid Chem. See also T. L. Hill, J. Chem. Phys. **19**, 261 (1951).

Anomalous X-Ray Diffraction Spectra in Graphite

JOSEPH S. LUKESH
Knolls Atomic Power Laboratory, General Electric Company, Schenectady, New York*
(Received June 28, 1951)

THE appearance in graphite powder diffraction patterns of weak diffraction spectra which cannot be accounted for on the basis of the classical hexagonal graphite structure has been observed by several investigators.[1–3] These have been interpreted by Lipson and Stokes[3] as being due to a rhombohedral modification which differs from the hexagonal form in the sequence of layer stacking. The classical structure is characterized by a stacking sequence which may be called $ABABAB\ldots$, indicating that alternate layers are structurally equivalent. Lipson and Stokes pointed out that an alternative sequence, $ABCABCABC\ldots$, was also possible and that this led to a rhombohedral cell which

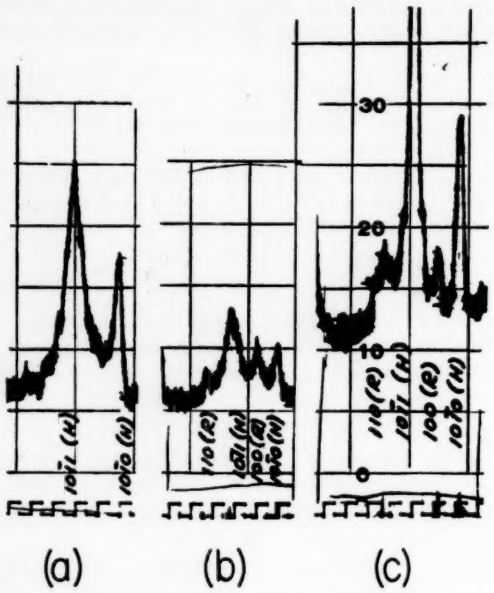

FIG. 1. Portion of spectrometer traces of powder patterns of graphite showing the introduction of new spectra. (a) Purified graphite as received. (b) Same sample after bromine treatment. (c) Natural graphite.

satisfactorily accounted for the observed anomalous diffraction spectra. Recent single-crystal work[4] which has shown the presence of other anomalous spectra which have twofold symmetry and are thus not due to a rhombohedral form,[5] has suggested a restudy of the problem of the origin of the extra lines on powder photographs.

Taylor and Laidler,[2] who first observed the anomalous spectra in x-ray patterns, found that they could be removed by wet oxidizing the graphite for several hours in a mixture of concentrated sulfuric and nitric acids. Purification in a mixture of hydrofluoric and hydrochloric acids, however, had no apparent effect. From this latter observation, they concluded that the extra lines were not due to impurities.

Since the extra x-ray spectra appear to be about as sharp as those from the classical structure, it is evident that there must probably exist domains of the *ABCABCABC*... stacking of the order of one thousand angstroms,[2] or some two to three hundred graphite layers. It is difficult to visualize a chemical process, oxidation or otherwise, which would alter the stacking sequence of a group of that many consecutive layers in an orderly manner. (Since the difference in free energy between the *ABABAB*... and *ABCABCABC*... stacking sequences is very small, selective oxidation of a rhombohedral domain seems improbable.) On the other hand, chemical removal of impurities would be expected to destroy a superstructure caused by such impurities.

In order to test whether the anomalous x-ray spectra could be caused by impurities, experiments have been conducted in which impurity atoms were deliberately introduced into a highly purified graphite. The specimen was made the anode of an electrolytic cell containing a saturated solution of potassium bromide. Power was supplied by a three-cell storage battery. Whether bromine was introduced into the graphite or oxidation occurred is not known at this time. A definite change in structure took place, however, as shown by x-ray diffraction patterns of the graphite before and after treatment. The pattern before treatment showed negligible evidence of the rhombohedral reflections. After the treatment, several new spectra were noted. These included peaks at the positions of all five of the rhombohedral reflections indexed by Lipson and Stokes as 100, 110, 211, 221 and $1\bar{1}1$; 100 and 110 appearing to have been considerably enhanced at the expense of $10\bar{1}0$ and $10\bar{1}1$. (All other rhombohedral spectra are coincident with classical hexagonal reflections.) For the first three the relative intensities, among themselves, are as reported by Lipson and Stokes.[3] However, 221 is much stronger. Portions of the spectrometer curves of the pure graphite before and after bromine treatment as well as that of a natural graphite specimen are reproduced in Fig. 1. The angular region shown corresponds to that illustrated by Taylor and Laidler.[2] The angular differences between peaks illustrated, in degrees 2θ, are listed in Table I.

TABLE I.

Reflections	$\Delta 2\theta$ Natural graphite	Brominated graphite	Calc
$10\bar{1}0$ (hex) → 100 (rhomb)	0°50′	0°50′	0°50′
$11\underline{0}$ (rhomb) → $10\bar{1}1$ (hex)	1°10′	1°10′	1°10′
$10\bar{1}1$ (hex) → $11\underline{0}$ (rhomb)	1°20′	1°20′	1°18′
$10\bar{1}0$ (hex) → $10\bar{1}1$ (hex)	2° 0′	2° 0′	2° 0′
100 (rhomb) → (110) (rhomb)	2°30′	2°30′	2°28′

From these measurements, it is clear that certain of the peaks resulting from the introduction of bromine or through oxidation are in excellent agreement with the anomalous peaks found in natural graphite as well as with those calculated from unit cell constants.

The appearance, after treatment of purified graphite with bromine, of spectra having the same Bragg angle as the rhombohedral spectra observed in natural graphite is suggestive, but not conclusive, of a possible common impurity origin for the two phenomena. The failure of halide acid treatment to remove the lines in natural material even after the graphite has been purified to zero ash might be explained if a volatile impurity remains in the structure, possibly iron chloride, chlorine itself, or an oxide.

In addition to those in the position of the rhombohedral lines, several other anomalous spectra appear after the bromide treatment. These are not accountable on the basis of the rhombohedral cell of Lipson and Stokes. Notable among these are lines at about 27°15′, 38°30′, and 63°30′. Insufficient data have been obtained as yet to allow interpretation of these additional spectra. However, all are increased in intensity by heat treatment of the brominated graphite for one hour at 250°C or on standing at room temperature overnight. Concurrent with the increase in intensity of the reflection at 27°15′ ($d=3.22$ *kx*) is a marked decrease in the intensity of 00.2 of graphite ($d=3.35$ *kx*). This indicates the probable formation of a compound (logically one of the lamellar compounds described by Riley[6]) at the expense of graphite. A point of importance in this connection is that the c_0 spacing of graphite does not measurably change during treatment.

The experimental work so far has been exploratory, and no conclusions can be drawn from it. It can only be stated that the treatment described introduces new spectra in the diffraction pattern, including lines having the same Bragg angle as those indexed as rhombohedral. Further work is in process which, it is hoped, will elucidate the meaning of the various anomalous spectra.

* The Knolls Atomic Power Laboratory is operated by the General Electric Company for the Atomic Energy Commission. The work reported here was carried out under Contract No. W-31-109 Eng-52.

[1] G. I. Finch and H. Wilman, Proc. Roy. Soc. (London) **A155**, 345 (1936).
[2] A. Taylor and D. Laidler, Nature **146**, 130 (1940).
[3] H. Lipson and A. R. Stokes, Proc. Roy. Soc. (London) **A181**, 101 (1942).
[4] Joseph S. Lukesh, Phys. Rev. **80**, 226 (1950).
[5] Joseph S. Lukesh, J. Chem. Phys. **19**, 383 (1951).
[6] H. L. Riley, Fuel Sci. Practice **24**, 8 (1945).

Decomposition of Hydrogen Peroxide by High Energy X-Rays*

EVERETT R. JOHNSON
Chemistry Department, Brookhaven National Laboratory, Upton, New York

(Received June 18, 1951)

DEAERATED, unbuffered solutions of hydrogen peroxide were irradiated with x-rays from a 2-Mev Van de Graaff generator. Doses were determined by Victoreen chambers, and

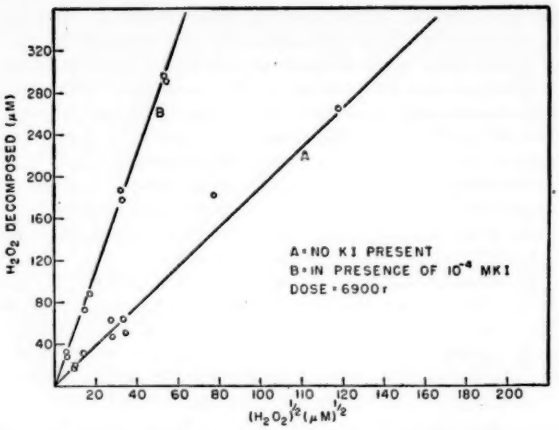

FIG. 1. Decomposition of H_2O_2 as a function of initial concentration.

air-saturated ferrous sulfate solutions (16.7 ± 0.5 μM Fe^{++} oxidized/1000 r). The decomposition was studied by both gas and spectrophotometric analyses. Material balances were usually within 5 percent and no poorer than 7 percent. Over the concentration range investigated ($1 \times 10^{-4} - 12.4 \times 10^{-3}$ M H_2O_2) the decomposition yield, in agreement with Fricke[1] (at a dose rate of 23 r/sec, for a total dose of 6900 r), was proportional to the square root of the initial peroxide concentration (curve A, Fig. 1). In the presence of 10^{-4} M KI the decomposition has the same concentration dependence (curve B, Fig. 1), and the rate is increased 2.43-fold.

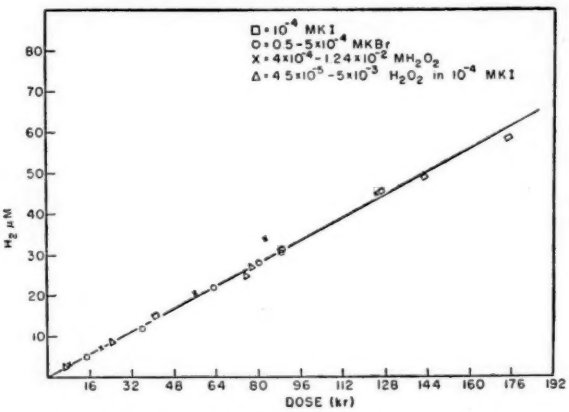

FIG. 2. Hydrogen yield from x-ray decomposition of some dilute unbuffered aqueous solutions.

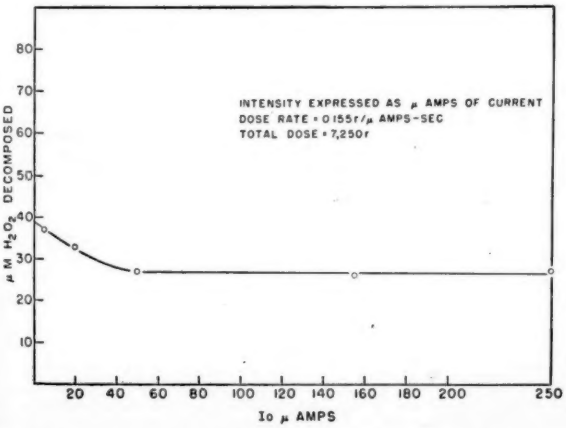

FIG. 3. Decomposition of 3.9×10^{-4} M H_2O_2 as a function of intensity. Dose rate $xI_0 = r$/sec.

The initial slope of the hydrogen yield from irradiation decomposition of hydrogen peroxide solutions is identical with that found by irradiating unbuffered KI, KBr, and KI+H_2O_2 solutions (Fig 2). The hydrogen evolved is believed to arise from the solvent and not the H_2O_2. For a dilute H_2O_2 solution (95 μM) the hydrogen yield is decreased after a dose of 10,000 r, possibly because of competition between the solvent decomposition products (H_2+O_2 or H_2O_2) and the hydrogen peroxide for free radicals (back reaction). The initial yield of hydrogen is 0.35 μM H_2/1000 r, and the ratio of μM Fe^{++} oxidized/1000 r in aerated acid $FeSO_4$ solutions to μM H_2 produced/1000 r in other solutions equals 47.7.

The decomposition of 3.9×10^{-4} H_2O_2 solution was found to be independent of intensity in the range of 3–38.7 r/sec, but below this value the decomposition yield increased with decreasing intensity (Fig. 3).

* Work carried out under the auspices of the AEC.

[1] H. Fricke, J. Chem. Phys. **3**, 364 (1935).

Possible Existence of a Symmetrical O···H···O Hydrogen Bond in Nickel Dimethylglyoxime

L. EDWARD GODYCKI, R. E. RUNDLE, ROGER C. VOTER, AND CHARLES V. BANKS
*Institute for Atomic Research and Department of Chemistry, Iowa State College, Ames, Iowa**

(Received July 6, 1951)

IN connection with a study of selective analytical reagents x-ray and infrared examinations of nickel dimethylglyoxime were made. These researches indicate that the O···H···O hydrogen bonds are unusually short and that vibration frequencies usually attributed to "free" or associated O—H are absent.

Nickel dimethylglyoxime is orthorhombic, space group Ibam, $a_0 = 16.6$, $b_0 = 10.4$, $c_0 = 6.49$A. For $Z = 4$, $\rho_{calc} = 1.63$ *vs* $\rho_{obs} = 1.61$ g/cc.[1] Nickel positions are 000, $00\frac{1}{2}$, $\frac{1}{2}\frac{1}{2}\frac{1}{2}$, $\frac{1}{2}\frac{1}{2}0$, and Patterson projections upon (001) resemble fouriers. The connexity of bonds is, without question, that shown in Fig. 1. The x-ray study has proceeded through one steepest descent refinement[2] and two three-dimensional fourier sections, $\rho(xy0)$. At this state of refinement, which is not final, bond distances are those shown in Fig. 1, and

$$R = \frac{\Sigma \big| \, |F_{obs}| - |F_{calc}| \, \big|}{\Sigma |F_{obs}|} = 0.15,$$

for ($hk0$) data, which include nickel contributions, while it is 0.19 for the first layer line data, which does not. Fourier synthesis indicates that the bonds are probably accurate to about 0.05A. The O···H···O distance, 2.42A, is significantly lower than any heretofore reported.[3]

Infrared spectrophotometric examination of nickel dimethylglyoxime, using both Nujol and perfluorokerosene mulls, reveals no absorption maxima in the range of 2.7 to 4.0 microns which are characteristic of either "free" or normally hydrogen bonded O—H. In dimethylglyoxime itself, the O—H fundamental stretching vibration frequencies give rise to a strong absorption maximum at about 3.1 microns. Dimethylglyoxime-d_2 was prepared by recrystallizing the parent compound from heavy water. A strong O—D absorption was found at about 4.2 microns. The nickel compound was also precipitated from heavy water solutions of dimethylglyoxime-d_2 and anhydrous nickel chloride to obtain ODO bonds, but infrared data indicated no absorption maximum in the region in which these maxima usually occur. The infrared spectra (2 to 26 microns) were carefully scrutinized to see if greatly displaced O···H···O and O···D···O absorption maxima were to be found, analogous to the greatly displaced F···H···F vibration frequencies found by Westrum and Pitzer[4,5] for the

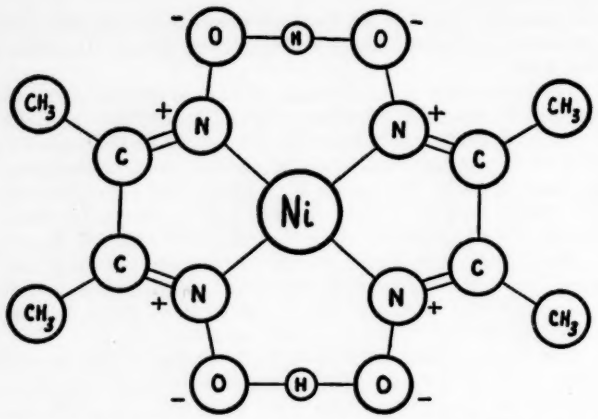

FIG. 1. Nickel dimethylglyoxime. Bond distances, A: Ni–N, 1.87; N–C, 1.27; N–O, 1.34; C–C, 1.50; C–CH_3, 1.50; O–H–O, 2.42.

bifluoride ion where the hydrogen bond is symmetrical. Though several appreciable differences were noted between the spectra of the H and D inner-complex compounds, it appears unwise at this time to make definite statements concerning the possible disposition of any absorption maxima due to O···H···O and O···D···O frequencies.

These two studies suggest that the O···H···O bond is unusually strong, and may well indicate a symmetrical bond (hydrogen in center). Donahue[6] has pointed out that Pauling's rule[7] predicts F···H···F=2.24 for the symmetrical case, *vs* 2.26A observed. The predicted distance for the symmetrical O···H···O bond is 2.32.

A full report of x-ray and infrared studies will be made later.

* Contribution No. 145 from the Institute for Atomic Research and the Department of Chemistry, Iowa State College, Ames, Iowa. Work performed in the Ames Laboratory of the AEC.

[1] Crystals were obtained from nitrobenzene solution but do not have lattice constants reported by M. Milone, Atti congr. intern. chim. 10th Congr. Rome **2**, 346 (1938). It is to be noted that Milone's observed and calculated densities are in severe disagreement.

[2] A. D. Booth, Proc. Roy. Soc. (London) **197**, 336 (1949).

[3] L. Pauling, *The Nature of the Chemical Bond* (Cornell University Press, Ithaca, New York, 1945), p. 311.

[4] E. F. Westrum, Jr., and K. S. Pitzer, J. Am. Chem. Soc. **71**, 1940 (1949).

[5] J. A. A. Ketelaar and W. Vedder, J. Chem. Phys. **19**, 654 (1951).

[6] J. Donahue, presented at American Chemical Society Meeting, Cleveland, April 9, 1951.

[7] L. Pauling, J. Am. Chem. Soc. **69**, 542 (1947).

Adsorption of Carbon Dioxide on a Nickel Single Crystal Using a Radioactive Tracer*

A. D. CROWELL† AND H. E. FARNSWORTH
Physics Research Laboratory, Brown University, Providence, Rhode Island‡

(Received July 13, 1951)

IN previous experiments to measure the amount of gas adsorbed on metal surfaces of known crystal orientation, chemisorption has been studied on evaporated metal films,[1,2] and physical adsorption has been studied on thin slices of a copper single crystal.[3,4] We are reporting some preliminary attempts to measure the amount of gas chemisorbed on a single face of one single crystal. By using C^{14} as a radioactive tracer, it has been possible to determine the amount of CO_2 chemisorbed on metal surfaces with areas of 1 to 2 cm^2. Several measurements have been made on polycrystalline copper, nickel, and silver, and on the (111) face of a nickel single crystal.

The following procedure was used. The specimen was placed in a vacuum chamber through a ground joint which was sealed on the outside edges with DPI Myvawax. The vacuum chamber was separated from the diffusion pumps and all stopcocks by a dry-ice trap as shown in Fig. 1. The specimen was outgassed by baking and by electron bombardment at red heat for many hours at pressures less than 10^{-6} mm Hg. CO_2 containing C^{14} was prepared by the acid method[5] from $BaCO_3$ and was introduced to pressures from 10^{-2} to 10^{-1} mm Hg measured on a Pirani gauge and at temperatures varying from room temperature to 200°C. After several minutes the CO_2 was withdrawn and the specimen was removed and placed before a thin window Geiger counter shielded by lead brick. A metal mask was placed over the specimen so that only the C^{14} on the desired surface was assayed.

The nickel crystal was cut parallel to the (111) crystal planes and the exposed face was polished mechanically and electrolytically and then rinsed in boiling distilled water, resulting in a face of approximately 1.5 cm^2. The crystal was mounted with a molybdenum backing so that during electron bombardment the crystal was not struck directly by electrons. To minimize dust as a factor, the surface was sprayed with distilled water from a clean syringe at the opening of the vacuum chamber just before the crystal was placed within the chamber. As a check on the efficacy of the process, portions of the crystal face were shielded with aluminum foil during counting, so that the distribution of adsorbed gas over the surface could be determined. Measurements showing uneven distribution were rejected.

Preliminary measurements on polycrystalline copper, nickel, and silver indicate that (1) CO_2 is irreversibly adsorbed on copper and nickel in observable quantities; (2) CO_2 is reversibly adsorbed on silver; (3) observable amounts of CO_2 are absorbed in nickel if exposure occurs near 400°C.

Measurable amounts of CO_2 were observed on the nickel crystal, but the results were not reproducible. Counting rates from 10 cpm to 260 cpm[6] were observed over a background of about 30 cpm under the same conditions of pressure and temperature during exposure to the CO_2. The irreproducibility is attributed to a changing surface from measurement to measurement due to

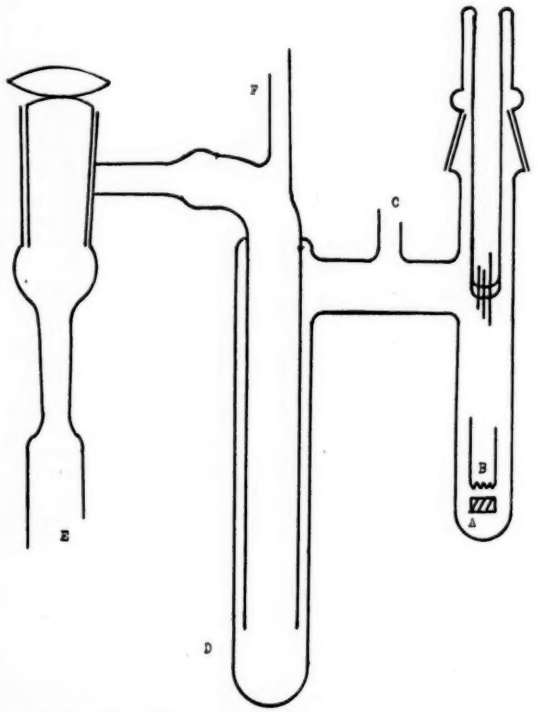

FIG. 1. Schematic diagram showing the position of the vacuum chamber with respect to the rest of the system. The specimen is located at A just below a tungsten filament B. Vacuum gauges are connected at C, and these and the chamber are separated from the rest of the system by dry ice trap D. The system is evacuated through tube E and the CO_2 is admitted and withdrawn through tube F.

exposure to the air during counting. It was observed that the larger readings were usually associated with higher outgassing temperatures during electron bombardment, but beyond this no consistency in the results could be found in spite of extreme care to obtain the same conditions of cleanliness and outgassing each time.

These experiments show that the chemisorption of gases on the small area available on single crystals can be studied by a tracer technique. In future measurements it appears desirable to use a method in which the surface is not exposed to the air between measurements.

* Part of a thesis submitted by A. D. Crowell in partial fulfillment of the requirements for the Ph.D. degree at Brown University.

† AEC Predoctoral Fellow, July 1, 1949, to June 30, 1950. Now at Amherst College, Amherst, Massachusetts.

‡ Assisted by the ONR and Research Corporation of New York.

[1] Beeck, Smith, and Wheeler, Proc. Roy. Soc. (London) **177A**, 62 (1941).
[2] O. Beeck, *Advances in Catalysis*, (Academic Press, New York, 1950). Volume II, 151.
[3] T. N. Rhodin, J. Am. Chem. Soc. **72**, 4343 (1950).
[4] T. N. Rhodin, J. Am. Chem. Soc. **72**, 5691 (1950).
[5] Calvin, Heidelberger, Reid, Tolbert, and Yankwich, *Isotopic Carbon* (John Wiley and Sons, Inc., New York, 1949).

[6] Order of magnitude calculations involving counting efficiency and specific activity of CO_2 indicate that 1 cpm corresponds to 10^{11} adsorbed CO_2 molecules.

The Polarized Infrared Spectrum of Potassium Bifluoride at −185°C*

ROGER NEWMAN AND RICHARD M. BADGER
The Gates and Crellin Laboratories of Chemistry, California Institute of Technology, Pasadena, California†

(Received July 6, 1951)

OBSERVATIONS on the reflection spectrum of potassium bifluoride have recently been reported[1] which appear to confirm the symmetrical linear structure of the bifluoride ion in this crystal. Some time ago absorption spectra of single crystals of KHF_2 using polarized infrared radiation were obtained in this laboratory which both confirm this work and supplement it. Owing to the improved resolution of complex absorption regions which we obtained at low temperatures it seems worthwhile to present these results briefly. The spectrum is possibly unique in the wealth of combination and overtone bands which arise from a crystal of structure so simple that a detailed interpretation may be anticipated.

Consideration of intensity, isotope shift, and polarization prompts the conclusion that the infrared active fundamentals of the bifluoride ion in KHF_2 are ν_2 (bending)$\cong$1230 cm^{-1} and ν_3 (antisymmetric stretch)$\cong$1425 cm^{-1}. Raman studies[2] have placed the symmetric stretching frequency ν_1 at about 600 cm^{-1}. Certain features of the fundamental bands deserve comment.

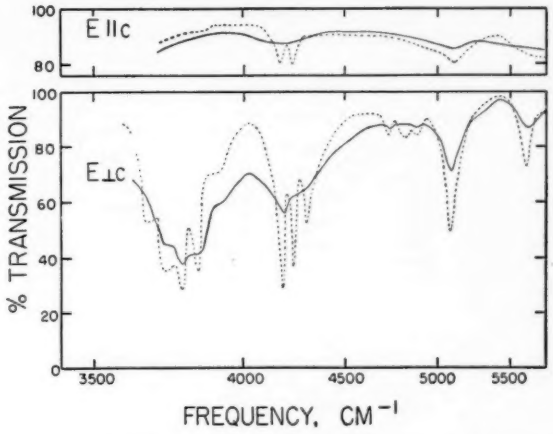

FIG. 2. Infrared spectra of KHF_2 (3300–5800 cm^{-1}) at 25°C (solid curve) and −185°C (dotted curve) in polarized light.

The fundamentals ν_2 and ν_3 differ greatly in breadth in the absorption spectrum of thin films and in reflection.[1] The half-width ν_2 is about 30 cm^{-1} and that of ν_3 about 200 cm^{-1}. In both KHF_2 and KDF_2 ν_3 showed no structure even at −185°C, but a narrowing of the band indicated that the breadth is at least in part due to interaction with lattice vibrations. It is surprising that such interactions are not equally manifest in the ν_2-band. Our results confirm the splitting of the degeneracy of ν_2 previously observed in reflection, and also an apparent anomaly in the ratio of intensities observed in the two polarization aspects. One should expect $I_{\parallel} \sim 2I_{\perp}$, but, in fact, $I_{\parallel} \sim I_{\perp}$.[3] The frequency of ν_3 is not unexpected, and is roughly that to be anticipated from the short F−F distance, but the relatively high value of ν_1 indicates a rather large positive bond-bond interaction constant in the potential function of the bifluoride ion.

As may be seen in Figs. 1 and 2 and Table I, in the range 1800–5000 cm^{-1}, the dominant absorption regions center on positions to be expected for members of the progression $\nu_3 + n\nu_1$. Structure observed in three of these regions can conceivably be due to the

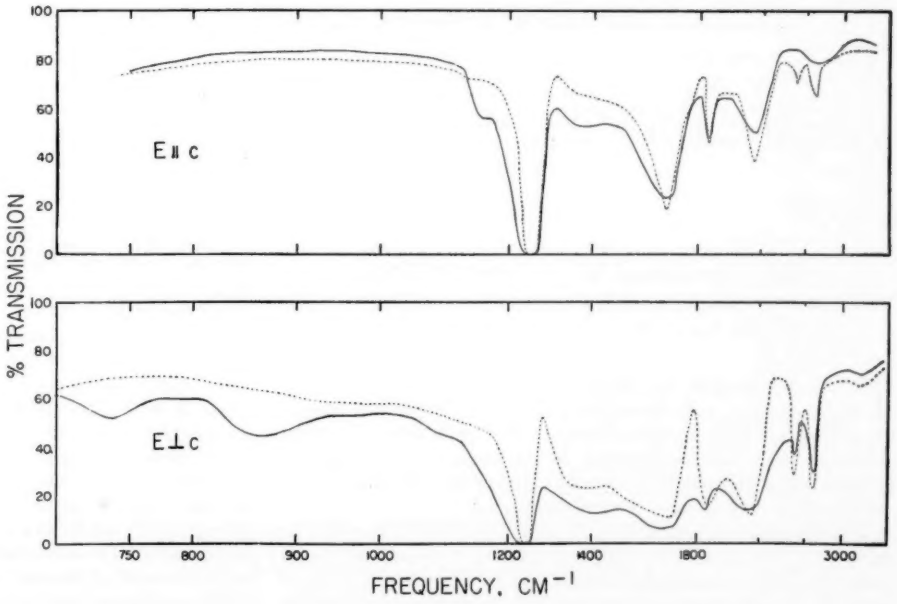

FIG. 1. Infrared spectra of KHF_2 (700–3300 cm^{-1}) at 25°C (solid curve) and −185°C (dotted curve) in polarized light.

TABLE I.

(obs) ⊥		ν(cm⁻¹) ∥	(calc)	I	Assignment
740				vw^b	ν_3-490
880			835	vw^b	$\nu_3-\nu_1$
[1170s]				vw	?
1230	=	1240		vs	ν_2
1425	≫	1425	1435	vs	ν_3
1700	=	1700		s	ν_3+460
1870	>	1870		s	$\nu_3+\nu_1$
2060	>	2060	2065	s	$\nu_3+\nu_1$
2420	>	2420		w	$\nu_2+2\nu_1$
2670	>	2670	2667	ms	$\nu_3+2\nu_1$
3240	≫	···	3241	w	$\nu_3+3\nu_1$
3660[a]		···		vw	$3\nu_2$?
3715		···		w	
3775		···	3787	w	$\nu_3+4\nu_1$?
3810		···		w	$(\nu_3+2\nu_2)$?
3890		···		vw	
4240	≫	4240[a]	4233	w	$3\nu_3$
4295[a]	≫	4295[a]	4305	w	$\nu_3+5\nu_1$
4335[a]		···		vw	$(\nu_3+2\nu_2+\nu_1)$?
4730		···		vvw	$(2\nu_3+\nu_2+\nu_1)$?
4820[a]		···	4795	vvw	$\nu_3+6\nu_1$
4890		···	4923	vvw	$3\nu_3+\nu_1$
5085	≫	5085		w	$(\nu_3+2\nu_2+2\nu_1)$?
5590		···		w	$(\nu_3+2\nu_2+3\nu_1)$?
	(6196)				$5\nu_2$ and $(\nu_3+2\nu_2+4\nu_1)$?
	(6735)				$(\nu_3+2\nu_2+5\nu_1)$?
	(7326)				$(\nu_3+2\nu_2+6\nu_1)$?

Frequencies in parentheses from Ketelaar (reference 1a).
Inequality signs indicate relative intensity in two polarizations relative to tetragonal axis.
[a] Observed only at −185°C. [b] Vanish at −185°C. s = shoulder.

near degeneracy of ν_2 and the doubling of ν_1 in the crystal. However, it is of interest that plausible assignments can be made to the individual maxima and that the overtones and combinations not involving ν_2 can be described, within the error of measurement, by a simple expression of the sort applicable to a gas spectrum. Namely, $\nu=v_3\omega_3+v_1\omega_1+v_3^2x_{33}+v_1^2x_{11}+v_1v_3x_{13}$, where $\omega_3=1447$, $\omega_1=614$, $x_{33}=-12$, $x_{11}=-14$, $x_{13}=30$. The progression $\nu_2\cong n\nu_1$ can be followed for only a short distance, but above 5000 cm^{-1} a series of moderately strong bands appear to represent the progression $\nu_3+2\nu_2+n\nu_1$. The spacing of the bands seems slightly irregular, and the first two members are in doubt. At least two bands of the spectrum appear to represent combinations with a frequency of unknown origin ∼460–490 cm^{-1}. This seems high for a lattice vibration but is difficult to explain otherwise. An exhaustive discussion of the spectrum must await a more satisfactory theory of overtone and combination bands in crystals than now exists.

* The work here described was supported by the ONR under Contract N6-ori-102, VI.
† Contribution No. 1597 from the Gates and Crellin Laboratories.
[1] J. A. A. Ketelaar and W. Vedder, J. Chem. Phys. **19**, 654 (1951).
[1a] See also J. A. A. Ketelaar, Rec. trav. chim. **60**, 523 (1941).
[2] L. Couture and J. P. Mathieu, Compt. rend. **230**, 1054 (1950).
[3] A similar phenomenon has been observed before and is as yet unexplained. See R. Newman and R. S. Halford, J. Chem. Phys. **18**, 1276 (1950).

High Resolution Mass Spectrometry

CLIFFORD E. BERRY AND S. M. ROCK
Consolidated Engineering Corporation, Pasadena, California
(Received July 12, 1951)

IN a recent note in this Journal, Kniebes *et al.*[1] showed mass spectra of ion pairs having similar m/e which were obtained on a commercial mass spectrometer.[2] The present note briefly discusses some factors involved in obtaining high resolution, presents some improved results, and explains the difficulty which Knieves *et al.* had in separating certain pairs.

The inherent resolving power of a mass spectrometer depends upon two factors: (a) the width of the ion beam at the focal plane, and (b) the mass dispersion of the instrument. The shape of peaks in a recorded spectrum depends upon these two factors

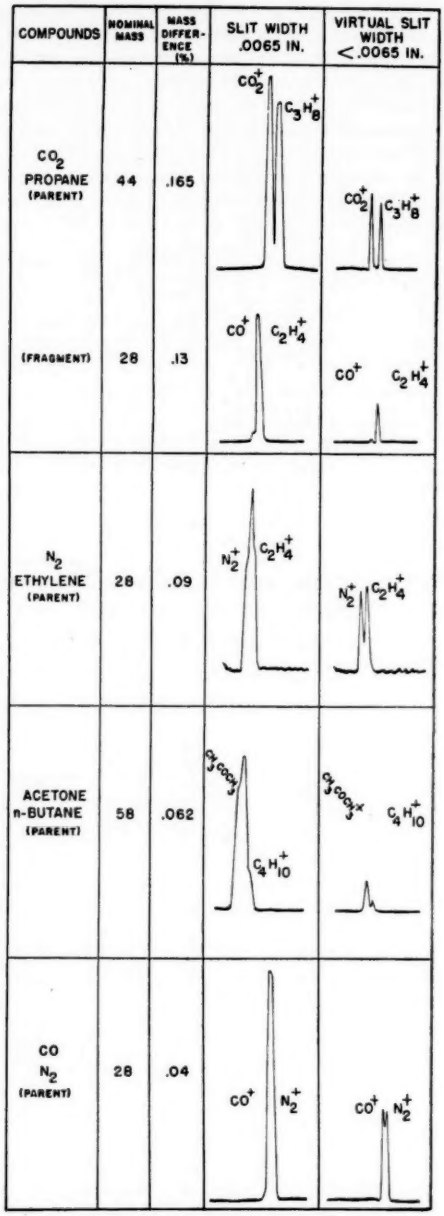

FIG. 1. Resolution of ion pairs. Resolution obtained on 180° analytical mass spectrometer, using narrow resolving slit (0.0065 in.). Improvement obtained by use of ion-optical means of reducing slit to virtual width less than 0.0065 in. is shown in column at right.

and also upon their relation to the width of the resolving slit. In general, two adjacent ion beams will show a clean separation when their dispersion is ⩾ the width of either beam plus the width of the resolving slit.

In analytical mass spectrometers it is necessary that the resolving slit be wider than the ion beam in order that the recorded peak height will be an accurate measure of the intensity of the beam. However, for certain qualitative or rough quantitative applications it is possible to use a resolving-slit width ⩽ the width of the ion beam. In the 180°, five-inch radius instruments used in reference 1 and for the work reported here, the apparent width of the resolving slit can be varied by an ion-optical method, the details of which will be published subsequently. We refer to the slit produced by this method as the *virtual* resolving slit, to distinguish it from the actual mechanical resolving slit.

The conditions under which we were able to attain improved

resolution were as follows: (a) the mechanical resolving slit width was 0.0065 inch (about 1/5 that used in the instrument of reference 1; (b) the electric field strength in the ionizing region was decreased to about 1/10 its normal value; (c) the ion lens system of the ion source was adjusted so as to obtain a minimum ion beam width at the focal point of the instrument. Under these conditions ion beam widths (for ions having only thermal energy initially) of approximately 0.0055 inch were obtained. (Ninety-eight percent of the ions were within this width.) Under the same conditions, 90 percent of the ions were found to lie within a width of 0.003 inch. Thus a considerable reduction of the slit width could be made before the intensity became too low.

Figure 1 shows the recorded peaks for a number of ion pairs, and illustrates the effect on the separation and relative intensity brought about by narrowing the virtual resolving slit.

Table I of reference 1 shows that in all but one case in which attempts to separate similar pairs failed, one or both of the ions in question were ionized fragments of a heavier molecule. It is well known that most such fragments possess considerable kinetic energy at the time of formation.[3,4] In instruments of the momentum filter type, such as were used by both Kniebes *et al.* and the writers, energy spread of the ions produces a broadening of a resolved beam, with consequent overlapping of closely adjacent beams. The inability of the instrument used by Kniebes *et al.* to separate CO^+ (carbon monoxide) and N_2^+, which have a $\Delta m/m$ of only 0.04 percent, was not due to excessive energy spread since these ions have only thermal energy initially. The most likely explanation of the difference between their results and ours in this instance is that the apparent sharpness of the virtual slit is improved when a smaller mechanical slit is used.

We wish to acknowledge the help of Miss Dorothy Comaford and Mr. Royce Howard in performing the experimental work.

[1] Kniebes, Katz, and Bernstein, J. Chem. Phys. **19**, 654 (1951).
[2] Consolidated Engineering Corporation, Model 21-103 Mass Spectrometer.
[3] H. D. Hagstrum and J. T. Tate, Phys. Rev. **59**, 354 (1941).
[4] C. E. Berry, Phys. Rev. **78**, 597 (1950).

A Theoretical Treatment of the Meta-Orienting Effect of Some Substituents in the Benzene Nucleus

F. L. J. Sixma
Laboratory for Organic Chemistry, University of Amsterdam, Amsterdam, Netherlands
(Received June 29, 1951)

ALTHOUGH the problem of the orienting effect in cationoid aromatic substitution is dealt with in a number of publications, there appears to be no semiquantitative treatment of the effect of the meta-directing substituents, such as the trichloromethyl group, the trimethylammonium group, and the carboxyl group. In the first and second type resonance interaction between the substituent and the benzene nucleus is absent or at least negligibly small; in the case of the carboxyl group and other substituents of this type, there will be no appreciable conjugation of the substituent with the pentadienate cation in the transition state of the reaction as Dewar[1] has pointed out. The directive power of these substituents is commonly ascribed to their $+I$-effect.[2]

We have tried to calculate the influence of the electric field of the substituent on the energy of the transition state of cationoid substitution reactions. As an example the calculation of the influence of a single positive point charge (e_y) on the energy of the four π-electrons in the pentadienate cation by the molecular orbital (LCAO) method is given. Besides the usual terms the Hamilton operator will contain a term V_k, the extra potential energy of an electron localized at carbon atom k in the ring (Fig. 1), due to the field of e_y; V_k is calculated from the charge e_y and the distance a_{yk}, taking the internal dielectric constant of the molecule as equal to 2.[3] The unperturbed wave functions

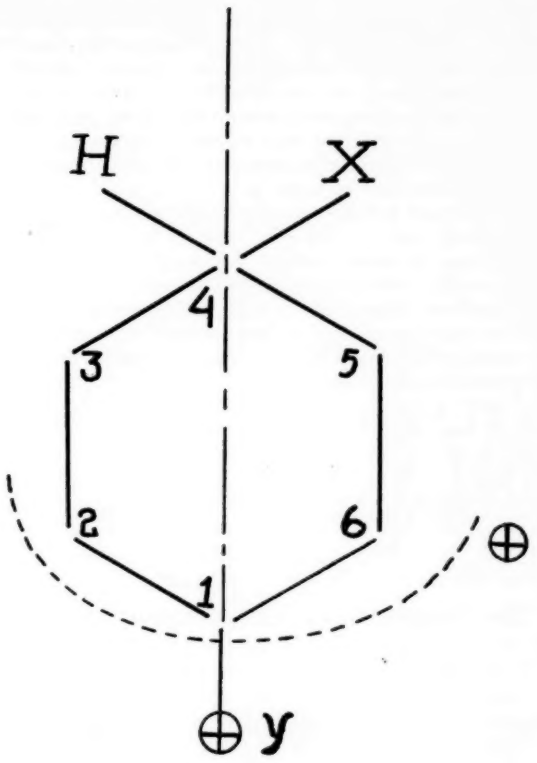

FIG. 1.

($V_k=0$) are[4]

$$\psi_j^0=\left[\sum_{k=1}^{5}\sin^2\left(\frac{j+1}{6}k\pi\right)\right]^{-\frac{1}{2}}\cdot\sum_{k=1}^{5}\sin\left(\frac{j+1}{6}k\pi\right)\cdot\varphi_k \quad (j=0,\cdots 4)$$

where φ_k is the p_z-orbital of the kth carbon atom. If we assume that the influence of the external field is small, we may write $E_j=E_j^0+E_j'$, where E_j' is calculated by a perturbation method:

$$E_j'=\left[\sum_{k=1}^{5}\sin^2\left(\frac{j+1}{6}k\pi\right)\right]^{-1}\cdot\sum_{k=1}^{5}\sin^2\left(\frac{j+1}{6}k\pi\right)\cdot V_k.$$

This yields for the difference of localization energy of a pair of π-electrons at the meta and para carbon atom (relative to Y)

$$E_3-E_4=\tfrac{1}{3}(V_1-V_2-2V_3+2V_4+V_5-V_6).$$

In the same way we obtain for the difference in localization energy at carbon atoms 2 and 4

$$E_2-E_4=V_4-V_2.$$

TABLE I. Percentage meta-isomer formed by cationoid substitution.

C_6H_5Y	Calc	Exp.[a]
$-CCl_3$	71	64
$-CF_3$	81	90
$-N(CH_3)_3+$	92[b]	100
$-CHO$	74	79
$-CONH_2$	84	69
$-COOH$	87	82, 85, 90
$-COCl$	90	90
$-COOCH_3$	86	73
$-CN$	87	80, 81, 88
$-CH(CN)_2$	67	68
$-CH_3$	22	3, 4
$-CH_2CN$	31	14
$-CH_2NH_3+$	54	49
$-CH_2NO_2$	74	48, 50
$-(CH_2)_2NO_2$	48	13

[a] C. C. Price, Chem. Revs. **29**, 37 (1941); L. F. Fieser, in H. Gilman, *Organic Chemistry* (John Wiley and Sons, Inc., New York, 1948), p. 203; A. E. Remick, *Electronic Interpretation of Organic Chemistry* (John Wiley and Sons, Inc., New York, 1949), p. 364.
[b] The positive charge on carbon atom 1 (due to the moment of the C_1-N bond) was neglected in the present calculation; this charge causes a further increase of the calculated amount of meta isomer.

As is usual in this type of calculation[5] we suppose these differences of the localization energies to be equal to the differences of the activation energies. As the activation entropies are constant to a good approximation,[6] we may calculate the percentage of meta isomer in the reaction product from the values of e_y and a_{yk}, which in turn are obtained from the data on bond distances and dipole moments from the literature. Some of the results of our calculations are shown in Table I.

The agreement between our results and the experimental values is surprisingly good for the first group of substituents. For the second group all theoretical values are higher than the experimental results, which is ascribed to the hyperconjugation of the $-CH_3$ and $-CH_2X$ group with the pentadienate cation, which tends to lower the energy of the transition state for ortho and para substitution. This effect of hyperconjugation was not taken into account in the present calculations.

[1] M. J. S. Dewar, *The Electronic Theory of Organic Chemistry* (The Clarendon Press, Oxford, 1949).
[2] We use the same convention of sign as Dewar (l.c.)
[3] J. G. Kirkwood and F. H. Westheimer, J. Chem. Phys. **6**, 506 (1938).
[4] E. Hückel, Z. Physik **76**, 628 (1932).
[5] F. L. J. Sixma, Rec. trav. chim. **68**, 915 (1949).
[6] F. E. C. Sheffer and W. F. Brandsma, Rec. trav. chim. **45**, 522 (1926).

The Vacuum Ultraviolet Spectrum of Allene

L. H. Sutcliffe and A. D. Walsh
Department of Chemistry, Leeds University, Leeds, England
(Received June 29, 1951)

Parr and Taylor have recently considered, theoretically, the electronic energy levels of allene.[1] They predict the first ionization potential to be 10.4*V* and the mean position of the first singlet-singlet and singlet-triplet transitions to be 5.1*V* (2431A). In view of this we should like briefly to report that we have photographed the far ultraviolet spectrum of allene. The spectrum has its most intense absorption in the region 1770–1600A (λ_{max} *ca* 1710A). Some vibrational structure is evident here. A weaker region of continuous absorption extends from *ca* 2030A to 1770A. The 1710A absorption probably corresponds to the absorption peak at *ca* 1815A of ethyl allene[2] ($\log\epsilon_{max}\sim3.8$) and the 2030–1770A region to the absorption beginning at *ca* 2300A in ethyl allene ($\log\epsilon\sim2.7$ to 3.1). At wavelengths between *ca* 1550A and 1200A strong discrete bands appear, many of which can be fitted into two Rydberg series converging to practically the same limit at 10.19*V*.

A full account of this work will be submitted for publication later.

[1] R. G. Parr and G. R. Taylor, J. Chem. Phys. **19**, 497 (1951).
[2] E. P. Carr and H. Stücklen, *Seventh Summer Conference on Spectroscopy* (John Wiley and Sons, Inc., New York, 1940), p. 128.

Rotational Isomerism in Hydrazine

E. L. Wagner and E. L. Bulgozdy
Department of Chemistry, State College of Washington, Pullman, Washington
(Received July 13, 1951)

The infrared and Raman spectra of anhydrous hydrazine have been obtained by several different workers[1] but there is still considerable disagreement both in the data and in its interpretation. In the course of an investigation involving the determination of the infrared and Raman spectra of anhydrous hydrazine and deutero-hydrazine it was found that there is a significant temperature dependence of these spectra, a fact which may account for the disagreement between different workers. Because of the recent interest in hydrazine and in substituted hydrazines some of our results are reported here.

For the sake of discussion let us consider only the four N–H stretching modes of hydrazine which all lie in the region above 3000 cm^{-1}. The appearance, non-appearance, polarization properties, and coincidences of these frequencies in the two spectra should clearly distinguish between the possible models for the hydrazine molecule, i.e., the *cis*-model (C_{2v}), the *trans*-model (C_{2h}), and the gauche models (C_2) which may be either the left and right staggered or the left and right semi-eclipsed configurations. Table I summarizes the expectations for these four modes in the two spectra. Four frequencies appear in both the infrared and Raman spectra of liquid hydrazine at 60°C. This would indicate that either of the two pairs of C_2 configurations are present. In solid hydrazine at −190°C only two sharp bands appear in either spectrum in this region and these are apparently not coincident. Further, both of the lines in the Raman spectrum appear to be polarized. This strongly indicates that the hydrazine molecules in a crystal at low temperature are almost entirely in the *trans*-configuration. Since the symmetry of a molecule in a crystal cannot be higher than that of the free molecule, liquid and gaseous hydrazine must consist of equilibrium mixtures of the *trans* and one pair of the C_2 isomers. Although this evidence does not indicate which of the two pairs of the C_2 modifications are the less stable forms of hydrazine, it is probable that they are the staggered forms. Measurements of the barrier heights separating the more stable *trans*-isomer from the less stable staggered isomers have not as yet been completed, but from the published dipole moment measurement (1.83*D*)[2] and on the assumption of tetrahedral angles and a N–H bond dipole of 1.42*D* one can calculate on the basis of the above picture that at room temperature there are approximately equal numbers of molecules in the three equilibrium configurations: *trans*, left and right staggered.

Table I. N_2H_4 fundamentals in the region above 3000 cm^{-1}.

Model	Raman spectrum	Infrared spectrum
C_{2h}	2 polar. lines; 0 depolar. lines	2—not common with Raman lines
C_{2v}	1 polar. lines; 3 depolar. lines	3—all in the Raman spectrum
C_2	2 polar. lines; 2 depolar. lines	4—all in the Raman spectrum

The conclusion reached here, that the stable form of hydrazine is the *trans*-configuration, is in disagreement with the theoretical prediction of Penny and Sutherland[3] that the *trans*-form is not stable. Furthermore, the reported space group of crystalline hydrazine,[4] C_{2h}^2, is not consistent with our results since there are no sites of C_{2h} symmetry in this space group. If the crystal is actually monoclinic with two molecules per unit cell, the space group C_{2h}^3 would be more acceptable than C_{2h}^2.

We are continuing the investigation on the temperature dependence of the intensities of the lines in the spectra of anhydrous hydrazine and deuterohydrazine in order to be able to estimate the barrier heights between the rotational isomers and will report our results in detail at a later date.

[1] S. Imanishi, Nature **127**, 782 (1931); L. Kahovec and K. Kohlrausch, Z. physik. Chem. **B28**, 96 (1937); J. Goubeau, Z. physik, Chem. **B45**, 237 (1940); W. Fresenius and J. Karweil, Z. physik. Chem. **B44**, 1 (1939).
[2] Audrieth, Nespital, and Ulich, J. Am. Chem. Soc. **55**, 673 (1933).
[3] W. Penny and G. Sutherland, J. Chem. Phys. **2**, 492 (1934).
[4] R. Collins and W. Lipscomb, Acta Cryst. **4**, 10 (1951).

Molecular Constants of the Ground State of the I_2 Molecule

D. H. Rank and William. M. Baldwin*
Physics Department, Pennsylvania State College, State College, Pennsylvania
(Received June 28, 1951)

Previously[1] one of us has shown that it was possible to determine the rotational and vibrational constants of the ground state of the I_2 molecule with considerable precision from Wood's green line resonance series. The measurements referred to were limited in precision by the necessity of using a small interferometer spacer since the dispersion of the spectrograph used was

insufficient to separate the interference patterns of the separate lines of the resonance doublets.

Making use of the light source described previously[2] in conjunction with a large Fabry and Perot etalon and crossing the interference pattern on a plane grating equipped with a camera of 16-foot focal length it has been possible to improve the precision of the earlier measurements by an order of magnitude. The interferometer spacer used was 21.35 mm in length. Calibration was made by means of the neon lines and the plates reduced making use of the method of exact fractions. We have photographed the resonance doublets up to and including $V=22$ with a relative precision of the wavelength measurements somewhat better than a thousandth of an angstrom unit.

It can easily be shown that the relationship between the rotational constants of the ground state and the separation of the components of the resonance doublets is given by the formula,

$$R(J_r-1)-P(J_r+1)=(4J_r+2)[B_e-\tfrac{1}{2}\alpha-(2J_r^2+2J_r+2)D_e-\alpha V]$$

where J_r refers to the rotational quantum number of the upper state and the other quantities have their usual significance. From the work of Loomis[3] on the absorption spectrum it is known that $J_r=34$. The value of D_e cannot be obtained from the resonance spectrum since a single rotational level of the ground state is involved in the primary absorption process. Since D_e must be very small, we have calculated its value from the well-known expression:

$$D_e=4B_e^3/\omega_e^2=4.55\times10^{-9}\ \text{cm}^{-1}.$$

It is unlikely that error in D_e will affect the value of B_e significantly since the total correction occasioned by the D_e term is only four times the probable error of the B_e determination.

A plot of $\Delta\nu$ for the resonance doublets against V yielded a perfectly straight line thus showing no indication of a quadratic variation of B with V. The R branch lines were fitted to a fifth-power equation making use of the previous determination[1] of the line for $V=36$ to supplement the present interferometer measurements. The mean scatter of the interferometer measurements from the fifth-power equation was 0.002 cm^{-1}. Values obtained for the molecular constants of the ground state of the iodine molecule are as follows in cm^{-1}:

$$\begin{aligned} B_e&=\ 0.037364\pm0.000003\\ \alpha&=\ 0.0001206\pm0.0000003\\ \omega_e&=214.248\\ X_e\omega_e&=\ 0.6074\\ Y_e\omega_e&=\ 0.00130\\ Z_e\omega_e&=\ 0.00000525\\ T_e\omega_e&=\ 0.00000016. \end{aligned}$$

The values obtained for the vibrational constants are consistent with those obtained earlier[1] within the probable error of the earlier measurements. The value of ω_e quoted in the earlier paper should have been 214.276 instead of 214.57 as stated. The latter value resulted from an arithmetical error in the determination of ω_e from the empirical equation. The value of B_e obtained in this work can be contrasted with the value obtained by Loomis[3] from the absorption bands, i.e., 0.037360±0.000003, which shows an overlapping of the probable errors of the two determinations.

* Now with Corning Glass Works, Corning, New York.

[1] D. H. Rank, J. Opt. Soc. Am. **36**, 239 (1946).
[2] D. H. Rank and R. E. Kagarise, J. Opt. Soc. Am. **40**, 89 (1950).
[3] F. W. Loomis, Bull. Natl. Research Council (US) **2**, Part 3, 287 (1926).

Space Charge in Electrolytes during Electrolysis

CHARLES W. TOBIAS
University of California, Berkeley, California
(Received June 18, 1951)

IN the May issue of this Journal, Ferguson and Schriever[1] reported about experiments demonstrating the existence of significant space charge in the electrolyte during the electrolysis of a neutral 0.0024*N* KCl solution using platinum electrodes. Reed and Schriever[2] earlier reported in this Journal the existence of macroscopic space charge during the electrolysis of neutral 0.0024*N* solutions of the salts of Ni, Cu, Al, Zn.

Gordon[3] and MacInnes, Shedlovsky, and Longsworth[4] severely criticized the experimental technique and the interpretation of data by Reed and Schriever by stating that

1. Irreversible electrodes are not suitable for the measurement of potential gradients because of "erratic behavior," irreproducibility, dependence of electrode potential on current density, and time.

2. During the electrolysis, concentration changes occur in the solution which are especially not negligible in the regions adjacent to the working electrodes. Convection due to specific gravity differences might complicate the situation.

Answering this criticism, Schriever[5,6] stated that

1. Since the potential deviation time curves were "quite" reproducible for any given position of the reference electrode in the cell, potential differences measured when the reference electrode was placed in various different positions along the axis of the cell gave a true representation of the variation of the potential gradient. If there was an error in the potential measurement, it had to be the same for all points along the column of electrolyte.

2. Overvoltage effects were taken in account in so far as the measurements were taken in each position 10 minutes after the current was started.

3. Concentration changes "must have been exceedingly small," since the current density was only 5×10^{-5} A/cm². Anyway, the shapes of the potential distribution curves could not be explained by phenomena occurring near the working electrodes. Approaching the cathode, the potential gradient should have increased if the depletion of ions had been the cause for the variation of the gradient. In most cases the opposite was observed.

Schriever and Ferguson's recent paper[1] on the $Pt/KCl_{(aq)}/Pt$ system indicates that throughout their experimental and interpretative efforts, some physiochemical facts were not taken into account.

The measured potential was the sum of the potential of the working electrode, the ohmic potential drop, and the potential of the reference electrode (neglecting the liquid junction potential). The authors claim that the potential of the working electrode in each run, 10 minutes after the current was started, assumed the same value! Schriever's space charge calculation method makes it necessary to *assume* that the conductivity was constant throughout the cell, and *that the potential of the reference electrode was independent of its position.*

In the experiments reported, *neutral* 0.0024*N* solutions of Cu, Zn, Ni, and Al salts were electrolyzed between the corresponding metal electrodes. The cathodic potentials at which Ni, Zn, and Al could be deposited were above the reduction potential of hydrogen ion from a neutral solution (0.41 volt). Actually, hydrogen liberation could occur at much lower potentials until the solution became saturated with it. In my opinion, the cathodic reaction in these experiments was hydrogen ion discharge, or the combined reduction of metal and hydrogen ions. As a result, hydroxides were formed in the vicinity of the cathode, bringing about significant changes in conductivity. (In electrochemical practice it has been known for many decades that the deposition of these metals in the pure state is not possible from neutral solutions.) Since the bulk concentration of hydrogen ions was only 10^{-7} g per liter, the current density applied in Schriever's experiments was by no means low; in fact, it was far above the limiting "diffusion-current" density. In none of Schriever's experiments can one justify the acceptance of steady-state conditions. The concentration of hydrogen ions indeed must have changed *not only* within the ΔX layer adjacent to the electrode. The interpretation of potential measurements would be extremely difficult under such circumstances.

The electrode reactions in the $Pt/KCl_{(aq)}/Pt$ cell are as follows:

$$\begin{aligned} &\text{cathode:}\quad 2H_2O+2e^-\rightarrow H_2+2OH^-,\\ &\text{anode:}\quad H_2O\rightarrow\tfrac{1}{2}O_2+2H^++2e^-. \end{aligned}$$

Consequently, the conductivity should increase appreciably both in the cathode and anode region! This fact is born out by the shape of Schriever's potential gradient curve.

In addition to the change in conductivity in the proximity of the electrodes, *the potential of the reference electrode varies also*, depending on its position along the axis of the cell. This variation is caused by the non-uniform metal and hydrogen ion concentration.* The potential values measured when the reference electrode was relatively close to the working electrode could not be interpreted without knowing (a) the potential of the reference electrode and (b) the conductivity of the solution between the working electrode and the reference.

Schriever *et al.* reported that the conductivity of the solutions was measured to be uniform throughout the cell. The conductivity measurements on which this statement was based must have been rather unreliable. The authors' repeated reference to "reproducibility" of results gives one the thought that the generous number of correction terms applied to the potential data made the method insensitive, in fact, unsuitable, to draw conclusions.

[1] W. Schriever and E. E. Ferguson, J. Chem. Phys. **19**, 609 (1951).
[2] C. A. Reed and W. Schriever, J. Chem. Phys. **17**, 935 (1949).
[3] A. R. Gordon, J. Chem. Phys. **18**, 146 (1950).
[4] MacInnes, Shedlovsky, and Longsworth, J. Chem. Phys. **18**, 233 (1950).
[5] W. Schriever, J. Chem. Phys. **18**, 146 (1950).
[6] W. Schriever, J. Chem. Phys. **18**, 763 (1950).
* Actually in the KCl experiment the reference was an *irreversible* oxygen electrode.

Space Charge in Electrolytes during Electrolysis: A Reply

WILLIAM SCHRIEVER
Physics Department, University of Oklahoma, Norman, Oklahoma
(Received June 28, 1951)

IN this reply to the letter by Charles W. Tobias it should first be pointed out that Reed and Schriever[1] reported data on $CuCl_2$, $ZnCl_2$, $Zn(C_2H_3O_2)_2$, and $NiCl_2$ as well as on the sulfates of Cu, Zn, Ni, and Al, and that potential determinations were made at one-minute intervals from 1 to 15 minutes.

By "neglecting liquid junction potential" it is assumed that Tobias means the "potential" between a layer very close to a current electrode and the remainder of column of electrolyte, since some concentration changes may have taken place in this layer. This "potential" *was* taken into account in the theory developed by Reed and Schriever (p. 936); it is included in e' and is referred to in the sentence, "Also concentration changes close to the electrodes may cause certain electromotive forces."

Tobias states that in our calculations it was "necessary to *assume* that the conductivity was constant throughout the cell." Reference to Reed and Schriever's paper (p. 936), will show that this was *not* the case. The resistivity (and therefore the conductivity) was assumed constant along the column *except* for a layer of thickness $\Delta\chi$ next to each current electrode, $\Delta\chi$ being sufficiently large to include the region where concentration change may have occurred. Earlier conductivity measurements (p. 937) showed that appreciable concentration changes did *not* occur in that part of the column where potential measurements could be made. Thus, the conductivity was *found* to be constant in the region under investigation.

According to Tobias, the "potential of the reference electrode varies also" because of the "non-uniform metal and hydrogen ion concentration." He also states that the hydrogen ions were produced at the anode. The mobility of the metal ion is such that it moved about 1 mm during the 15-minute interval that the current passed, whereas the hydrogen ion moved about 6 mm during the same time. Schriever and Ferguson's[2] deviation-time curves show that the deviations were essentially constant after not more than 5 minutes. Thus, the ions moved only about $\frac{1}{3}$ mm and 2 mm, respectively, by the time the calculated field strength and space charge values existed. Thus, it appears impossible that the concentrations of the hydrogen and potassium ions could have changed a measurable amount at a distance greater than a very few mm from the electrodes. Any change in potential of the reference electrode caused by the changes in concentrations next to the current electrodes would be constant at any specific time of passage of the current, for all positions of the reference electrode along the column. Such a constant term would not cause any changes in the potential-gradient and space-charge distributions. The space charge effects in KCl existed out into the solution to points nearly 100 mm from the cathode and 50 mm from the anode. Thus it appears that the potential of the reference electrode could not have changed as it moved along the column, for the reasons specified above in this paragraph.

Would not conductivity changes near the two current electrodes be greatest near the electrode surfaces and decrease in a regular manner with distance from the electrode? Granting that in KCl solution there was an increase in conductivity near each electrode, then, if this were the only effect, the potential gradient should decrease only; actually, both an increase and a decrease near each electrode were observed. Also, how can one account for significant concentration changes up to 100 mm from the cathode, when the ions can move only 2 or 3 mm at most during the 15 minutes that the current existed?

In Reed and Schriever's[1] work with Ni electrodes they found for $NiCl_2$ a *decreasing* potential gradient from 1 to 40 mm from the cathode, and then an increasing gradient out to 90 mm followed by a decreasing gradient further away. In $NiSO_4$ they found an *increasing* potential gradient from 1 to 40 mm from the cathode followed by a decreasing gradient out to 90 mm. If concentration changes were the correct explanation, why should the gradient curves be so different for the same electrodes treated in exactly the same manner? The gradient curve for $CuSO_4$ was similar to that of $NiCl_2$. How can significant concentration changes occur so far from the electrodes with a current density of only 5×10^{-5} amp/cm^2 in 15 minutes? How can concentration changes cause both a decreasing and an increasing gradient in the neighborhood of the cathode in $NiCl_2$?

The relative conductivity measurements reported by Reed and Schriever[1] (p. 937) were reliable. The rigid electrode assembly was calibrated by immersing it in several solutions having both slightly larger and slightly smaller known concentrations, and the measurements were reproducible. The measuring current was 1000 cycle ac, and the bridge-balance was observed with the aid of an electron tube amplifier. We could have measured a change in conductivity one-eighth as great as was required to account for the change in gradient. We were unable to detect any change whatever anywhere along the column of electrolyte.

We applied three corrections. The chemical emf of the exploring electrode has already been discussed above. The correction obviously required because of the shape and size of the exploring electrode is certainly nothing serious. The standard-curve method, which corrected for the unavoidable changes in the current-electrode surfaces with time, is certainly not serious. Are not the important facts that the data were reproducible *in spite of* these corrections, and that, in the crucial regions, the observed "deviations" were large in comparison with the variations in these deviations? Three corrections may be a "generous number of correction terms"; however, the significant fact is that these corrections were *not* estimates concocted to make data fit a preconceived idea, but actual measured values fully explained in the publications. They appear to be fully justified. Just how can they prevent the drawing of reliable conclusions when the corrected data were reproducible?

Some of the items mentioned above as well as other important considerations are discussed in two earlier Letters[3] to the Editor; these have a direct bearing on this discussion.

[1] C. A. Reed and W. Schriever, J. Chem. Phys. **17**, 935 (1949).
[2] W. Schriever and E. E. Ferguson, J. Chem. Phys. **19**, 609 (1951).
[3] W. Schriever, J. Chem. Phys. **18**, 146 and 763 (1950).

Solid Diffusion in Chromatography

HENRY C. THOMAS
Sterling Chemistry Laboratory, Yale University, New Haven, Connecticut
(Received July 12, 1951)

ONE of the most troublesome problems in the interpretation of kinetic behavior in chromatography on deep beds is posed by the finite rate of diffusion in the solid adsorbent or exchanger. In some current work on exchange adsorption in montmorillonite clays the experimental data indicate that solid diffusion may play an important part. To get a clearer idea of the effects to be expected in the simple case of isotopic exchange, where a linear isotherm is to be found, the problem has been solved for a slightly idealized case. An interesting conclusion which is susceptible to direct experimental check appears on the basis of this calculation. In so far as the writer is aware, this prediction of the theory has not been noticed before. Attention is called to it in the hope that others may have data presently available with which to check the prediction. (Experiments to this end are now in progress in this laboratory.)

The column of length x is supposed to be packed with spheres of exchanger of radius a. The column, having been equilibrated with a solution of concentration c_0, is eluted with an identical solution carrying an appropriate tracer. The diffusion problem may then be phrased as follows:

$$[\partial^2(rq)/\partial r^2]-(\dot{V}/D)\partial(rq)/\partial y=0, \quad x\geq 0, \quad y\geq 0, \quad 0\leq r\leq a, \tag{1}$$

$$\partial q/\partial r=0, \quad r=0, \tag{2}$$

$$Kq(x, y, a)=c(x, y), \quad r=a, \tag{3}$$

$$q(x, 0, r)=0, \quad y\leq 0, \tag{4}$$

$$c(0, y)=c_0, \quad x=0, \quad y\geq 0, \tag{5}$$

$$\partial c/\partial x=-(\mu D/a\dot{V})[\partial q/\partial r]_{r=a}. \tag{6}$$

The significance of the various quantities is apparent: $q(x, y, r)$ and $c(x, y)$ are volume concentrations in adsorbent and in solution, respectively; $y=\dot{V}t-mx$=volume downstream (where m is free space per unit length of column); μ, three times the volume of exchanger in unit column length. D is the diffusion constant in the solid; it is supposed to be small compared with the diffusion constant in the liquid, so that no liquid film diffusion need be considered. The relations being all linear, the problem is immediately soluble by the method of the laplace transform. The most interesting integral to be calculated is

$$\frac{c}{c_0}=\frac{1}{2\pi i}\int \exp\left\{\frac{Dy}{a^2\dot{V}}z^2-\frac{\mu Dx}{a^2\dot{V}K}(z\coth z-1)\right\}\frac{dz}{z}, \tag{7}$$

where the path of integration is an infinite circuit around the imaginary axis, enclosed the pole at $z=0$ and the essential singularities at $z=\pm n\pi i$, $n=1, 2, 3, \cdots$. The result of this calculation can be put in the form

$$\frac{c}{c_0}=1-2\sum_{n=1}^{\infty}\exp(k\omega_n^2)\times\left\{J_1(2\kappa)+\sum_{m=1}^{\infty}\frac{(-)^m}{m!}J_{m+1}(2\kappa)\left[\frac{d^m}{ds^m}F(s)\right]_{s=0}\right\} \tag{8}$$

in which $\omega_n=n\pi i$, $\kappa=\mu Dx/a^2\dot{V}K$, $k=Dy/a^2\dot{V}$,

$$F(s)=\exp\{k\omega_n^2(2+s)s-\kappa s-\kappa S(s)-\ln(1+s)\}$$

and

$$S(s)=-\sum_{\nu=1}^{\infty}\frac{2^{2\nu}B_\nu}{(2\nu)!}(n\pi)^{2\nu}(1+s)s^{2\nu-1}.$$

The J_m are bessel functions; the B_ν are Bernoulli numbers. This result is useful for computation only with κ small; other methods must be applied to obtain usable results for more interesting values of κ.

The prediction mentioned above is, however, independent of the computation of the integral. It is apparent that

$$c/c_0=f(Dy/\dot{V}a^2, \quad \mu Dx/\dot{V}Ka^2), \tag{9}$$

so that if one sets up two columns, one with spheres of nearly equal radius, say, a, and of length x, and the other with spheres of radius θa and of length $\theta^2 x$ (together with any small adjustments necessary to keep μ constant), the breakthrough curve of the second column should be immediately deducible from that of the first by multiplying the values of y for given c/c_0 by θ^2. (This is, of course, a sufficient condition for conservation; it is not in general necessary.) In the kinetics for liquid film diffusion the corresponding prediction is $a\rightarrow\theta a$, $x\rightarrow\theta x$, then $y\rightarrow\theta y$, for given c/c_0. In cases where one type of kinetics is largely dominant, this observation should make possible a decision between the two types of kinetics using deep beds of exchanger.

This work has been done as a part of work at Yale University under contract with Brookhaven National Laboratory, Upton, New York.

The Infrared Spectra of $DC^{12}N$ and $DC^{13}N$

W. S. RICHARDSON*
Mallinckrodt Chemical Laboratory, Harvard University, Cambridge, Massachusetts†
(Received July 11, 1951)

THE ν_1-vibration of the molecule HCN has never been unambiguously observed in the vapor phase infrared spectrum because of the very small change of dipole moment associated with this vibrational mode. However, if the hydrogen atom is replaced by deuterium, the form of the normal mode is changed and the vibration has an easily observable absorption intensity. The spectrum of DCN has been investigated in detail by Bartunek and Barker,[1] but they failed to observe ν_1, presumably because of the small size and low deuterium enrichment of their sample. Actually, this band is readily observable using a pressure of 10 cm Hg of DCN in a 5-cm cell.

The sample of DCN was prepared by adding solid KCN to a sirupy mixture of D_2O and P_2O_5 and collecting the evolved product in a cold trap. In the preparation of $DC^{13}N$ the KCN used was enriched to 63 percent in C^{13} (Eastman Kodak Company, Rochester, New York). In each case the product contained a small amount of the hydrogen compound; some of the frequencies of $HC^{13}N$ are recorded below, although they are not used in any of the calculations.

The spectra were measured using a Baird Associates, Inc., Model B infrared recording spectrophotometer (NaCl prism). The spectra of undesirable components of the isotopic mixtures were eliminated by using a comparison cell filled to the appropriate pressure with these components. The frequency ν_1 for $DC^{12}N$ was measured using a CaF_2 prism in the Perkin-Elmer Model 12B spectrometer at Mellon Institute. The fundamental frequencies of the various isotopic forms of hydrocyanic acid are collected in Table I.

The product rule ratios for the stretching modes of the isotopic pair $DC^{12}N$ and $DC^{13}N$ are

$$\begin{aligned}\omega_1\omega_3/\omega_1^i\omega_3^i&=[(M/M^i)\cdot(m^i/m)]^{\frac{1}{2}}=1.0228,\\ \nu_1\nu_3/\nu_1^i\nu_3^i&=1.0232,\end{aligned} \tag{1}$$

where ω and ν are the zeroth order and observed frequencies, respectively, M is the molecular weight, m is the mass of the carbon atom, and i denotes $DC^{13}N$.

By using the stretching frequencies of $DC^{12}N$ and $DC^{13}N$ it is possible to compute the three force constants in the most general

TABLE I.

Molecule	$HC^{12}N$	$HC^{13}N$	$DC^{12}N$	$DC^{13}N$
ν_1	2089.0[a]	—	1928	1916
ν_2	712.1[b]	706.3	568.9[c]	—
ν_3	3312.0[c]	3295	2629.3	2585

[a] C. R. Kastler, Compt. rend. **194**, 858 (1932).
[b] K. N. Choi and E. F. Barker, Phys. Rev. **42**, 777 (1932).
[c] P. F. Bartunek and E. F. Barker, Phys. Rev. **48**, 516 (1935).

quadratic potential function for the stretching vibration:

$$2V = f_{CD}\Delta r_{CD}^2 + f_{CN}\Delta r_{CN}^2 + 2f_{12}\Delta r_{CD}\Delta r_{CN}. \quad (2)$$

The resulting force constants are

$$f_{CD} = 5.626,$$
$$f_{CN} = 19.15\times10^5 \text{ dynes/cm}, \quad (3)$$
$$f_{12} = -0.22.$$

The other sets of force constants arising from this calculation can be eliminated on the basis of the invariance of potential constants on isotopic modification and the large positive value of f_{12}(+3.8 $\times10^5$ dynes/cm), which seems unreasonable.

If the value of f_{12} obtained above is carried over to $HC^{12}N$ (f_{12} is small and does not affect the principal force constants strongly), one obtains $f_{CN}=18.1\times10^5$ and $f_{CH}=5.76\times10^5$ dynes/cm. The fact that f_{CH} comes out higher than f_{CD} is rather surprising, since the effect of neglecting anharmonicity differences generally leads to deviations with f_{CD} greater than f_{CH}. Similarly, if we use the force constants of Eqs. (3) to compute the stretching frequencies of HCN, the results are in rather better agreement with the observed frequencies than one would expect considering normal anharmonicity differences.

Finally, it may be noted that the C—D force constant is rather lower and the C≡N force constant rather higher than the corresponding force constants obtained from structurally related molecules.

* Present address: Mellon Institute, Pittsburgh, Pennsylvania.
† The research reported in this paper was made possible by support extended Harvard University by the ONR under Contract N5ori, Task Order V.

Isotope Effect in the Oxidation of Carboxyl-C^{14} Acetic Acid*

E. A. Evans† and John L. Huston
Department of Chemistry, Oregon State College, Corvallis, Oregon
(Received July 13, 1951)

SEVERAL recent studies of isotope fractionation effects occurring in the formation of acetic acid by decarboxylations of malonic acid have involved wet combustions of these two acids.[1-3]

In the course of work in this laboratory involving the study of anhydrous acetic acid as an ionizing solvent, it has been noted that the wet combustion procedure is, itself, subject to an isotope rate effect when applied to the rather difficultly oxidizable acetic acid. In other words, $CH_3C^{12}O_2H$ is oxidized more rapidly than $CH_3C^{14}O_2H$; and unless precautions are taken to insure complete combustion of a sample of acetic acid, a low specific activity is found.

In studying this isotope effect, the CO_2 formed during a wet combustion of carboxyl-C^{14} acetic acid‡ by the procedure of Van Slyke and Folch[4] was collected as two consecutive fractions of roughly the same weight, absorbed in barium hydroxide solutions, and counted as barium carbonate on copper planchets. Blanks due to atmospheric CO_2 or SO_3 from the oxidizing mixture were negligible.

A number of runs were made in investigating this effect, during the course of which several revisions were made in our experimental procedure. The isotope effect was consistently observed in all these runs. For six consecutive combustions which were made after the last revision an average value of 1.06, with an average experimental deviation of ±0.02, was obtained for the ratios of the specific activities of the second fractions to those of the first fractions. The nature of the combustion procedure and the lack of precision inherent in the counting technique are such that correlation of the size of the effect with the relative amounts of the two fractions was not considered feasible.

* Research supported in part by AEC.
† Du Pont Fellow, 1950–1951.
[1] A. Roe and M. Hellmann, J. Chem. Phys. **19**, 660 (1951).
[2] J. Bigeleisen and L. Friedman, J. Chem. Phys. **17**, 998 (1949).
[3] Lindsay, Bourns, and Thode, Can. J. Chem. **29**, 192 (1951).
‡ The acid was formed *in situ* by the addition of sodium acetate to the oxidation fluid. Approximately 50 mg of the salt was used in each run.
[4] Van Slyke and Folch, J. Biol. Chem. **136**, 509 (1940).

Vibrational Structure of the Hydrocarbon Flame Bands*

George M. Murphy and L. Schoen†
Chemistry Laboratories of Washington Square College, and Research Division, University Heights, New York University, New York, New York
(Received July 13, 1951)

A VIBRATIONAL analysis of the hydrocarbon flame band system has been carried out based on two active modes of vibration in the wavelength region 2500 to 4000A. It has been found that the frequencies of all but five of the bands reported by Vaidya[1] may be expressed by means of the six progressions $(0,0)\rightarrow(v_1'',0)$, $(0,1)\rightarrow(v_1'',0)$, $(1,0)\rightarrow(v_1'',0)$, $(0,2)\rightarrow(v_1'',0)$, $(0,0)\rightarrow(v_1'',1)$, and $(0,2)\rightarrow(v_1'',1)$, where $v_1''=0,1,2\cdots9$. The arrangement of bands is given in Tables I and II, where the wave-

TABLE I.

V_1' V_2'	(0, 0)		(0, 1)		(1, 0)		(0, 2)
$V_1''V_2''$							
(0, 0)	*39,476*						
	1876						
(1, 0)	*37,600*	1066	*38,666*			2110	*39,710*
	1859		1858				1850
(2, 0)	*35,741*	1067	*36,808*	1223	*36,964*	2119	*37,860*
	1832		1829				1829
(3, 0)	33,909	1070	*34,979*			2122	*36,031*
			1819				
(4, 0)			*33,160*		*33,307*		
(5, 0)	*30,302*						
	1761						
(6, 0)	*28,541*	1059	*29,600*	1221	*29,762*		
	1743		1742		1752		
(7, 0)	*26,798*	1060	*27,858*	1212	*28,010*	2109	*28,907*
	1727		1721		1720		1711
(8, 0)	*25,071*	1066	*26,137*	1219	*26,240*	2125	*27,196*
			1706				
(9, 0)			*24,431*				

number differences are indicated by numbers placed between the columns and rows. The horizontal differences have been taken between the first row and succeeding rows, thus giving the energies between the lowest level and the higher vibrational levels of the excited state.

The frequency of any band in the system may be expressed with sufficient accuracy by an equation of the type

$$\nu = \nu_{00} + \omega_1'^0 V_1' + X_{11}'^0 V_1'^2 + \omega_2'^0 V_2' + X_{22}'^0 V_2'^2 - \{\omega_1''^0 V_1'' + X_{11}''^0 V_1''^2 + \omega_2''^0 V_2'' + X_{22}''^0 V_2''^2 + X_{12}''^0 V_1 V_2\},$$
$$V_1''=0,1,2\cdots9,\ V_2'=1,2,\ V_1'=V_2''=1,$$

where ν_{00} is the energy of the pure electronic transition. The ω_i^0 terms represent vibrational frequencies referred to the lowest ($v_1=0$, $v_2=0$) level and the x_{ij} factors the corresponding anharmonicity terms. The calculated values for the constants of this equation are $\nu_{00}=39{,}463$ cm^{-1}, $\omega_1'^0=X_{11}'^0=1219$ cm^{-1}, $\omega_2'^0=1070$ cm^{-1}, $\omega_1''^0=1880$ cm^{-1}, $\omega_2''^0+X_{22}''^0=1532$ cm^{-1}, $X_{22}''^0=-5.68$ cm^{-1}, $X_{11}''^0=-10.15$ cm^{-1}, and $X_{12}''^0=-4.50$ cm^{-1}. From the values obtained, the two active vibrational modes have been interpreted as C=O stretching and C—H deformation vibrations, and it is inferred that the emitter of the flame bands will contain these groupings. The observed frequencies in the lower state are in

TABLE II.

V_1', V_2'	(0, 0)	(0, 2)
V_1'', V_2''		
(0, 1)		*40,068*
		1882
(1, 1)		*38,186*
		1853
(2, 1)		*36,333*
(3, 1)		
(4, 1)		
(5, 1)	*28,789*	
	1753	
(6, 1)	*27,036*	
(7, 1)		*27,410*
(8, 1)		
(9, 1)		

good agreement with the corresponding ones in the infrared absorption spectrum of formaldehyde,[2] 1744 and 1503 cm^{-1}, respectively.

The occurrence of an isotopic shift in the system when the flame of a deuterated hydrocarbon is used as a source of excitation[3] has demonstrated that at least one hydrogen atom is involved in the structure of the emitter. Lack of sufficient data regarding equilibrium distances and the configurations of polyatomic molecules, particularly in excited electronic states, has not permitted an unambiguous calculation thus far of the isotope effect for specific cases utilizing the vibrational scheme described above.

* The work described in this paper was done with the support of the ONR, Department of the Navy, and the Office of Air Research, Department of the Air Force, under Contract N6Ori-11, Task Order 2, as part of Project Squid.

† Present address: U. S. Bureau of Mines, Pittsburgh, Pennsylvania.

[1] W. M. Vaidya, Proc. Roy. Soc. (London) **A147**, 513 (1934).
[2] G. Herzberg, *Infrared and Raman Spectra* (D. Van Nostrand Company, Inc., New York, 1945).
[3] G. M. Murphy, and L. Schoen, J. Chem. Phys. **19**, 380 (1951).

Liesegang Ring Formation Arising from Diffusion of Ammonia and Hydrogen Chlorine Gases through Air

ELLEN L. SPOTZ AND JOSEPH O. HIRSCHFELDER
Naval Research Laboratory, University of Wisconsin, Madison, Wisconsin
(Received July 9, 1951)

A COMPLICATED structure of Liesegang rings is formed when ammonia and hydrogen chloride diffuse together from opposite ends of an air-filled tube. The rings are composed of a smoke of solid ammonium chloride particles. A detailed explanation of this phenomena is difficult; however, significant clues can be obtained by fixing attention on the time of formation of the first ring.[1] Experimentally, it was found that at 298°K in a tube 8 mm in diameter 40 cm long connected to a bottle of 12*N* hydrochloric acid on one end and a bottle of 9*N* ammonium hydroxide in the other end, the first ring began to form after 300 seconds. From simple diffusion theory, it is easy to determine the concentration of the ammonia and of the hydrogen chloride gases as a function of time and position up to the time of formation of the first ring. Such a calculation indicates that at the position of the first ring after 300 seconds the concentration product of the gases is

$$p\mathrm{NH_3}p\mathrm{HCl}=9.2\times10^{-4}\ \text{atmos}^2.$$

However, according to the thermodynamical measurements of Stephenson,[2] the equilibrium concentration product is

$$[p\mathrm{NH_3}p\mathrm{HCl}]_{\text{equilibrium}}=1.04\times10^{-16}\ \text{atmos}^2.$$

If the NH_4Cl had started to precipitate when the equilibrium concentration product was exceeded, the first ring would have been observed to form after only 14 seconds (instead of 300 seconds). If there had been convection currents in our diffusion tube, the equilibrium concentration product would have been exceeded in a time much smaller than the 14 seconds. Thus, we conclude that the Liesegang ring formation involves more than a thousandfold supersaturation of the individual gases. This supersaturation phenomena is typical of all nucleation phenomena.[3] From the standpoint of nucleation our experimental data can be interpreted as showing that of the order of a hundred molecules need to join in forming a critical cluster and the critical cluster requires a free energy of activation, ΔF_{act}, of 18,000 cal/mole. In forming these nuclei, it is necessary not only for the NH_3 and the HCl molecules to join in the cluster but they must also react simultaneously to form the NH_4Cl. From theoretical considerations it appears that the forces between a single NH_3 and a single HCl molecule are homopolar, whereas the forces within a NH_4Cl crystal are ionic. Therefore, it is not surprising that a critical size of NH_4Cl nucleus is necessary in order to exhibit the strong ionic forces which would render further growth of the nucleus comparatively easy. We intend to study this system further and determine more of the properties of the critical nuclei as well as develop a complete quantitative explanation of the Liesegang ring formation in the NH_3-HCl system. Furthermore, we are interested in the effect of external radiation on catalyzing the nuclei formation and thereby producing a Wilson-Cloud chamber with tracks made up of solid NH_4Cl particles.

The authors wish to acknowledge the financial support of the Navy Bureau of Ordnance through their contract NORD-9938 with the University of Wisconsin.

[1] The work discussed in this letter is described in great detail in the Ph.D. dissertation of Ellen L. Spotz, "Some properties of gases and gaseous reactions," University of Wisconsin (1950).
[2] C. C. Stephenson, J. Chem. Phys. **12**, 318 (1944).
[3] H. Reiss, J. Chem. Phys. **18**, 529 (1950).

The Effect of Variation of *Z* upon the Theoretically Computed Energy Levels of Benzene*

HARRISON SHULL AND FRANK O. ELLISON
Department of Chemistry and Institute for Atomic Research, Iowa State College, Ames, Iowa
(Received June 28, 1951)

THEORETICAL calculations of the energies of the lower excited levels of benzene by the method of antisymmetrized products of molecular orbitals were made by Goeppert-Mayer and Sklar,[1] with the neglect of many two-center and all three- and four-center integrals. The moderately good agreement with experiment which they secured has been shown by several investigators to be fortuitous, inasmuch as many of the neglected integrals are of magnitudes comparable to the calculated energy separations. The calculations of these investigators have been summarized by Roothaan and Parr,[2] and the best results reported by them are in rather good agreement with experiment.

There has recently been, however, some question as to the proper assignment for the observed lowest triplet state and lowest excited singlet state of benzene.[3-5] Craig has pointed out the unanimity of agreement of the theoretical calculations by both valence bond and molecular orbital methods in predicting $3_{B_{1u}}$ and $1_{B_{2u}}$ for these states, respectively. Within the framework of the approximate methods as a whole, only two nontheoretical parameters appear, these being the skeletal carbon-carbon distance and the effective nuclear charge, *Z*, in the Slater atomic orbitals used in these calculations. Of these two parameters, there is very considerable question as to the proper choice of *Z*. It has been general practice to use the same *Z* for molecules as determined by the variation method for the free atom (3.18 for C). It is not at all apparent that this is necessarily the best choice. In particular, the trend in molecular binding is toward the united atom approximation; and one might well expect that for bonding orbitals at least, a higher *Z* would apply in molecules. On the other hand, for π-electron systems, it is tempting to think of the π-electrons as being unusually well shielded by the bonding σ-electrons. Computations by Bayliss,[6] using the free electron model, sug-

gested the possibility that a considerably lower value of Z (near 1) might be more satisfactory for the π-electron systems.

Preliminary calculations in the Mayer-Sklar approximation indicated that use of $Z=1$ would yield absurd results. For Z values slightly below 2.7, however, this approximate method produced inversion of the theoretically calculated positions of the B_{1u} and B_{2u} levels in both the singlet and triplet systems. Since sensitivity to Z of this kind would seriously open to question the present theoretical assignments, it was felt worth while to repeat these calculations, including all previously neglected integrals (but not including configuration interaction). For these calculations Z values of 2.268, 2.740, and 3.180 were used together with carbon-carbon distance of 1.40A. The results are summarized in Table I. It is clear that the energy separations between the states

TABLE I. Calculated energy levels (ev) of benzene as a function of Z.

	Z=2.268	2.740	3.180	Observed
$^1E_{1u}$	11.9	10.6	9.6	7.0
$^1B_{1u}$	8.8	7.6	6.8	6.2[a]
$^1B_{2u}$	7.9	6.6	5.4	4.9
$^3B_{2u}$	8.0	6.5	5.2	..
$^3E_{1u}$	7.4	5.6	4.1	..
$^3B_{1u}$	6.9	4.7	2.9	3.8
$^1A_{1g}$	0.0	0.0	0.0	0.0

[a] For another possible assignment of this observed level, see reference 7.

are slowly varying functions of the parameter Z and hence that no reversal occurs in the complete calculations. This serves once again to emphasize the extreme importance of including all three- and four-center integrals in theoretical calculations. In addition, these results considerably strengthen the theoretical assignment of the benzene levels. The order of the lowest excited levels has also been shown to be preserved when configuration interaction is taken into account,[7] and it is not likely that calculations including both configuration interaction and a change in Z value will change this situation.

In the process of computing approximate values for the three- and four-center repulsion integrals, both the Sklar[8] and Mulliken[9] approximations were studied by comparing their validity in the two-center integrals for various Z values. It can be shown by actual computation for two-center repulsion integrals that the Sklar approximation is always somewhat greater than (or in the limit equal to) the exact value of the integral. When the two charge centers as formulated by the Sklar method happen to coincide in the case of two-center integrals, the approximated values become much larger than the true values. It is likely that the same situation will prevail in three- and four-center integrals. Approximate values of integrals computed by the Mulliken method were not uniformly higher than the exact values for the two-center integrals, but in those cases where they were lower than the exact, the deviation was not large. It is suggested that in future computations using these approximations, one should use that approximation for each integral which gives the lower value to that integral. This criterion favors the Mulliken approximation perhaps 80 to 90 percent of the time. The results reported in this paper were calculated by using a mixture of the two approximations which tended to eliminate those integrals of the Sklar method that were expected to be much too high, but the procedure did not conform exactly to that recommended here.

* Contribution No. 143 from the Institute for Atomic Research and Department of Chemistry, Iowa State College, Ames, Iowa. This work was supported in part by the Ames Laboratory of the AEC.

[1] M. Goeppert-Mayer and A. L. Sklar, J. Chem. Phys. **6**, 645 (1938).
[2] C. C. Roothaan and R. G. Parr, J. Chem. Phys. **17**, 1001 (1949).
[3] H. Shull, J. Chem. Phys. **17**, 295 (1949).
[4] D. S. McClure, J. Chem. Phys. **17**, 665 (1949).
[5] D. P. Craig, J. Chem. Phys. **18**, 236 (1950).
[6] N. S. Bayliss, J. Chem. Phys. **17**, 1353 (1949).
[7] Parr, Craig, and Ross, J. Chem. Phys. **18**, 1561 (1950).
[8] A. L. Sklar, J. Chem. Phys. **7**, 990 (1939).
[9] R. S. Mulliken, J. Chem. Phys. **46**, 497, 675 (1949).

Directed Valence in As_4 and P_4

MITSUO MASHIMA
Faculty of Liberal Arts, Saga University, Saga-ken, Japan
(Received July 17, 1951)

THE best $s-p-d$ hybrid bond orbital[1] (with the maximum strength 3) is

$$\tfrac{1}{3}s+(1/3^{\frac{1}{2}})p_z+(5^{\frac{1}{2}}/3)d_z.$$

Hultgren[2] has stated that three best bond orbitals of this type may be formed at mutual angles of 73°9′ and 133°37′; but these bond orbitals have not been adapted to actual molecules.

We can obtain trigonal pyramidal, equivalent bond orbitals which have mutual angles of 73°9′ and strength 3. These are

$$\psi_1=\tfrac{1}{3}s+\tfrac{1}{3}\{2(6-6^{\frac{1}{2}})/5\}^{\frac{1}{2}}p_x+\tfrac{1}{3}\{(2+3\cdot6^{\frac{1}{2}})(6-6^{\frac{1}{2}})/10(7-2\cdot6^{\frac{1}{2}})\}^{\frac{1}{2}}p_z$$
$$+\tfrac{1}{3}\{2(7-2\cdot6^{\frac{1}{2}})/5\}^{\frac{1}{2}}d_{xy}+\tfrac{1}{3}\{2(2+3\cdot6^{\frac{1}{2}})/5\}^{\frac{1}{2}}d_{y+z}$$
$$+\tfrac{1}{3}\{73-28\cdot6^{\frac{1}{2}}/5(7-2\cdot6^{\frac{1}{2}})\}^{\frac{1}{2}}d_z,$$

$$\psi_2=\tfrac{1}{3}s-\tfrac{1}{3}\{6-6^{\frac{1}{2}}/10\}^{\frac{1}{2}}p_x+\{6-6^{\frac{1}{2}}/30\}^{\frac{1}{2}}p_y$$
$$+\tfrac{1}{3}\{(2+3\cdot6^{\frac{1}{2}})(6-6^{\frac{1}{2}})/10(7-2\cdot6^{\frac{1}{2}})\}^{\frac{1}{2}}p_z-\tfrac{1}{3}\{7-2\cdot6^{\frac{1}{2}}/10\}^{\frac{1}{2}}d_{xy}$$
$$-\{7-2\cdot6^{\frac{1}{2}}/30\}^{\frac{1}{2}}d_{x+y}-\tfrac{1}{3}\{2+3\cdot6^{\frac{1}{2}}/10\}^{\frac{1}{2}}d_{y+z}$$
$$+\{2+3\cdot6^{\frac{1}{2}}/30\}^{\frac{1}{2}}d_{x+z}+\tfrac{1}{3}\{73-28\cdot6^{\frac{1}{2}}/5(7-2\cdot6^{\frac{1}{2}})\}^{\frac{1}{2}}d_z,$$

$$\psi_3=\tfrac{1}{3}s-\tfrac{1}{3}\{6-6^{\frac{1}{2}}/10\}p_x-\{6-6^{\frac{1}{2}}/30\}^{\frac{1}{2}}p_y$$
$$+\tfrac{1}{3}\{(2+3\cdot6^{\frac{1}{2}})(6-6^{\frac{1}{2}})/10(7-2\cdot6^{\frac{1}{2}})\}^{\frac{1}{2}}p_z-\tfrac{1}{3}\{7-2\cdot6^{\frac{1}{2}}/10\}^{\frac{1}{2}}d_{xy}$$
$$+\{7-2\cdot6^{\frac{1}{2}}/30\}^{\frac{1}{2}}d_{x+y}-\tfrac{1}{3}\{2+3\cdot6^{\frac{1}{2}}/10\}^{\frac{1}{2}}d_{y+z}$$
$$-\{2+3\cdot6^{\frac{1}{2}}/30\}^{\frac{1}{2}}d_{x+z}+\tfrac{1}{3}\{73-28\cdot6^{\frac{1}{2}}/5(7-2\cdot6^{\frac{1}{2}})\}^{\frac{1}{2}}d_z.$$

(The z axis coincides with the C_3 axis of the trigonal pyramid.) When an angle between the directions of three equivalent bond orbitals is introduced as a parameter to these bond functions, variation of strength of these bond orbitals with varying of the angle may be illustrated, and the degrees of hybridization of the bonds may be estimated by use of experimental values of bond angles.

The fourth orthogonal hybrid function ψ_4 which contains all of the residual s parts may be constructed in the direction of the C_3 axis, and other five functions orthogonal to $\psi_1, \cdots, \psi_4$ can be set up.

These hybrid bond orbitals may be applied to As_4 and P_4. It is reported that As_4, P_4 molecules have bond angles[3,4] 60°, the four atoms lying at the tetrahedron corners and the bonds along the tetrahedron edges. Hultgren[2] has applied $p-d$ hybrid bond orbitals (with strength 2.773) to such a configuration. Assuming that an s function is used in hybridization, we can obtain stronger bond orbitals than these; $s-p-d$ trigonal pyramidal bond orbitals have strength 2.970 (only slightly less than that of the best $s-p-d$ hybrid bond orbital) at bond angle 60°.

It seems to be more probable that $s-p-d$ hybrid orbitals are used in the bond formation in As_4 and P_4; the unshared pair occupies the fourth hybrid function (containing all of the residual s parts) which has 76.5 percent s character at bond angle 60°. Further details on this work will be reported elsewhere.

[1] L. Pauling, J. Am. Chem. Soc. **53**, 1367 (1931).
[2] R. Hultgren, Phys. Rev. **40**, 891 (1932).
[3] Maxwell, Hendricks, and Mosley, J. Chem. Phys. **3**, 699 (1935).
[4] H. J. Bernstein and J. Powling, J. Chem. Phys. **18**, 1018 (1950).

Erratum: On the Latent Heat of Fusion and the Hole Theory

[J. Chem. Phys. **19**, 502 (1951)]

N. R. MUKHERJEE
Department of Chemistry and Chemical Engineering, University of Washington, Seattle, Washington

IN the Letter to the Editor of the above title, Table II was cited incorrectly. Table II was calculated from Eq. (8) of the Letter.

Carrier-Free Radioisotopes from Cyclotron Targets. XVII. Preparation and Isolation of Fe^{59} from Cobalt*

JEANNE D. GILE, WARREN M. GARRISON, AND JOSEPH G. HAMILTON
Crocker Laboratory, Radiation Laboratory, and Divisions of Medical Physics, Experimental Medicine, and Radiology, University of California, Berkeley and San Francisco, California
(Received July 5, 1951)

THE radionuclide, Fe^{59}, produced by the nuclear reaction[1] $Co^{59}(d, 2p)$ has been isolated without the use of added isotopic carrier by a separation procedure based on the observation that Fe^{59} forms radiocolloidal aggregates[2] which may be removed by filtration. The radio-iron was produced by bombarding a cobalt metal target with 20-Mev deuterons in the 60-inch cyclotron at the Crocker Laboratory. The only other transmutation products formed concurrently by deuteron bombardment of cobalt include 2.6-hr Mn^{56} (from n, α-reaction) which was allowed to decay out prior to chemical separation and approximately 10^5-year Ni^{59} (from d, $2n$ reaction), which is too long-lived to be produced in detectable amounts by the bombardments reported here.

The target was 10-mil thick foil of "iron-free" cobalt[3] silver-soldered to a water-cooled copper probe. Approximately 100 milligrams of the bombarded surface was removed by dissolution in 12 N HCl. After centrifugation, the solution was diluted with an equal volume of water and neutralized to pH 9 with 15 N NH_4OH to give a clear "solution" which was slowly drawn through a Whatman No. 50 filter paper. The carrier-free Fe^{59} was quantitatively retained on the filter as adsorbed radiocolloid. The filter was washed first with dilute NH_4OH until Co could not be detected in the filtrate and then washed with distilled water. Over 98 percent of the Fe^{59} remained on the filter paper. The activity was then removed with 6 N HCl solution which was evaporated to incipient dryness and diluted to 0.1 N at which pH the Fe^{59} remained in true solution.

The Fe^{59} was identified by the assigned 46-day[4] half-life and by the 0.46-Mev and the 0.26-Mev beta-particles which have been reported.[5] The gamma-radiation had a half-thickness in lead of 11 g/cm², which agrees with the previous observations.[5] Chemical separation of an aliquot amount of the activity in the Fe fraction after the addition of Ni, Co, Fe, and Mn carriers further identified the activity as Fe^{59}.

We wish to thank Professor G. T. Seaborg for helpful suggestions, Mr. T. Putnam and Mr. B. Rossi and the crew of the 60-inch cyclotron for bombardments, and Miss Margaret Gee for assistance in counting.

* This document is based on work performed under Contract No. W-7405-eng-48-A for the AEC.
[1] G. T. Seaborg and I. Perlman, Revs. Modern Phys. **20**, 585 (1948).
[2] O. Hahn, *Applied Radiochemistry* (Cornell University Press, Ithaca, New York, 1936).
[3] The cobalt target was prepared by Mr. R. W. Dunn of the Donner Laboratory. Spectrographic analysis showed the iron content to be less than 20 ppm.
[4] H. H. Hopkins, Jr., Phys. Rev. **77**, 717 (1950).
[5] Deutsch, Dowining, Elliott, Irvine, and Roberts, Phys. Rev. **62**, 3 (1942).

Carrier-Free Radioisotopes from Cyclotron Targets. XVIII. Preparation and Isolation of Cr^{51} from Vanadium*

JEANNE D. GILE, WARREN M. GARRISON, AND JOSEPH G. HAMILTON
Crocker Laboratory, Radiation Laboratory, and Divisions of Medical Physics, Experimental Medicine, and Radiology, University of California, Berkeley and San Francisco, California
(Received July 5, 1951)

DEUTERON bombardment of vanadium[1] produces 26-day Cr^{51} by the nuclear reaction $V^{51}(d, 2n)Cr^{51}$. This paper reports a radiochemical isolation of carrier-free Cr^{51} from a vanadium target which had been bombarded with 19-Mev deuterons from the 60-inch cyclotron at the Crocker Laboratory. The possible radioisotopes of titanium (from the n, p and d, $2p$ reactions) and scandium (from the n, α-reactions) were allowed to decay out prior to the separation.

A 2-mm layer of "chromium-free" vanadium[2] powder supported on a grooved water-cooled copper target plate by a 0.25-mil tantalum foil was bombarded for 100 microampere hours at a beam intensity of 8 microamperes. After aging, the bombarded vanadium was dissolved in a minimum volume of 6N HNO_3. Ten milligrams of Fe^{+++} were added and the solution was slowly poured into an excess of boiling 10 percent NaOH solution. The Cr^{51} carried quantitatively on the $Fe(OH)_3$ precipitate which was then redissolved and reprecipitated as above. Three such cycles were required to remove last traces of sodium vanadate. The final $Fe(OH)_3$ precipitate containing the Cr^{51} was redissolved in 6N HNO_3 previously saturated with Br_2 and reprecipitated by the addition of dilute NaOH. The temperature of the solution was maintained at approximately 90°C. Under these conditions, the carrier-free Cr^{51} as chromate was retained in the solution which was then made 1N in HNO_3 and saturated with SO_2, 2 milligrams of Fe^{+++} was added and precipitated by the addition of dilute NH_4OH. The $Fe(OH)_3$ precipitate containing the Cr^{51} was washed, dissolved in 6N HCl, and Fe was extracted with ether. The HCl solution was evaporated to dryness on 20 milligrams of NaCl. The carrier-free Cr^{51} was redissolved quantitatively in 2 ml of water at pH 5 to give an isotonic saline solution for biological investigation.

The activity was identified by half-life determinations, by absorption measurements, and by chemical separation with added carriers. The decay curve was followed for 5 half-lives and showed a single period of 26 days which agrees with previously published values.[3,4] Absorption measurements in lead showed the 0.32-Mev gamma-ray reported[5,6] for Cr^{51}. In a chemical separation using added Cr, V, Ti, and Sc carriers, over 98 percent of the activity was recovered in the Cr fraction.

We wish to thank Professor G. T. Seaborg for helpful suggestions, Mr. T. Putnam, Mr. B. Rossi, and the crew of the 60-inch cyclotron for bombardments, and Miss Margaret Gee for assistance in counting.

* This document is based on work performed under Contract No. W-7405-eng-48-A for the AEC.
[1] G. T. Seaborg and I. Perlman, Revs. Modern Phys. **20**, 585 (1948).
[2] Spectrographic analysis showed less than 0.001 percent of chromium to be present.
[3] H. H. Hopkins, Jr., Phys. Rev. **77**, 717 (1950).
[4] H. H. Hopkins, Jr., and B. B. Cunningham, Phys. Rev. **73**, 406 (1948).
[5] F. N. D. Kurie and M. Ter-Pogossian, Phys. Rev. **74**, 677 (1948).
[6] Kern, Mitchell, and Zaffarano, Phys. Rev. **76**, 94 (1949).

The Raman Spectra of Methylbromosilanes

HIROMU MURATA
The Osaka Municipal Technical Research Institute, Osaka, Japan
AND
SEICHI HAYASHI
Kanazawa Teachers College, Kanazawa University, Kanazawa, Japan
(Received July 9, 1951)

THE Raman spectra of tetrabromosilane and tetramethylsilane have been reported by several investigators. We have measured the Raman spectra of methyltribromosilane, dimethyldibromosilane, and trimethylbromosilane, and the following Raman lines (cm^{-1}) have been observed:

$SiBr_3CH_3$	98 (9s)e, k	453(4b)e, k	1396 (4b)e, k
	153 (8s)$e\pm$, k	746(5s)e, k	2898 (8s)e, k
	186 (8s)$e\pm$	1249(1s)e, k	2977 (7s)e, k
	314(10s)$e\pm$, k	1320(3s)e, k	
$SiBr_2(CH_3)_2$	118 (8s)$e\pm$, k	426(2s)e, k	1325 (3s)e, k
	166 (4s)$e\pm$, k	682(5s)e, k	1395 (4b)e, k
	208(9bb)$e\pm$, k	797(2s)e, k	2902 (9b)e, k
	355(10b)$e\pm$, k	1265(1s)e, k	2975 (9b)e, k

TABLE I. The vibrational frequencies of methylbromosilanes (cm^{-1}).

	$SiBr_4$		$SiBr_3(CH_3)$			$SiBr_2(CH_3)_2$			$SiBr(CH_3)_3$			$Si(CH_3)_4$	
		Obs		Obs	Calc		Obs	Calc		Obs	Calc		Obs
$\delta(Br-Si-Br)$	E	90	E	98	95	A_1	118	122		...	...		...
$\delta(CH_3-Si-CH_3)$		...		...	...	A_2	166	164	E	178	175	E	202
$\delta(Br-Si-Br)$	F_2	137	A_1	153	156	B_2	208	197	A_1	213	212	F_2	239
$\delta(Br-Si-CH_3)$		...	E	186	190	A_1	208	202	E	242	240		...
$\delta(CH_3-Si-CH_3)$		...		...	...	B_1	208	210		...	...		...
$\nu(Si-Br)$	A_1	249	A_1	314	316	A_1	355	359	A_1	374	420	A_1	598
$\nu(Si-Br)$	F_2	487	E	453	490	B_2	426	494		...	...		
$\nu(Si-CH_3)$		...	A_1	746	750	A_1	682	720	A_1	635	675	F_2	696, 863
$\nu(Si-CH_3)$		...		...	...	B_1	797	783	E	758	782		

$SiBr(CH_3)_3$	178 $(8b)e\pm$	635$(9b)e\pm, k$	1258 $(1s)e, k$
	213 $(4s)e\pm, k$	697$(3s)e, k$	1325 $(5s)e, k$
	242 $(5s)e\pm, k$	758$(3s)e, k$	1398 $(5b)e, k$
	374 $(7b)e\pm, k$	850$(2s)e, k$	2904$(10b)e, k$
			2973$(10b)e, k$.

Using the method and force constants described by T. Shimonouchi,[1] we have calculated the skeletal vibrations of these molecules. The calculated frequencies are in good agreement with the observed, the assignment of which is adequately made as shown in Table I, where A denotes totally symmetric, B antisymmetric, E twofold degenerate, and F threefold degenerate vibrations of the tetrahedral molecule, respectively. Similar to the case of $(CH_3)_2SiCl^2$ in $Si-CH_3$ stretching frequencies of $(CH_3)_3SiBr$, two Raman lines, 697 and 850, are left to be assigned as shown in Table I, and it may be probable that each of A and E vibrations of this molecule is split into two lines by Fermi-resonance. Thus it is seen that the Raman spectra of methylbromosilanes provide another typical example of a sequence[3] of $XY_4 \rightarrow XZ_4$.

[1] T. Shimanouchi, J. Chem. Phys. **17**, 245, 848 (1949).
[2] J. Duchesne, J. Chem. Phys. **16**, 1006 (1948); Shimanouchi, Tsuchiya, and Mikawa, J. Chem. Phys. **18**, 1306 (1950).
[3] Lecomte, Volkringer, and Tchakrian, Compt. rend. **204**, 1927 (1937).

20th Anniversary
of the
AMERICAN INSTITUTE OF PHYSICS

OCTOBER 23–27 **HOTEL SHERMAN** **CHICAGO, ILLINOIS**

A Joint Meeting of the American Institute of Physics and its Founder Societies

- **AMERICAN PHYSICAL SOCIETY (OCT. 25–27)**
- **OPTICAL SOCIETY OF AMERICA (OCT. 23–25)**
- **ACOUSTICAL SOCIETY OF AMERICA (OCT. 23–25)**
- **SOCIETY OF RHEOLOGY (OCT. 24–26)**
- **AMERICAN ASSOCIATION OF PHYSICS TEACHERS (OCT. 25–27)**

The American Crystallographic Association, an Affiliated Society of the American Institute of Physics, will participate in the Anniversary Meeting.

On Thursday, October 25, there will be an all-day symposium organized upon the theme "physics today", which will feature invited papers by:

ENRICO FERMI—THE NUCLEUS
E. U. CONDON—THE ATOM
J. C. SLATER—THE SOLID STATE
HARVEY FLETCHER—ACOUSTICS
EDWIN H. LAND—OPTICS
K. K. DARROW—PHYSICS AS SCIENCE AND AS ART

A JOINT BANQUET on Thursday evening, October 25, will have Senator Brien McMahon and K. T. Compton as guest speakers.

AN INDUSTRIAL EXHIBIT of scientific instruments and apparatus will provide manufacturers with an excellent opportunity to show their products to men who are responsible for many of the major scientific and technological advances of the past twenty years.

A PLACEMENT SERVICE for the benefit of employers and potential employees will be available during the meeting, and space in the Hotel Sherman will be reserved for this purpose.

Address inquiries to: The Secretary, American Institute of Physics, 57 East 55th Street, New York 22, New York